CORRIGENDA

Page	Line	Corrections
2	4	Replace "profiles for each phase" by "profiles, one for each phase".
27	18	Replace "Each flow pattern" by "Each of the flow patterns".
39	5	Substitute "both for the cases of "by "for both".
51	17	Replace "its analytical" by "their analytical".
53	2	Substitute "seems to over-predict the void fractions for 1.013" by "overlpredict the void fractions for 1.013 bar".
73	28	Replace "0.5 and 10" by "0.5 and when $e_g = e_\ell = 0.5$".
79	12	Substitute "and specific enthalpy" by "and energy".
80	8	Replace "rate of creation of energy" by "sum of thermal energy sources".
110	14	Replace the sentence "bubbly flows .... achieved" by "two-phase axisymmetric flows which occupy one or two regions of a pipe each of which is filled by a homogeneous mixture of the two phases. Such flows are usually referred to as homogeneous, annular-separated or wispy-annular and are easily studied".
113	12	Substitute "the obtained predictions" by "the predictions obtained".
114	4	Replace "can be only" by "can only be".
115	12	Replace "assumed here velocity profiles" by "velocity profiles assumed here".

ANALYSIS OF TWO-PHASE FLOW BASED ON A VELOCITY PROFILE MODEL.

by

Andreas Nikolaos Skouloudis

M.Sc.,D.I.C.

November 1983.

A thesis submitted for the degree of

Doctor of Philosophy

In the Faculty of Engineering

University of London.

Nuclear Power Section

Department of Mechanical Engineering

Imperial College of Science and Technology

London SW7 2BX.

ABSTRACT

This thesis is concerned with the physical modelling of laminar and turbulent two-phase flows with liquid and vapour entrainment.

The proposed analytical model is based on two different power law velocity profiles for each phase and has been used for the prediction of the void fraction and pressure drops for annular types of two-phase flow. This model is then extended by allowing the liquid and vapour phases to be entrained into each other. Thus by suitably choosing the entrainment ratios bubbly and wispy-annular flows can be analysed. Encouraging comparisons are made with a wide range of experimental results for the void fraction and pressure drop in uniformly heated flows.

For two-phase flows under non-uniform heat flux distributions the conservation equations for mass, momentum and energy are solved numerically. When the velocity profile model is integrated in these equations an interesting numerical scheme is developed, with a finite difference approximation only for the terms containing the mass flux, pressure and specific enthalpy. The details of the calculation procedure are presented and the conditions for achieving accurate results are considered.

The physical modelling is further improved by using a simple representation of entrainment for the liquid phase and the whole scheme is then used for the prediction of burnout in forced convective boiling in vertical upflows with uniform and non-uniform heat flux distributions. The results show an encouraging agreement with experiment.

Dedicated to
my wife
Photoula
and my
Parents.

ACKNOWLEDGEMENTS

My first and foremost gratitude is to my supervisor Dr S J Peerless for his constant and sincere encouragement throughout my stay at the College. His utmost interest in my work together with his inspiring ideas are the invaluable elements on which this thesis is based. I should never forget the endless hours we spent together discussing various aspects of my work.

The present study has been carried out partially under a fellowship from the International Atomic Energy Agency. I am grateful to all the staff of the Fellowships and Training Section for their valuable assistance which has been greatly appreciated. In particular, I wish to extend my thanks to Professor N Chrisochoedes of the Nuclear Research Centre "Demokritos", Dr S B Hammond of the IAEA and Miss A T Duerden for their constant interest and support to my work, and for keeping a very friendly contact with the IAEA authorities. However, the views expressed in this work are entirely mine and not necessarily those of the IAEA.

My stay at Imperial College has been enriched by the help, suggestions and discussions of all the members of staff of the Nuclear Section and Dr J A Mason from the Reactor Centre to whom I wish to express my sincere gratitude. I am also indebted to all those colleagues with whom I have participated in both scientific and social discussions. These include : Mr P Begleris, Dr A H Hadid, Mr G Ioannon, Mr N Zarimbas and many others.

I also wish to acknowledge the assistance provided for the presentation of this thesis by Mr R J G Edwards of "Manpower" Ltd,for his expert handling of the typing arrangements,and Miss Jane Toplis for her diligent typing which is very much appreciated.

For the support, encouragement and dedication given to me through all the stages of my life by my wife and our parents, my gratitude cannot be expressed in words. I wonder if I can ever return even a small fraction of the kindness they have shown to me.

Last but not least I wish to acknowledge how limited is the human mind even when we try to describe the mechanisms involved with the interaction of only two-phases. But we all hope that one day, our eyes might see, our ears hear, and our mind understand.

London 1983

A N Skouloudis

You may hear and hear, but you will never understand; you may look and look, but you will never see. For this people's mind has become gross; their ears are dulled, and their eyes are closed. Otherwise, their eyes might see, their ears hear, and their mind understand;

The Acts 28 26-28

ΑΚΟΗ ΑΚΟΥΣΕΤΕ ΚΑΙ ΟΥ ΜΗ ΣΥΝΗΤΕ, ΚΑΙ ΒΛΕΠΟΝΤΕΣ ΒΛΕΨΕΤΕ ΚΑΙ ΟΥ ΜΗ ΙΔΗΤΕ ΕΠΑΧΥΝΘΗ ΓΑΡ Η ΚΑΡΔΙΑ ΤΟΥ ΛΑΟΥ ΤΟΥΤΟΥ, ΚΑΙ ΤΟΙΣ ΩΣΙ ΒΑΡΕΩΣ ΗΚΟΥΣΑΝ, ΚΑΙ ΤΟΥΣ ΟΦΘΑΛΜΟΥΣ ΑΥΤΩΝ ΕΚΑΜΜΥΣΑΝ, ΜΗΠΟΤΕ ΙΔΩΣΙ ΤΟΙΣ ΟΦΘΑΛΜΟΙΣ ΚΑΙ ΤΟΙΣ ΩΣΙΝ ΑΚΟΥΣΩΣΙ ΚΑΙ ΤΗ ΚΑΡΔΙΑ ΣΥΝΩΣΙ.

The Acts 28 26-28

CONTENTS

CHAPTER 2 : THE VELOCITY PROFILE MODEL

CHAPTER 3 : THE EFFECTS OF ENTRAINMENT IN ANNULAR TYPES OF FLOW

NOMENCLATURE

A	:	flow area
c	:	8.74
d	:	pipe diameter
E	:	energy
e_1, e_2	:	entrainment ratios
f_E	:	exchange factor
f_R	:	relaxation factor
$G \equiv \langle \rho u \rangle$	:	mass flux
g	:	gravitational acceleration
h	:	specific enthalpy
$h_{g\ell}$	:	$h_g - h_\ell$
i	:	internal energy
j	:	volumetric flux
j_g^+	:	dimensionless vapour flux defined in chapter 5
ℓ	:	Prandtl mixing length
L	:	total length of the test section
L_B	:	length over which evaporation occurs
$\dot{m}$	:	mass flow rate
$\dot{M}$	:	momentum flow rate
n	:	power law exponent
p	:	local pressure

$\dot{q}'$	:	heat transfer rate per unit length
$\dot{q}''$	:	heat transfer into the system via the channel wall
$\dot{q}'''_V$	:	internal heat generation rate per unit volume
Re_ℓ	:	$\rho_\ell \, j_\ell \, d \, / \, \mu_\ell$
R_D^2	:	density ratio $\rho_2 \, / \, \rho_1$
R_V^2	:	viscosity ratio $\mu_2 \, / \, \mu_1$
S	:	slip ratio $\bar{u}_2 \, / \, \bar{u}_1$
s	:	distance from entrance
s^+	:	dimensionless distance defined in chapter 5
U^2	:	$\overline{u^2} \, / \, \bar{u}^2$
U^3	:	$\overline{u^3} \, / \, \bar{u}^3$
u	:	local velicity
We	:	effective Weber number as defined in chapter 5
x	:	mass-dryness fraction
y	:	$r_o - r$
Z	:	wetted perimeter
$< \; >$	:	averaged value

Greek symbols

α	:	void fraction
$\Delta\rho$	:	density difference
Δp	:	pressure drop
Δz_i	:	$(\delta s_i + \delta s_{i-1})$ /2
δs	:	cell length
δt	:	time increment
ε_p, ε_h	:	errors from finite difference approximation of the derivatives
Θ	:	inclination to horizontal
μ	:	viscosity
ρ	:	density
ρ_A	:	area-averaged density (Chapter 4)
ρ_E	:	energy-averaged density (Chapter 4)
ρ_H	:	enthalpy-averaged density (Chapter 4)
ρ_F	:	flow-averaged density (Chapter 4)
ρ_M	:	momentum-averaged density (Chapter 4)
σ	:	surface tension
τ	:	shear stress

Subscripts

ac	:	accelerational component
BO	:	burnout quantity
e	:	equivalent
fr	:	frictional component
g	:	vapour phase
gℓ	:	property change during evaporation
gr	:	gravitational component
h	:	hypothetical quantity
i	:	axial discretisation property
in	:	inlet value
j	:	time discretisation property
ℓ	:	liquid phase
max	:	maximum quantity
N	:	normalised value
out	:	output quantity
s	:	separation
T	:	total flow quantity
w	:	conditions at the wall
1	:	property for region 1
2	:	property for region 2
−	:	average value

LIST OF FIGURES

LIST OF TABLES

Chapter 1.

Introduction.

Contents :

CHAPTER 1

INTRODUCTION

1-1 The Problem Considered

Knowledge of the flow of a liquid and its vapour along a pipe or a duct has become increasingly important in recent years. In power generation plants, nuclear reactors and chemical process plants, there is great safety and economic incentive to be able to examine the behaviour of certain key phenomena, such as burnout under the extreme temperature and flow conditions associated with mixed liquid and vapour flows. The advantages gained by such studies are that optimum efficiency could be obtained and greater emphasis could be put on refining the design and operational methods.

The analysis of two-phase flows is made easier if it can be established that the flow is either laminar or turbulent and whether any separation or secondary flow effects occur, in the same way as for single phase flow. However, it is of greater importance to know the topology or geometry of the flow. Experience has shown that for such flows the liquid and vapour can take up a variety of configurations. Each flow pattern depends on the conditions of pressure, flow, heat flux and channel geometry and are usually classed in flow patterns for vertical or horizontal co-current flows. These flow patterns are shown in figures 1.1 and 1.2 together with the special case where the two-phase mixture is created by liquid evaporation in heated channels.

In the investigation of such flows, the knowledge of the division of the flow between the two phases is usually important. The associated parameters are the fraction of the total flow area occupied by vapour

(void fraction), and the ratio of the vapour mass flow rate to the total (mass-dryness fraction). In addition to these parameters, it is usually desired for design purposes to know the two-phase flow friction factor as well as how the liquid and vapour are intermixed in each of flow patterns which are likely to occur.

Several methods have been proposed throughout the years to describe the relation of all those parameters associated with the flow of the two fluids. These methods can be classed as semi-empirical and analytical; the most important of these are presented in section 1-3. The constraints of the first category are that the correlations produced are limited by the application range of the experiments on which they are based; and for the second category the limitations are due to the severe physical assumptions made about the character of the flow.

With the ever increasing computer facilities now available it has become relatively easy to analyse two-phase flows in complex flow boundaries. Numerous computer codes are already proposed with various degrees of complexity as shown by Fabic (Fa76). However in effect all those codes suffer from lack of understanding of the actual physical mechanisms and they need semi-empirical models for the friction factors and the slip velocity between the two phases.

This thesis represents a different approach to the subject in the sense that a numerical method is developed based on the physical mechanisms of the flow. This method is developed in such a way that it could easily describe bubbly, wispy-annular and annular flow patterns in circular flow areas, with or without heat input, where the two phases are assumed in thermal equilibrium. Flow patterns other than those mentioned above are not covered in this thesis. That is because the excluded flow patterns are not expected to have a significant contribution in flows

with energy transfer, and because those patterns are very difficult to study with a theoretical model.

1-2 The Present Contribution

So far the most successful method of analysing two-phase flow problems was to use a semi-empirical correlation for the frictional pressure component, then calculate the shear stress distribution in the channel and then the velocity profile from corresponding single phase turbulence models. The aim of the present investigation is to reverse that approach and start from an assumed velocity profile with the correct boundary conditions of zero velocity at the wall and maximum velocity at the centre, which also retains the continuity of velocity and shear stress at the interface between the two phases.

After obtaining the relations for the division of the flow the frictional pressure drop is easily calculated. This model can be also substituted into the flow conservation equations which are then modified to account for entrainment of the phases into each other. For the conservation equations a finite difference scheme is developed which can be applied to predict burnout in flows with complex heat flux distributions.

Throughout the present work a variety of experimental comparisons are carried out to examine the accuracy of the predictions and to validate certain aspects of its physical modelling. For the burnout calculations comparison with other semi-empirical models indicates the advantages gained from the use of a purely numerical method which is based on a simple analytical approach. Parametric effects from the present model are also presented.

1-3 Survey of Previous Work

Due to the wide range of conditions over which two-phase flow is likely to exist in power and process plants this subject has received considerable attention during the past two decades. Numerous works have been also published examining the safety aspects in various industrial plants arising from the existence of such flows. Most of these publications have concentrated on trying to predict the frictional pressure drop as well as trying to correlate the fractions of the total flow and area parameters referring to each individual phase. The result of such studies is that many correlations are formulated without reference to any particular flow regime. These correlations are easy to use and sufficiently accurate for many purposes within their range of validity, but they give little insight into the physics of the system. Some of these most popular are briefly described below, and they are classed as either semi-empirical, or analytical. Some comments are also made about a number of well known experimental works.

1-3.1 Semi-empirical Studies

Most of the semi-empirical two-phase models have been based on the work by Lockhart and Martinelli (Lo49) who in 1949 produced equations based on the ratios of frictional pressure gradient in two-phase flow to the frictional pressure gradients for the liquid and vapour phases flowing alone in the same tube with the same flow rates as in the two-phase flow. Their equations were derived for horizontal flow data near to atmospheric pressures in unheated tubes. Since then this method has been adopted in many different ways, of which the most important transformation was that by Chisholm (Ch73). He used a physical property coefficient which was the square root of the ratio of the vapour to liquid frictional pressure gradient when the total mixture flows as vapour or liquid respectively. However the method retained its

semi-empirical character and could not be used easily in evaporating flows with non-uniform heat flux distributions.

On similar lines, Martinelli and Nelson (Ma48) used the ratio of frictional two-phase pressure drop to the frictional pressure drop of the liquid flowing alone in the tube with a flow rate equal to the total flow rate of the two-phase flow. Thom in 1964 (Th64) also recommended the use of this correlation with different multipliers for uniformly heated pipe flows. For the calculation of those multipliers Thom used a constant slip between the two phases at constant pressure. Unfortunately experiments have shown that this ratio also depends on the ratio of the liquid and vapour mass flow rates.

Hughmark and Pressburg (Hu62)carried out tests on vertical upward cocurrent air-liquid flows without heat input for six different liquids. Their correlation aims to determine the effects of density, viscosity and surface tension on the void fraction and pressure drop. This correlation calculates the total pressure drop with an average absolute error of about 11% for 563 experimental points.

1-3.2 Analytical Models

In contrast to the semi-empirical studies the analytical models are mainly based on the actual flow regime, so the correlations produced are dependent on the physical assumptions made.

One of the earliest analytical models for bubbly flow regimes was that of Bankoff (Ba60). This model assumed that there is no local slip in the bubbly flow; instead, single radial profiles for the velocity and void fraction were used. This model is not suitable for mixtures with large bubbles which begin to coalesce, especially for conditions approaching the all-vapour flow, because in that region the void fraction is considerably underestimated.

Levy in 1960 (Le60) proposed a momentum exchange model with equal frictional and head loss for the liquid and vapour phases. This model was not very successful in comparisons with experiment and was substituted in 1966 (Le66) by a model which considered the momentum and mass-transfer component for the interfacial shear force. This latter model showed that the momentum component is dominant within the liquid film while for the vapour core the mass-transfer component is the most important term. The interfacial shear stress for the vapour core was calculated from an empirical correlation based on experimental results. This work demonstrated the importance of the continuity of shear stress at the interface between liquid and vapour which can by no means be taken equal to the wall shear stress.

A rather simpler approach was proposed by Smith (Sm70) in 1970. His model assumes an annular liquid flow, surrounding a core flow of vapour with entrained water droplets, both of which are assumed to have equal velocity heads. For the best fit over a wide range of experimental results, Smith suggested that the entrained liquid component of the core flow should be 40% by mass.

All the above models are "one-dimensional" in a sense that at any station in the pipe, each of the flow properties including the velocity, has a single value for each of the phases. The two phases are to some extent independent of each other except that together they fill the whole flow area and they are assumed to be in thermal equilibrium.

Westmoreland (We57) in 1957 suggested a two dimensional velocity profile model for two-phase annular flow which was based on two different velocity profiles which varied with the radius according to 1/nth power law. He joined those profiles at the liquid-vapour interface by continuity of shear-stress and velocity, but rather unexpectedly he used laminar shear laws for the interface, even for turbulent two-phase flows.

The Westmoreland model can be regarded as a forerunner of the models presented in this thesis. It was not apparently developed, perhaps because of the difficulty in performing the complicated numerical calculations at that period.

However the advantage of the Westmoreland approach is that wall shear stress is calculated directly from the velocity profile that corresponds to the phase next to the wall. This method of calculating wall shear stress was successfully used by D H Rooney (Ro67) for natural circulation velocity prediction.

It may be noted at this point that none of the above models predicts any variation of void fraction with mass flow rate.

1-3.3 Survey of Experimental Works

The experimental approach, although always more expensive, is essential for the validation of the theoretical ideas and provides detailed factual knowledge about the actual flow conditions. The main aim of experimental work is to provide the missing link between the ratios of the flow (e.g. void-fraction) properties which correspond to each phase. Secondly, to examine the two-phase friction effects and if possible relate those to the relationship established for the ratios of the flow and geometry properties.

Several experimental works have been carried out so far, from which the most important are those by Haywood et. al. (Ha61), Rouhani and Becker (Ro63) and Anderson and Mantzouranis (An60). Those experiments covered wide ranges of operating conditions, geometries, with or without heat input, with different two-phase components and used different measuring techniques. The operating conditions for these experiments are given in the next chapters where comparisons are made with theoretical predictions, but here the main emphasis and the aims set by those experiments are briefly described.

Haywood et. al. (Ha61) made measurements for the void-fraction and pressure drop with boiling water in heated and unheated tubes arranged vertically or horizontally. The purpose of these experiments was to examine the dependence of the results at different mass flow rates and operating pressures. For the void fraction a gamma-ray attenuation method was used. Their results showed the importance of the slip velocity between the two-phases in the prediction of the pressure drop.

Rouhani and Becker (Ro63) measured void fractions in small tubes using boiling heavy water vertical flows. A wider range of operating pressures was covered by these experiments and the void fraction measurements were obtained by the (γ - n) reaction which occurs when heavy water is irradiated with gamma rays.

The experiments by Anderson and Mantzouranis (An60) were conducted with air-water mixtures flowing in an unheated vertical tube of 11 mm bore. Measurements of the void fraction were made by isolating the test section and measuring the height of the liquid. The aim of these experiments was to provide void fractions and pressure drops for conditions approaching the all-gas flow. Also, special attention was given to measuring the entrainment of liquid droplets in the gas core, by the method of separation from the liquid flowing in the annular film.

Even for these experiments remains a considerable degree of uncertainty with regard to the actual flow patterns covered by the range of the operating conditions. However the general support is that the examined flows are mostly of an annular type.

As for entrainment, its existence has been confirmed although it has not been yet fully described. Unfortunately, the development of sophisticated analytical models depends very much on the understanding of the actual physical conditions.

1-4 Outline of the Thesis

The main body of the thesis consists of five chapters. Chapter two contains the development and application of the velocity profile model in annular two-phase flows where the liquid and vapour phases are flowing completely separated with a smooth interface between them. The equations are derived for laminar and turbulent flows and comparisons are made with experimental results which are close to the assumed physical representation. The parametric studies in the same chapter help to identify the influence on the predictions of the new parameters introduced by the velocity profile model.

In chapter three the velocity profile model is extended for flows with both liquid and vapour entrainment. Some interesting comparisons with experiment are shown in this chapter including results for flow in an annular passage.

In chapter four the generalised forms of the conservation equations are simplified by making use of the velocity profiles assumed in this model and a general numerical solution scheme is proposed, suitable for two-phase flows with non-uniform heat-flux distributions.

In chapter five the numerical scheme is used for prediction of burnout length and mass dryness fraction with various heat-flux distributions. For the nearest possible representation of entrainment, a semi-empirical model has been introduced as part of the numerical scheme.

The general discussion of the model and the conclusions derived from its use are given in chapter six. Also the achievements of the present work are stated, and suggestion for future work are made. The remaining sections of the thesis contain the figures and tables for the previous chapters organised in a single appendix, a list of the cited references, and appendices that provide supplementary information to some of the chapters in the main text.

Chapter 2.

The Velocity Profile Model.

Contents :

CHAPTER 2

THE VELOCITY PROFILE MODEL

2-1 Introduction to the model

In the investigation of the flow of a liquid and its vapour along a pipe or duct, knowledge of the division of the flow between the two phases is usually important. The associated parameters which are often used in the application of conservation laws in such flows are:

(a) The void fraction, "α" which is defined as the ratio of the vapour flow area to the total;

(b) The mass dryness fraction, "x", defined as the ratio of vapour mass flow rate to the total flow rate.

Values of local dryness fraction are normally readily obtainable from the initial values of the flow and the conditions of heat transfer when thermal equilibrium is assumed. But for the void fraction α the absence of comprehensive analysis of two phase flow, generally makes the dependence on experimental measurements unavoidable.

Alternatively we could relate the local values of dryness fraction and void fraction to each other, but in order to achieve this, existing models require some simplifying assumptions about the character of the flow. Such assumptions, as mentioned at the introduction chapter, involve simplifications of the conservation equations thus producing results with limited ranges of application.

Frequently it has been assumed (Wa69, Le60) that the frictional pressure gradient for the liquid component is approximately equal to the frictional gradient for the liquid phase flowing alone in a tube with the same cross sectional area as that of the liquid in the combined flow. As

shown by the two velocity profiles of Figure 2.1, it is highly unlikely that the two cases will produce similar wall shear stresses, and therefore pressure gradients. With the continuous line in this diagram is drawn a hypothetical velocity profile which allows continuity of velocity and shear stress at the interface between the two phases. This is the main idea behind the velocity profile model which offers the obvious advantage of avoiding discontinuities at the interface, and relates directly the void fraction and mass dryness fraction.

2-2 Description of the velocity profile model

The velocity profile model describes steady, axisymmetric two-phase annular pipe flows in which the two phases can be regarded as flowing separately, divided by a clearly-defined hypothetical surface of separation. The most obvious feature of the proposed model is that the two-dimensional velocity profile for the two phases is not given by a single relation over the complete flow passage. Instead, for each phase a different velocity relationship is used.

In each part of the flow passage the velocity is taken to vary with radius according to relations similar to those used in the analysis of single-phase flow. Thus for turbulent two-phase flows the velocity is taken to vary with radius following a 1/nth power law relation while for laminar flows parabolic relations are used.

When the two parts of the velocity profiles are matched by ensuring continuity of velocity and shear stress at the surface of separation, the shape of the combined profile will also depend on whether the heavier phase is flowing in the annular region next to the wall or the circular central region, which we will call regions 1 and 2 respectively. As either phase could be taken to occupy regions 1 and 2 it is useful to define as "L1V2" the case where liquid flows in the region next to the

wall and vapour in the central region, with "V1L2" referring to the reverse case. The two cases are shown respectively in figures 2.2(a) and 2.2(b).

In the following sections the relations between the associated two-phase flow parameters are derived both for the cases of laminar and turbulent flows. The terms laminar and turbulent flow are used in the same sense as for single phase flow.

2-2.1 Laminar two-phase velocity profiles

Laminar parabolic velocity profiles are used for regions 1 and 2 and the two parts of the velocity profile are given by

$$(u_1/u_{max,1}) = (1 - r^2/r_o^2) \qquad r_s \leq r \leq r_o \qquad (2.2.1)$$

$$(u_2/u_{max,2}) = (1 - r^2/r_h^2) \qquad 0 \leq r \leq r_s \qquad (2.2.2)$$

when liquid flows next to the wall, subscript 1 and 2 refer to liquid (ℓ) and vapour (g) respectively; the converse is true when vapour flows next to the wall. The surface of radius r_s is the surface of separation between the two phases and r_h is a hypothetical dimension used in specifying the velocity profile for the phase in region 2.

From equations (2.2.1) and (2.2.2), the continuity of velocity at the surface of separation ($r = r_s$) gives :

$$u_{max,1}\left(1 - \frac{r_s^2}{r_o^2}\right) = u_{max,2}\left(1 - \frac{r_s^2}{r_h^2}\right) \qquad (2.2.3)$$

Similarly, from the continuity of laminar shear stress at the interface gives a second relation between the maximum velocities and the geometric parameters. So

$$\mu_1 \left(\frac{du_1}{dy}\right)_{r = r_s} = \mu_2 \left(\frac{du_2}{dy}\right)_{r = r_s} \qquad (2.2.4)$$

where $y \equiv r_o - r$. When we substitute the relevant velocities from equations (2.2.1) and (2.2.2) we obtain:

$$\mu_1 \frac{u_{max,1}}{r_o^2} = \mu_2 \frac{u_{max,2}}{r_h^2} \qquad (2.2.5)$$

Hence from equations (2.2.3) and (2.2.5) the ratio of the maximum velocities is given by :

$$\frac{u_{max,1}}{u_{max,2}} = R_V^2 \left(\frac{r_o}{r_h}\right)^2 = \left(\frac{r_o}{r_h}\right)^2 \left(\frac{r_h^2 - r_s^2}{r_o^2 - r_s^2}\right) \qquad (2.2.6)$$

Where $R_v \equiv (\mu_2/\mu_1)^{1/2}$. Further rearrangement leads to

$$(r_h/r_s)^2 = 1 + R_V^2 \ (r_o^2/r_s^2 - 1) \qquad (2.2.7)$$

But from the definition of void fraction as the ratio of the vapour flow area to the total, it is quickly seen that:

$$\begin{cases} (r_s/r_o)^2 = 1 - \alpha & \text{when vapour flows next to the wall.} \\ (r_s/r_o)^2 = \alpha & \text{when liquid flows next to the wall.} \end{cases} \qquad (2.2.8)$$

From (2.2.7) and (2.2.8) the geometric parameters of the combined profiles can be derived when the void fraction is known. Unfortunately the void fraction is very difficult to determine and we usually have to work from the mass dryness fraction instead. So we also have to derive an expression for the mass-dryness fraction based on the geometric and kinematic parameters. For that purpose the mass flow rates in region 1 and 2 are obtained in the normal way as :

$$\dot{m}_1 = \int_{A_1} \rho_1 u_1 dA = 2\pi\rho_1 u_{max,1} \int_{r_s}^{r_o} \left(1 - \frac{r^2}{r_o^2}\right) r dr \qquad (2.2.9)$$

$$\dot{m}_2 = \int_{A_2} \rho_2 u_2 dA = 2\pi\rho_2 \, u_{max,2} \int_0^{r_s} \left(1 - \frac{r^2}{r_h^2}\right) r dr \qquad (2.2.10)$$

When equation (2.2.6) is used together with the relevant integrals from table 2.1 the ratio of mass flow rates becomes :

$$\frac{\dot{m}_2}{\dot{m}_1} = R_D^2 \left[\frac{r_s^2}{r_o^2 - r_s^2}\right]\left[\frac{2r_h^2 - r_s^2}{r_h^2 - r_s^2}\right] \qquad (2.2.11)$$

where $R_D = (\rho_2/\rho_1)^{1/2}$. Since by definition,

$$x = \dot{m}_g / (\dot{m}_g + \dot{m}_\ell) \qquad (2.2.12)$$

then the ratio of mass flow rates can be expressed in terms of mass dryness fraction as :

$$\frac{\dot{m}_2}{\dot{m}_1} = \frac{1 - x}{x} \quad \left\{ \text{when vapour flows next to the wall.} \right.$$

$$\frac{\dot{m}_2}{\dot{m}_1} = \frac{x}{1 - x} \quad \left\{ \text{when liquid flows next to the wall.} \right. \qquad (2.2.13)$$

From equations (2.2.13) and (2.2.11) an explicit relation between the mass-dryness fraction and the kinematic and geometric parameters is obtained.

Alternatively equations (2.2.11), (2.2.13), (2.2.7) and (2.2.8) constitute an implicit relationship between α and x. In which ever way we express equation (2.2.11) there is a single solution everywhere in the range of real physical conditions, i.e. for $0 \leq x \leq 1$ and $0 \leq \alpha \leq 1$. In table 2.2 the important relations of the present analysis are summarised for laminar two-phase flows.

2-2.2 Turbulent two-phase velocity profiles

In a similar way as for laminar flows the turbulent velocity profiles corresponding to each flow region of figure 2.2 are given by the

following power law relations :

$$(u_1/u_{max,1}) = (1 - r/r_o)^{1/n} \qquad r_s \leq r \leq r_o \qquad (2.2.16)$$

$$(u_2/u_{max,\ 2}) = (1 - r/r_h)^{1/n} \qquad 0 \leq r \leq r_o \qquad (2.2.17)$$

in which the subscripts 1,2 together with h and s have the same meaning as for equations (2.2.1) and (2.2.2).

When the two parts of the velocity profile are matched by ensuring continuity of velocity at the surface of separation ($r = r_s$) it is found that :

$$u_{max,\ 1}\ (1 - \frac{r_s}{r_o})^{1/n} = u_{max,\ 2}\ (1 - \frac{r_s}{r_h})^{1/n} \qquad (2.2.18)$$

For the continuity of shear stress at the interface the ratio of turbulent viscosities must be known and for that purpose a single phase turbulence model is assumed applicable. To avoid unnecessary complication of the calculations at this stage, the Prandtl mixing length hypothesis is used and the turbulent shear stress expressions are taken as :

$$\tau_1 = \rho_1\ \ell_1^2 |du_1/dy|\ (du_1/dy)$$
$$\tau_2 = \rho_2\ \ell_2^2 |du_2/dy|\ (du_2/dy) \qquad (2.2.19)$$

where ℓ is the mixing length, which in general varies with radius. When τ_1 and τ_2 are used to express the shear stress continuity at the surface of separation we assume that the values of ℓ for the two-phases are equal i.e. that $\ell_1 = \ell_2$. When equations (2.2.16) and (2.2.17) are substituted in equation (2.2.19) the continuity of shear stress at r_s gives :

$$\rho_1\ \frac{u^2_{max,1}}{r_o^2}\ (1 - \frac{r_s}{r_o})^{\frac{2}{n} - 2} = \rho_2\ \frac{u^2_{max,2}}{r_h^2}\ (1 - \frac{r_s}{r_h})^{\frac{2}{n} - 2} \qquad (2.2.20)$$

From equations (2.2.18) and (2.2.20) the ratio of maximum velocities is :

$$\frac{u_{max,1}}{u_{max,2}} = R_D\left(\frac{r_o}{r_h}\right)^{1/n}\left(\frac{r_h - r_s}{r_o - r_s}\right)^{\frac{1-n}{n}} = \left(\frac{r_o}{r_h}\right)^{1/n}\left(\frac{r_h - r_s}{r_o - r_s}\right)^{1/n} \quad (2.2.21)$$

with $R_D \equiv (\rho_2 / \rho_1)^{1/2}$. When re-arranged the last two terms in the last equation can be expressed as :

$$(r_h / r_s) = 1 + R_D (r_o / r_s - 1) \quad (2.2.22)$$

Equations (2.2.22) and (2.2.8) constitute the relationship between the void fraction and the geometric parameters for turbulent two-phase flows.

In the usual way the mass flow rates are given by :

$$\dot{m}_1 = 2\pi\rho_1 u_{max,1} \int_{r_s}^{r_o} (1 - \frac{r}{r_o})^{1/n} \, r \, dr \quad (2.2.23)$$

$$\dot{m}_2 = 2\pi\rho_2 u_{max,2} \int_{0}^{r_s} (1 - \frac{r}{r_h})^{1/n} \, r \, dr \quad (2.2.24)$$

and the ratio of mass flow rates is

$$\frac{\dot{m}_2}{\dot{m}_1} = R_D^3 \left[\frac{r_h \left(\frac{r_h}{r_h - r_s}\right)^{\frac{n+1}{n}} - r_h - \left(\frac{n+1}{n}\right) r_s}{\left(\frac{n+1}{n}\right) r_s + r_o} \right] \quad (2.2.25)$$

As for the laminar case, the last equation is an explicit relation between x (equation 2.2.13) the geometric and kinematic parameters, or an implicit relation between x and α (using equations 2.2.13, 2.2.8 and 2.2.22). Which ever method of expression we choose there is a single solution for equation (2.2.25) in the range $0 \leq \alpha \leq 1$ and $0 \leq x \leq 1$.

Thus by applying the continuity of velocity and shear stress of the surface of separation between the two phases we have obtained a

two-dimensional model for annular axisymmetric laminar or turbulent flows which satisfies the zero slip condition at the pipe wall. For turbulent flows the present model possesses a small flexibility since the profile exponent 1/n can be varied empirically to satisfy local flow conditions. In the following chapters n is taken to be 7 except where stated otherwise. A summary of the most important relations derived from the velocity profile model are shown in table 2.2

2-3 The ratio of the average velocities of the vapour and liquid phases

From the usual definition of mass flow rate, the ratio of mass flow rates in region 1 and 2 is expressed as :

$$\frac{\dot{m}_2}{\dot{m}_1} = \frac{\rho_2 \int_{A_2} u_2 \, dA}{\rho_1 \int_{A_1} u_1 \, dA} = \frac{\rho_2 \, \bar{u}_2 \, A_2}{\rho_1 \, \bar{u}_1 \, A_1} \qquad (2.3.1)$$

Therefore the ratio of the average velocities of the vapour and liquid phases, S, may be expressed as :

$$S \equiv \frac{\bar{u}_2}{\bar{u}_1} = \left(\frac{\dot{m}_2}{\dot{m}_1}\right)\left(\frac{\rho_1}{\rho_2}\right)\left(\frac{A_1}{A_2}\right) \qquad (2.3.2)$$

But from their definition $\dot{m}_2 / \dot{m}_1$ = function(x) and A_2 / A_1 = function(α), so if the velocity ratio S is somehow related to either the void fraction (α) or the dryness fraction (x) we may obtain from equation (2.3.2.) a unique relation between x and α.

Unfortunately, incomplete understanding of the phenomena associated with the interaction of the two phases made many authors rely on empirical expressions in order to represent the ratio S in terms of mass-dryness fraction. With every such empirical expression a different correlation between x and α was produced through equation (2.3.2). In

fact the success of the slip expression, S = fn(x), determined how accurately the void fraction was related to the mass dryness fraction.

However for the two-dimensional velocity profile model the ratio S does not seem to have any significant contribution in the development of the relation between "x" and "α". Nevertheless it is worthwhile to examine to what extent the ratio S is influenced by the independent parameters introduced in the description of the velocity profile model. So by substitution of equations (2.2.11) and (2.2.25) into equation (2.3.2), the ratio S, for the laminar and turbulent cases is given respectively by :

$$S = \left[\frac{2r_h^2 - r_s^2}{r_h^2 - r_s^2} \right] \qquad \text{(Laminar)} \qquad (2.3.3)$$

$$S = R_D \left(\frac{r_o^2 - r_s^2}{r_s^2} \right) \left[\frac{r_h \left(\frac{r_h}{r_h - r_s} \right)^{\frac{n+1}{n}} - r_h - \left(\frac{n+1}{n} \right) r_s}{\left(\frac{n+1}{n} \right) r_s + r_o} \right] \qquad (2.3.4)$$

(Turbulent)

It is obvious from equation (2.2.2) and (2.3.4) that the ratio of the average velocities of the vapour and liquid phases depends on the ratios of the geometric parameters r_h/r_s and r_s/r_o as well as the density ratio R_D. Where r_h/r_s is a function of the void fraction α, and the density or viscosity ratio as shown by equations (2.2.8) and (2.2.7), (2.2.22) for laminar or turbulent flows.

It is also important to emphasise the dependence of the turbulent velocity profile correlation on the exponent n. By analogy to single phase flow this exponent can be taken to vary for different Reynolds numbers. Such a relation between n and Reynolds numbers requires a consistent set of experimental results at different mass flow rates and

this task should be left for future experimental work. In the absence of information of this kind the power exponent will be considered as an independent variable for the parametric studies in section 2.5 and is taken to be 7 everywhere else.

All the independent parameters required in the calculation of the velocity ratio S are finally shown in table 2.3 which also contains the parameters used by a number of empirical relations proposed since 1949.

2-4 The Pressure Gradient

Consider a channel of constant shape and cross sectional area, inclined at an angle Θ to the horizontal, in which steady two-phase flow is allowed. An integral momentum balance can be written over the cross sectional area of the channel for a control volume limited with two planes at a distance δs apart. The resultant equation in the usual way is as follows :

$$\int_{A_T}\left[p - \left(p + \frac{dp}{ds}\delta s\right)\right] dA - \int_{Z} \tau_w \delta s dZ - \int_{A_T}(\rho g \sin\Theta)\delta s dA = \frac{d\dot{M}}{ds}\delta s \qquad (2.4.1)$$

where p is the pressure at a given point in the cross-section, τ_w is the wall shear stress at a point around the periphery Z, A_T the total flow area, ρ the local density which is weighted on a area basis and $\dot{M}$ is the local momentum flow rate.

The main advantage of using the velocity profile model in comparison to existing models is that it provides a rational basis for the direct calculation of axial pressure gradient from equation (2.4.2), for which consistent relations for τ_w and $\dot{M}$ are provided from the shape of the velocity profile. The velocity, and hence the mass flux is not necessary to be considered constant over the whole region and the velocity profile

method takes into account the highly peaked profiles (He70) when liquid flows next to the wall (figure 2.2)

Equation (2.4.1) can be easily interpreted as showing the axial pressure gradient to consist of three pressure components, which are best described by the following :

$$-\frac{dp}{ds} - \frac{Z}{A_T}\tau_w - \frac{1}{A_T}\int_{A_T} \rho g \sin\Theta dA = \frac{1}{A_T}\frac{d\dot{M}}{ds} \qquad (2.4.2)$$

for which the shear stress on the channel wall is taken as constant, irrespective of peripheral position or of the phase which is in contact with the wall. This assumption is certainly valid only for the case of round tube where $Z/A_T = 4/d$. However at this stage it might be possible to extend this assumption to cases where the principle of equivalent hydraulic diameter gives acceptable results.

For steady, annular, axisymmetric flow with no liquid or vapour entrainment, the three components of axial pressure gradients are evaluated from the following expressions for laminar or turbulent two-phase flows.

2-4.1 Frictional Pressure Gradient

For the frictional component, $Z\tau_w/A_T$, the shear stress is calculated from the profile of the phase flowing in the region next to the wall. A similar method to that of Reference (Ro67) is employed, in which the conditions at the wall are calculated from the complete u_1 profile shown in figure 2.2, as if the fluid occupying that region filled the whole tube area. For steady, fully developed, uniform density laminar or turbulent flows the relevant expressions are given by (Sc55) as :

$$\tau_w = \frac{16}{4}\left[\frac{\rho_1 \bar{u}_{1T}\, r_o}{\mu_1}\right]^{-1} \qquad (\rho_1 \bar{u}_{1T}^2) \qquad \text{(Laminar)} \quad (2.4.3)$$

$$\tau_w = \left[c \frac{\bar{u}_{1T}}{u_{max,1}} \right]^{-\frac{2n}{n+1}} \left[\frac{\rho_1 \bar{u}_{1T} r_o}{\mu_1} \right]^{-\frac{2}{n+1}} (\rho_1 \bar{u}_{1T}^2) \qquad (2.4.4)$$

(Turbulent)

where the standard value for c when n = 7 is 8.74. Also $\bar{u}_{1T}$ is taken to be the average velocity over the whole flow area, i.e. :

$$\bar{u}_{1T} = \frac{1}{A_T} \int_{A_T} u_1 dA \qquad (2.4.5)$$

The use of $\bar{u}_{1T}$in equations (2.4.3) and (2.4.4), is similar to the approach of reference (We57) and has the advantage of retaining the continuity of velocity and shear stress at the interface. On the contrary, the use of $\bar{u}_1$, in equations (2.4.3) and (2.4.4), approximates the wall shear stress with the shear stress of a hypothetical flow of phase 1 over the whole tube area, but with mass flow rate equal to that of phase 1 flowing only in the region next to the wall. For laminar or turbulent flows the ratio of the average velocities $\bar{u}_{1T}$ and $\bar{u}_1$ is given by the following equations :

$$\frac{\bar{u}_{1T}}{\bar{u}_1} = \left[1 - \left(\frac{r_s}{r_o} \right)^2 \right]^{-1} \qquad \text{(Laminar)} \qquad (2.4.6)$$

$$\frac{\bar{u}_{1T}}{\bar{u}_1} = \left[1 - \left(\frac{r_s}{r_o} \right)^2 \right] \left[\frac{r_o}{r_o - r_s} \right]^{\frac{n+1}{n}} \left[\frac{n+1}{n} \left(\frac{r_s}{r_o} \right) + 1 \right]^{-1} \qquad (2.4.7)$$

(Turbulent)

The last two expressions are derived by substitution of u_1, into equation (2.4.5) using equations (2.2.1) and (2.2.16) together with the integrals of table 2.1

2-4.2 Gravitational Pressure Gradient

The gravitational component is expressed in the standard way for annular two-phase flow when the local density is weighted on a area basis through the void fraction α thus :

$$\frac{1}{A_T}\int_{A_T} \rho g \sin\Theta dA = [\alpha\rho_g + (1-\alpha)\rho_\ell]\, g \sin\Theta \qquad (2.4.8)$$

Obviously the last equation is applicable for both laminar and turbulent flows; the difference for those two cases is only on the way "α" is expressed in terms of the mass-dryness fraction "x".

2-4.3 Acceleration Pressure Gradient

The acceleration component of axial pressure gradient in equation (2.4.1) takes into account the change of momentum in and out of the control volume. As expected for adiabatic flows this term is zero, because there is no change of momentum, and the two-dimensional velocity profile in not affected from any external sources. But for the case of diabatic flows, the velocity profile model seems to predict acceleration pressure gradients which are up to 1/3 of the frictional gradient and it is impossible to neglect this term from the momentum equation. The velocity profile method has the obvious advantage that allows the calculation of the accelerational pressure gradient directly from the velocity profiles for the two parts of the flow. Thus :

$$\frac{1}{A_T}\frac{d\dot{M}}{ds} = \left(\frac{1}{A_T}\right)\frac{d}{ds}\left(\rho_1 \int_{A_1} u_1^2 dA + \rho_2 \int_{A_2} u_2^2\, dA\right) \qquad (2.4.9)$$

where $\dot{M}$ is the momentum flow rate. Equation (2.4.9) can be expressed in terms of the geometrical ratios r_h/r_s, r_s/r_o and the kinematic parameters but such a representation is avoided here for simplicity. However this relation is easily obtained by substitution of equations (2.2.16) and (2.2.17), for turbulent flow, or of equations (2.2.1) and (2.2.2), for

laminar flow, into equation (2.4.9). The deduced integrals for region 1 and 2, for laminar and turbulent flows can be found among the contents of table 2.1.

2-4.4 Evaluation of total Pressure Drop

For the total change of pressure in a given length of pipe, L, the integrals of the frictional, gravitational and accelerational gradients are calculated over the length L and added together for steady flows.

In this section the total change of pressure is calculated for the particular case of uniformly heated pipe flow where the mass-dryness fraction varies linearly along the pipe. If we ignore variation of fluid properties and assume that the kinematic and potential energy terms are negligible, then the energy conservation equation is expressed by :

$$dx / ds = \dot{q}' / \dot{m}_T h_{g\ell} \qquad (2.4.10)$$

where $\dot{q}'$ is the heat transfer rate per unit length, $h_{g\ell}$ the specific enthalpy of vaporisation. For equation (2.4.10) the two phases are are assumed to be in thermal equilibrium. If in addition, L_B is the pipe length measured from the station where $\alpha = 0$ and the liquid is just saturated then the total pressure drop is :

$$\Delta p = \Delta p_{fr} + \Delta p_{gr} + \Delta p_{ac} \qquad (2.4.11)$$

In the last equation the integrated pressure gradients over the distance L_B are obtained from the following expressions :

$$\Delta p_{fr} = \frac{Z}{A_T} \frac{L_B}{x_{out}} \int_0^{x_{out}} \tau_w \, dx \qquad (2.4.12)$$

$$\Delta p_{gr} = \rho_\ell g \sin\Theta \left[L_B + \frac{\rho_g - \rho_\ell}{\rho_\ell} \left(\frac{L_B}{x_{out}} \right) \int_0^{x_{out}} \alpha \, dx \right] \qquad (2.4.13)$$

$$\Delta p_{ac} = \frac{1}{A_T} \cdot (\dot{M}_{out} - \dot{M}_{in}) =$$

$$= \frac{1}{A_T} \left[\rho_1 \int_{A_1} u_1^2 dA + \rho_2 \int_{A_2} u_2^2 dA \right]_{out} - \frac{1}{A_T} \left[\rho_\ell \int_{A_T} u_{in}^2 dA \right] \qquad (2.4.14)$$

Inspection of equations (2.4.12) to (2.4.14) together with equations (2.4.3) or (2.4.4.) shows that for the components of total pressure drop the following integrals remain to be calculated :

$\int_0^{x_{out}} \alpha(x)dx$ where the void fraction is a function of mass dryness fraction.

$\int_0^{x_{out}} (\bar{u}_{lT})\, dx$ for the Laminar wallshear stress or,

$\int_0^{x_{out}} (\bar{u}_{lT})^{2n/(n+1)}\, dx$ for the Turbulent wall shear stress.

As seen from the sections 2-2.1 and 2-2.3 α and x can be expressed in terms of r_h/r_s and r_s/r_o. Similarly $\bar{u}_{lT}$ depends on the same geometric ratios as seen from equations (2.4.6) and (2.4.7); where $\bar{u}_l$, from its definition can be expressed (equation 2.3.1) as $\bar{u}_l = \dot{m}_l/\rho_l A_l$ with $\dot{m}_l$ and A_l, related to the mass dryness fraction and void fraction respectively.

It is obvious that the previous integrals, expressed in terms of r_h, r_s and r_o, are very complex and its analytical calculation practically impossible. Therefore, those integrals are calculated by the method of bisection until the evaluated numbers are bounded by a number close to the accuracy of the computer. Further details about the

numerical method are included as part of the appendix B, which describes the interactive computer package called VELPRO.

At this stage it must be emphasised that the analysis for the total pressure drop presented in this section, is not only applicable to uniform heat fluxes where the fluid properties are constant. Similar calculations could be made when the heat flow is non-uniform and the properties are allowed to vary significantly along the axis. But for those cases a finite difference solution scheme is necessary as described in chapter 4.

2-5 Comparison with Experiment

In its present simple form, the validity of the velocity profile model can be demonstrated by comparisons with experimental results for the void fraction, the ratio of average vapour and liquid velocities and pressure drops at various mass-dryness fraction. Six different experimental sources are used for comparisons, with a wide range of operating and flow conditions. A summary of those conditions can be found in table 2.4. In the predictions by the velocity profile method liquid is taken to flow next to the wall (L1V2) accept where otherwise stated. The predictions for void fractions from the velocity profile model are also compared with the theoretical correlations of S L Smith (Sm70) and J R S Thom (Th64) whenever that is possible.

In figures 2.3 and 2.4 the present model is compared with results for void fractions in horizontal and vertical unheated pipes reported by H C Larson (La57) and H Isbin (Is57). The observed void fractions were up to 0.85 for mass-dryness fractions in the region 0.01 to 0.7. For the void fraction measurements Isbin used a Selenium gamma source with a half-life of 127 days. With the attenuation method applied at different chordal positions across the flow area it is confirmed that the liquid

phase occupies the region next to the wall. Good agreement is obtained for both sets of experimental results although the profile method seems to over-predict the void fractions for 1.013 where the density ratio for the two phases has a high value. Of course this ratio is significantly changed by the theoretical model of S L Smith where density in the gas core is severely changed by the recommended 40% entrainment of liquid.

For the results of R A Egen et. al (Eg57) shown in figure 2.5 for vertical flows at high pressures in heated channels, the velocity profile gives better results than the model proposed by Smith. In the same graph the observed increase of void fraction with mass flux might be partially explained by increasing the value of the exponent n. This dependence is shown in figure 2.5 for mass fluxes 949 and 1220 Kg/m^2s, at 1261 KW/m^2 heating flux with values of 7 and 8 for n.

Haywood et. al. (Ha61), in 1961, presented a well-known series of experimental results covering a wide range of operating conditions in heated or unheated pipe flows. Measurements of void fractions taken by the gamma ray absorption method with Cs-137 at different scanning positions across the flow area, confirmed that liquid was flowing close to the wall. Predictions as shown by figure 2.6 are in good agreement with experiment, as well as with the other theoretical models. It is interesting to observe how the scattering effect in the actual measurements is minimised at high operating pressures where the liquid and vapour densities are more nearly equal.

In figure 2.7 are shown void fractions for boiling heavy water in a vertical tube measured by a (γ,n) reaction method which occurs when heavy water is irradiated by gamma rays. The method is described by Rouhani and Becker in reference (Ro63). Since it is not known which phase flowed next to the wall the predictions from the velocity profile model are plotted for both cases. It seems that for dryness fractions less than

0.02 the high values of void fraction might be partially explained by the velocity profile model when vapour is assumed in region 1. Even so it is not possible to take into account the deviations at 49 and 59 bar. A more general look through the experimental curves seems to show that it is unlikely that they are going to pass through the points (0,0) and (1,1) as thermodynamic equilibrium requires; that is probably the reason why the velocity profile method overpredicts the void fractions.

An alternative form of comparisons, for all the results presented in the previous figures, could be shown by plotting predicted void fractions against observed values for steam-water and heavy water mixtures. Figures 2.8 and 2.9 are the corresponding graphs for the two mixtures when the velocity profile method is used and figures 2.10 and 2.11 when similar predictions are made by the S L Smith model. As shown by figures 2.8 and 2.10, the velocity profile model in its present simple form agrees with most experimental results more or less to within the ± 10% lines especially at high operating pressures. For low pressures there is a tendency to give high predictions at high values of void fraction. This suggests that some form of entrainment should be assumed thus modifying the density of the phases in region 1 and 2 respectively. For given amounts of entrainment the effect on the densities assumed in each region will of course be greater at low operating pressures where the density difference between the actual phases is large. However, one should expect the amount of the phases entrained to be greater at high values of void fraction where the ratio of the vapour flow rate to that of the liquid is high. The same comments can be also made for the heavy water mixtures as is shown by figures 2.9 and 2.11.

In figure 2.12 the ratio of the average velocities of the vapour and liquid phases S, is plotted against mass dryness fraction at

various operating pressures together with results obtained by Haywood et. al. (Ha61) for a 1-in bore horizontal heated pipe. Such a ratio, often called slip ratio, when expressed in terms of either void fraction or mass dryness fraction constitutes an alternative way of expressing the relation between x and α. Proof of that can be found in section 2-3, but here it is interesting to see how sensitive S is in comparisons with experimental values. As seen from figure 2.12 there is a considerable scatter of experimental points especially for low operating pressures. In the same figure are drawn the lines of the predictions from the velocity profile method with various power law exponents. As seen from figure 2.12 at low operating pressures, exponents lower than 4 might provide better agreement for dryness fractions less than 0.1. Exactly the reverse behaviour is observed for 144.8 bar (2100 psia) where a power law exponent higher than 7 seems to be more appropriate. A more or less less similar impression about the dependence of S on the value of the power law exponent is obtained by inspection of figures 2.13 and 2.14. Here S is plotted against the ratio of volumetric flow rates of the vapour and liquid phases for the tests of Chisholm and Laird (Ch58). It is obvious that at high mass flow rates S is accurately predicted for power law exponents between n = 7 and n = 9 when the ratio of volumetric flow rates is below the value of 4. For the range of volumetric flow rates between 4 and 15 the experimental values lie between the lines for power law exponents 3 and 5, and for higher ratios of volumetric flow rates, power exponents between 2 and 3 should provide satisfactory comparisons with experimental results. No firm recommendations about the dependence of slip ratio on n and mass flow rate can be given in the absence of consistent experimental data over a wide range of operating conditions, including the relevant information on entrainment, which will also influence significantly the overall ratios of average velocities.

Comparisons between the experimentally determined pressure drops reported by R W Haywood et. al. (Ha61) and those predicted from the velocity profile model are shown in figures 2.15 to 2.19. The graphs correspond to heated and unheated pipes vertically or horizontally positioned; the pressure drops are normalised by dividing by $\rho_\ell \bar{u}_{in}^2$ where $\bar{u}_{in}$ is the average velocity at the inlet of the test section

$$(x = 0 \text{ and } \alpha = 0) \quad \text{i.e. :} \quad \Delta p_N \equiv \Delta p / (\rho_\ell \bar{u}_{in}^2)$$

Figures 2.15 and 2.16 for vertical flows are complicated by the existence of the gravitational component in pressure drop, nevertheless it is possible to see that the agreement obtained is generally good. Even better agreement is shown in figures 2.17 and 2.19 for horizontal flows. In these graphs for pressure drops, the intercepts on the vertical axes indicate the normalised pressure drops for uniform density liquid flow throughout the test section. An alternative form of comparison is shown in figure 2.20 where the experimental values from figures 2.15 to 2.19 are plotted against the predicted values. Nearly all the points lie within the ± 15% lines.

2-6 Parametric Effects on the Predictions by the Velocity Profile Method

The most obvious feature of the two-dimensional velocity profile model is that it provides a method which directly relates the void fraction and pressure drops to the mass dryness fraction, while exhibiting a greater degree of flexibility than other existing models. The purpose of the parametric studies in this section is to show how the predictions from the model are influenced by the geometric and kinematic parameters introduced during its development.

It has already been seen in sections 2-2 and 2-3 that the void fraction (α), and the ratio of the average velocities of the vapour and

liquid phases (S) can be expressed by relations of the following form :

$$\begin{bmatrix} \alpha \\ S \end{bmatrix} = \text{Function}\left(x, \begin{bmatrix} R_D \\ R_V \end{bmatrix}, n(\dot{m}_T), \begin{bmatrix} \text{Laminar} \\ \text{Turbulent} \end{bmatrix}, \begin{bmatrix} \text{L1V2} \\ \text{V1L2} \end{bmatrix} \right) \quad (2.6.1)$$

where R_D and R_V are the density and viscosity ratios, and obviously depend on the operating pressure. In the following figures "α" and "S" are plotted against the mass dryness fractions for a number of possible combinations of the independent variables in equation (2.6.1). With the usual notations L1V2 and V1L2 we are referring respectively to the case of liquid flowing in region 1 and vapour in region 2, and vice versa for the case V1L2.

At constant operating pressure of 50 bar, figure 2.21 shows how the predictions for laminar and turbulent flows compare for the cases of L1V2 and V1L2. It is easily observed that for L1V2 the void fractions when $x \to 1$ in laminar flows may be as much as 50% lower than for turbulent flows. The reverse is true for V1L2 but this time as x asympotically approaches zero. Also in figure 2.21 is shown the dependence of the void fractions predicted by different power exponents n. An increase of the power law exponent from the value of 7 to 9 increases the void fractions predicted for L1V2, whether for the case of V1L2 such an increase gives slightly lower void fractions.

In figures 2.22 and 2.23 the predicted void fractions are shown for laminar and turbulent flows at various operating pressures when liquid flows next to the wall. Lines of constant slope are observed for low operating pressures when the flow is laminar and for the very high pressures in turbulent flows.

The void fractions predicted for various operating pressures are drawn in figure 2.24 with the power law exponent taken as 7 for the cases L1V2 and V1L2. Variations of pressure seem to affect the predicted void fraction equally, whichever phase flows in region 1.

Similar diagrams are produced for the ratio of the average velocities of the vapour and liquid phases, S. In figure 2.25, as for figure 2.21, it is shown for the cases L1V2 and V1L2, how S varies with mass dryness fraction in laminar and turbulent flows. The lines for the case L1V2 seem to asympotically approach infinity when x = 1 both for laminar and turbulent flow conditions. A rather unexpected behaviour is observed for the ratio S in the V1L2 case, where the various lines seem to approach constant values at the intercepts with the vertical axis at x = 1. This is because for all vapour flows, region 2 is reduced to the centre line with $r_s = 0$. So the average liquid velocity corresponds to the maximum velocity of a single phase velocity profile. Therefore the ratio S becomes the ratio of average over maximum velocity which of course has a constant value. In a similar way for the case L1V2, S approaches infinity for x = 1 because now the average velocity in region 1 is zero.

In figure 2.26 the effects of different operating pressures are shown when L1V2. With increasing pressures at the same dryness fraction lower values of S are observed. Figure 2.27 shows a similar effect but for the cases L1V2 and V1L2. For V1L2 the pressure effects seem to diminish as x approaches 1.

The boundary conditions that correspond to the intercepts with the vertical axes at x = 0, x = 1 in the previous graphs are summarised in the tables 2.5 and 2.6. Thus it is proved that physical reality is represented even in those extremes such as x = 0 and x = 1 both for L1V2 and V1L2. Therefore in its present simple form, the velocity profile method with the continuity of velocity and shear stress at the surface of separation seem to show a significant advance on most existing one dimensional models.

Chapter 3.

The Effects of Entrainment in Annular Types of Flow.

Contents :

CHAPTER 3

THE EFFECTS OF ENTRAINMENT IN ANNULAR TYPES OF FLOW

3-1 Introduction

In the development of the velocity profile model for annular two-phase flow in the previous chapter, the two phases were regarded as flowing separately with a smooth interface between them. But in reality the situation is more complex, and this interface is influenced by several hydrodynamic mechanisms that contribute significantly to the mass, energy and momentum transfer across it. Those mechanisms produce a very wavy interface with significant entrainment of liquid and vapour. In reality the entrainment mechanisms are unstable processes which might reach some form of dynamic equilibrium with the deposition mechanisms, but only after considerable flow lengths. This equilibrium is usually called hydrodynamic equilibrium, in which the amount of liquid entrainment is balanced by the droplet deposition, and similarly for the vapour bubbles.

Several mechanisms of liquid entrainment have been identified so far, described in the literature by Hewitt et. al. (He70) and M Ishii (Is82). The most important of those mechanisms are shown schematically in figure 3.1. But for annular types of flow with a liquid film, there is also the possibility that vapour bubbles are present in the liquid region, because of nucleation of dissolved vapour at the solid-liquid interface, and the occlusion of vapour bubbles in the liquid region as a direct result of surface wave action.

In general the two-phases must be treated as entrained into each other and not in hydrodynamic equilibrium, for the realistic

representation of the actual physical conditions in evaporation flows. In this chapter, attention is concentrated on the improvement of the velocity profile model so that it incorporates the entrainment of liquid and vapour. Thus, the range of application of the proposed equations is extended to include implicitly the effects of the presence at a wavy interface, between the two flow regions.

The equations are first formulated so as to allow entrainment, by arbitrarily introducing a fraction of the phase entrained into the other region. For the equations proposed here, this fraction is taken to vary with position along the flow axis for given liquid and vapour mass flow rates, geometry and physical properties. Where inadequate information is available about the entrainment fraction , it is treated as constant in the calculations of the present chapter.

3-2 The velocity profile model with entrained liquid and vapour

As for the simple velocity profile model given in section 2-2, we assume again similar velocity profiles applicable within each of the two regions of the flow passage shown in figure 3.2. Each region is assumed to be occupied mainly by either the liquid or vapour phase, with some of the other phase uniformly mixed in with it. This mixing is taken to be sufficiently intimate to allow the velocity to be assigned a single value at each point.

As before, the shape of the velocity profile will depend on whether the heavier mixture is flowing in the annular region next to the wall (1), or the central circular region (2); the two cases are shown in figure 3.2 (a) and (b). The expressions used for the two parts of the velocity profile, are the parabolic type of equations (equations 2.2.1) and (2.2.2) for laminar flow or the 1/nth power law type of equations (equations 2.2.16) and 2.2.17) shown in section 2-2, for turbulent flow.

We make the usual assumption of local thermodynamic equilibrium between the vapour and liquid phases at any cross-section of the pipe, so that the familiar concept of dryness fraction, x, can be used to relate the total mass flow rates of vapour and liquid, $\dot{m}_g$ and $\dot{m}_\ell$:

$$x = \frac{\dot{m}_g}{\dot{m}_g + \dot{m}_\ell} \qquad (3.2.1)$$

In a similar way, mass dryness fractions can be defined for each region of the flow as follows :

$$x_1 = \frac{\dot{m}_{g1}}{\dot{m}_{g1} + \dot{m}_{\ell 1}} \quad \text{and} \quad x_2 = \frac{\dot{m}_{g2}}{\dot{m}_{g2} + \dot{m}_{\ell 2}} \qquad (3.2.2)$$

Where $\dot{m}_{g1}$, $\dot{m}_{g2}$ are the vapour mass flow rates for region 1 and region 2 and $\dot{m}_{\ell 1}$, $\dot{m}_{\ell 2}$ are the corresponding values for the liquid phase. The flow rates, for uniform mixtures in each region, are defined in the usual way as :

$$\dot{m}_{g1} = \rho_g \bar{u}_1 A_{g1} \quad \text{and} \quad \dot{m}_{g2} = \rho_g \bar{u}_2 A_{g2} \qquad (3.2.3)$$

$$\dot{m}_{\ell 1} = \rho_\ell \bar{u}_1 A_{\ell 1} \quad \text{and} \quad \dot{m}_{\ell 2} = \rho_\ell \bar{u}_2 A_{\ell 2} \qquad (3.2.4)$$

Where A_{g1} and A_{g2} are the vapour flow areas in region 1 and 2 respectively; $A_{\ell 1}$ and $A_{\ell 2}$ are similar areas for the liquid phase. Then the mean density of each of the mixtures is easily expressed in terms of the relevant dryness fraction :

$$\frac{1}{\bar{\rho}_1} = \frac{x_1}{\rho_g} + \frac{1 - x_1}{\rho_\ell} \quad , \quad \frac{1}{\bar{\rho}_2} = \frac{x_2}{\rho_g} + \frac{1 - x_2}{\rho_\ell} \qquad (3.2.5)$$

and the mass flow rates in the two regions are

$$\dot{m}_1 = \dot{m}_{g1} + \dot{m}_{\ell 1} = \bar{\rho}_1 \int_{A_1} u_1 dA \qquad (3.2.6)$$

$$\dot{m}_2 = \dot{m}_{g2} + \dot{m}_{\ell 2} = \bar{\rho}_2 \int_{A_2} u_2 dA \qquad (3.2.7)$$

Where $A_1 = A_{g1} + A_{\ell 1}$ and $A_2 = A_{g2} + A_{\ell 2}$ are the flow areas for region 1 and 2 respectively.

We may also define local void fractions, in the usual way :

$$\alpha_1 = \frac{A_{g1}}{A_{g1} + A_{\ell 1}} \quad , \qquad \alpha_2 = \frac{A_{g2}}{A_{g2} + A_{\ell 2}} \tag{3.2.8}$$

But the main difficulty in defining the properties for each region, arises from ignorance about the effective viscosities for such mixtures. A relatively simple correlation (Co72) which is frequently used in the analysis of homogeneous types of two phase flow, is :

$$\frac{1}{\bar{\mu}_1} = \frac{x_1}{\mu_g} + \frac{1 - x_1}{\mu_\ell} \quad , \qquad \frac{1}{\bar{\mu}_2} = \frac{x_2}{\mu_g} + \frac{1 - x_2}{\mu_\ell} \tag{3.2.9}$$

So far, the physical laws describing mass-transfer at the surface of separation are not sufficiently developed to provide a basis for direct incorporation into the present model. We can, nevertheless, introduce the idea of entrainment into the model by introducing an "entrainment ratio". Since entrainment occurs in both directions as described in the literature (He70), there will in general, be two entrainment ratios in each of the two flow cases shown in figure 3.2. For the case in which liquid predominates in region 1 (next to the wall),

$$e_1 \equiv \frac{\dot{m}_{\ell 2}}{\dot{m}_\ell} = \frac{(1 - x_2)\,\dot{m}_2}{(1 - x)\,\dot{m}_T} \tag{3.2.10}$$

$$e_2 \equiv \frac{\dot{m}_{g1}}{\dot{m}_g} = \frac{x_1\,\dot{m}_1}{x\,\dot{m}_T} \tag{3.2.11}$$

Entrainment ratio is thus defined as the portion of the total flow rate of a phase which flows in the region in which that phase is not the predominant one.

Following the definition of the entrainment ratios we may express the regional void fractions in terms of the phase densities, overall

mass-dryness fraction and entrainment ratios. From equations (3.2.3) and (3.2.4)

$$\frac{A_{g1}}{A_{\ell 1}} = \left(\frac{\rho_\ell}{\rho_g}\right)\left(\frac{\dot{m}_{g1}}{\dot{m}_{\ell 1}}\right) \qquad (3.2.12)\ , \qquad \frac{A_{g2}}{A_{\ell 2}} = \left(\frac{\rho_\ell}{\rho_g}\right)\left(\frac{\dot{m}_{g2}}{\dot{m}_{\ell 2}}\right) \qquad (3.2.13)$$

from where, by using equations (3.2.10) and (3.2.11), it follows that :

$$\frac{A_{g1}}{A_{\ell 1}} = \left(\frac{\rho_\ell}{\rho_g}\right)\left(\frac{e_2}{1 - e_1}\right)\left(\frac{x}{1 - x}\right) \qquad (3.2.14)$$

$$\frac{A_{g2}}{A_{\ell 2}} = \left(\frac{\rho_\ell}{\rho_g}\right)\left(\frac{1 - e_2}{e_1}\right)\left(\frac{x}{1 - x}\right) \qquad (3.2.15)$$

Substitution of equations (3.2.14), (3.2.15) into the definitions of the void fraction for each region (equation 3.2.8) yields the expressions

$$\frac{\alpha_1}{1 - \alpha_1} = \left(\frac{\rho_\ell}{\rho_g}\right)\left(\frac{e_2}{1 - e_1}\right)\left(\frac{x}{1 - x}\right) \qquad (3.2.16)$$

$$\frac{\alpha_2}{1 - \alpha_2} = \left(\frac{\rho_\ell}{\rho_g}\right)\left(\frac{1 - e_2}{e_1}\right)\left(\frac{x}{1 - x}\right) \qquad (3.2.17)$$

Equations similar to (3.2.10) to (3.2.17) can be set up for the case when vapour is the predominant phase next to the wall. Such expressions are shown in table 3.1 for comparisons of the two possible combinations.

3-2.1 <u>The void fraction, mass-dryness fraction relationship</u>

The two parts of the velocity profile shown in figure 3.2 are matched by ensuring continuity of velocity and shear stress at the interface, r_s, in exactly the same way as shown in sections 2-2.1 and 2-2.2. For the turbulent case we still use the Prandtl's mixing length hypothesis at the interface, with equal mixing- lengths for the two mixtures. Consequently, the corresponding relations of the geometric parameters are :

$$\left(r_h / r_s\right)^2 = 1 + \bar{R}_v^2 \left(r_o^2 / r_s^2 - 1\right) \qquad \text{[Laminar]} \qquad (3.2.18)$$

$$(r_h / r_s) = 1 + \bar{R}_D (r_o / r_s - 1) \qquad \text{[Turbulent]} \qquad (3.2.19)$$

where $\bar{R}_V = (\bar{\mu}_2 / \bar{\mu}_1)^{1/2}$ and $\bar{R}_D = (\bar{\rho}_2 / \bar{\rho}_1)^{1/2}$ (3.2.20)

The shape of the velocity profile established by the last equations, can be related to the mass flow rates of the two phases and the entrainment ratios; the result is :

$$\frac{\dot{m}_2}{\dot{m}_1} = \bar{R}_D^{\,2} \left[\frac{r_s^2}{r_o^2 - r_s^2} \right] \left[\frac{2r_h^2 - r_s^2}{r_h^2 - r_s^2} \right] \qquad \text{[Laminar]} \qquad (3.2.21)$$

$$\frac{\dot{m}_2}{\dot{m}_1} = \bar{R}_D^{\,3} \left[\frac{r_h \left(\frac{r_h}{r_h - r_s} \right)^{\frac{n+1}{n}} - r_h - \left(\frac{n+1}{n} \right) r_s}{\left(\frac{n+1}{n} \right) r_s + r_o} \right] \qquad \text{[Turbulent]}$$

These are the same equations as for the simple model (2-2), but here the ratio of total mass flow rates in region 1 and 2 is not only a function of dryness fraction but also depends on the entrainment ratios. By using equations (3.2.6, 3.2.7) and (3.2.10, 3.2.11) for liquid dominating region 1 the LHS of equations (3.2.21) can be expressed as :

$$\frac{\dot{m}_2}{\dot{m}_1} = \frac{(1 - e_2) \dot{m}_g + e_1 \dot{m}_\ell}{(1 - e_1) \dot{m}_\ell + e_2 \dot{m}_g} = \frac{(1 - e_2) x + e_1 (1 - x)}{(1 - e_1) (1 - x) + e_2 x} \qquad (3.2.22)$$

For the overall void fraction (α) and mass dryness fraction (x) relationship, the expression of void fraction in terms of the geometric parameters remains to be established. This is easily obtained from the ratio of total area occupied by vapour and liquid. From the definitions of the void fractions in region 1 and 2.

$$\frac{\alpha}{1 - \alpha} = \frac{A_{g1} + A_{g2}}{A_{\ell 1} + A_{\ell 2}} = \frac{\left(\frac{\alpha_1}{1-\alpha_1} \right) + \left(\frac{\alpha_2}{1-\alpha_2} \right) \frac{A_{\ell 2}}{A_{\ell 1}}}{1 + \left(\frac{A_{\ell 2}}{A_{\ell 1}} \right)} \qquad (3.2.23)$$

where the ratio $A_{\ell 2}/A_{\ell 1}$ is obtained from the ratio of the flow areas in region 2 and region 1 i.e. :

$$\frac{A_{g2} + A_{\ell 2}}{A_{g1} + A_{\ell 1}} = \frac{r_s^2}{r_o^2 - r_s^2} \quad \text{or} \quad \frac{A_{\ell 2}}{A_{\ell 1}} = \left(\frac{r_s^2}{r_o^2 - r_s^2}\right)\left(\frac{1 - \alpha_2}{1 - \alpha_1}\right) \tag{3.2.24}$$

When equation (3.2.24) is substituted in equation (3.2.23) the relationship between the void fraction and the geometric parameters is given by :

$$\frac{\alpha}{1 - \alpha} = \left[\frac{\alpha_1 + \alpha_2 \left(\frac{r_s^2}{r_o^2 - r_s^2}\right)}{(1 - \alpha_1) + (1 - \alpha_2)\left(\frac{r_s^2}{r_o^2 - r_s^2}\right)}\right] . \tag{3.2.25}$$

Where of course, α_1 and α_2 can be expressed in terms of the dryness fraction, x and the entrainment ratios, as shown by equations (3.2.16) and 3.2.17).

Equations (3.2.25) and (3.2.21) together with equations (3.2.22) and (3.2.18/19) implicitly define the relationship between x and α, which has a single solution for all values for x and α between 0 and 1. This solution can only be found numerically when the local entrainment ratios has been expressed in terms of either the void fraction (α) or the mass-dryness fraction (x). All calculations presented in this chapter were carried out by the computer program VELPRO after the entrainment option had been switched on as described in appendix B.

In its present form the velocity profile model possesses greater flexibility than its original state described in chapter 2. In addition to the dependence of the power law exponent on the Reynolds number, the results now depend on the local entrainment ratios. It should be emphasised that by varying the local entrainment ratios we are able to

simulate any operating conditions between the two extreme cases of homogeneous and completely separated types of two-phase flows.

3-2.2 The pressure gradient

Following the same method as for the earlier version of the velocity profile model, described in section 2-4, the force-momentum relation applied to steady pipe flow yields the result

$$-\frac{dp}{ds} - \frac{Z}{A_T}\tau_w - [\,\alpha\rho_g + (1-\alpha)\rho_\ell\,]\,g\sin\Theta = \frac{1}{A_T}\frac{d\dot{M}}{ds} \qquad (3.2.26)$$

The main difference in the last equation being that for the wall shear stress and the change of momentum we must take into account the vapour and liquid entrainment. As frequently described in the literature (He70, Is82), such phenomena depend among other things at the condition of the interface, the thickness of region 1 in figure 3.2, the local heat flux, the local liquid and vapour velocities, and on whether the mixture has reached hydrodynamic equilibrium. Therefore the entrainment ratios that will be used for the pressure gradients in equation (3.2.26) must be treated as strongly varying properties at least in the direction of flow.

In a similar way as for equations (2.2.3) and (2.2.4), for the simple model, the wall shear stress, τ_w, is calculated from the velocity profile of a hypothetical homogeneous fluid flow, in which the whole pipe is filled with the mixture occupying region 1. For this hypothetical flow the distribution of the velocity u_1 is extended to the pipe axis. The calculation uses the standard parabolic and power law profiles and gives

$$\tau_w = \frac{16}{4}\left[\frac{\bar{\rho}_1\bar{u}_{1T}\,r_o}{\bar{\mu}_1}\right]^{-1} \qquad (\bar{\rho}_1\bar{u}_{1T}^{\,2}) \qquad \text{[Laminar]} \quad (3.2.27)$$

$$\tau_w = \left[c \frac{\bar{u}_{1T}}{u_{max,1}} \right]^{-\frac{2n}{n+1}} \left[\frac{\bar{\rho}_1 \bar{u}_{1T} r_o}{\bar{\mu}_1} \right]^{-\frac{2}{n+1}} (\bar{\rho}_1 \bar{u}_{1T}^2) \quad (3.2.28)$$

[Turbulent]

where $\bar{\rho}_1$ and $\bar{\mu}_1$ are given by equations (3.2.5) and (3.2.9) and obviously depend on the entrainment ratios. The parameter c is again a numerical factor with the value 8.74 when n = 7. For the previous two equations $\bar{u}_{1T}$ represents the average velocity of the assumed hypothetical flow when the profile of u_1 has been extended to the pipe axis. The hypothetical average velocity $\bar{u}_{1T}$ is significantly different from $\bar{u}_1$ which corresponds to the average velocity in region 1 only. The ratio of those two average velocities is expressed again in terms of r_h and r_s by equations (2.4.6) and (2.4.7). The main difference now, when entrainment is allowed, arises in the definition of $\bar{u}_1$ which is given by

$$\bar{u}_1 = \frac{\dot{m}_1}{\bar{\rho}_1 A_1} = \frac{\dot{m}_{g1} + \dot{m}_{\ell 1}}{\bar{\rho}_1 (A_{g1} + A_{\ell 1})} \quad (3.2.29)$$

where $\dot{m}_1$ and $\bar{\rho}_1$ depend on the entrainment ratios e_1 , e_2 ; also A_1 is equal to $\pi(r_o^2 - r_s^2)$. For the case of liquid being the predominant phase in region (1) then

$$\dot{m}_1 = (1 - e_1) (1 - x) \dot{m}_T + e_2 x \dot{m}_T \quad (3.2.30)$$

similarly

$$\dot{m}_1 = (1 - e_1) x \dot{m}_T + e_2 (1 - x) \dot{m}_T \quad (3.2.31)$$

when vapour dominates the same region.

The last term in equation (3.2.26), which represents the acceleration pressure gradient, is easily obtained by standard

integration over the two parts of the combined velocity profile shown in figure 3.2. :

$$\frac{1}{A_T}\frac{d\dot{M}}{ds} = \frac{1}{A_T}\frac{d}{ds}\left[\bar{\rho}_1 \int_{A_1} u_1^2 dA + \bar{\rho}_2 \int_{A_2} u_2^2\, dA\right] \qquad (3.2.32)$$

where A_1 and A_2 are as defined in section 3-2.

3-2.3 Calculation of the total pressure drop

For steady-state flow in a constant-cross-section duct where x is taken to vary linearly in the axial direction, then the total pressure drop over the length L_B , measured from the inlet of the test section where the liquid is just saturated, is given by

$$\Delta p = \Delta p_{fr} + \Delta p_{gr} + \Delta p_{ac} \qquad (3.2.33)$$

where :

$$\Delta p_{fr} = \frac{Z}{A_T}\left(\frac{L_B}{x_{out}}\right)\int_0^{x_{out}} \tau_w\, dx \qquad (3.2.34)$$

$$\Delta p_{gr} = \rho_\ell g \sin\Theta \left[L_B + \frac{\rho_g - \rho_\ell}{\rho_\ell}\left(\frac{L_B}{x_{out}}\right)\int_0^{x_{out}} \alpha\, dx\right] \qquad (3.2.35)$$

$$\Delta p_{ac} = \frac{1}{A_T}\left(\dot{M}_{out} - \dot{M}_{in}\right) =$$

$$= \frac{1}{A_T}\left[\bar{\rho}_1 \int_{A_1} u_1^2 dA + \bar{\rho}_2 \int_{A_2} u_2^2 dA\right]_{out} - \frac{1}{A_T}\left[\rho_\ell \int_{A_T} u_{in}^2 dA\right] \qquad (3.2.36)$$

The last equations are derived for negligible change of physical properties along the flow axis. This assumption is used in the present section in order to simplify the equations and is eliminated in the more general use of equations described in chapter 4.

It is easily understood from equations (3.2.34) to (3.2.36) together with equations (3.2.27) and (3.2.28) that, when the two phases are entrained into each other the following integrals must be calculated numerically :

$$\int_0^{x_{out}} \alpha(x,e_1,e_2)\, dx$$ where e_1 and e_2 also depend on the local mass-dryness fraction

$$\int_0^{x_{out}} \bar{\mu}_1\, \bar{u}_{1T}\, dx$$ for the wall shear stress in Laminar flows.

$$\int_0^{x_{out}} (\bar{\rho}_1)^{\frac{n-1}{n+1}} (\bar{\mu}_1)^{\frac{2}{n+1}} (\bar{u}_{1T})^{\frac{2n}{n+1}}$$ for the wall shear stress in Turbulent flows.

The programme VELPRO calculates those integrals by the method of bisection up to a specified accuracy. Of course the entrainment ratios has been treated as local properties so e_1 and e_2 are found for every value of x by cubic spline interporation to a specified table of entrainment ratios. This table of entrainment ratios, at various mass dryness fractions, must be supplied as part of the input data.

Application of the proposed model in its present form requires, a table of known entrainment ratios, a statement about which phase is the predominant one in each of the flow regions and a suitable value of the power law exponent. In the absence of such information, comparison with experimental results will seem to be rather tentative.

3-3 Experimental Comparisons

In the comparisons which follow, calculations are made with the modified version of the velocity profile model for different amounts of liquid and vapour entrainment. Whenever the experimental entrainment

ratios are not given, arbitrary values are used, with no attempt to optimise the agreement by varying the chosen ratios. The purpose of such comparisons is mainly an attempt to demonstrate the importance of entrainment phenomena under operating, flow or geometry parameters summarised in table 3.2.

As shown by table 3.2, the comparison with experiment are carried out for vertical and horizontal, diabatic and adiabatic types of two-phase flow, in pipes or in an annulus. The corresponding figure numbers are also included in table 3.2 for ease of reference to the graphs where the comparison are made.

Throughout the comparisons presented it has been assumed that the liquid phase is predominantly next to wall in region 1. The exponent for the power law has been taken as 7 except where otherwise stated. For the pressure drop graphs, the actual pressure has been normalised against $\rho_\ell \bar{u}_\ell^2$ for all-liquid flow at the same total mass flow rate.

The first comparisons presented here are with the experimental results of Anderson and Mantzouranis (An60) who measured void fraction for wide ranges of flow rate and mass-dryness fraction for adiabatic air-water flow at atmospheric pressures. Their measurements also included values of the flow rate of entrained liquid in the central core flow; the way in which this varied is shown in figure 3.3, where values of the entrainment ratio, e_1 , (as defined by equation 3.2.10) are plotted against mass-dryness fraction for various mass flow rates of the liquid phase.

The corresponding calculations for the velocity-profile model have been carried out in several ways.

(a) Without any allowance for entrainment, using both laminar and turbulent versions of the model, with values of 2 and 7 for the velocity exponent n in the latter case. The calculated values

of void fraction are drawn as single curves against mass-dryness fraction in figure 3.4

(b) Also shown in figure 3.4 are two sets of curves obtained from calculations with the laminar and turbulent models, and using the appropriate values of entrainment ratio as shown in figure 3.3.

The very small values of Reynolds number that correspond to the mass flow rates used in this particular set of experiments, is an indication that the actual flow might have been laminar. However, under laminar conditions, it is difficult to explain the measured values of the entrainment ratio, e_1. The fact that the flow was not laminar, is also confirmed in figure 3.4 by comparing the void fractions predicted by the laminar velocity profile and the actual measurements. As shown in the same figure, better agreement is achieved for turbulent velocity profiles with n = 2, which is a reasonable value due to the small Reynolds numbers. This agreement could become even better when we use the entrainment ratios drawn in figure 3.3.

The upper two lines in figure 3.4 show the void fractions predicted by the velocity profile model with n = 7, and by the correlation proposed by S L Smith (Sm). It might be useful to mention again that this last correlation is derived for 40% entrainment of the liquid phase in the gas core, nevertheless it seems to overpredict the actual voids, especially at low dryness fractions.

Comparisons for a different set of flow conditions are shown in figures 3.5 and 3.6. Here pressure drops are plotted against mass-dryness fraction for four different operating pressures, in vertical and horizontal pipe flows. In this comparison some of the vapour phase is entrained by the liquid. Entrainment in this direction has a greater influence on the calculated values of the wall shear stress, and

therefore on the calculated pressure gradient. As shown in the previous chapter for similar tests (Ha61) the obtained is excellent over a wide range of experimental values even without introducing entrainment. However, inspection of figures 3.5 suggests that this agreement could be improved by increasing the gas entrainment ratio for low values of dryness fraction, where the line for homogeneous flow ($e_g = 1.0$) gives the best fit.

Figure 3.6 shows comparison with the Haywood (Ha61) results for flows in unheated vertical tubes at three different inlet velocities for the same range of operating pressures as for horizontal flows. Similarly for these operating conditions the flow can be adequately modelled by assuming complete separation of the two phases, without any entrainment. Here the difference between the homogeneous ($e_g = 1.0$, $e_\ell = 0.0$) and the separated type of predictions is more distinct mainly at low inlet velocities. In both figures 3.5 and 3.6 is clearly shown the decreasing contribution of entrainment on the predicted pressure drop as pressure increases and the density difference between the two phases decreases. This is also confirmed by figure 3.7 where the same predicted and observed pressure drops are plotted in a different way for the four operating pressures. Results are contained within the 10% lines both for the case of constant vapour entrainment and the case of complete separation between the two phases.

The effects of vapour entrainment on the pressure predictions at three different pipe diameters are investigated in figures 3.8, 3.9 and 3.10 for various mass flow rates. Those figures correspond to the same range of mass fluxes at approximately equal operating pressures of 70 bar. In each of those graphs are drawn the lines predicted by the velocity profile model for gas entrainment ratios of 0.0, 0.5 and 10; the latter value represents the case in which all the vapour is entrained, so

that the whole tube is filled with a homogeneous mixture, and the first value when the phases are not intermixed. It is obvious from the mentioned plots that the experimental points are coming closer to the lines for a single homogeneous mixture as the mass-flow rate increases. From a detailed observation of figures 3.8(α), 3.9(α) and 3.10(α), it is suggested that higher entrainment ratios are necessary for the predictions by the present model to agree with measurements in the larger diameter tubes, in similar mass fluxes. The same suggestion can be made from figures 3.9 (d), 3.10(e) and 3.9(f), 3.10(f). However this is only a tendency and needs to be investigated further from a more consistent set of experimental results.

The influence of another geometrical parameter on the predictions is examined in figures 3.11 and 3.12. In those graphs, pressure drops are plotted for two different lengths of 0.53 and 0.91 meters for a test section without heat input and for a variety of mass fluxes. Inspection of figures 3.11(a) and 3.12(a), for the same mass fluxes, indicates that the scatter of the experimental observations are at approximately similar distances from the drawn lines of the theoretical predictions. This is also true from the comparison of figures 3.11(c), 3.12(b), as well as figures 3.11(e), 3.12(e) and figures 3.11(f), 3.12(f). The conclusion that is drawn from such comparisons, is that good agreement between theory and experiment is obtained with the same values of gas entrainment ratio, irrespective of the length of the test pipe in adiabatic flows. This is an indication that for the lengths shown in figure 3.11 and 3.12 the entrainment and deposition mechanisms have already reached the hydrodynamic equilibrium, as defined in section 3-1.

By the final set of comparisons, described in table 3.2, the application of the velocity profile model is investigated in non-circular flow areas. For the predictions in such geometries, the familiar concept

of the equivalent hydraulic diameter has been used in the usual way. In figure 3.13 are drawn the observed pressure drops at various mass-flow rates in a vertically positioned annulus without heat flux. Again for low mass fluxes the obtained pressures are predicted better by the lines corresponding to the separated type of flow. For increasing mass-flow rates the entrainment ratios required for the best agreement with experimental observations must be slightly increased. However, above 2000 kg/m^2-s the measured pressure drops lie between the theoretical lines for the separated and homogeneous flow which are predicted by the velocity profile model. Pressure drops for low dryness fraction are generally closer to the lines of zero entrainment, whereas for higher dryness fractions the homogeneous flow predictions are in closer agreement. As shown by figure 3.31(d to h) there is a transition region for the experimental pressure drops around mass-dryness fraction of about 0.2, which possibly corresponds to the region where a change of the flow pattern might take place.

However it must be emphasised that the application of the proposed model in non-axisymmetric types of flows, where the 1/nth power law velocity profile is not valid, is highly questionable. On the other hand the profile model, as it stands, is capable of demonstrating the importance of entrainment phenomena and the change of flow pattern in a better way than any of the existing theories compared by M Muscettola in (Mu63).

3-4 Concluding Remarks

As shown by the experimental comparisons of the previous section the contribution of entrainment is of significant nature in annular types of flow, especially at high mass flow rates where the interface between the two flow regions is strongly disturbed by momentum and mass transfer. It

is inevitable that any purely empirical correlation for the entrainment ratios will be of a limited range of application due to the complexity of the interface phenomena. This is clearly shown by figure 3.14, where predicted pressure drops are plotted against the observed values for a selected number of mass fluxes taken form figures 3.10 and 3.11.

Neither the predictions shown in the upper graph of figure 3.14, for the homogeneous - mixture model (gas entrainment ratio = 1), nor for the entrained type of flow (with $e_g = 0.5$) of the lower graph, gives satisfactory agreement with the experimental results. Especially for the homogeneous case in the lower mass fluxes, the difference between predicted and observed values can be as poor as fifty per cent. However, when a certain amount of vapour is entrained into the liquid phase, the pressure drops can be more or less evenly contained between the fifteen per cent confidence lines.

It must be appreciated that even with the added feature of inter-phase entrainment, the velocity profile model remains a highly-idealised representation of two-phase flow phenomena. Nevertheless, the liquid and vapour entrainment as treated by the equations of the present chapter has a general range of application. For this statement to be more realistic the local entrainment ratios must be calculated internally by an analytical model. This is a desirable improvement which is described in detail, in chapter 5, where the velocity profile model is used to produce results for complex physical situations, such as the burnout in uniformly and non-uniformly heated pipes.

Chapter 4.

Generalised Two-Phase Flow Concervation Equations.

Contents :

CHAPTER 4

GENERALISED TWO-PHASE FLOW CONSERVATION EQUATIONS

4-1 Introduction

For the more general application of the velocity profile model in two-phase flows under heat fluxes other than uniform, it is necessary to consider in detail the physical laws that describe the flow conditions. These laws are the well known conservation laws that guarantee the conservation of mass momentum and energy between two reference points in the flow channel. Often the conservation equations are derived first in a very general form that corresponds to the phenomenological basis of the flow and are simplified at the application stage by excluding the terms that have no significant influence in the particular type of flow being considered.

In recent years, there has been intense interest in developing detailed numerical schemes for the two-phase flow conservation equations expressed in three dimensional form, to describe the flow in complex geometries. But those schemes have the disadvantage that they treat the distribution of the two phases in a rather empirical way. The same is also true for the relative velocities and temperatures for the two phases, with the average values in each control volume calculated from empirical equations suitable for flows in one direction.

For the development of the present numerical study we wish to solve the conservation equations for the whole flow in one-dimensional form (i.e. axially), rather than the more complicated two-dimensional form. This is only achieved by defining the transverse velocity distribution and effectively the transverse distribution of temperature, density and

specific enthalpy in a way similar to that described in chapter 2 and 3. Thus with the present study we make full use of the assumed distribution of the phases in the flow area.

In the next sections, the equations are first introduced in the most general form, and are then reduced to a form suited to the present study. The numerical solution procedure is also explained and finally the numerical predictions are presented for pipe flows with heat fluxes similar to those found in some types of industrial and nuclear plants.

4-2 Basic Equations

The fundamental equations which govern the properties of a general compressible flow are the conservation equations of mass, momentum and specific enthalpy. These equations together with the equation of state, relating the local densities to pressure and enthalpy, will define the conditions at specified points or stations in any flow field.

Throughout the present work, the control volume used to describe the conservation equations is of the type shown in figure 4.1, and refers to the flow in the axial direction of two homogeneous mixtures of liquid and vapour. Those mixtures are assumed to occupy two separate flow regions with a smooth interface between them. The derived conservation equations for such separated types of flow are also applicable for homogeneous flows when both regions 1 and 2 are filled with the same mixture.

Therefore for the control volume, described in figure 4.1, the usual conservation of mass, momentum and energy expressed in a differential form gives :

$$\frac{\partial}{\partial t}\int_{A_T} \rho \, dA + \frac{\partial}{\partial s}\int_{A_T} \rho u \, dA = 0 \qquad (4.2.1)$$

$$\frac{\partial}{\partial t}\int_{A_T} \rho u \, dA + \frac{\partial}{\partial s}\int_{A_T} \rho u^2 \, dA = A_T \frac{\partial p}{\partial s} - g\sin\Theta \int_{A_T} \rho \, dA - Z\tau_w \quad (4.2.2)$$

$$\frac{\partial}{\partial t}\int_{A_T} \left[h - \frac{p}{\rho} + \frac{u^2}{2} + gs\sin\Theta \right] \rho \, dA + \quad (4.2.3)$$

$$+ \frac{\partial}{\partial s}\int_{A_T} \left[h + \frac{u^2}{2} + gs\sin\Theta \right] \rho u \, dA = \dot{q}''Z + \dot{q}'''_V A_T$$

where u varies with position across the flow area A_T ; of course A_T is equal to the sum of A_1 and A_2 which are the flow areas for region 1 and 2. The right hand side of equation (4.2.2) is the sum of the forces acting on the control volume, and the right hand side of equation (4.2.3) is the rate of creation of energy. In the usual way, τ_w represents the wall shear stress given by equations (3.2.27) or (3.2.28), Z is the wetted perimeter, $\dot{q}''$ is the heat flux through the channel walls and $\dot{q}'''_V$ is the internal thermal energy generation per unit volume.

It is desirable to reduce the equations (4.2.1), (4.2.2) and (4.2.3) for the whole flow area into one-dimensional form by taking the average of flow properties in the transverse direction, thus avoiding the solution of conservation equations in the more complicated two-dimensional form. To achieve this we must somehow define the transverse velocity distribution as well as the distributions of temperature, density, specific enthalpy and pressure. By using the velocity profile model we introduce the transverse distributions shown in figure 4.2, while retaining the advantage of velocity and shear stress continuity at the surface of separation between regions 1 and 2.

4-2.1 Assumptions and Simplifications

It is probably worth-while summarising briefly the assumptions and simplifications used in the conservation equations, before describing how the equations are to be solved. In general, the assumptions and simplifications can be classed as referring to the geometric, physical and kinematic parameters of the flow.

The following can be classed as geometric assumptions :

(G1) Axisymmetric flows.

(G2) Co-current flows.

(G3) Circular flow area.

(G4) Smooth interface between regions 1 and 2.

Under the assumption G3 it might be possible to include also flows in ducts of non-circular cross-section, when the principle of the equivalent hydraulic diameter is expected to be a reasonable approximation.

The physical conditions of the flow are described by the following :

(P1) Thermal equilibrium.

(P2) Liquid and Vapour entrainment.

(P3) Compressibility of the phases.

(P4) Homogeneous mixtures in region 1 and 2.

Entrainment of the two phases is usually described by empirical models and therefore has a limited range of application.

The third class of assumption refers to the local kinematic conditions. Thus :

(K1) Different velocity profiles in each region.

(K2) Continuity of velocity and shear stress at the interface.

Some of the stated conditions can be subject for further improvements, as described in chapter 6, together with other topics for future consideration.

4-2.2 Composite-averaged equations

One of the main complexities of the two-phase flow conservation equations is that many of their terms are different from single phase relations and contain the parameters x and α. It has been common practice to transform those equations to a form similar to single-phase flow, so that the solution proceeds according to the relatively easy calculation schemes for single-phase equations. Frequently, during this transformation process, the multi-dimensionality of the flow is lost because of the complexity of the operations, also because the derived relations usually contain implicit assumptions about the flow regime.

In the same way as for single-phase flows, the flow conservation equations can be expressed in a simpler form by making use of the term mass flux which is the mass flow rate per unit flow area. For flows in which the total flow area is divided into two, the average value of mass flux is defined by :

$$G \equiv \langle \rho u \rangle \equiv \frac{1}{A_T} \int_{A_T} \rho u \, dA = \frac{1}{A_T} \left[\bar{\rho}_1 \int_{A_1} u_1 \, dA + \bar{\rho}_2 \int_{A_2} u_2 \, dA \right] \qquad (4.2.4)$$

where the average densities are as defined by equation (3.3.5) for each flow region.

Further simplifications are necessary for the equations (4.2.2) and (4.2.3), in order to express in average form the integrals containing the velocity in higher order than one. There are various methods which could achieve this. One, for instance, can employ different average velocities for the mass, momentum and energy equations but that will in effect, introduce different mass fluxes into the conservation equations. To avoid this, it is thought to be better to use a different value of

average density for each of the conservation equations; these are defined as :

$$\rho_A \equiv \langle\rho\rangle = \frac{1}{A_T}\int_{A_T} \rho \, dA \tag{4.2.5}$$

$$\rho_F \equiv \frac{\langle\rho u\rangle}{\langle u\rangle} = \frac{\int_{A_T} \rho u \, dA}{\int_{A_T} u \, dA} \tag{4.2.6}$$

$$\rho_M \equiv \frac{\langle\rho u\rangle^2}{\langle\rho u^2\rangle} = \frac{\left[\int_{A_T} \rho u \, dA\right]^2}{A_T \int_{A_T} \rho u^2 dA} \tag{4.2.7}$$

$$\rho_E \equiv \left(\frac{\langle\rho u\rangle^3}{\langle\rho u^3\rangle}\right)^{1/2} = \left[\frac{\left(\int_{A_T} \rho u \, dA\right)^3}{A_T^2 \int_{A_T} \rho u^3 dA}\right]^{1/2} \tag{4.2.8}$$

Because of the way they are defined ρ_A, ρ_F , ρ_M and ρ_E are called area, flow, momentum and energy averaged densities. Further description of these densities are given in section 4-2.3.

The space-averaged conservation equations of mass, momentum and energy are obtained by substitution, in equations (4.2.1), (4.2.2) and (4.2.3) of the definitions of the average densities and of the mass flux.

Thus for channels with constant cross-sectional area the equations become :

$$\underline{\text{Mass}} \quad : \quad \frac{\partial \rho_A}{\partial t} + \frac{\partial G}{\partial s} = 0 \tag{4.2.9}$$

$$\underline{\text{Momentum}} \quad : \quad \frac{\partial G}{\partial t} + \frac{\partial}{\partial s}\left(\frac{G^2}{\rho_M}\right) = \frac{\partial p}{\partial s} - \frac{Z}{A_T}\tau_w - g\rho_A \sin\Theta \tag{4.2.10}$$

$$\underline{\text{Energy}} \quad : \quad \frac{1}{A_T}\frac{\partial}{\partial t}\left(\int_{A_T} \rho h \, dA\right) + \frac{1}{A_T}\frac{\partial}{\partial s}\left(\int_{A_T} h\rho u \, dA\right) = \dot{q}''\frac{Z}{A_T} + \dot{q}'''_V + \frac{\partial p}{\partial t} - \frac{1}{2}\frac{\partial}{\partial t}\left(\frac{G^2}{\rho_M}\right) - \frac{1}{2}\frac{\partial}{\partial s}\left(\frac{G^3}{\rho_E^2}\right) - gG\sin\Theta \tag{4.2.11}$$

Further simplification of the last equation can be achieved by expressing the integrals of enthalpy and enthalpy flux as :

$$\int_{A_T} \rho h \, dA = \int_{A_g} \rho_g h_g \, dA + \int_{A_\ell} \rho_\ell h_\ell \, dA = A_T[\alpha\rho_g h_g + (1-\alpha)\rho_\ell h_\ell] \tag{4.2.12}$$

$$\int_{A_T} \rho u h \, dA = \int_{A_g} \rho_g u_g h_g dA + \int_{A_\ell} \rho_\ell u_\ell h_\ell \, dA = \dot{m}_T[\, x h_g + (1-x)h_\ell \,] \tag{4.2.13}$$

The local mean value of specific enthalpy, h, for the flow are is :

$$h = x\, h_g + (1-x)\, h_\ell = h_\ell + x\, h_{g\ell} \tag{4.2.14}$$

and in order to express equation (4.2.12) in terms of h we have to define an additional flow-averaged density as :

$$\rho_H \equiv \frac{\alpha\, \rho_g h_g + (1-\alpha)\, \rho_\ell h_\ell}{x\, h_g + (1-x)\, h_\ell} \tag{4.2.15}$$

From equations (4.2.12), (4.2.13), (4.2.14) and (4.2.15) the conservation

equations are expressed in a differential form as :

$$\underline{\text{Mass}} \quad : \quad \frac{\partial \rho_A}{\partial t} + \frac{\partial G}{\partial s} = 0 \tag{4.2.16}$$

$$\underline{\text{Momentum}} \quad : \quad \frac{\partial G}{\partial t} + \frac{\partial}{\partial s}\left(\frac{G^2}{\rho_M}\right) = \frac{\partial p}{\partial s} - \frac{Z}{A_T}\tau_w - g\rho_A \sin\Theta \tag{4.2.17}$$

$$\underline{\text{Energy}} \quad : \quad \frac{\partial}{\partial t}\left(\rho_H h\right) + \frac{\partial}{\partial s}\left(Gh\right) = \dot{q}'' \frac{Z}{A_T} + \dot{q}'''_V + \frac{\partial p}{\partial t} - \frac{1}{2}\frac{\partial}{\partial t}\left(\frac{G^2}{\rho_M}\right) - \frac{1}{2}\frac{\partial}{\partial s}\left(\frac{G^3}{\rho_E^2}\right) - gG\sin\Theta \tag{4.2.18}$$

This set of conservation equations can be solved, when the average densities are expressed as functions of the local enthalpy, h, and pressure, p.

4-2.3 Auxiliary Information

For the velocity profile model, with the transverse distribution of properties shown in figure 4.2, it is possible to express the average densities defined in the last section as :

$$\rho_A = f_1 \bar{\rho}_1 + f_2 \bar{\rho}_2 \tag{4.2.19}$$

$$\frac{1}{\rho_F} = \frac{f_1}{\bar{\rho}_1} + \frac{f_2}{\bar{\rho}_2} \tag{4.2.20}$$

$$\frac{1}{\rho_M} = \frac{f_1}{\bar{\rho}_1} + \frac{f_2}{\bar{\rho}_2} \tag{4.2.21}$$

$$\frac{1}{\rho_E^2} = \frac{f_1}{\bar{\rho}_1^2} + \frac{f_2}{\bar{\rho}_2^2} \tag{4.2.22}$$

where f_1 and f_2 are functions of x,α, and the local entrainment ratios of the liquid and vapour phase, e_1 and e_2 . The corresponding terms for f_1

and f_2, in these equations, are calculated from the transverse distribution of the flow parameters as described in Appendix C and the analytical expressions obtained are shown in table 4.1.

At this stage it is worthwhile to examine typical values of the first three average densities, at different operating pressures and for two different exponents of the power law velocity profile. As shown by figures 4.3 and 4.4 the differences between the average densities are greater for small operating pressures, and also become smaller when vapour flows in the region next to the wall. Also an increase of the power law exponent seem to have no significant effect on the calculated densities. In figures 4.3 and 4.4 the curves for the energy-averaged density are omitted for clarity, because they are close to those for the momentum averaged density.

It is also considered helpful to examine to what extent the ratio $\overline{u^2}/\bar{u}^2$, for the power law velocity profiles of figure 4.2, differs from unity, which is usually assumed for the conservation equations without transverse velocity variation. As shown by figure 4.5, this ratio could achieve values up to 1.06 for the highly peaked velocity profiles, when liquid flows next to the wall, at 69 bar. An increase in the operating pressure produces lower values of the same ratios as is shown in figure 4.6, for 155 bar. This ratio is not directly related with the equations presented here, but is a useful indication of the uncertainty introduced by the one-dimensional approach, where the transverse velocity variation is ignored.

4-2.4 The General Form of the Conservation Equations

When the average densities, described in the last section, are expressed as functions of local enthalpy and pressure it is possible to describe the conservation equations of flow in a single form which will contain only the time and space derivatives of mass-flux, pressure and

specific enthalpy. However, a closer inspection of table 4.1 shows that the various average densities are also functions of the local entrainment ratios, e_1 and e_2 . Undoubtedly these entrainment ratios should be related to the local properties of h and p but such a relationship is not yet established by the existing entrainment models. Therefore in order to be able to take into account time and space variations of the average densities, due to changes in the entrainment ratio, we must for the time being treat those quantities as independent variables.

From the standard expressions for partial derivatives in terms of the independent variables it is easily shown that :

$$\frac{\partial \rho}{\partial \xi} = \left(\frac{\partial \rho}{\partial h}\right)\frac{\partial h}{\partial \xi} + \left(\frac{\partial \rho}{\partial p}\right)\frac{\partial p}{\partial \xi} + \left(\frac{\partial \rho}{\partial e_1}\right)\frac{\partial e_1}{\partial \xi} + \left(\frac{\partial \rho}{\partial e_2}\right)\frac{\partial e_2}{\partial \xi} \qquad (4.2.23)$$

where ξ stands for either space, s, or time, t, and ρ can be any of the average densities $\rho_A, \rho_F, \rho_M, \rho_E$ and ρ_H. When the last equation is used for the density derivatives in (4.2.16), (4.2.17) and (4.2.18) the three flow-conservation equations can be rearranged to the following general form :

$$\sum_{\kappa=1}^{3} \psi_{\kappa\lambda} \frac{\partial Y_\kappa}{\partial t} = \sum_{\kappa=1}^{3} \Phi_{\kappa\lambda} \frac{\partial Y_\kappa}{\partial s} + S_\lambda \qquad (4.2.24)$$

where the expressions for $\psi_{\kappa\lambda}$ $\Phi_{\kappa\lambda}$ and S_λ can be deduced from the parent equations (4.2.16), (4.2.17) and (4.2.18). The subscript λ = 1 to 3 refers to the mass, momentum and energy equations respectively and the parameters Y_κ are defined by :

$$Y_1 \equiv G \quad , \quad Y_2 \equiv p \quad , \quad Y_3 \equiv h \qquad (4.2.25)$$

The expressions for $\psi_{\kappa\lambda}$ $\Phi_{\kappa\lambda}$ and S_λ are shown in tables 4.2 and 4.3, where for simplicity the partial derivatives in equation (4.2.23) are

represented by :

$$D_h(\rho) = \left(\frac{\partial \rho}{\partial h}\right), \quad D_{e1}(\rho) = \left(\frac{\partial \rho}{\partial e_1}\right)$$
$$D_p(\rho) = \left(\frac{\partial \rho}{\partial p}\right), \quad D_{e2}(\rho) = \left(\frac{\partial \rho}{\partial e_2}\right) \qquad (4.2.26)$$

In a control volume where p and h are known, the partial derivatives shown in (4.2.26) are easily calculated from the thermodynamic relationships and the equations of the velocity profile model.

4-3 Finite - Difference Equations

Discretisation of the differential equations described by (4.2.24), over a small control volume, gives the finite-difference form of the conservation equations. The discretisation is performed over a staggered difference scheme on the Eulerian mesh shown in figure 4.7. Each cell in this grid, is of length δs, and its centre is designated by (i) for variations in the axial direction and by (j) for the advance in time from (t) to $(t+\delta t)$. In the usual way for staggered grid systems, the state variables such as pressure, specific enthalpy and densities, are those obtained at the centre of the mesh cell, and the flow variables, such as velocity and mass flux, at the cell boundaries. This arrangement of variables, represented by figure 4.8 for a typical cell, has several advantages. First, the velocity components are stored at convenient locations for continuity of mass flow rate, and second, the location of pressure and enthalpy at the centre, provides the actual pressure and enthalpy gradients across the cell boundaries.

There are various ways to discretise the system of first order differential equations described by (4.2.24). Most of these methods will differ only as far as stability and the speed of convergence is

concerned. Usually a simple implicit discretisation scheme is proved to be adequate, thus equation (4.2.24) becomes :

$$\sum_{\kappa=1}^{3} \psi_{\kappa\lambda} \, (Y_{\kappa}^{i,j+1} - Y_{\kappa}^{i,j}) = \left(\frac{\delta t_j}{\delta s_i}\right) \sum_{\kappa=1}^{3} \Phi_{\kappa\lambda} (Y_{\kappa}^{i,j+1} - Y_{\kappa}^{i-1,j+1}) + S_{\lambda} \, \delta t_j \tag{4.3.1}$$

Further rearrangement of the terms in this equation gives :

$$\sum_{\kappa=1}^{3} Y_{\kappa}^{i,j+1} \left(\psi_{\kappa\lambda} - \frac{\delta t_j}{\delta s_i} \Phi_{\kappa\lambda}\right) = \sum_{\kappa=1}^{3} \left(\psi_{\kappa\lambda} Y_{\kappa}^{i,j} - \frac{\delta t_j}{\delta s_i} \Phi_{\kappa\lambda} Y_{\kappa}^{i-1,j+1}\right) + S_{\lambda} \delta t_j \tag{4.3.2}$$

The unknown quantities in these equations are Y_1, Y_2 and Y_3 at the advanced time step $(t_j + \delta t_j)$, which are easily calculated from the system of equations for $\lambda = 1$ to 3, i.e. for the conservation of mass, momentum and energy.

Although the numerical scheme has been developed for transient solutions it is used in this thesis for predictions in steady two-phase flows. The steady flow system of the conservation equations becomes :

$$\frac{\partial G}{\partial s} = 0 \tag{4.3.3}$$

$$\Phi_{22} \frac{\partial p}{\partial s} + \Phi_{32} \frac{\partial h}{\partial s} = - S_2 \tag{4.3.4}$$

$$\Phi_{23} \frac{\partial p}{\partial s} + \Phi_{33} \frac{\partial h}{\partial s} = - S_3 \tag{4.3.5}$$

Hence it is easily shown that :

$$G = \text{constant} \tag{4.3.6}$$

$$\frac{\partial p}{\partial s} = \frac{\Phi_{32} S_3 - \Phi_{33} S_2}{\Phi_{22} \Phi_{33} - \Phi_{23} \Phi_{32}} \tag{4.3.7}$$

$$\frac{\partial h}{\partial s} = \frac{\Phi_{23} S_2 - \Phi_{22} S_3}{\Phi_{22} \Phi_{33} - \Phi_{23} \Phi_{32}} \tag{4.3.8}$$

From equations (4.3.7) and (4.3.8) it is obvious that for known pressure and enthalpy in a cell the pressure and enthalpy gradients are easily calculated.

4-3.1 The Solution Procedure

As described above the properties describing the motion of the two phases are determined numerically by advancing the local flow conditions through a series of small increments, using finite-difference approximations to the equations of motion. The calculation sequence is of a standard predictor-corrector type and consists of the following steps :

(i) Predictor stage - The pressure and enthalpies along the whole test section are guessed using a typical Euler's formula for the first estimate of properties at i+1. Thus ,

$$h_{i+1}^{(1)} = h_i + \left(\frac{\delta s_{i+1} + \delta s_i}{2}\right)\left(\frac{\partial h}{\partial s}\right)_i^{(1)} \qquad (4.3.9)$$

$$p_{i+1}^{(1)} = p_i + \left(\frac{\delta s_{i+1} + \delta s_i}{2}\right)\left(\frac{\partial p}{\partial s}\right)_i^{(1)} \qquad (4.3.10)$$

where $\frac{\partial h}{\partial s}$ and $\frac{\partial p}{\partial s}$ are obtained from (4.3.7) and (4.3.8) for known $p_i^{(1)}$ and $h_i^{(1)}$.

(ii) Corrector stage - The previous estimate is corrected by using a mean slope for the axial derivatives, based on the values for i and i+1, i.e. :

$$h_{i+1}^{(2)} = h_i + \left(\frac{\delta s_{i+1} + \delta s_i}{2}\right)\left[f_E\left(\frac{\partial h}{\partial s}\right)_{i+1}^{(1)} + (1-f_E)\left(\frac{\partial h}{\partial s}\right)_i \right] \qquad (4.3.11)$$

$$p_{i+1}^{(2)} = p_i + \left(\frac{\delta s_{i+1} + \delta s_i}{2}\right)\left[f_E\left(\frac{\partial p}{\partial s}\right)_{i+1}^{(1)} + (1-f_E)\left(\frac{\partial p}{\partial s}\right)_i \right] \qquad (4.3.12)$$

where f_E is an exchange factor for the mean slope. Further details about this factor are presented in the next section.

(iii) Check for convergence - The relative errors from the predictor and corrector stage are calculated by :

$$\varepsilon_h = (h_{i+1}^{(2)} - h_{i+1}^{(1)}) / h_{i+1}^{(1)} \qquad (4.3.13)$$

$$\varepsilon_p = (p_{i+1}^{(2)} - p_{i+1}^{(1)}) / p_{i+1}^{(1)} \qquad (4.3.14)$$

when those numbers are approximately equal to the accuracy of the calculating machine multiplied by 1000, then the solution procedure is considered to have converged sufficiently.

(iv) When the criteria in step (iii) are not satisfied then a new value for $(\frac{\partial h}{\partial s})_{i+1}^{(1)}$ and $(\frac{\partial p}{\partial s})_{i+1}^{(1)}$ is calculated for the following enthalpies and pressures :

$$h_{i+1} = h_{i+1}^{(1)} + f_R (h_{i+1}^{(2)} - h_{i+1}^{(1)}) \qquad (4.3.15)$$

$$p_{i+1} = p_{i+1}^{(1)} + f_R (p_{i+1}^{(2)} - p_{i+1}^{(1)}) \qquad (4.3.16)$$

where f_R is a relaxation factor introduced to ensure stability and to influence the speed of convergence. Step (iv) is a new predictor stage and the solution procedure iterates between (ii) and (iv) until convergence has been achieved.

The advantages of the present scheme, together with other computational details, are described in the next section.

4-3.2 Computational Details

(i) Initial Conditions.

Generally speaking the predictor-corrector method is a rather less expensive iterative method that gives stable solutions for sufficiently small grids, where the truncation errors from the finite-difference approximation of the differential equations are known. The major

difference of the method is that it requires the conditions at the entrance of the test section. Thus the inlet values of pressure, enthalpy and mass-flux must be known.

(ii) The truncation error.

The order of the error introduced in the numerical scheme by the finite-difference approximation of derivatives, depends on the value of the exchange factor, f_E, assumed in equations (4.3.11) and (4.3.12). Thus when $f_E = 0$ we have the familiar Eulerian method which is locally accurate to the second order. This is easily seen from the application of Taylor's theorem at station i, i.e. :

$$Y_i = Y_{i-1} + \frac{\Delta z_i}{1!} Y'_{i-1} + \frac{\Delta z_i^2}{2!} Y''_{i-1} + \frac{\Delta z_i^3}{3!} Y'''_{i-1} + \ldots \qquad (4.3.17)$$

similarly for station i-2, the same theorem gives :

$$Y_{i-2} = Y_{i-1} + \frac{\Delta z_{i-1}}{1!} Y'_{i-1} + \frac{\Delta z_{i-1}^2}{2!} Y''_{i-1} + \frac{\Delta z_{i-1}^3}{3!} Y'''_{i-1} + \ldots \qquad (4.3.18)$$

where $\Delta z_i \equiv \frac{1}{2}(\delta s_i + \delta s_{i-1})$ and $\Delta z_{i-1} \equiv \frac{1}{2}(\delta s_{i-1} + \delta s_{i-2})$.

By subtraction of equation (4.3.18) from (4.3.17), with the assumption $\delta s_i - \delta s_{i-1} \cong 0$, it is found that :

$$Y'_{i-1} = \frac{Y_i - Y_{i-2}}{\Delta z_i + \Delta z_{i-1}} + \varepsilon \left(\Delta z_i^3 , \Delta z_{i-1}^3 \right) \qquad (4.3.19)$$

The last expression is a central difference approximation of the derivative at station i-1 from the values at i-2 and i. A similar central difference between i-1 and i gives :

$$Y_i = Y_{i-1} + \left(\frac{\delta s_i + \delta s_{i-1}}{2}\right) Y'_{i-1/2} + \varepsilon \left(\delta s_i^3, \delta s_{i-1}^3\right) \qquad (4.3.20)$$

The derivative $Y'_{i-1/2}$ can be expressed in terms of Y_i and Y_{i-1} from the

following central difference expressions between (i+1/2, i-3/2), (i+1/2, i-1/2) and (i-1/2, i-3/2),

$$Y'_{i-1/2} = \frac{Y_{i+1/2} - Y_{i-3/2}}{\delta s_i + \delta s_{i-1}} + \varepsilon \left(\delta s_i^3 , \delta s_{i-1}^3 \right) \qquad (4.3.21)$$

$$Y'_i = \frac{Y_{i+1/2} - Y_{i-1/2}}{\delta s_i} + \varepsilon \left(\delta s_i^3 \right) \qquad (4.3.22)$$

$$Y'_{i-1} = \frac{Y_{i-1/2} - Y_{i-3/2}}{\delta s_{i-1}} + \varepsilon \left(\delta s_{i-1}^3 \right) \qquad (4.3.23)$$

Substitution of the last equations in (4.3.20) gives :

$$Y_i = Y_{i-1} + \Delta z_i \left[\left(\frac{\delta s_i}{\delta s_i + \delta s_{i-1}} \right) Y'_i + \left(\frac{\delta s_{i-1}}{\delta s_i + \delta s_{i-1}} \right) Y'_{i-1} \right] + \varepsilon(\delta s_i^3, \delta s_{i-1}^3) \qquad (4.3.24)$$

when equations (4.3.11) and (4.3.12) are compared with the last equation it is obvious that f_E is defined by :

$$f_E \equiv \left(\frac{\delta s_i}{\delta s_i + \delta s_{i-1}} \right) \qquad (4.3.25)$$

and that the truncation error, ε, is of the third order.

(iii) Grid size dependence.

Equation (4.3.24) also shows that for higher accuracies, the mesh size must be chosen small enough to resolve the expected spatial variations of the dependent variables. A large number of mesh points will increase prohibitively the required memory space and execution time. However before any realistic comparisons can be made, it is necessary to see the effects of grid size on the predictions. Figure 4.9 shows the pressure drop, mass-dryness fraction and void fraction for four different sizes of (equally-spaced) grids. From these diagrams it is obvious that the accuracy of the predictions is quite similar for values of δs / L between 0.010 and 0.005. The most sensitive of the parameters is the void fraction which seems to be significantly affected mainly in the

region where evaporation starts. It is therefore desirable to use mesh increments of varying length with the smaller lengths in the regions where significant changes of thermal or flow conditions are expected.

4-4 Numerical Predictions

The purpose of the numerical predictions shown in this chapter is to examine the effects of various shapes of heat-flux distribution, when entrainment of liquid and vapour is allowed.

For liquid flowing in the region next to the wall, the semi-empirical method proposed by Ishii and Mishima (Is22) is included in the numerical scheme to calculated the liquid entrainment ratio. A description of this model and the way it is incorporated, is given in the next chapter, together with other physical phenomena associated with the problem of burnout. For the entrainment ratio of vapour into the liquid phase there are no models suitable for direct calculations. Entrainment of this kind is probably a combined effect of evaporation as well as occlusion by waves; in the absence of more precise information this ratio is arbitrarily taken to be half the local value of the liquid entrainment ratio.

In the following graphs the effects of entrainment on the predictions are shown for three different steady heat flux distributions similar to those typically found in nuclear power plants. By comparing the results predicted by the same entrainment model, it is also seen how the distribution of heat input affects the calculated pressure drop, void fraction entrainment ratio and film thickness, for the case with liquid predominating in the outer flow region. The average value of the heat flux in the results presented is taken to be 800 kW/m^2, the inlet temperature is 265.4 °C and the operating pressure is 68.9 bar (1000 psia).

The contribution of entrainment is partially investigated by drawing the lines of the two extreme cases, i.e. for fully separated and completely homogeneous ($e_g = 1$, $e_\ell = 0$) types of two-phase flow; the latter case being that for complete entrainment between the two regions. It is observed that for the predicted pressure drops in figures 4.10(a) to 4.12(a), the differences can be as large as fifty per cent over the 3.66 metres of the test section. The homogeneous flow predicts lower pressure drops than the separated type, but the void fraction in homogeneous flow is 10 to 13% higher than when no mixing occurs. The void fraction predictions are shown in figures 4.10(b) to 4.12(b).

Those graphs also show that entrainment of the liquid phase only has little effect on the calculated pressure drop, whereas for the void fraction the results lie everywhere between the homogeneous and separated flow lines. Different conclusions are made for the pressure drop when both liquid and vapour entrainment is allowed. In this latter case the predictions are closer to the line for completely homogeneous mixture.

Inspection of figures 4.13 to 4.16 gives a rather more complete picture of the effects of heat flux distribution on the predictions made with the current numerical scheme. These figures compare the predictions for the pressure drop, entrainment ratio, void fraction and film thickness for the three different heat-fluxes when the liquid entrainment ratio is calculated by the Ishii and Mishima model. As shown by figure 4.13, the pressure drops predicted for the exponential heat-flux are 15 to 20% lower than for the other two heat flux shapes, and the same observation is made from figure 4.14 for the liquid entrainment ratio.

Similar comparisons for the void fraction and film thickness are made in figures 4.15 and 4.16 which show how those quantities are influenced by the various heat flux distributions. From those figures, it is seen that vapour is generated in shorter distances for uniform heat

flux, and the thickness of the liquid film is reduced faster for the chopped cosine distribution.

Because of the equality of the average heat inputs the total amounts of vapour generated and entrained at the exit of the test section are nearly equal, whatever heat flux distribution is chosen. However, there are important differences of the local conditions at various distances along the flow axis, which justify the use of detailed entrainment models and numerical schemes even for steady two-phase flow.

Chapter 5.

Burnout Predictions with the Velocity Profile Model.

Contents :

CHAPTER 5

BURNOUT PREDICTIONS WITH THE VELOCITY PROFILE MODEL

5-1 Definitions

In many industrial and nuclear plants, where heat transfer is likely to take place under high enough surface temperatures and/or heat fluxes, it is desirable to examine the conditions under which a severe deterioration of the heat transfer process can take place. This deterioration is usually called burnout and is defined in the literature (e.g., He82) as :

(1) The condition under which a small increase in the surface heat flux leads to an inordinate increase in the wall temperature, for systems where the heat flux is controlled.

(2) The condition under which a small increase in the wall temperature leads to an inordinate decrease in heat flux, in systems where the wall temperature is controlled.

For the purposes of this chapter, the term burnout is treated as being synonymous with similar proposed terms such as, "critical heat flux" and "dryout".

Burnout is a very complicated phenomenon due to the several possible physical mechanisms that create it, and the correspondingly large number of independent variables that influence its occurrence. A great deal of effort has been spent in trying to describe this phenomenon, and a large number of detailed reviews have been published on the subject, such as (He82), (He78), (Be77), (Ma75), (La75) etc. Most of these works refer to a number of alternative mechanisms of burnout, from which the more reasonably well established are :

(i) The formation of a hot spot under a growing bubble.

(ii) Near-wall bubble crowding and inhibition of vapour release.

(iii) Film dryout in annular flows.

In this chapter we are examining only liquid film dryout in annular types of flow, with the predictions from the numerical scheme of chapter 4 being compared with experimental results, under uniform and non-uniform heat flux distributions.

5-2 Dryout in annular flows

This form of burnout is most likely to occur at the high quality region for most practical systems which are several metres long. It is well understood (Is61, He82) that this type of burnout is controlled by the processes of liquid loss from the film, such as of evaporation and liquid entrainment, and liquid addition from droplet deposition. As a result of these processes, burnout occurs near the point where the liquid film flow rate at the channel wall is zero; however a significant amount of liquid may remain present in the tube as entrained droplets at the location of burnout.

According to the outline given above, the key to the accurate prediction of burnout in annular flow, is an adequate description of the liquid entrainment and deposition rates, as well as the description of effects of the heat flux on entrainment and deposition. It is usually expected (He81) that nucleate boiling within the liquid film could give rise to bursting of bubbles at the interface between the two mixtures in region 1 and 2 shown in figure 3.2. This will consequently release more droplets into the vapour core. On the other hand, the evaporation process leads to a flux of vapour away from the interface and this might sweep away droplets that would otherwise have been deposited. Those effects are very difficult to distinguish, and to a certain extent,

experiments (He63, Be67, Ke70) have shown that their contribution to entrainment and deposition is rather small.

However, with the current state of the numerical method described in chapter 4, we could consider the presence of vapour bubbles in the liquid film and how this is affecting the prediction of burnout.

Reasonably accurate predictions of burnout in annular flows could be achieved by applying the standard conservation equations of chapter 4 together with a suitable semi-empirical model describing the entrainment and deposition processes.

5-2.1 Entrainment model

For the liquid entrainment ratio in annular flows with a liquid film, we can use a simple correlation proposed by Ishii and Mishima (Is82b). Basically, this correlation consists of two equations proposed for two different regions of entrainment, namely the entrance region (following a relatively smooth introduction of liquid film) and the quasi-equilibrium region. The correlation is expressed in terms of dimensionless quantities such as the vapour volumetric flux, distance and liquid Reynolds number and can identify the necessary distance for the development of entrainment. It has been claimed by the proposing authors that this correlation can supply accurate information about liquid entrainment over wide ranges of experimental data for steam-water flows although in their original paper (Is82b) comparisons are shown only for air-water systems.

The equation proposed for the quasi-equilibrium region for the liquid entrainment ratio e_ℓ^*, on the basis of experimental data, is :

$$e_\ell^* = \tanh \left(7.25\ 10^{-7}\ We^{1.25}\ Re_\ell^{0.25}\right) \qquad (5.2.1)$$

where the effective Weber and Reynolds numbers are :

$$We = \frac{\rho_g j_g^2 d}{\sigma} \left(\frac{\Delta\rho}{\rho_g}\right)^{1/3} \qquad (5.2.2)$$

$$Re_\ell = \left(\frac{\rho_\ell j_\ell d}{\mu_\ell}\right) \qquad (5.2.3)$$

In these equations σ is the surface tension, $\Delta\rho$ is the density difference, and the volumetric fluxes, j_g and j_ℓ, are given by :

$$j_g = \frac{xG}{\rho_g} \text{ and } j_\ell = \frac{(1-x)\,G}{\rho_\ell} \qquad (5.2.4)$$

For the entrance region Ishii and Mishima defined the dimensionless vapour flux, j_g^+, and distance, s^+, according to :

$$j_g^+ = j_g \left[\frac{\sigma g \Delta\rho}{\rho_g^2}\left(\frac{\rho_g}{\Delta\rho}\right)^{2/3}\right]^{-0.25} \qquad (5.2.5)$$

$$s^+ = \frac{L_B}{d}\sqrt{\frac{Re_\ell}{j_g^+}} \qquad (5.2.6)$$

which are used in the entrainment ratio correlation, given by :

$$e_\ell = \left[1 - \exp(-10^{-5}(s^+)^2)\right] e_\ell^* \qquad (5.2.7)$$

This correlation must be used until entrainment reaches a quasi-equilibrium value which, as shown by Ishii and Mishima, is achieved where :

$$s^+ \geq 600 \qquad (5.2.8)$$

The onset of liquid entrainment has been also studied by Ishii and Grolmes (Is75) considering a force balance at the crest of roll waves. They determined that entrainment occurs when the vapour volumetric flux

exceeds a critical value, j_c, which for $Re_\ell > 1635$ is given by :

$$\frac{\mu_\ell j_c}{\sigma}\sqrt{\frac{\rho_g}{\rho_\ell}} = \begin{cases} N_\mu^{0.8} & \text{for } N_\mu < 1/15 \\ 0.115 & \text{for } N_\mu > 1/15 \end{cases} \qquad (5.2.9)$$

and for $Re_\ell < 1635$ by :

$$\frac{\mu_\ell j_c}{\sigma}\sqrt{\frac{\rho_g}{\rho_\ell}} = \begin{cases} 11.78\, N_\mu^{0.8}\, Re_\ell^{-1/3} & \text{for } N_\mu < 1/15 \\ 1.35\, Re_\ell^{-1/3} & \text{for } N_\mu > 1/15 \end{cases} \qquad (5.2.10)$$

where the velocity number N_μ is defined from :

$$N_\mu \equiv \mu_\ell \left(\rho_\ell \sigma \sqrt{\sigma/g\Delta\rho}\right)^{-0.5} \qquad (5.2.11)$$

This is not the only model that could be used to calculate the entrainment ratio for the liquid phase. It has been chosen here because of its simplicity, although in the near future it is desirable to substitute it by a more detailed model (e.g., Hu73) involving the rates of entrainment and deposition.

5-2.2 The numerical scheme for the entrainment models

This section outlines briefly the modifications of the numerical scheme, described in section 4-3.1, required to implement the Ishii and Mishima entrainment model as part of the calculations.

The liquid entrainment ratio evaluated by equations (5.2.1) and/or (5.2.7) depends on the local mass dryness fraction. Therefore, for known values of pressure and specific enthlapy, the steps of the calculational cycle for entrainment are as follows :

(a) Calculate the local mass-dryness fraction x.

(b) Examine if entrainment has reached quasi-equilibrium.

(c) If the answer in step (b) is yes, calculate the liquid entrainment ratio from equation (5.2.1), or from equation (5.2.7) if the answer is no.

(d) Approximate the derivative of the liquid entrainment ratio with :

$$\frac{\partial e_\ell}{\partial s} = \frac{(e_\ell)_i - (e_\ell)_{i-1}}{\frac{1}{2}\ (\delta s_i + \delta s_{i-1})} \qquad (5.2.12)$$

(e) Calculate the pressure and specific enthalpy gradients from equations (4.3.7) and (4.3.8).

This sequence is repeated for every new estimate of pressure and specific enthalpy, generated by the predictor-corrector numerical of section 4-3.1.

The liquid entrainment ratio and the thickness of the liquid film, calculated from the present numerical scheme, for a diabatic pipe flow with a chopped cosine distribution are shown in figure 5.1 (a and b). The various lines correspond to different grid sizes, and indicate that, for equidistant cells, we must choose :

$$\delta s_i \leq 0.010\ L$$

to achieve near-independence from the imposed grid.

In the numerical scheme, the location of burnout is defined as the region where the mass flow rate of the liquid in the region next to the wall is reduced to zero. This definition is in accordance with the approach used at Harwell (Wh74) for a number of comparisons with experimental results.

However, some authors (Ha64, Zu66) investigating the stability of dry patches forming in liquid films, considered the forces acting on the interface and recommended relations for the critical film thickness. When the film thickness becomes lower than the critical value the film is considered to be broken up, and a dry patch is formed in that region. For films flowing over heated surfaces, Zuber in 1966 (Zu66) proposed an equation that predicts this critical thickness for laminar flows

motivated by gravity. This criterion has been also built into the numerical scheme as a different method for locating burnout, although its application must be restricted to the conditions it has been proposed.

5-3 Burnout Predictions

In general the critical heat flux $\dot{q}''_{BO}$ for burnout in a channel with given geometry and fluid is a function of the hydraulic diameter d, test section L, inlet subcooling Δh_{in}, mass flux G and pressure. Thus :

$$\dot{q}''_{BO} = \text{fn } (d, L, \Delta h_{in}, G, p) \qquad (5.3.1)$$

The inlet subcooling, in this equation, can be replaced by the mass-dryness fraction x_{BO} at the location of burnout using a heat balance relationship so :

$$\dot{q}''_{BO} = \text{fn } (d, L, x_{BO}, G, p,) \qquad (5.3.2)$$

The six variables in this equation are not independent, and any change in operating conditions affects at least two of the variables listed. For constant d, L, G and p equation (5.3.2) represents a relation between burnout heat-flux against the mass-dryness fraction at the location of burnout. This is usually represented by a nearly straight line in the $(\dot{q}''_{BO}, x_{BO})$ plane with the exception of very short channel lengths.

Alternatively for constant $\dot{q}''_{BO}$, d, G, p, equation (5.3.2) implies a relationship between x_{BO} and L_B; where L_B is the length from the point at which bulk saturation conditions are obtained.

These two different representations are completely interchangeable for uniformly heated channels when a heat balance relation is used. However, for non-uniformly heated channels they usually indicate different degrees of agreement with experimental results.

In the comparisons that follow results for uniform and non-uniform heat flux distributions are presented. In some of the figures are also shown the lines from proposed empirical correlations for the burnout heat-flux in uniformly heated channels. All the predictions by the velocity profile model were carried out for n = 7 with zero vapour entrainment except where otherwise stated.

5-3.1 Results for Burnout with Uniform Heat Flux

Figure 5.2 is a plot of the burnout mass-dryness fraction against the boiling length (i.e. the distance between the point of bulk saturation conditions and the point of burnout). In this graph are shown the experimental data by Bennett et. al. (Be65), for four different mass fluxes, in uniformly heated steam-water flow at 69 bar. Round tubes, 12.6 mm in diameter were used for this experiment.

In the same figure are shown the predictions by the velocity profile model when the liquid mass flow rate in the region next to the wall was reduced to zero. The predictions are in encouraging agreement with the experimental data though there are greater deviations at the higher mass fluxes probably due to the inadequacy of the entrainment model. The effects of the mass flux and the trend with the boiling length is correctly predicted over the examined range of boiling lengths. However one should not try to extrapolate the lines for the very short distances because it is not known if burnout in that region will occur due to film dryout or even possible due to the other mechanisms mentioned in section 5-1. In the same figure are also drawn the lines obtained by the Bowring correlation (Bo72). This correlation gives predictions with the same trend as the velocity profile model, although it overpredicts considerably the mass dryness fraction for the smaller mass fluxes.

Similar agreement is obtained when the same experimental results are transferred to the $\dot{q}''_{BO}$, x_{BO} diagram. In the diagram shown in figure

5.3 are again drawn the predictions by the velocity profile model and the Bowring correlation.

5-3.2 Results for Burnout with Chopped Cosine Heat Flux

The burnout data of Keeys et. al. (Ke72) with chopped cosine heat-flux distribution have been analysed for different mass fluxes in a round tube 12.6 mm in diameter and a total test section of 3.66 metres. The extrapolation length for the chopped cosine heat flux distribution was 0.273 metres, therefore the ratio of the maximum to the average heat flux was 1.4. The inlet subcooling, in this particular set of experiments, was around 100 kJ/kg ; the exact values are given in brackets next to the small triangle points in figure 5.5.

The burnout positions obtained experimentally by Keeys et. al. are shown in figure 5.4 and the resulting average heat fluxes are shown in figure 5.5 as a function of mass velocity. In figure 5.4 are also drawn the predictions from the velocity profile model when the liquid mass-flow rate in the region next to the wall was zero either with or without vapour entrainment in the liquid film. In the absence of any information about vapour entrainment the vapour entrainment ratio was taken to be 0.2 times the value of the local liquid entrainment ratio as predicted by the Ishii and Mishima model. Also in the same figure are shown the predictions from the velocity profile model when the point of burnout was calculated from the critical film thickness model, discussed in the last paragraph of section 5-2.2. This criterion developed for laminar flows is not particularly useful for the present experiments, and as expected is in considerable disagreement with observed burnout lengths. The last line in figure 5.4 corresponds to the predictions by the CISE (Be64) boiling length correlation, for the burnout heat flux drawn in figure 5.5.

The predictions in figure 5.4 show a good agreement with the general trend of the experimental points. This figure indicates that the present model is capable of accurate predictions provided we have enough knowledge about the actual physical phenomena that produce burnout.

The superiority of the present model is even better illustrated in figure 5.6 where the local burnout heat flux is plotted against the mass-dryness fraction at burnout, for different mass flow rates. The continuous line is the best fit to the data of Keey et. al. (Ke70) and the dashed lines correspond to the predictions obtained by the present numerical method without vapour entrainment. The position of burnout in these predictions corresponds to the point where the liquid film flow rate is reduced to zero.

5-3.3 Burnout for Uniform Heat Flux with Cold Patch

Burnout data obtained at 68.9 bar by Bennett et. al. (Be66) are also presented in table 5.1 for a pipe 12.6 mm in diameter with a total length of 4.2073 metres. This pipe was uniformly heated with the exception of 60.96 mm test section, which was unheated (Cold Patch). In table 5.1 are presented the experimental and predicted burnout lengths for four different locations of the unheated section. The agreement is generally good, with the predicted locations within 7% of the actually observed lengths.

5-4 Conclusions

As shown from the application of the velocity profile model in uniform and non-uniform heat flux distributions an encouraging agreement is achieved with experimental burnout. However the comparisons made in this chapter are not intended for explaining the complex phenomenon of burnout. Nevertheless it is indicated the flexibility of the model to

use various criteria for burnout, and its capability for accurate predictions.

To a certain extent the accuracy of the predictions depends on how successful entrainment is taken into account in the calculations. This is clearly shown in figure 5.4 where both liquid and vapour entrainment are used.

In order to improve the agreement of burnout predictions, it is desirable to alter the entrainment correlation so that entrainment and deposition rates of liquid droplets and vapour bubbles are used directly in the calculations. It is also desirable to examine in detail the conditions under which hydrodynamic equilibrium is established between the entrainment and deposition mechanisms.

Chapter 6.

Concluding Chapter.

Contents :

CHAPTER 6

CONCLUDING CHAPTER

6-1 General Conclusions

An analytical model of the flow of liquid and its associated vapour phase has been developed and applied to adiabatic and diabatic flows with heat-flux distributions typical of those found in nuclear plants. The main novelties of the method are that two homogeneous liquid and vapour mixtures with different transport properties are considered to be flowing in two different flow regions with a compound velocity profile.

In general there are many different ways by which the phases could be mixed into each other, and the nature of the resulting flow regimes usually varies with channel geometry and orientation as described in chapter 1. The analytical model that has been developed here is capable of describing bubbly flows, wispy annular, annular with liquid droplets and separated types of flow; this is easily achieved by properly choosing the values of the entrainment ratios that has been introduced in chapter 3. For the accurate prediction of the local flow conditions in evaporating channels with the present model, it is possible to simulate the transition between the different types of flow by suitably choosing the values of the entrainment ratios along the flow axis. The application of the model is not restricted to the types of flow where the liquid phase is predominantly in the region close to the wall. With the same model it is possible to describe exceptional cases where the vapour generated by boiling at the channel wall remains close to the wall, also cases where bubbles concentrate preferentially near the wall which usually happens during rewetting of hot surfaces. The assumed velocity

profiles for the two cases with liquid or vapour predominant in region 1 can be significantly different, as shown by the three dimensional picture of figure 6.1 for flow without entrainment.

In effect, the shape of the velocity profile obtained by the present model also depends on the actual flow regime. Thus, the parabolic profiles for laminar flows produce significantly different results than the power law profiles as described in the parametric studies of chapter 2. In reality the value of the power exponent must be properly established by a consistent set of experimental measurements at different Reynolds numbers. This is particularly important for the ratio of average velocities of the vapour and liquid phases, as described in chapter 2.

For the application of the velocity profile method in diabatic flows with complex heat distributions, when the properties of the two phases vary significantly along the channel, it is necessary to use the finite difference form of the flow conservation equations. By defining the suitable average densities, these equations could be transformed to a type similar to that for single-phase flow. With the velocity profile model the equations can by expressed only by derivatives of the independent properties of the flow, like mass flux, pressure and enthalpy which could be discretised by a variety of methods. In this way complex two-phase flows can be analysed with a fast numerical procedure which gives accurate predictions with moderately small grid lengths ($\delta s/L < 0.01$).

For the realistic simulation of actual two-phase flows, it is necessary to include as part of the numerical scheme, theoretical or semi-empirical models to calculate the local entrainment ratios. Thus, the flow conditions predicted in each axial location of the flow channel,

are influenced by the accuracy of the model which calculates the upstream entrainment ratios.

One of the particularly useful applications of the current numerical scheme with a realistic entrainment model, is the prediction of burnout in pipe flows. As described in chapter 5, the numerical predictions constitute an important advancement in comparison with results produced by standard empirical correlation. It is surprising how accurate are the predictions made by the current scheme in a variety of heat and flow conditions.

In conclusion, the present velocity profile cannot claim to be more than a simplified description of the complex velocity profiles that represent physical reality. Nevertheless it gives better description of two-phase flows than "one-dimensional" models and allows a more realistic representation of a number of flow regimes. However, further development is desirable, which to a considerable extent depends on the existence of more detailed observation of actual two-phase flows. Some suggestions are made in section 6-3.

6-2 Achievements of the Present Study

The achievements of the work presented in this thesis can best be summarised in relation to the objectives stated in chapter 1.

(1) An analytical model has been developed which proves to be superior to other existing models wherever comparisons with similar experimental conditions were possible. The model contains a certain degree of flexibility in the arrangement of the two phases into the flow area; also the actual shape of the velocity profiles can be allowed to vary according to a chosen exponent. Entrainment of the two phases is also taken into account during the derivation of the model.

(2) Full use of the assumed radial variation of velocity is very helpful in the description of the flow conservation equations for two-phase mixtures. This enables the introduction of a fast numerical scheme, which is then extended to describe steady flows with complex heat-flux distributions.

(3) Experimental comparisons with well established data found in the literature, showed that the model is capable of satisfactory predictions of void fraction, pressure drop and for the conditions which are most likely to produce burnout in heated pipe flows.

(4) It has been shown in chapters 3,4 and 5 that the accuracy of the obtained predictions is significantly affected by the local values of liquid and vapour entrainment ratios.

6-3 Topics for Future Consideration

The present method of two-phase flow modelling can be improved in two different stages. The first category of improvements refer to the relatively easy modifications of the velocity profile model as described in the present thesis. At the second stage of improvement , some suggestions can be made on how the model should be extended to give a more precise representation of two-phase flow. This latter type of improvements also includes topics for further experimental work, that is closely associated with the development of the analytical model.

6-3.1 Easy improvements of the current model.

In its general form the velocity profile model is closely connected with the conservation laws for the flow in a passage, as discussed in chapter 4. Therefore improvements can be achieved either by adding some extra features to the analytical model for a better description of the

flow conditions or by developing further the current solution scheme. Such improvement are shown schematically in figure 6.2.

(i) Improvements of the analytical model

The system of conservation equations, described in chapter 4, can be only solved after establishing a relation between the entrainment ratios and the local flow conditions. Thus, one of the first future considerations, is to examine how accurate are the predictions for different models of entrainment. Ultimately, it is desirable to use an entrainment model based on the local entrainment and deposition rates, like the model proposed by Hutchinson and Whalley (Hu73). This model is already under active consideration but, to a certain degree, success in this direction will be limited by the difficulty in proposing a correlation for the equilibrium concentration of droplets in the vapour core. Calculations for the entrainment ratio in the region next to the wall, will also depend on the availability of suitable entrainment models.

As discussed in chapter 3, at the moment it is assumed that the two phases are arranged in two homogeneous mixtures for each of the flow regions shown in figure 3.2; the homogeneous assumption is used to indicate that the liquid and vapour portions present in region 1 travel with the same average velocity $\bar{u}_1$, and similarly for region 2. This of course is an approximation, and it would be more realistic if we were to allow the small vapour bubbles and liquid droplets to travel with different velocities from the surrounding phase. This could be easily achieved by introducing two slip ratios $\bar{u}_{g1}/\bar{u}_{\ell 1}$ and $\bar{u}_{g2}/\bar{u}_{\ell 2}$ which will be related empirically to the local transport properties of the mixtures.

On the basis of experimental observations included in the discussion of chapters 2 and 3, it is necessary to establish a relation between the power law exponent n and the local Reynolds number. This task could be easily achieved when a consistent set of experimental measurements is available at various mass-flow rates, operating pressures and pipe diameters.

A rather important advancement of the current use of the velocity profile model could be achieved by examining how the present representation of the flow affects the calculation of the heat transfer coefficients. At this stage one of the many semi-empirical methods found in literature could be used, but ultimately it will best if an analytical model could be proposed based on the assumed here velocity profiles and detailed information about the temperature distribution in the flow passage.

(ii) Improvements of the numerical scheme

The finite difference equations described in chapter 4 have been derived for both steady and time-dependent solutions,although in the thesis steady flow comparisons with experiment are only presented. It is therefore desirable to examine the predictions of the present numerical scheme in comparison with transient experimental results. Before this is achieved, it is necessary to investigate the limitations imposed by the use of one of the explicit or implicit differencing schemes used in approximating the conservation equations.

Frequently it is also desirable to start the numerical solution procedure with a different combination of input parameters. For most practical applications where one has to simulate the performance over a complete system, it is necessary to use the total pressure drop over a test length rather than the mass-flow rate which has been assumed so far

in section 4-3.2. An iterative scheme starting from a guessed mass-flow rate is probably a suitable improvement in this direction.

6-3.2 Extension of the velocity profile method

The extension of the velocity profile model seems to be desirable in three main directions. These are, firstly, improvements of the model for more complex geometries of the flow passage; secondly, better understanding of flow conditions and thirdly consider how the current representation of the two-phases could incorporate a more realistic description of thermal effects. It is inevitable that such improvements require consistent experimental measurements, which will examine the accuracy of the predictions, as well as establish the correlations for the independent parameters that describe the velocity profile and determine the entrainment ratios of the two phases. A schematic representation of directions that could be pursued are shown in figure 6.3.

Perhaps the most obvious first extension is the simulation of two-phase, non-axisymmetric flows, such as the flows in annulus or inclined pipes. Experimental work is also necessary for such geometries mainly to investigate the contribution of entrainment and deposition in complex shapes of interface. As a first approximation, the concept of the equivalent hydraulic diameter might be useful in the analytical model, but in reality one has to develop velocity profiles suitable for non-circular passages which will be then integrated over the flow area in the similar way as described in this thesis. It is also worthwhile to extend the present model to study steady and transient two-phase flows in pipes with sudden expansion and contractions of the flow area.

Further development of the model could be achieved by improvement of the actual flow regime. One could modify the model to account for flow reversal, of either one or both of the two mixtures and that will be a very useful extension in analysing quenching and reflooding phenomena.

The conditions of the interface should be also subject of further consideration. The Prandtl's mixing length hypothesis for the interface might not be a good approximation under certain conditions, and one should consider using different turbulence models. At the moment, this task seem to introduce further complexity in the calculations which might not be desirable at this stage.

The numerical method itself could be developed to simulate shock waves which is of some importance, particularly during very fast flow transients.

Experimental observations are also necessary to investigate the conditions that produce vapour entrainment in the liquid film. Aim of such experiments is to produce a realistic semi-empirical model that could be used in calculating the entrainment ratio in the region next to the wall.

Experiments must be also performed to examine the conditions under which laminar two-phase flow could be achieved, and define the corresponding critical Reynolds number for the transition to turbulent flow.

On the basis of the current velocity profile model, where vapour or liquid could be taken to be the predominant phase next to the wall, it is necessary to examine by experiments the conditions which are most likely to give liquid or vapour in region 1. It might be also necessary to examine the transition region between those two types of annular flow in diabatic two-phase flows.

The simulation of the flow so far assumes that liquid and vapour are in thermal equilibrium. In reality this is an idealisation which is very rarely true. In most cases, thermal non-equilibrium must be taken into account together with the relative temperature distribution in the radial direction.

An important advancement of the current solution scheme could be to extend the analytical model to describe the effects of coolant evaporation on the transient heat generation in reactor channels. This requires significant modifications on the heat transfer part of the solution, but because of the simplicity of the current numerical scheme those modifications can be safely incorporated in the program without prohibitively increasing the computational time.

Finally in order to examine the accuracy of the thermal predictions we need to make comparisons under transient thermal conditions. Further experiments are therefore necessary for the transient burnout calculations as well as for quenching and reflooding in channels with a sudden reduction of the flow area.

Appendix A.

Figures and Tables .

A - 1. Figures for Chapter 1 .

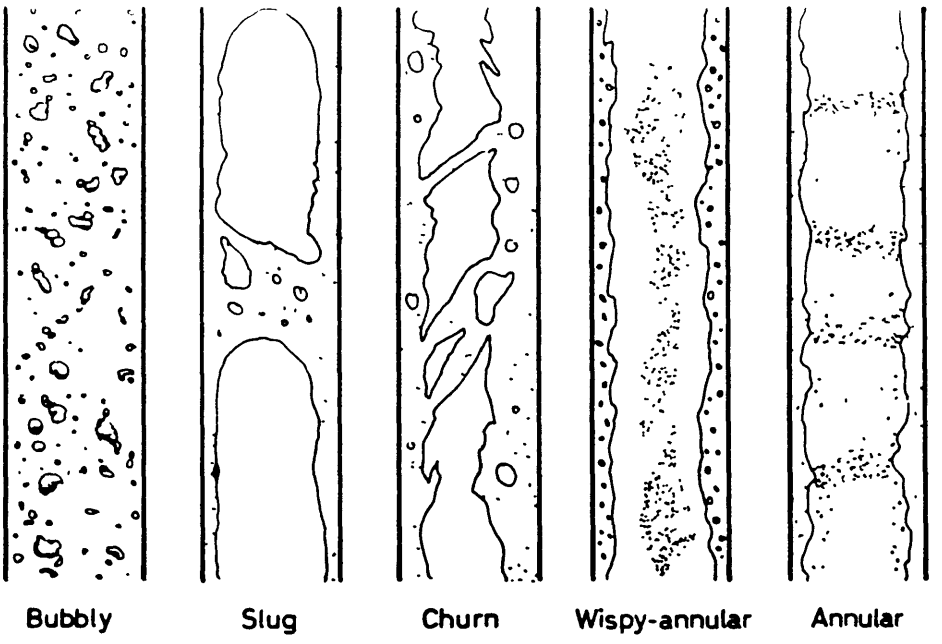

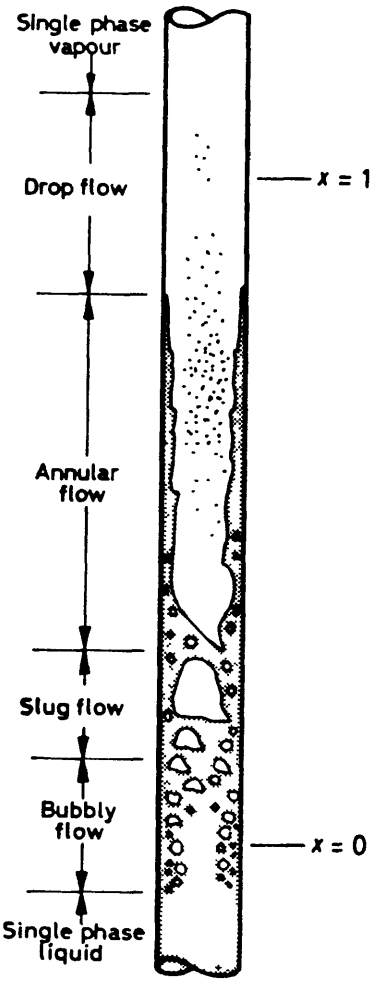

1.1 Flow patterns in vertical co-current flow (Co72).

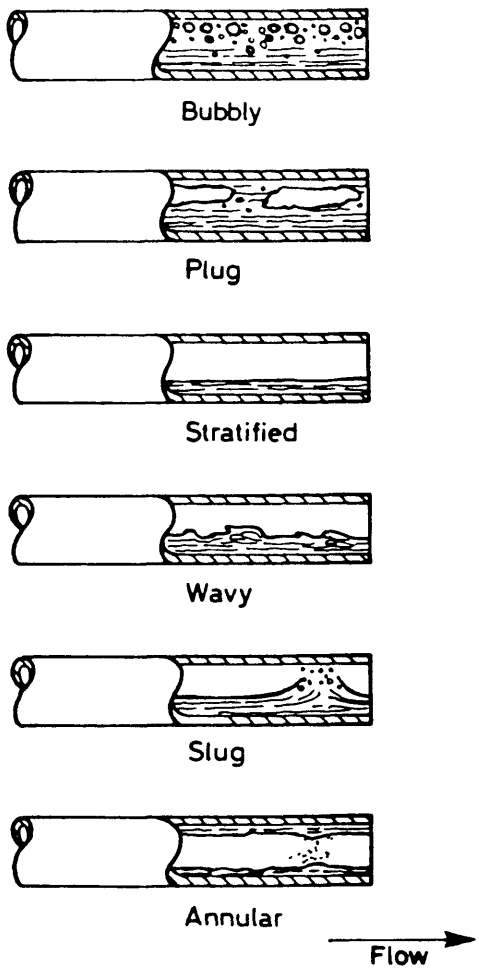

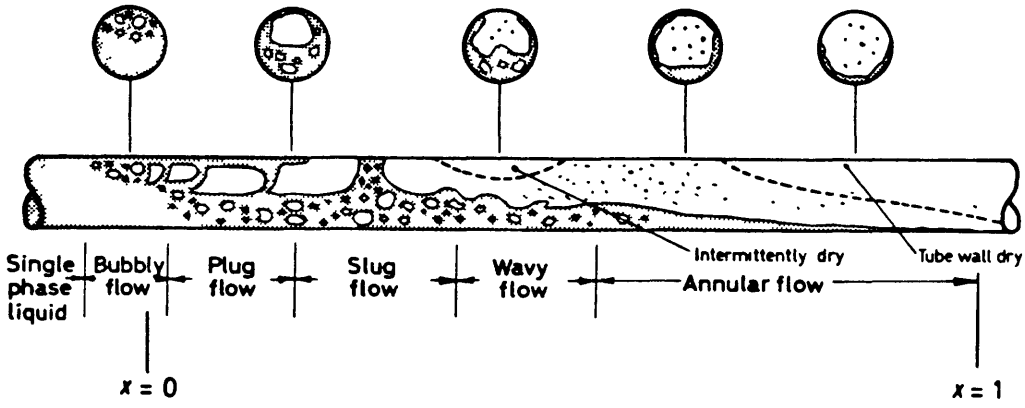

1.2 Flow patterns in horizontal flow (Co72).

A - 2.1 Figures for Chapter 2.

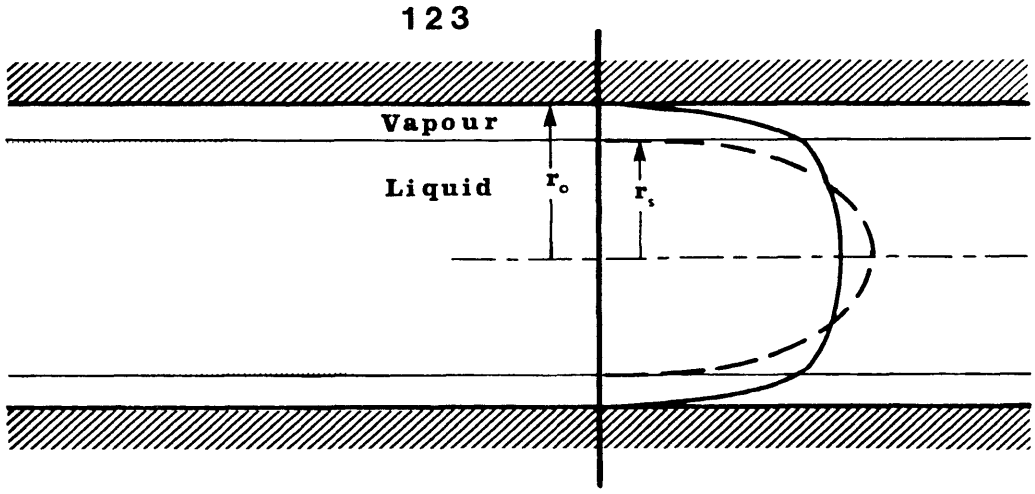

2.1 Approximations used for the velocity profile in annular two-phase flow.

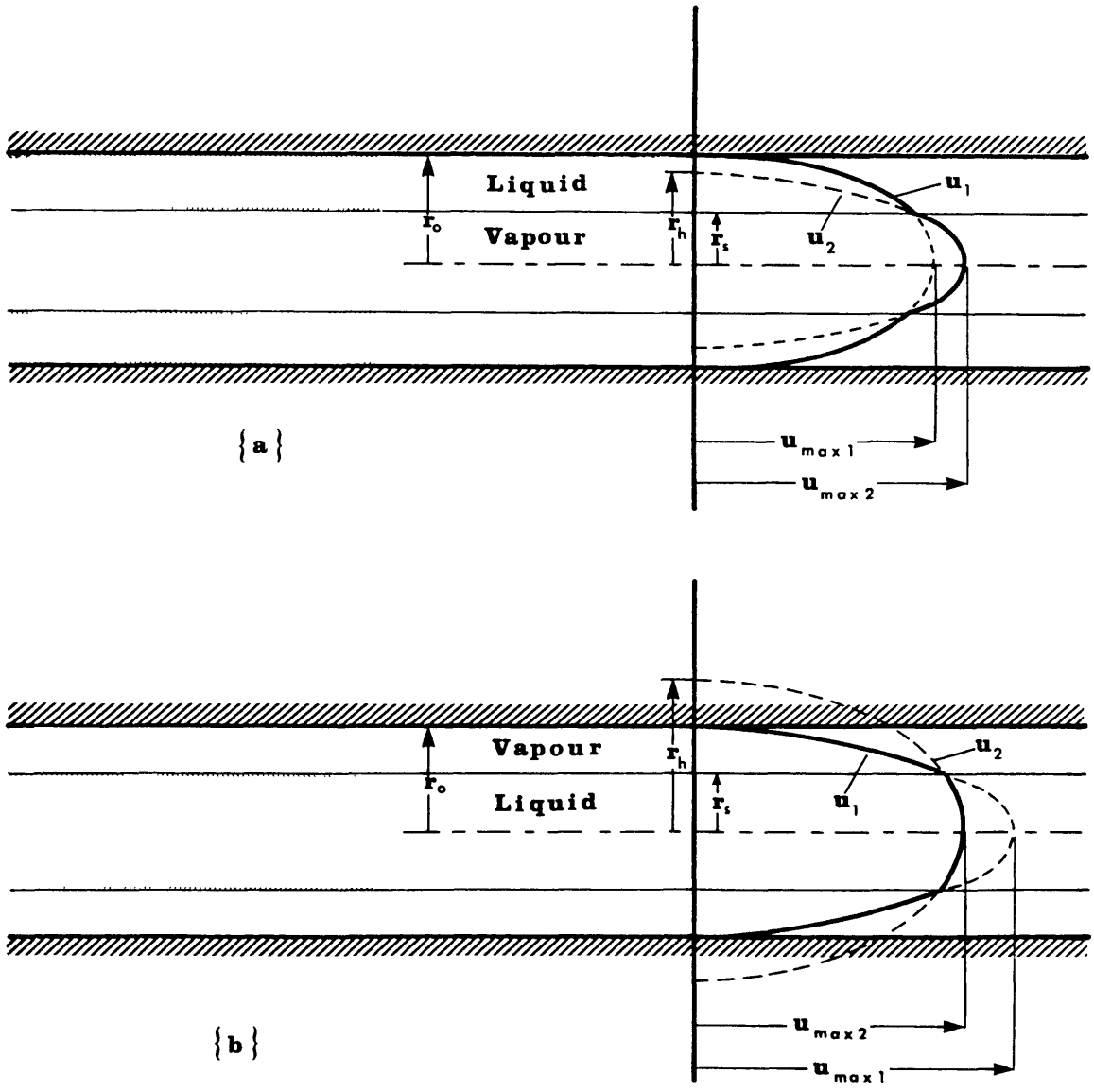

2.2 The assumed velocity profiles used by the presend model for annular two-phase flow; (a) L1V2 (b) V1L2.

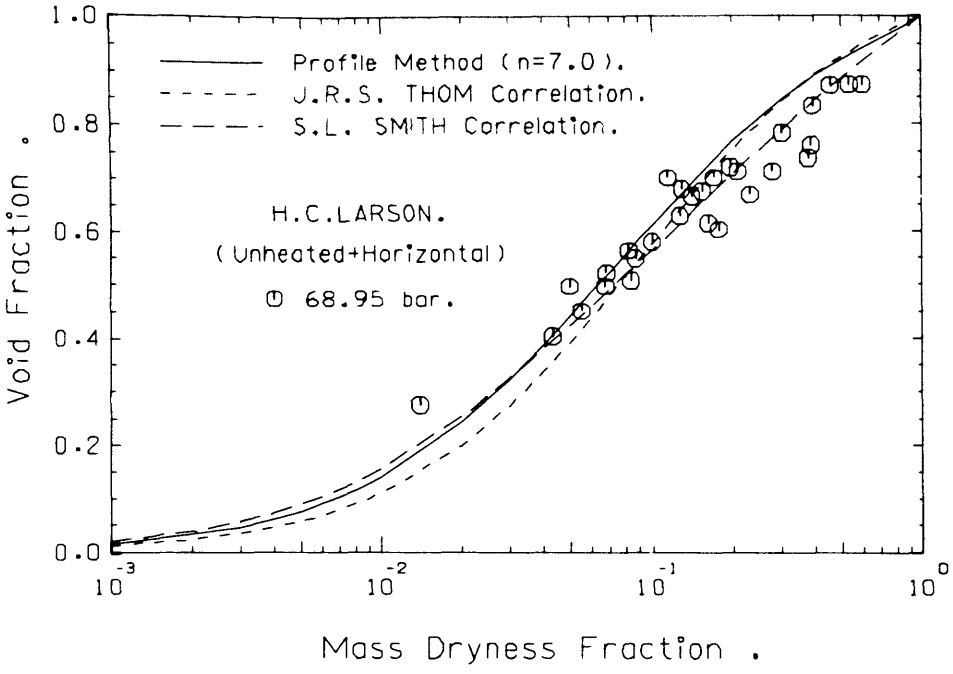

2.3 **The void fraction, mass-dryness fraction relation in a horizontal unheated pipe.**

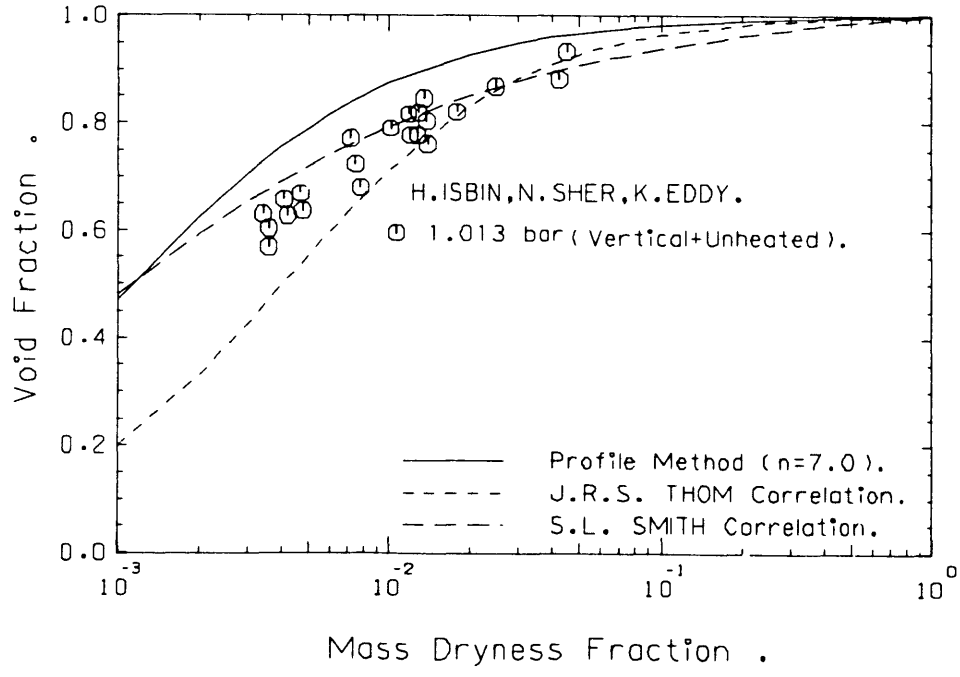

2.4 **The void fraction, mass-dryness fraction relation in a vertical unheated pipe.**

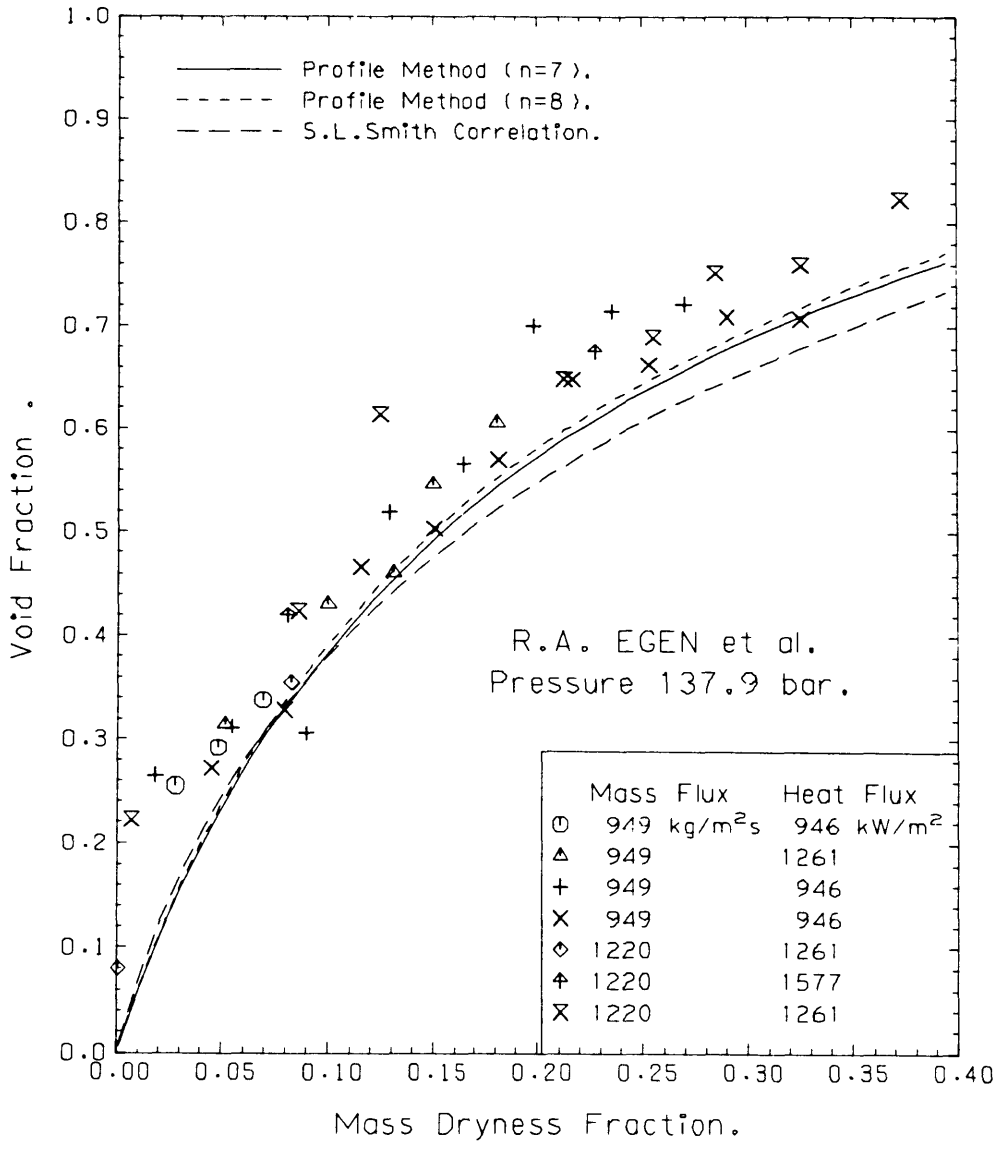

2.5 The void fraction, mass-dryness fraction relation in a vertical heated pipe.

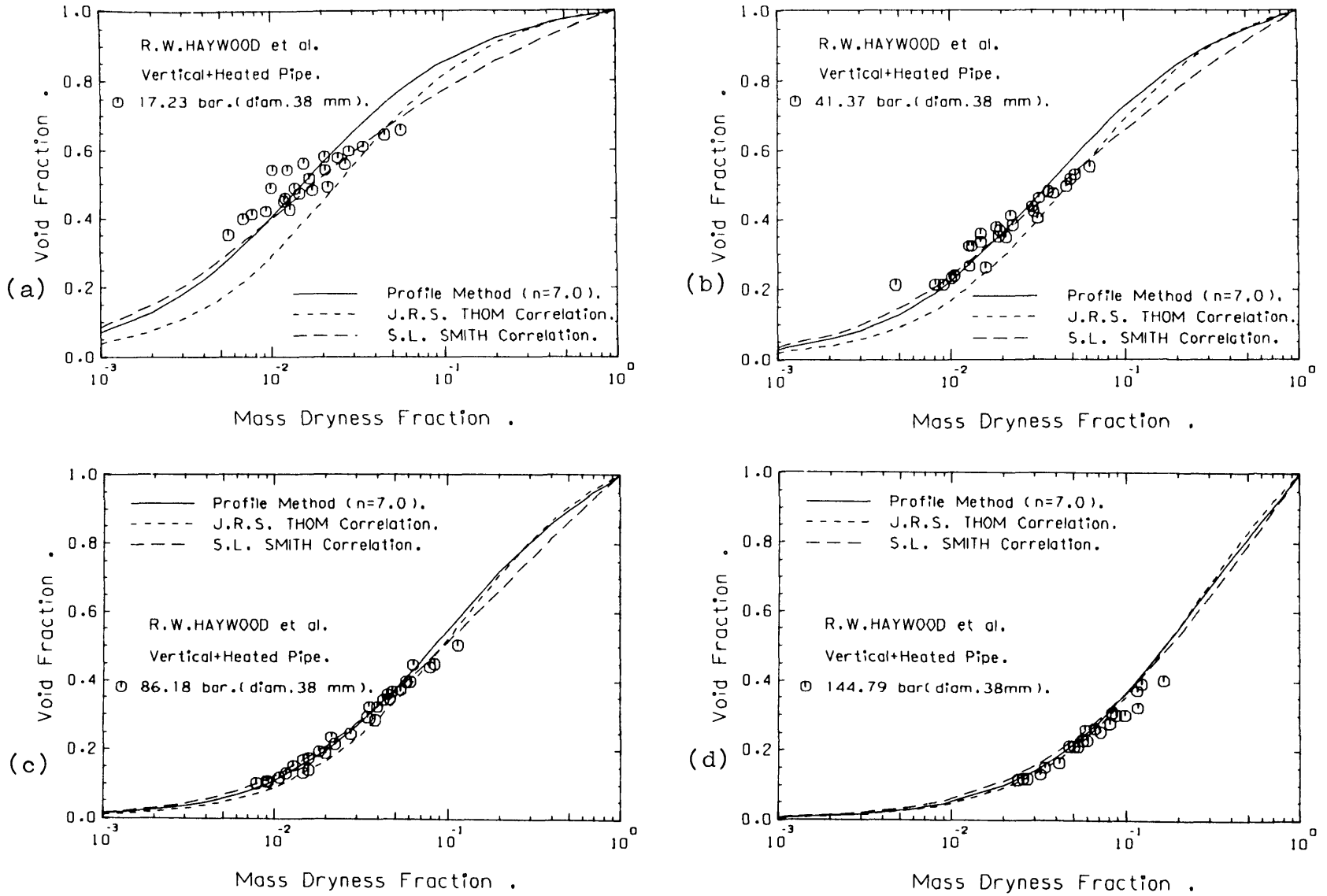

2.6 The void fraction, mass-dryness fraction relation for boiling water in a vertical heated pipe.

(a)

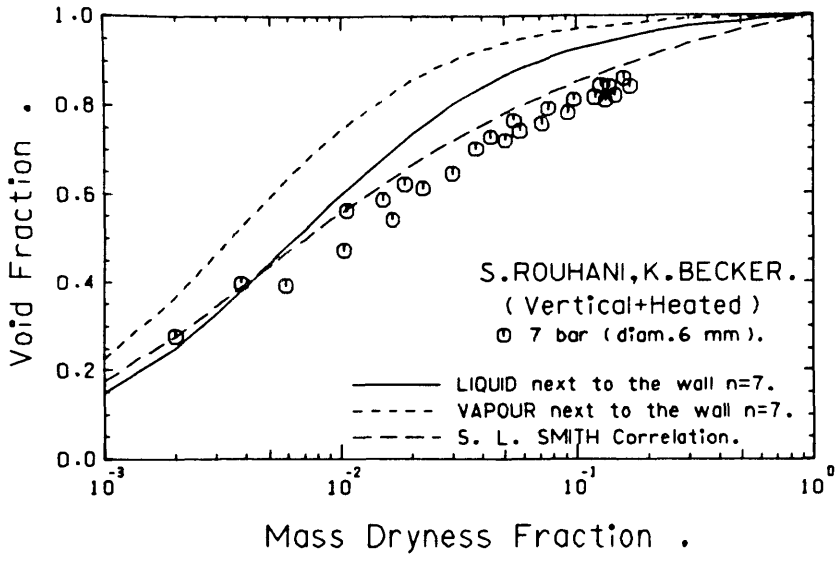
Void Fraction .
1.0
0.8
0.6
0.4
0.2
0.0
10^{-3}
10^{-2}
10^{-1}
10^{0}
S.ROUHANI, K.BECKER.
(Vertical+Heated)
① 7 bar (diam.6 mm).
LIQUID next to the wall n=7.
VAPOUR next to the wall n=7.
S. L. SMITH Correlation.
Mass Dryness Fraction .

(b)

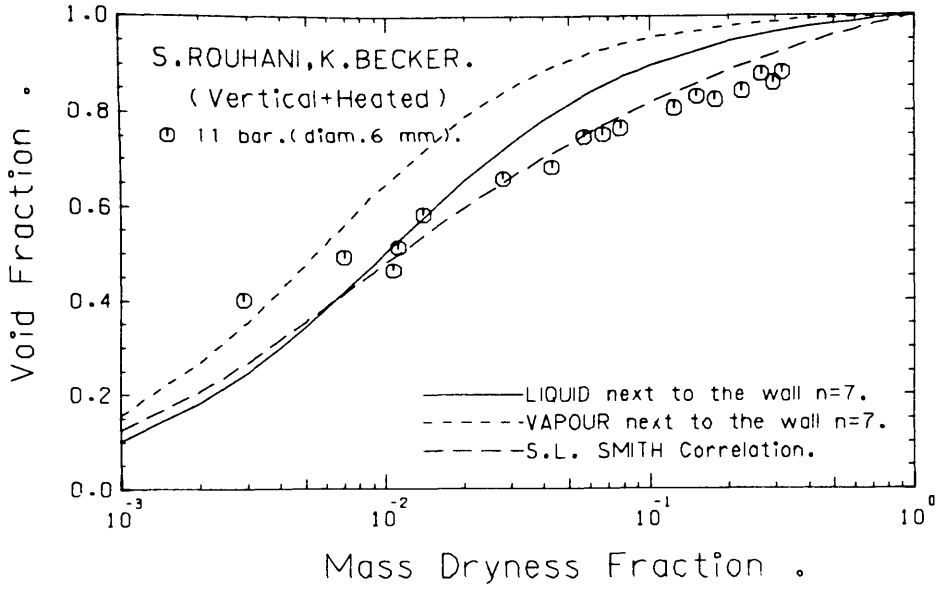
Void Fraction .
1.0
0.8
0.6
0.4
0.2
0.0
10^{-3}
10^{-2}
10^{-1}
10^{0}
S.ROUHANI, K.BECKER.
(Vertical+Heated)
① 11 bar.(diam.6 mm).
LIQUID next to the wall n=7.
VAPOUR next to the wall n=7.
S.L. SMITH Correlation.
Mass Dryness Fraction .

(c)

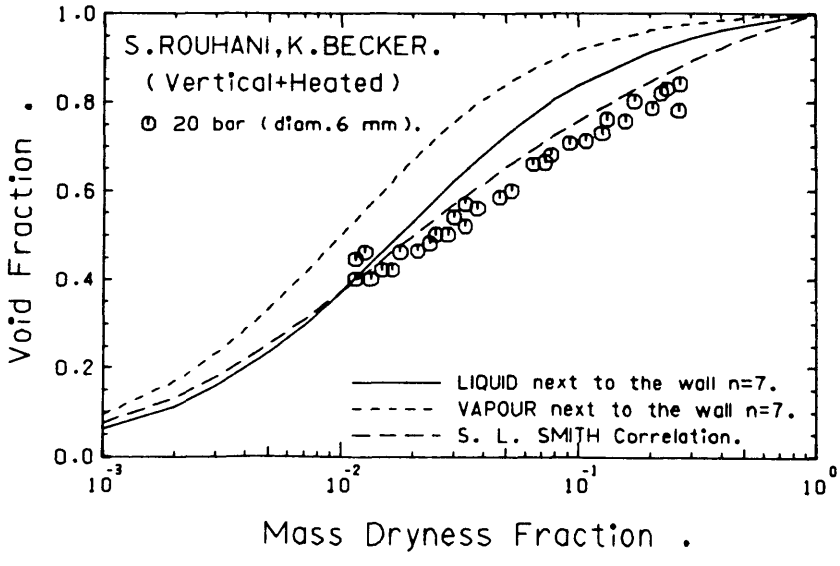
Void Fraction .
1.0
0.8
0.6
0.4
0.2
0.0
10^{-3}
10^{-2}
10^{-1}
10^{0}
S.ROUHANI, K.BECKER.
(Vertical+Heated)
① 20 bar (diam.6 mm).
LIQUID next to the wall n=7.
VAPOUR next to the wall n=7.
S. L. SMITH Correlation.
Mass Dryness Fraction .

(d)

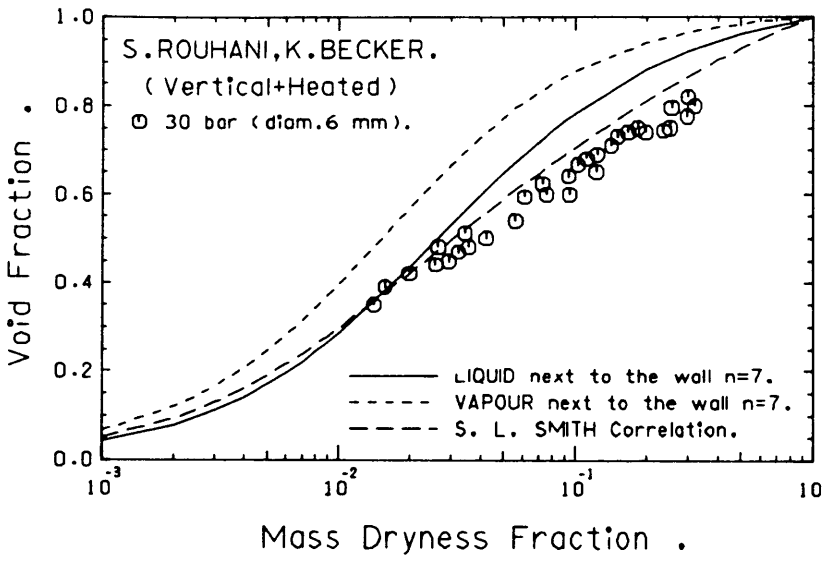

(e)

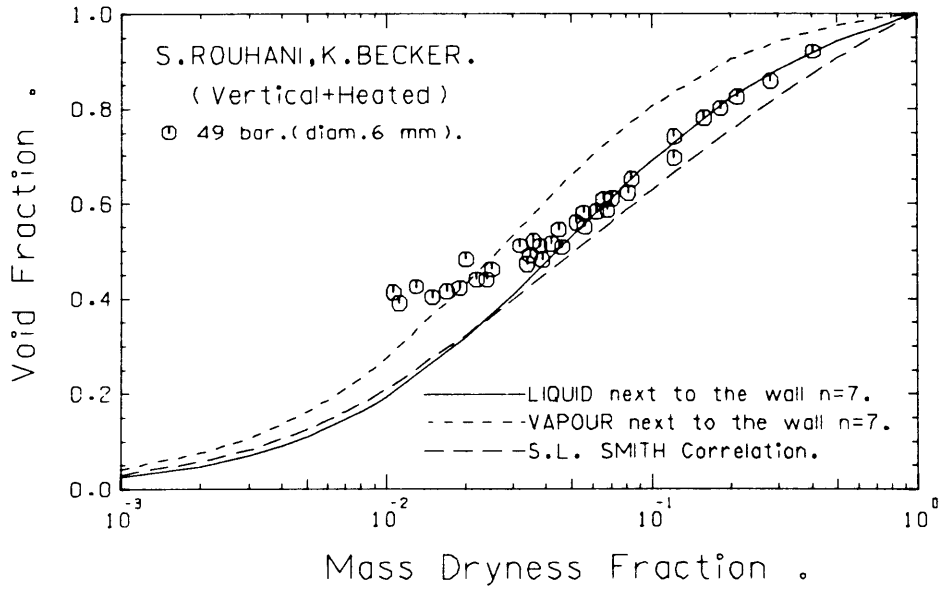

(f)

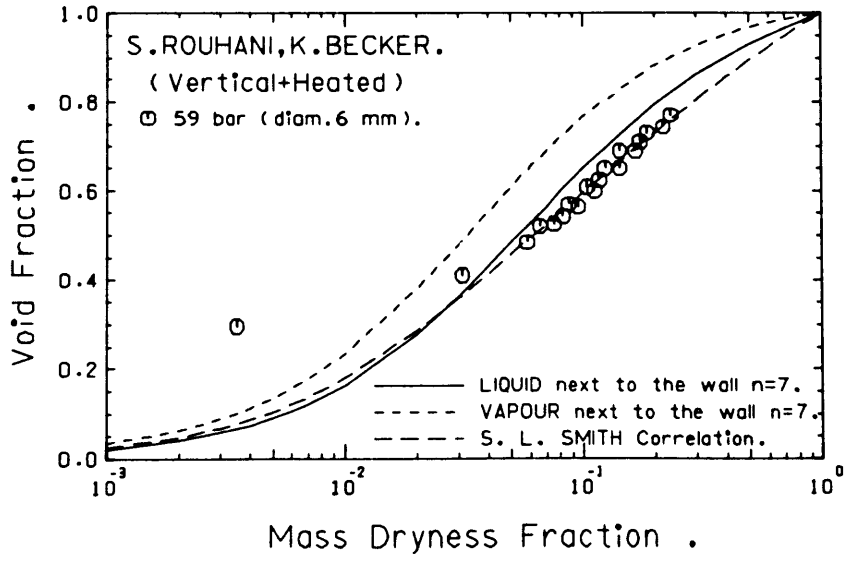

2.7 The void fraction, mass-dryness fraction relation for boiling heavy water in vertical pipe.

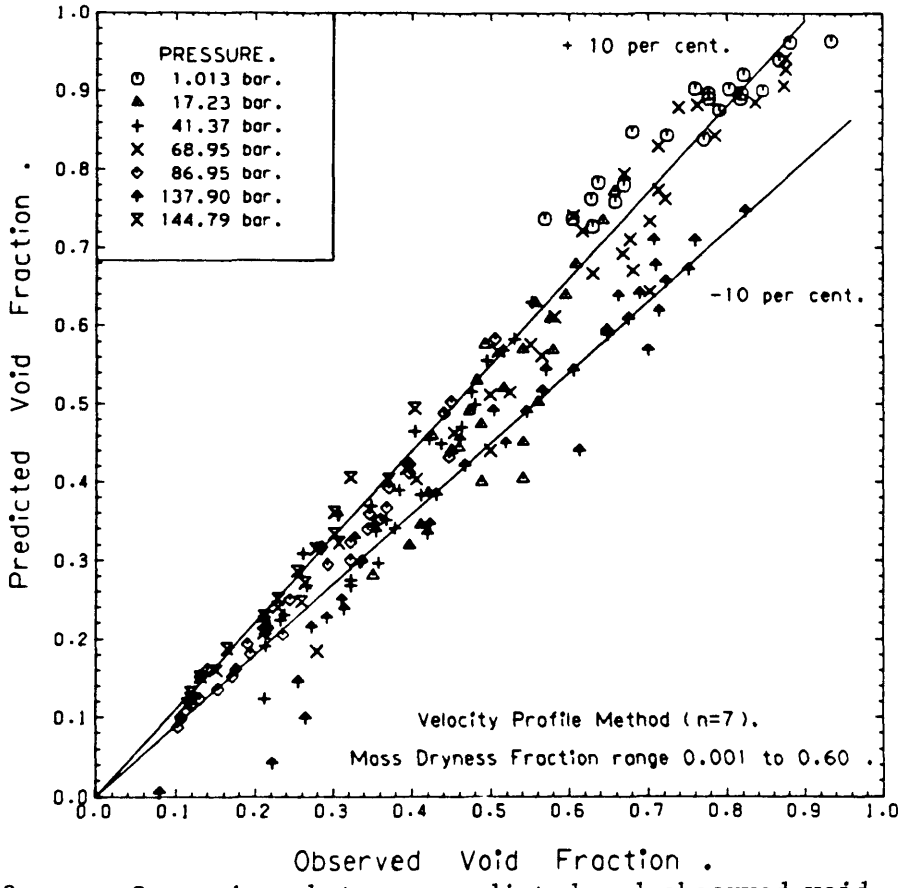

2.8 Comparison between predicted and observed void fractions for steam-water flows.

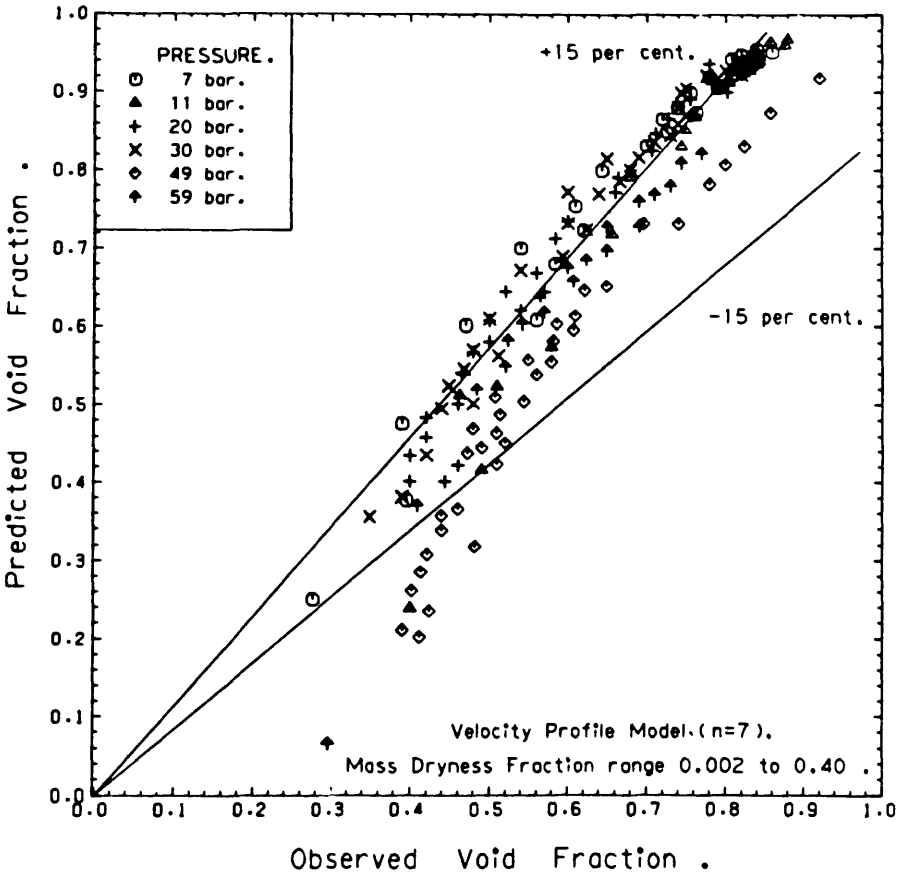

2.9 Comparison between predicted and observed void fraction for boiling heavy water flows.

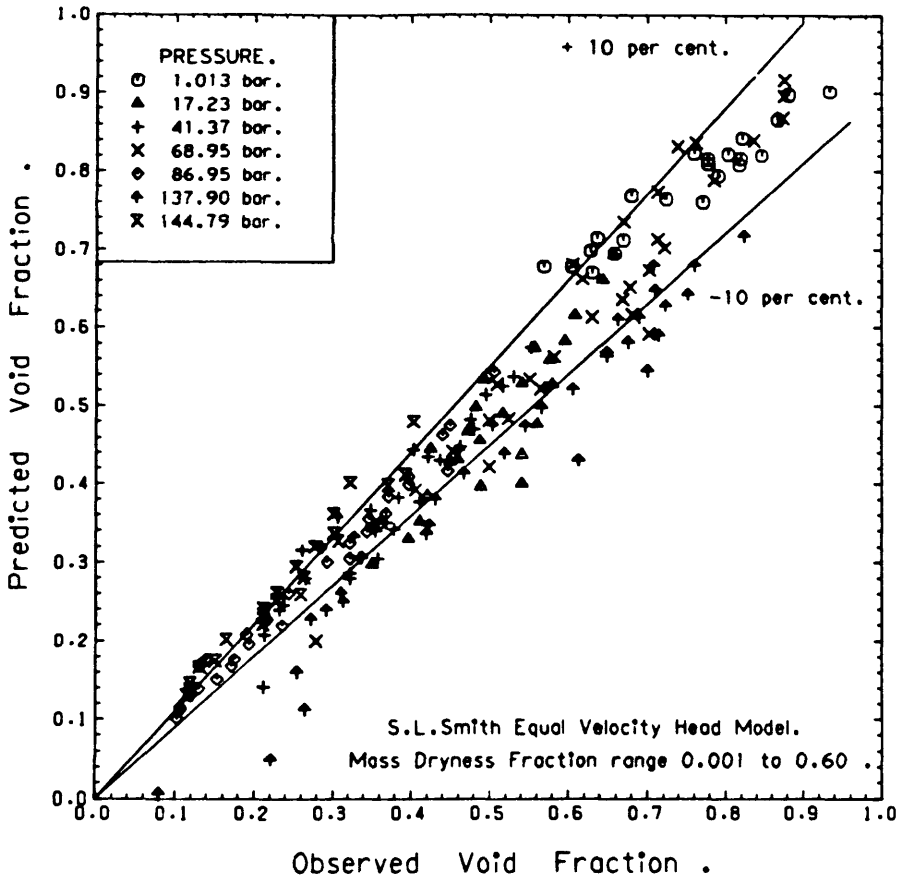

2.10 Predicted and observed void fractions by S L Smith for steam-water flows.

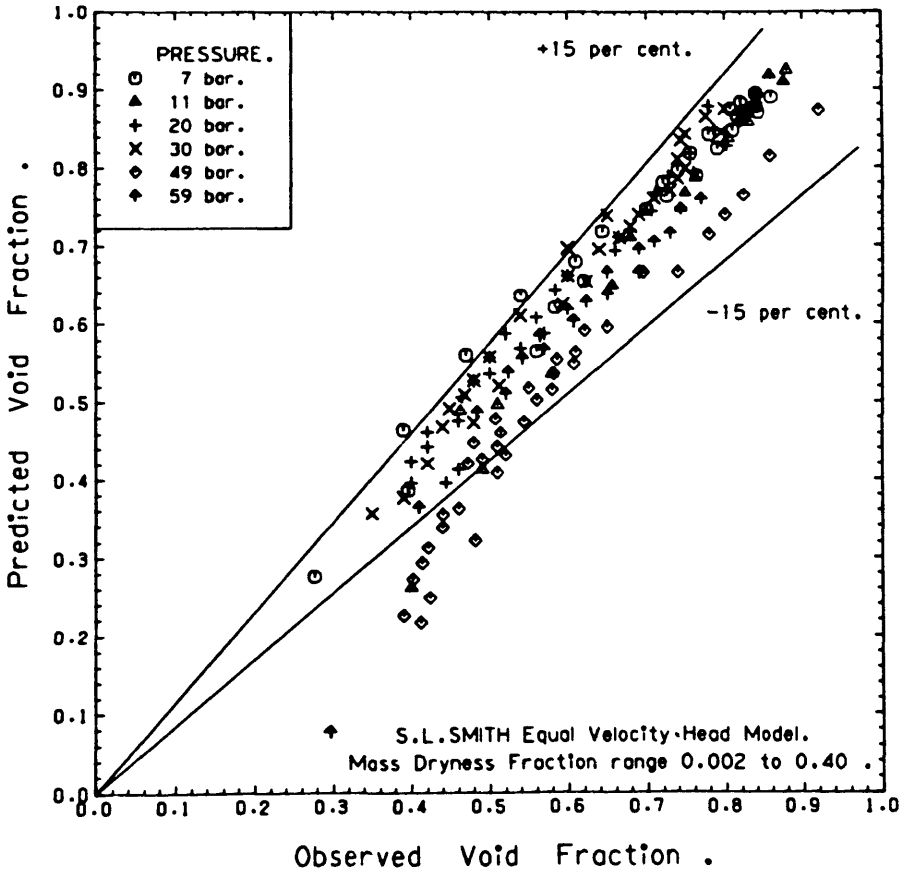

2.11 Predicted and observed void fractions by S L Smith for boiling heavy water flows.

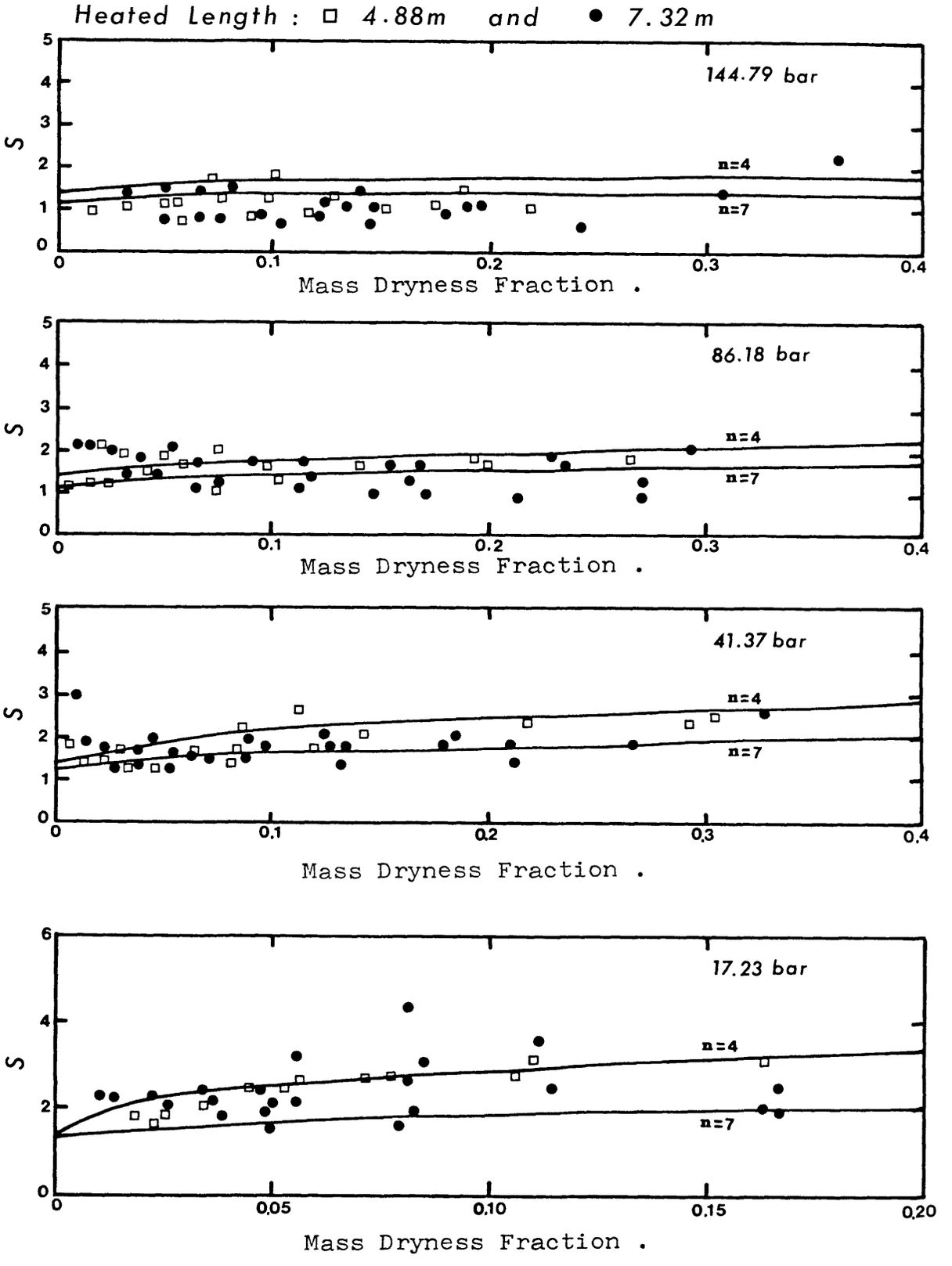

2.12 The ratio of average vapour and liquid velocities (S) as a function of mass dryness fraction for a 25.4 mm tube (L1V2).

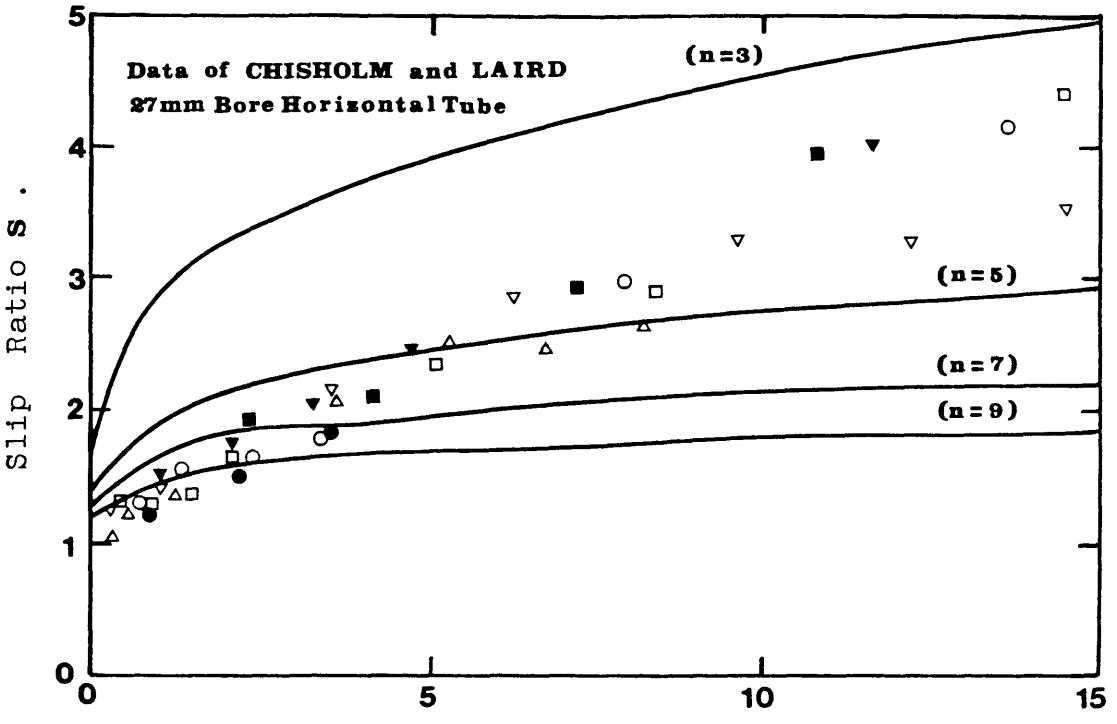

2.13 The ratio **S** for small ratios of gas to liquid volume flow rates (L1V2).

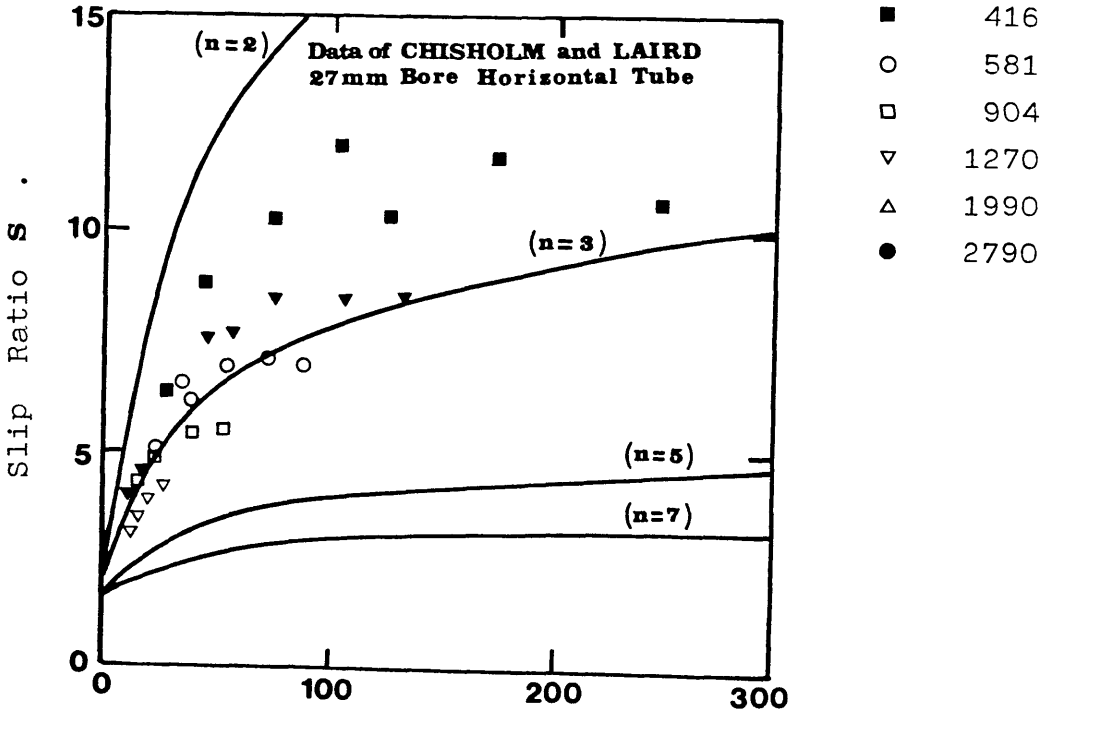

2.14 The ratio **S** for high ratios of gas to liquid volume flow rates (L1V2).

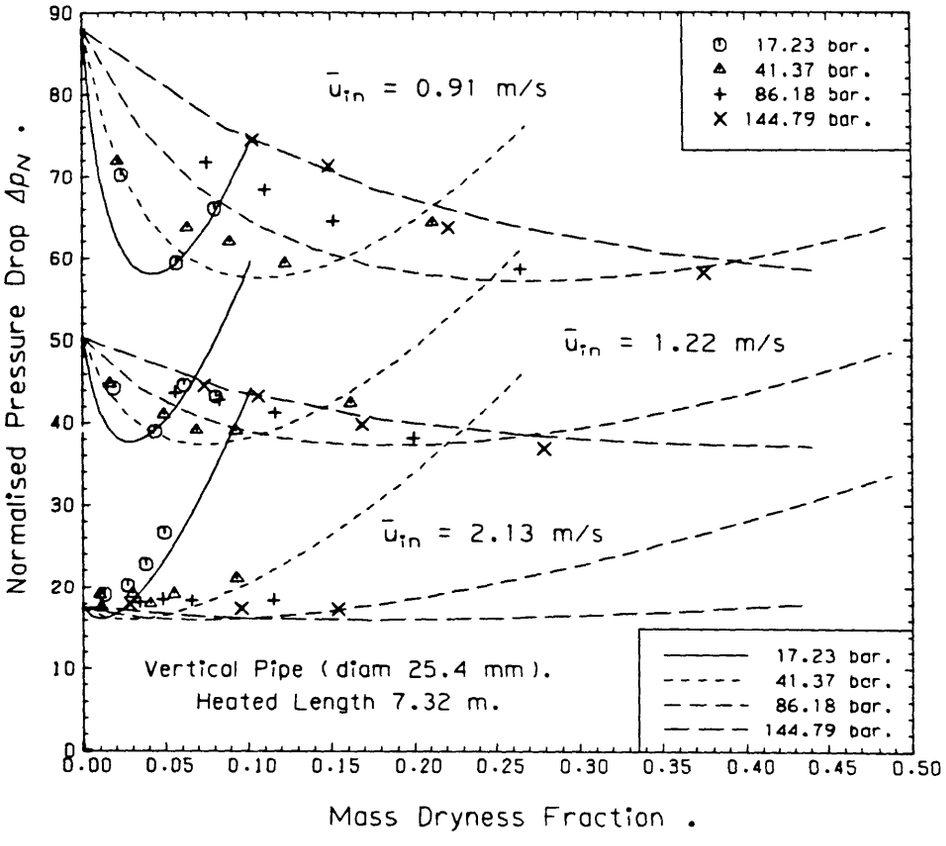

2.15 Normalised pressure drop for vertical heated pipe flow (25.4 mm diameter).

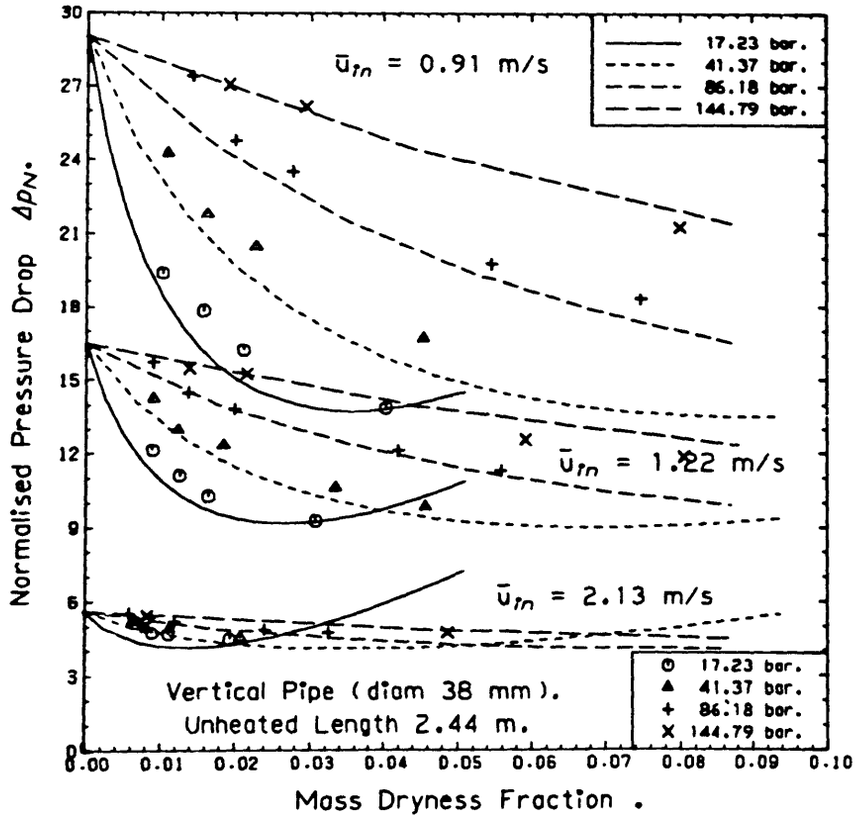

2.16 Normalised pressure drop for vertical unheated pipe flow (38 mm diameter).

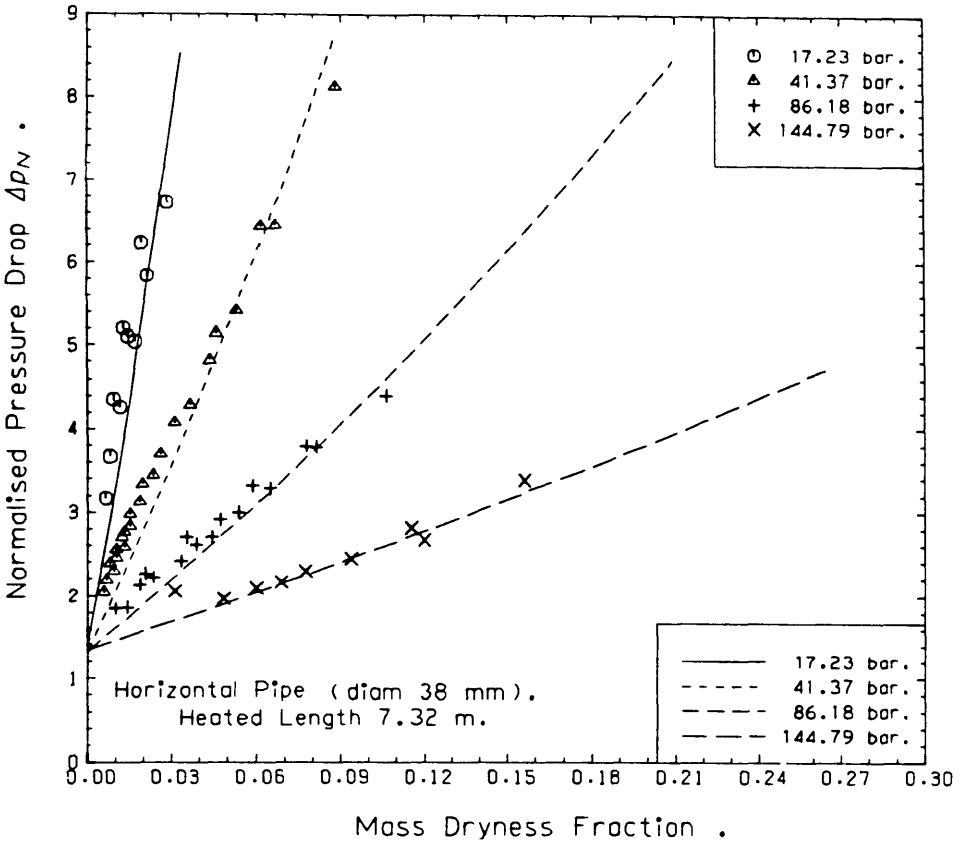

2.17 Normalised pressure drop for horizontal heated pipe flow (38 mm diameter).

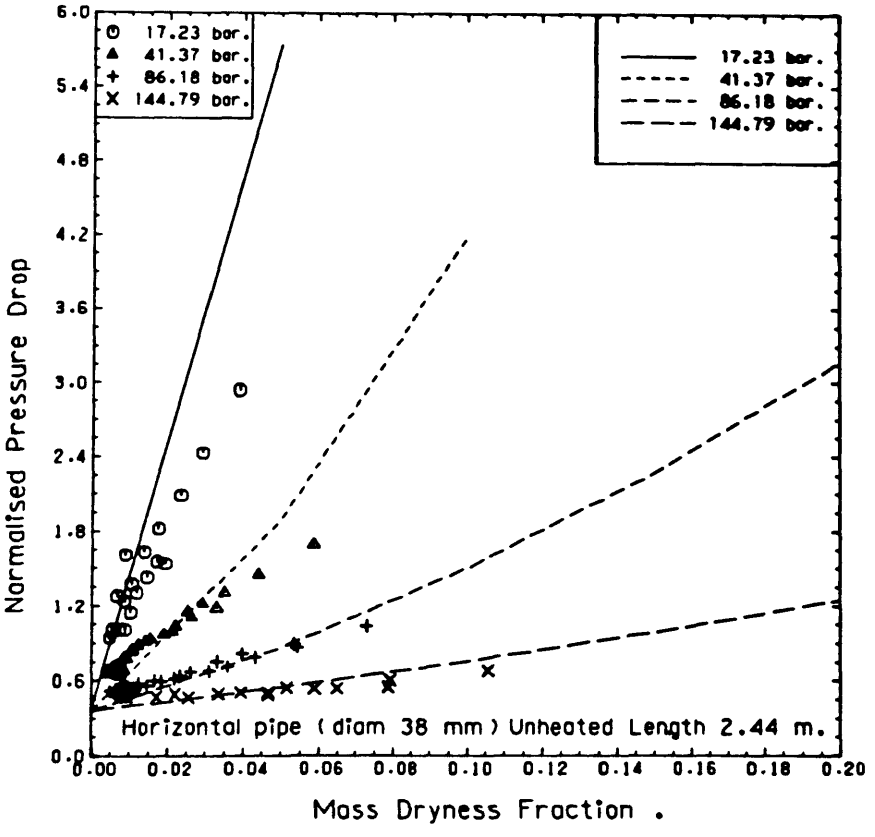

2.18 Normalised pressure drop for horizontal unheated pipe flow (38 mm diameter).

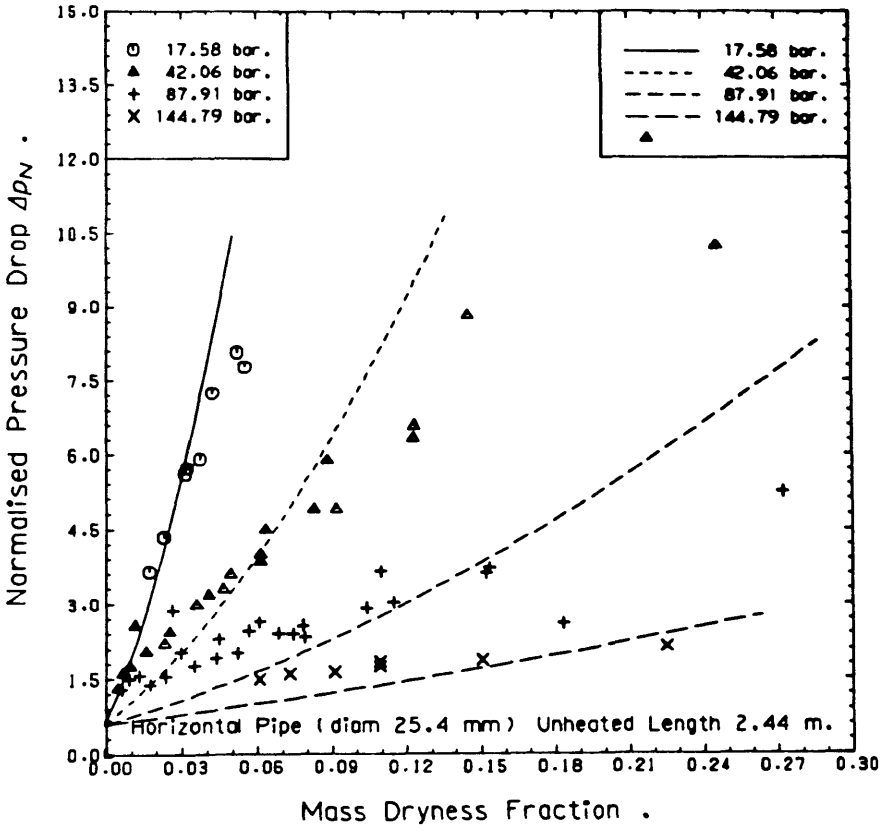

2.19 Normalised pressure drop for horizontal unheated pipe flow (25.4 mm diameter).

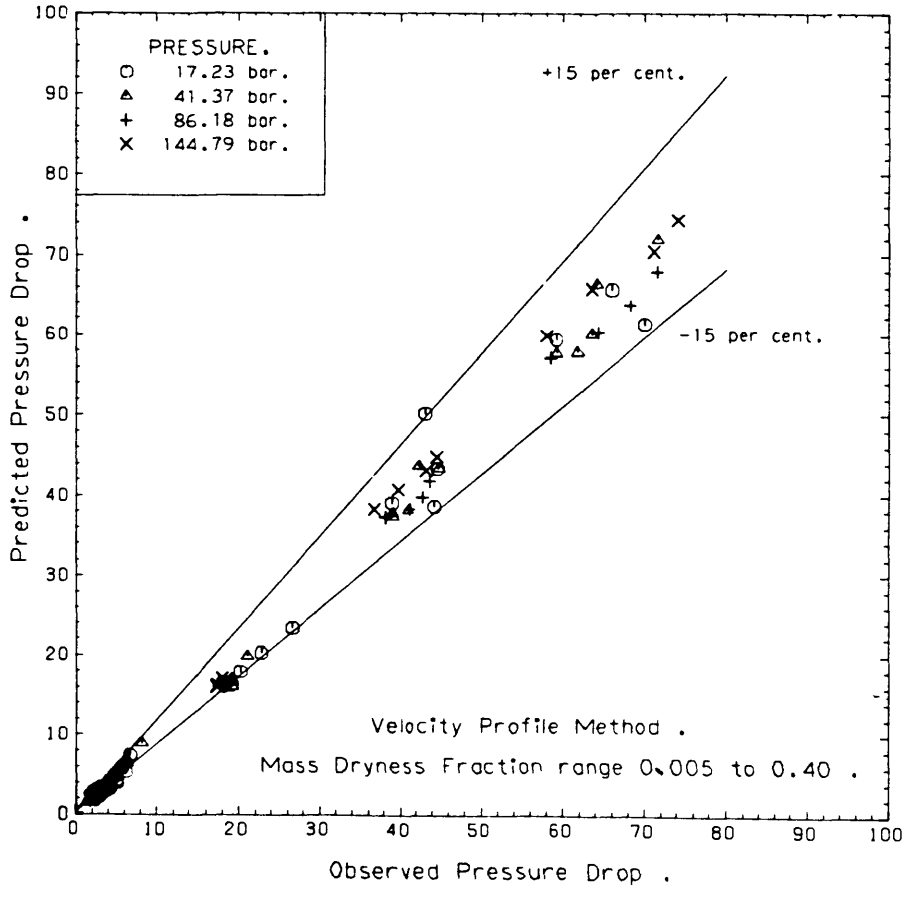

2.20 Comparison between predicted and observed pressure drop.

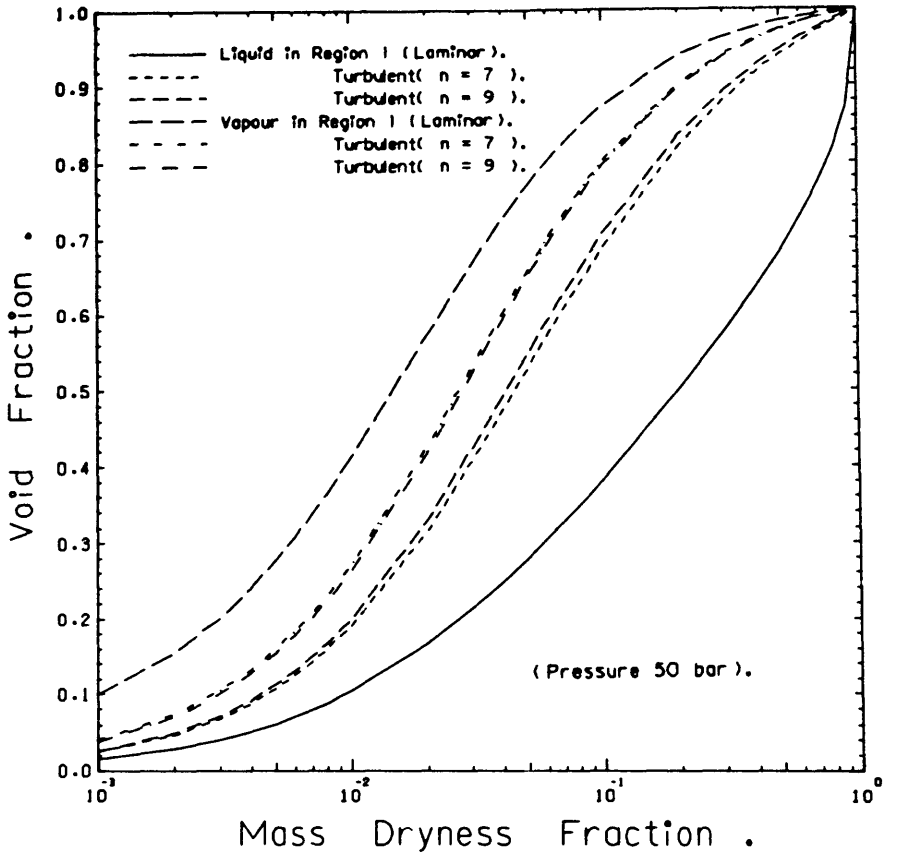

2.21 Predicted void fractions for laminar and turbulent flows for L1V2 and V1L2.

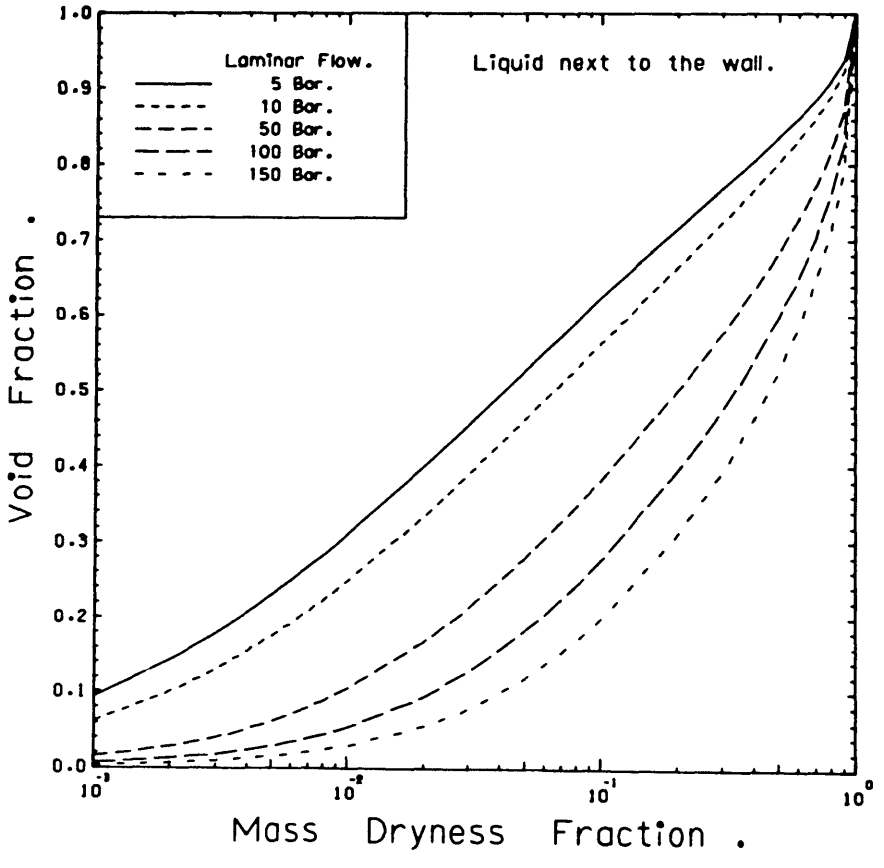

2.22 Predicted void fractions for laminar flows at different operating pressures.

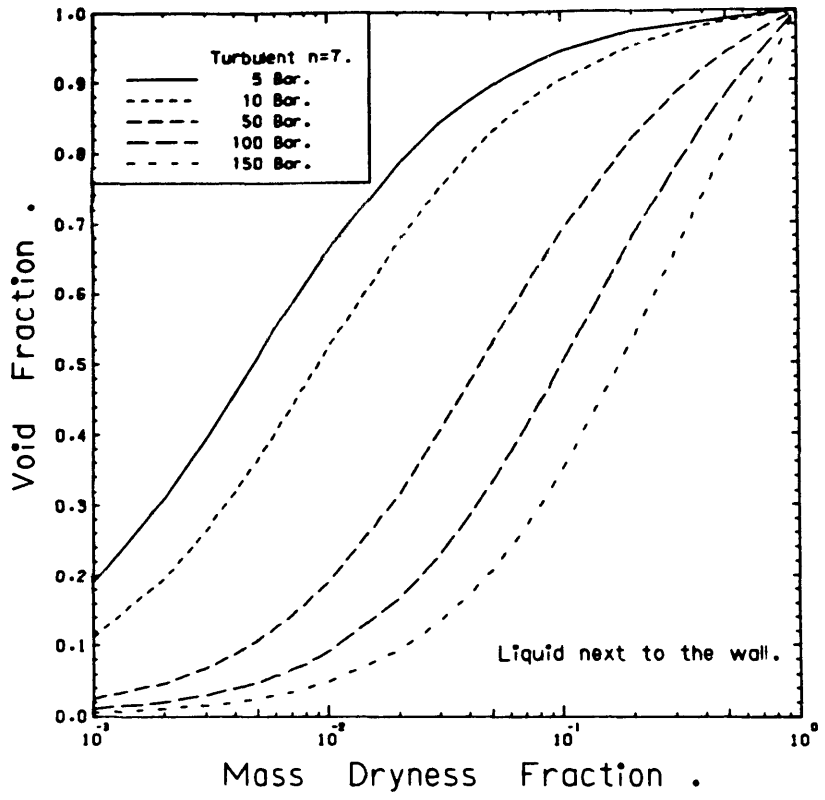

2.23 Predicted void fractions for turbulent flows at different operating pressures.

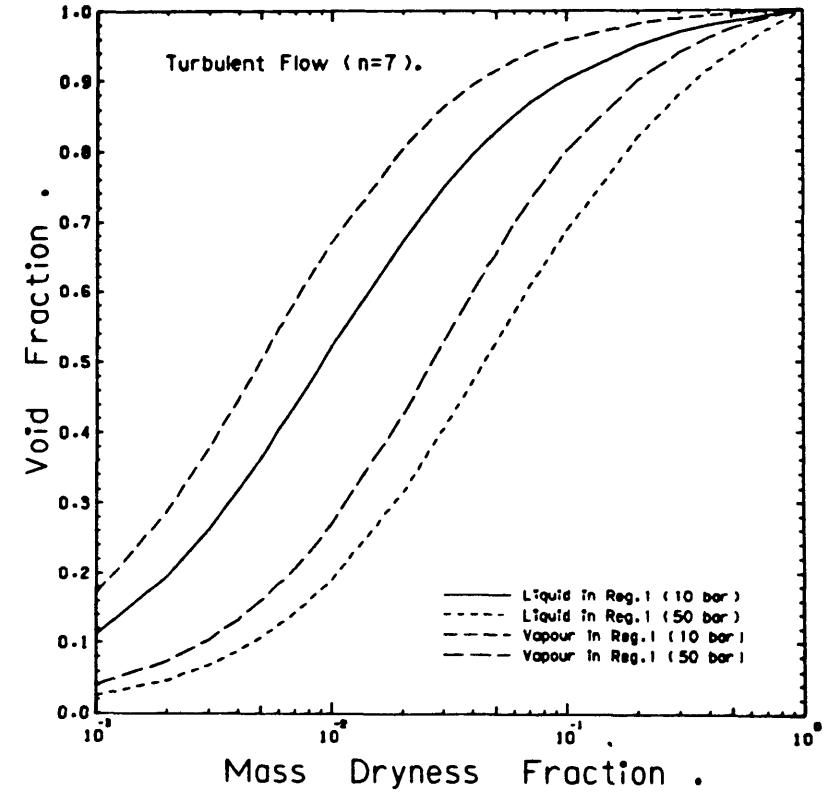

2.24 Predicted void fractions at different operating pressures for liquid or vapour next to the wall.

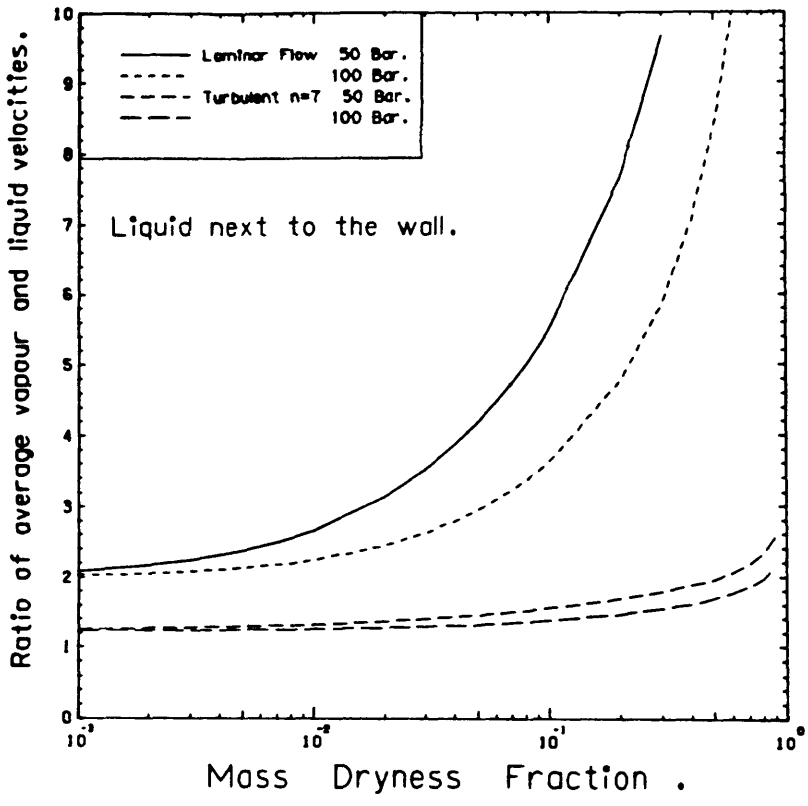

2.26 The ratio of average vapour and liquid velocities (S) at different operating pressures.

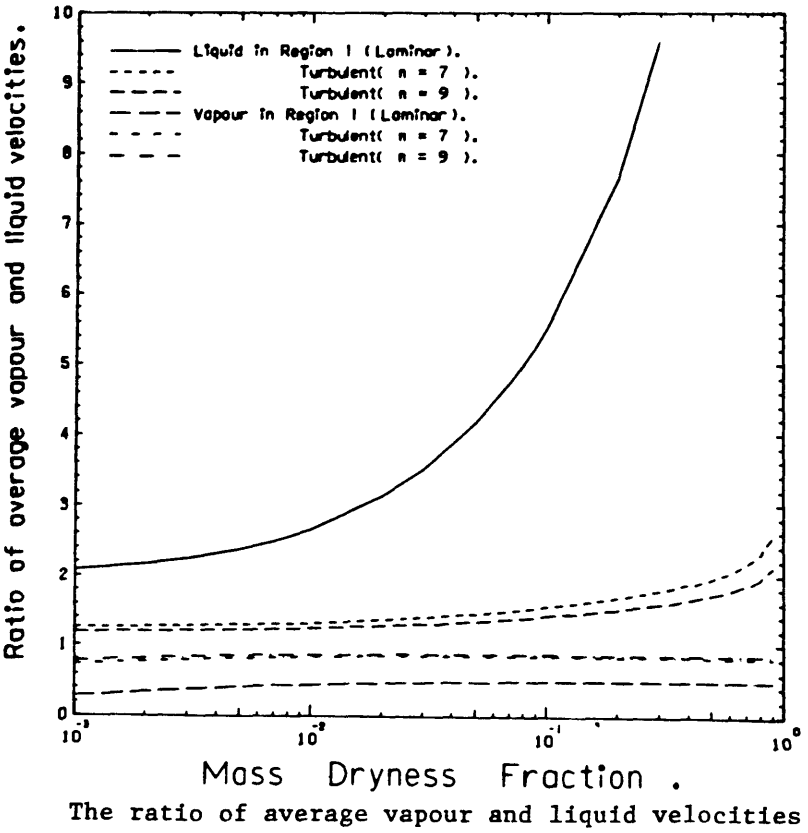

2.25 The ratio of average vapour and liquid velocities (S) for laminar and turbulent flows when L1V2 and V1L2.

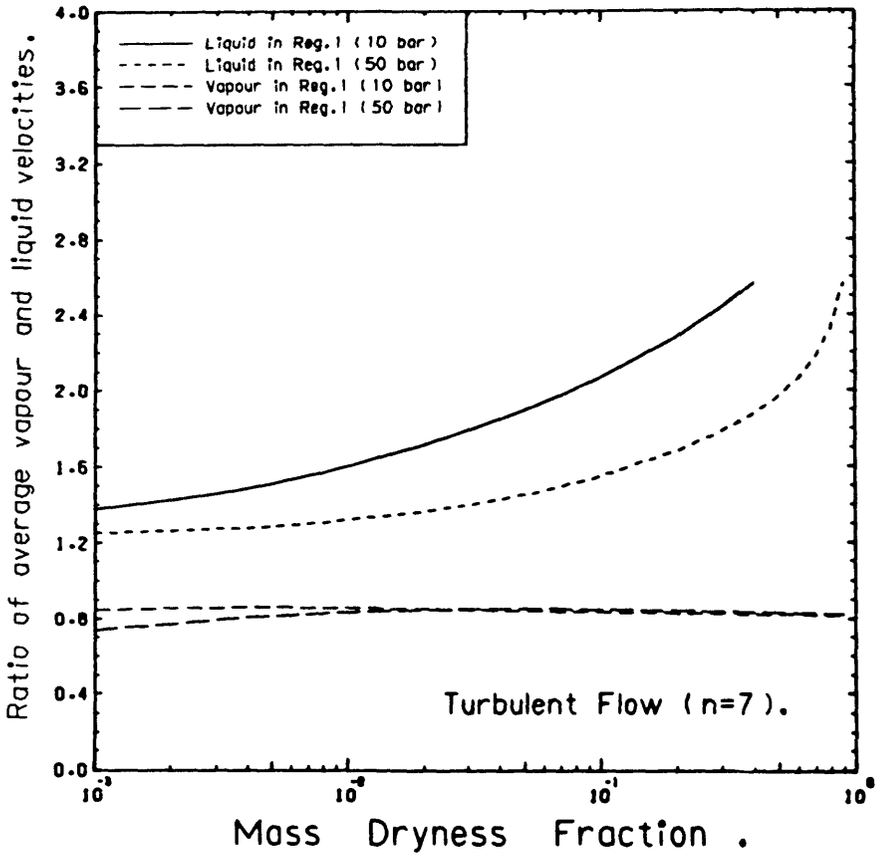

2.27 The ratio of average vapour and liquid velocities at different operating pressures for liquid or vapour next to the wall.

A - 2.2 Tables for Chapter 2.

LAMINAR FLOW

$$\int_{r_s}^{r_o} \left(1 - \frac{r^2}{r_o^2}\right) r\, dr = \frac{1}{4r_o^2} \left[r_o^2 - r_s^2 \right]^2$$

$$\int_{0}^{r_s} \left(1 - \frac{r^2}{r_h^2}\right) r\, dr = \frac{r_s^2}{4r_h^2} \left[2r_h^2 - r_s^2 \right]$$

$$\int_{r_s}^{r_o} \left(1 - \frac{r^2}{r_o^2}\right)^2 r\, dr = \frac{1}{2r_o^4} \left[\frac{1}{3} (r_o^6 - r_s^6) - r_o^2 r_s^2 (r_o^2 - r_s^2) \right]$$

$$\int_{0}^{r_s} \left(1 - \frac{r^2}{r_h^2}\right)^2 r\, dr = \frac{r_s^2}{2r_h^4} \left[r_h^4 - r_h^2 r_s^2 + \frac{1}{3} r_s^4 \right]$$

TURBULENT FLOW

$$\int_{r_s}^{r_o} \left(1 - \frac{r}{r_o}\right)^{1/n} r\, dr = r_o \left(\frac{n}{n+1}\right) \left(\frac{n}{2n+1}\right) \left(1 - \frac{r_s}{r_o}\right)^{\frac{n+1}{n}} \left[\left(\frac{n+1}{n}\right) r_s + r_o \right]$$

$$\int_{0}^{r_s} \left(1 - \frac{r}{r_h}\right)^{1/n} r\, dr = r_h \left(\frac{n}{n+1}\right) \left(\frac{n}{2n+1}\right) \left(1 - \frac{r_s}{r_h}\right)^{\frac{n+1}{n}} \left[r_h \left(\frac{r_h}{r_h - r_s}\right)^{\frac{n+1}{n}} - r_h - \left(\frac{n+1}{n}\right) r_s \right]$$

$$\int_{r_s}^{r_o} \left(1 - \frac{r}{r_o}\right)^{2/n} r\, dr = r_o \left(\frac{n}{n+2}\right) \left(\frac{n}{2n+2}\right) \left(1 - \frac{r_s}{r_o}\right)^{\frac{n+2}{n}} \left[\frac{2n+1}{n} r_s + r_o \right]$$

$$\int_{0}^{r_s} \left(1 - \frac{r}{r_h}\right)^{2/n} r\, dr = r_h \left(\frac{n}{n+2}\right) \left(\frac{n}{2n+2}\right) \left(1 - \frac{r_s}{r_h}\right)^{\frac{n+2}{n}} \left[r_h \left(\frac{r_h}{r_h - r_s}\right)^{\frac{n+2}{n}} - r_h - \left(\frac{n+2}{n}\right) r_s \right]$$

2.1 List of the important integrals used by the velocity profile model.

Two-phase Flow Parameters	Laminar	Turbulent
Density Ratio (R_D)	$R_D \equiv (\rho_2/\rho_1)^{1/2}$	$R_D \equiv (\rho_2/\rho_1)^{1/2}$
Viscosity Ratio (R_V)	$R_V \equiv (\mu_2/\mu_1)^{1/2}$	$R_V \equiv \left[\frac{\mu_2}{\mu_1}\right]_t^{1/2} = \left[\frac{\rho_2}{\rho_1}\right]^{1/4}$
Ratio of Relative Pipe Radius	$\left[\frac{r_h}{r_o}\right]^2 = \left[\frac{r_s}{r_o}\right]^2 + R_V^2\left[1 - \frac{r_s^2}{r_o^2}\right]$	$\left[\frac{r_h}{r_o}\right] = \left[\frac{r_s}{r_o}\right] + R_D\left[1 - \frac{r_s}{r_o}\right]$
Maximum Velocity Ratio	$\frac{u_{max,2}}{u_{max,1}} = \left[\frac{1}{R_V}\frac{r_h}{r_o}\right]^2 = \left[\frac{r_h}{r_o}\right]^2\left[\frac{r_o^2 - r_s^2}{r_h^2 - r_s^2}\right]$	$\frac{u_{max,2}}{u_{max,1}} = \left[\frac{1}{R_D}\frac{r_h}{r_o}\right]^{1/n} = \left[\frac{r_h}{r_o} \cdot \frac{r_o - r_s}{r_h - r_s}\right]^{1/n}$
Mass Flow Rate Ratio	$\frac{\dot{m}_2}{\dot{m}_1} = R_D^2\left[\frac{r_s^2}{r_o^2 - r_s^2}\right]\left[\frac{2r_h^2 - r_s^2}{r_h^2 - r_s^2}\right]$	$\frac{\dot{m}_2}{\dot{m}_1} = R_D^3\left[\frac{r_h\left(\frac{r_h}{r_h - r_s}\right)^{\frac{n+1}{n}} - r_h - \left(\frac{n+1}{n}\right)r_s}{\left(\frac{n+1}{n}\right)r_s + r_o}\right]$
Average Velocity Ratio	$\frac{\bar{u}_2}{\bar{u}_1} = \left[\frac{2r_h^2 - r_s^2}{r_h^2 - r_s^2}\right]$	$\frac{\bar{u}_2}{\bar{u}_1} = R_D \cdot \frac{r_o^2 - r_s^2}{r_s^2}\left[\frac{r_h\left(\frac{r_h}{r_h - r_s}\right)^{\frac{n+1}{n}} - r_h - \left(\frac{n+1}{n}\right)r_s}{\left(\frac{n+1}{n}\right)r_s + r_o}\right]$

2.2 The two-phase flow parameters of the velocity profile model in laminar and turbulent flows.

Reference	Correlation for $S \equiv \bar{u}_2/\bar{u}_1$
Lockhart and Martinelli (Lo49)	$S = \left(\frac{x}{1-x}\right)\left(\frac{\rho_g}{\rho_\ell}\right)\left(\frac{1-\alpha}{\alpha}\right)$ where $\alpha = fn\ (X)\ ,\ X \equiv \left[\left(\frac{dp}{ds}\right)_\ell \Big/ \left(\frac{dp}{ds}\right)_g\right]^{1/2}$
Hughmark (Hu62)	$S = \left(\frac{x}{1-x}\right)\left(\frac{\rho_g}{\rho_\ell}\right)\left(\frac{1-\alpha}{\alpha}\right)$ where $\alpha = k\,\beta$ with $\beta = \frac{x}{x + (\rho_g/\rho_\ell)(1-x)}$ $k = fn\left(Re\ ,\ \frac{G^2}{\rho_\ell^2\, gd}\ ,\ 1-\beta\right)$
Thom (Th64)	$S = fn\left(\rho_\ell/\rho_g\right)$
Smith (Sm70)	$S = e + (1-e)\left[\frac{\rho_\ell/\rho_g + e(1/x - 1)}{1 + e(1/x - 1)}\right]^{1/2}$ with $e \equiv 0.40$
Chisholm (Ch73)	$S = \left[x\left(\frac{\rho_\ell}{\rho_g}\right) + 1 - x\right]^{1/2}$
Bryce (Br77)	$S = \left[\frac{1-\alpha}{A - \alpha + (1-A)\,\alpha^B}\right]$ where $A = fn\left(p, G, x, \rho_g, \rho_\ell\right)$ $B = fn\left(p, \rho_g, \rho_\ell\right)$
Velocity Profile (1983)	$S = fn\left(\frac{r_h}{r_o}, \frac{r_s}{r_o}, \frac{\rho_g}{\rho_\ell}, n\right)$ where $\frac{r_s}{r_o} = fn(\alpha)$, $\frac{r_h}{r_s} = fn(\alpha, \rho_g/\rho_\ell)$ and $n = fn(G)$.

2.3 Slip correlations for steam-water flows with liquid next to the wall.

References	Two-phase mixture	Range of Experimental Conditions.					Description.
		p(bar)	$\dot{q}''$(kW/m^2)	G(kg/m^2-s)	d(mm)	$\theta°$	
Larson (La57).	Steam-Water	68.98	0			0.0	Void fraction and pressure drop for mass-dryness fractions up to 0.80 .
Isbin et.al. (Is57)	Steam-Water	1.013	0	292 - 876	22.0	90.0	Void fraction and pressure drop measurements for mass-dryness fractions up to 0.04 .
Egen et.al. (Eg57)	Steam-Water	137.9	946-1577	949 - 1220		90.0	Void fraction measurements for mass-dryness fractions up to 0.40 .
Chisholm and Laird (Ch58).	Air - Water	1.1 to 1.7	0	190 - 2800	27.0	0.0	Ratios of average velocities of the vapour and liquid phases , and pressure drops. Pipe length 2.44 metres.
Haywood et.al. (Ha61)	Steam-Water	17.2 to 145.0	20 - 140	750 - 1950	25.4 38.1	0.0 90.0	Void fraction and pressure drop measurements for mass-dryness fraction up to 0.4 . Pipe length up to 7.32 metres.
Rouhani and Becker (Ro63).	Heavy-Water	7.0 to 50.3	380-1200	650 - 2050	6.0	90.0	Void fraction measurements for mass-dryness fraction up to 0.38 . Pipe length 2.5 m.

2.4 Range of Experimental conditions for the tests used in comparisons.

Two-phase flow Parameters	LAMINAR		TURBULENT	
	$x \longrightarrow 0$	$x \longrightarrow 1$	$x \longrightarrow 0$	$x \longrightarrow 1$
Interface radius	$r_s = r_o$	$r_s = 0$	$r_s = r_o$	$r_s = 0$
Ratio of Relative Pipe Radius	$\frac{r_h}{r_o} = 1$	$\frac{r_h}{r_o} = R_V$	$\frac{r_h}{r_o} = 1$	$\frac{r_h}{r_o} = R_D$
Maximum Velocity Ratio	$\frac{u_{max,2}}{u_{max,1}} = \frac{1}{R_V}$	$\frac{u_{max,2}}{u_{max,1}} = 1$	$\frac{u_{max,2}}{u_{max,1}} = \frac{1}{R_D}$	$\frac{u_{max,2}}{u_{max,1}} = 1$
Mass Flow rate Ratio $(\dot{m}_2/\dot{m}_1)$	∞	0	∞	0
Ratio of average velocities of Region 2 and 1	∞	$\frac{\bar{u}_2}{\bar{u}_1} = 2$	∞	$\frac{\bar{u}_2}{\bar{u}_1} = \frac{(n+1)(2n+1)}{2n^2}$

2.5 Boundary conditions for all liquid and all vapour flows when vapour is next to the wall.

Two-phase flow Parameters	LAMINAR		TURBULENT	
	$x \rightarrow 0$	$x \rightarrow 1$	$x \rightarrow 0$	$x \rightarrow 1$
Interface radius	$r_s = 0$	$r_s = r_o$	$r_s = 0$	$r_s = r_o$
Ratio of Relative Pipe Radius	$\frac{r_h}{r_o} = R_V$	$\frac{r_h}{r_o} = 1$	$\frac{r_h}{r_o} = R_D$	$\frac{r_h}{r_s} = 1$
Maximum Velocity Ratio	$\frac{u_{max,2}}{u_{max,1}} = 1$	$\frac{u_{max,2}}{u_{max,1}} = \frac{1}{R_V}$	$\frac{u_{max,2}}{u_{max,1}} = 1$	$\frac{u_{max,2}}{u_{max,1}} = \frac{1}{R_D}$
Mass Flow rate Ratio $(\dot{m}_2/\dot{m}_1)$	0	∞	0	∞
Ratio of average velocities of Region 2 and 1	$\frac{\bar{u}_2}{\bar{u}_1} = 2$	∞	$\frac{\bar{u}_2}{\bar{u}_1} = \frac{(n+1)(2n+1)}{2n^2}$	∞

2.6 Boundary conditions for all liquid and all vapour flows when liquid is next to the wall.

A - 3.1 Figures for Chapter 3.

Shearing of roll - waves.

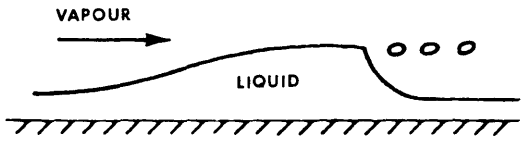

(a)

Wave undercut.

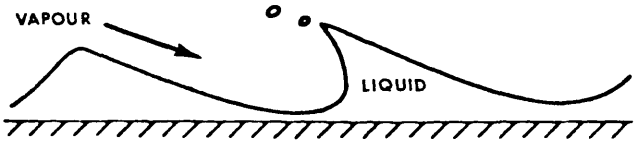

(b)

Bubble burst.

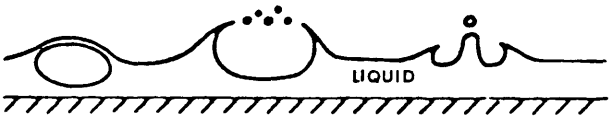

(c)

Impingement of large drops.

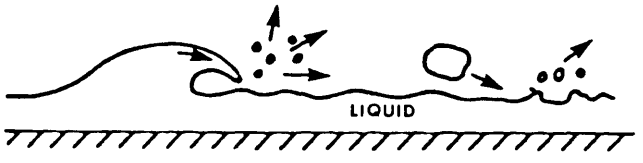

(d)

Liquid-bulge disintegration.

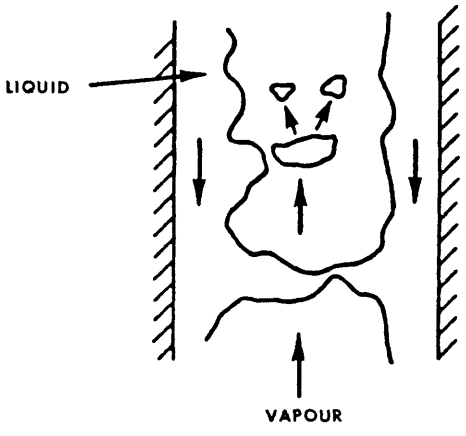

(e)

3.1 Various physical pictures of entrainment.

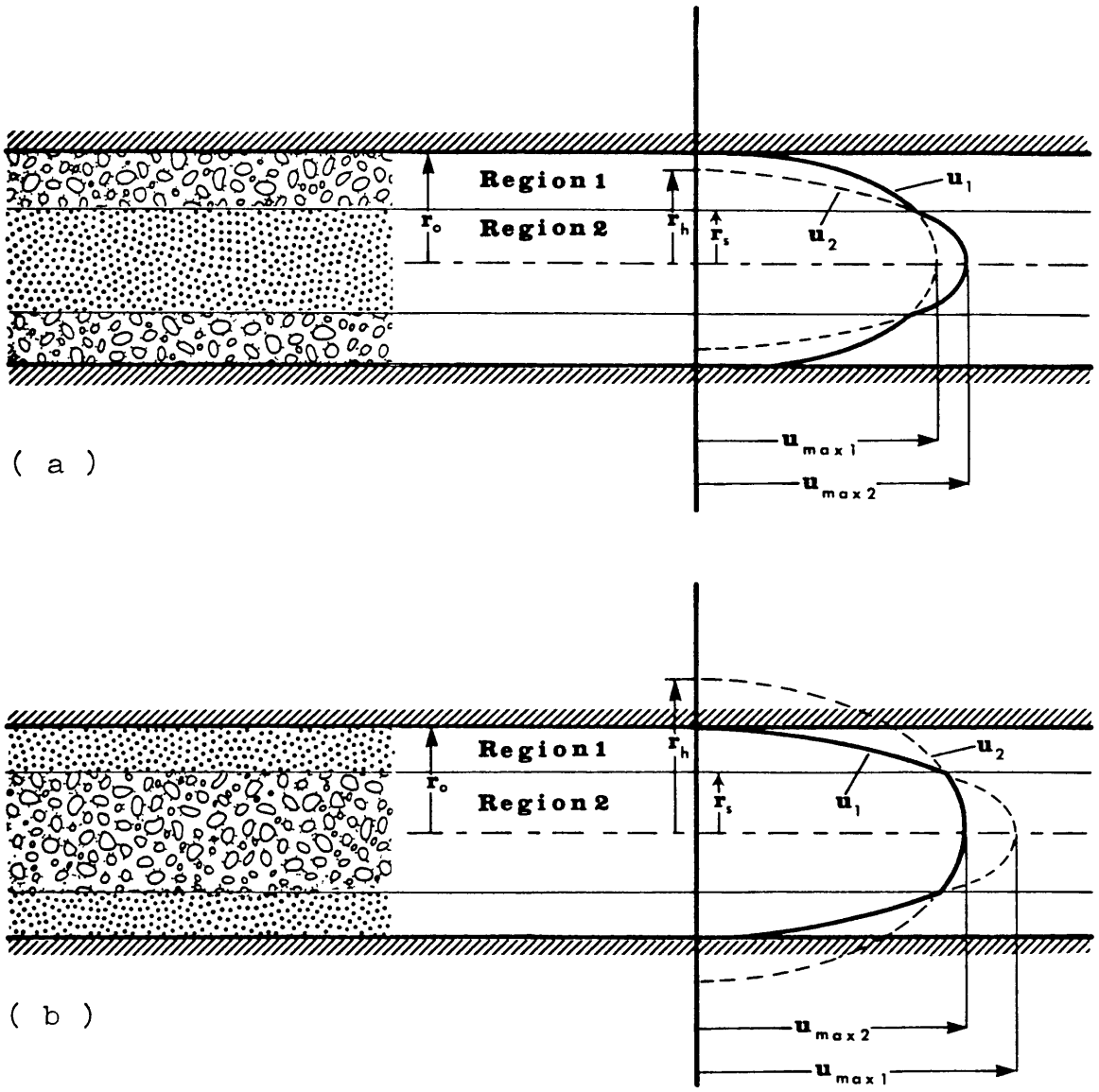

3.2 The assumed velocity profiles with (a) liquid and (b) vapour predominant in region 1.

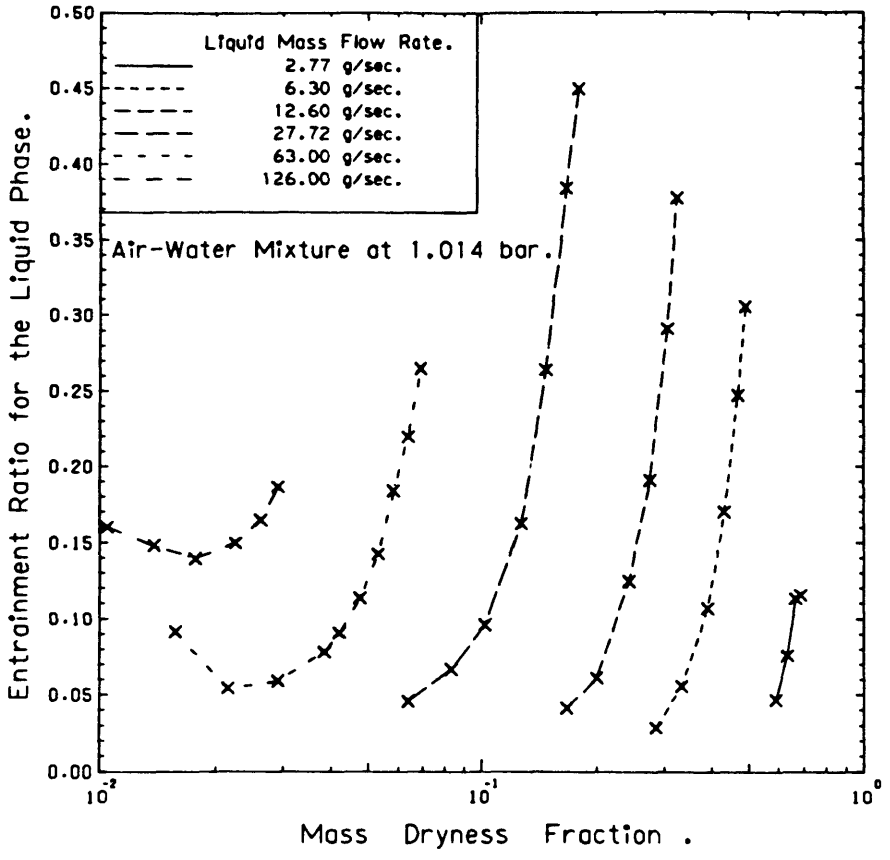

3.3 The measured entrainment ratios for the liquid.

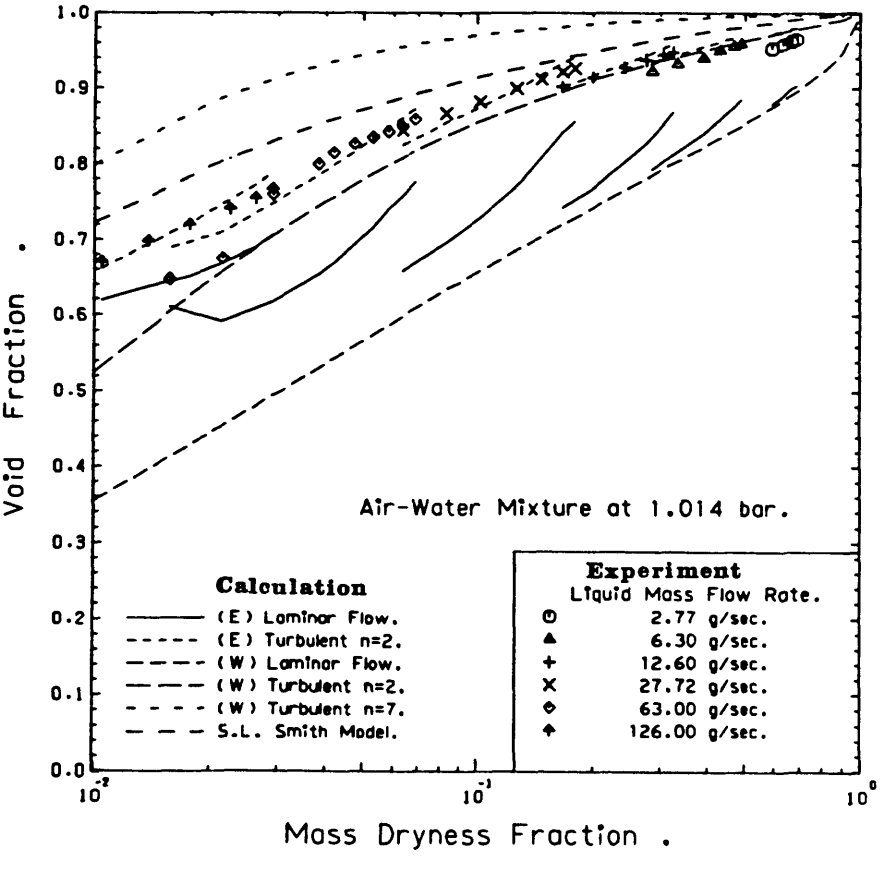

(E) Experimental Entrainment Ratios.
(W) Without Entrainment .

3.4 Experimental and predicted void fractions at different mass flow rates.

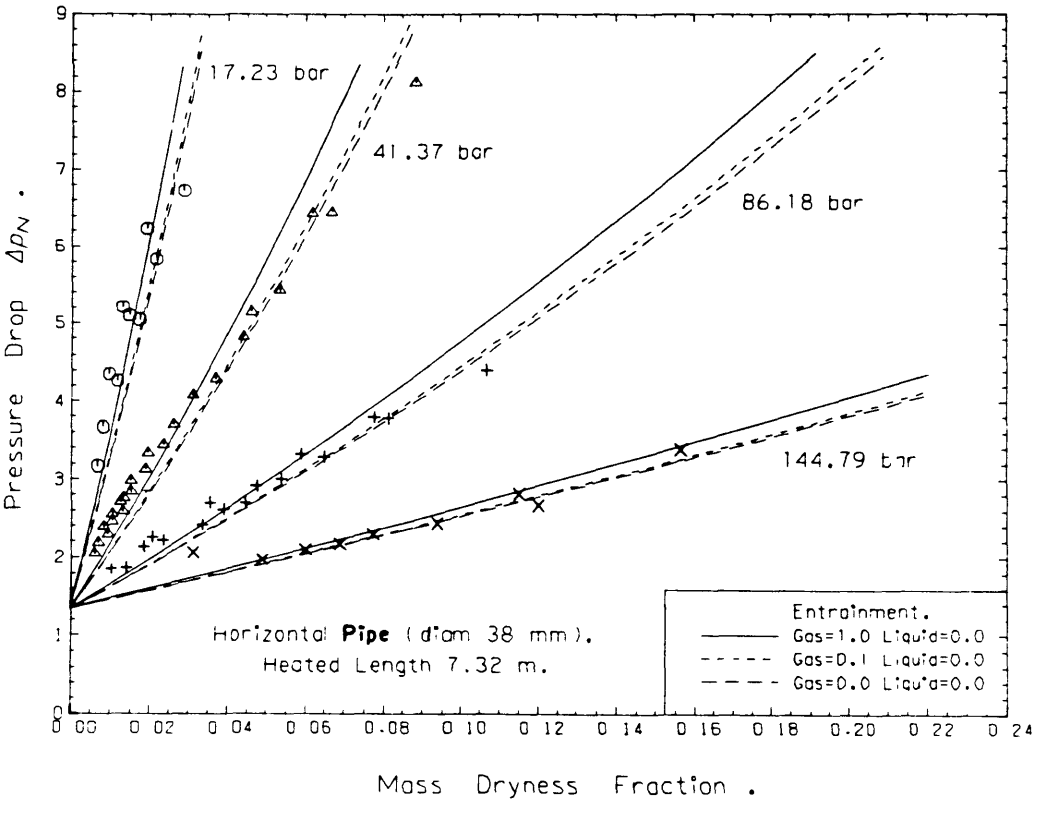

3.5 Normalised pressure drop in horizontal pipe flows with heat input.

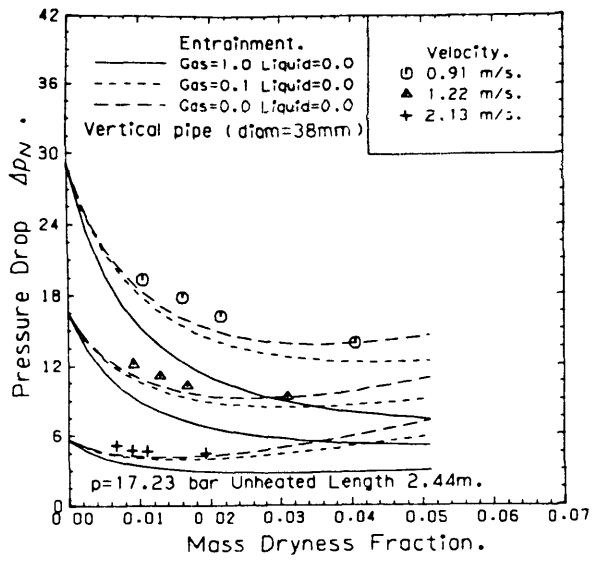

(a)

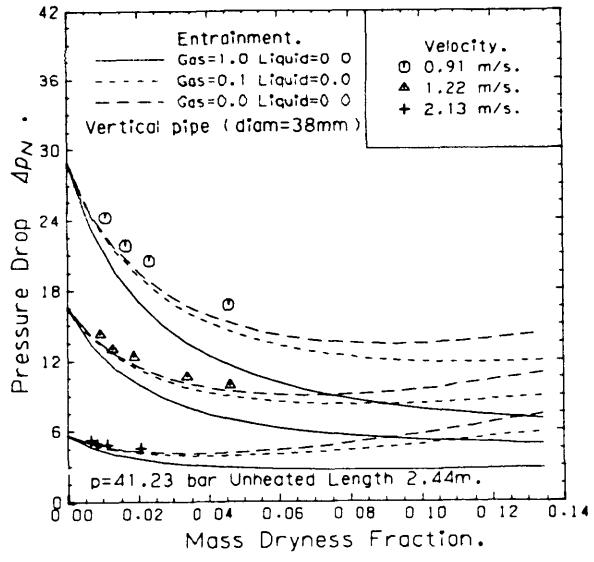

(b)

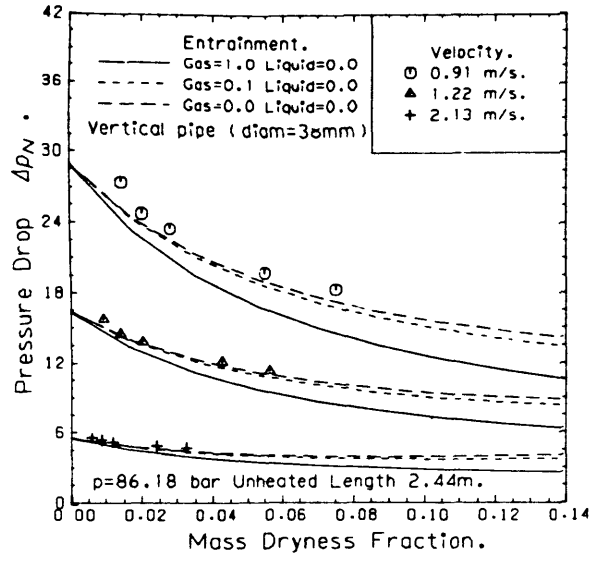

(c)

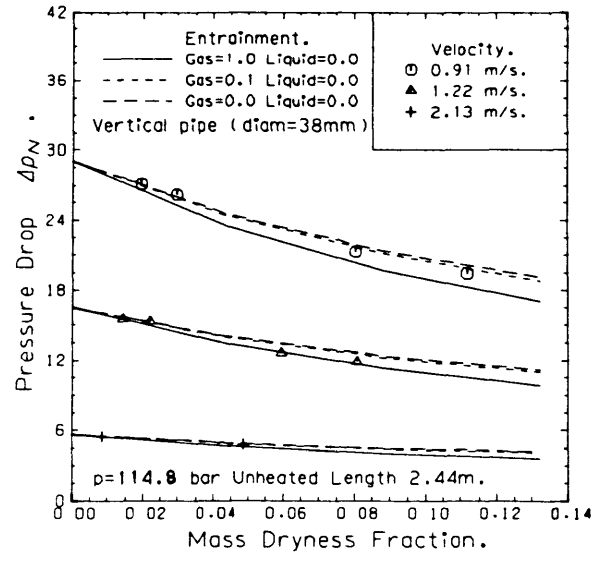

(d)

3.6 Normalised pressure drop in vertical unheated pipe.

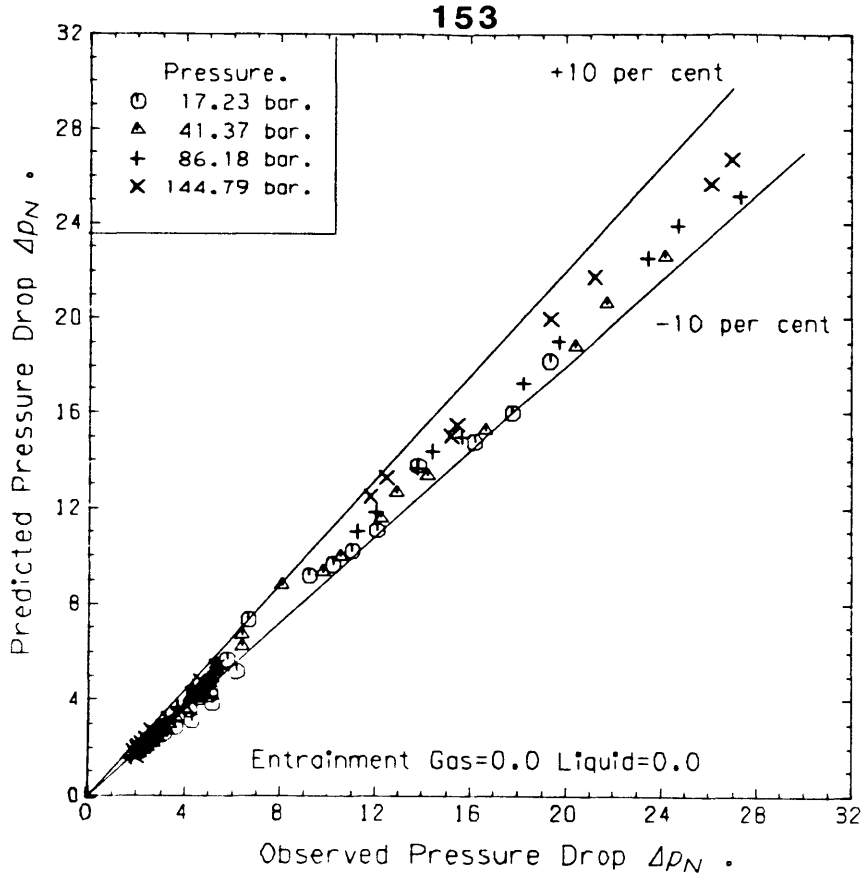

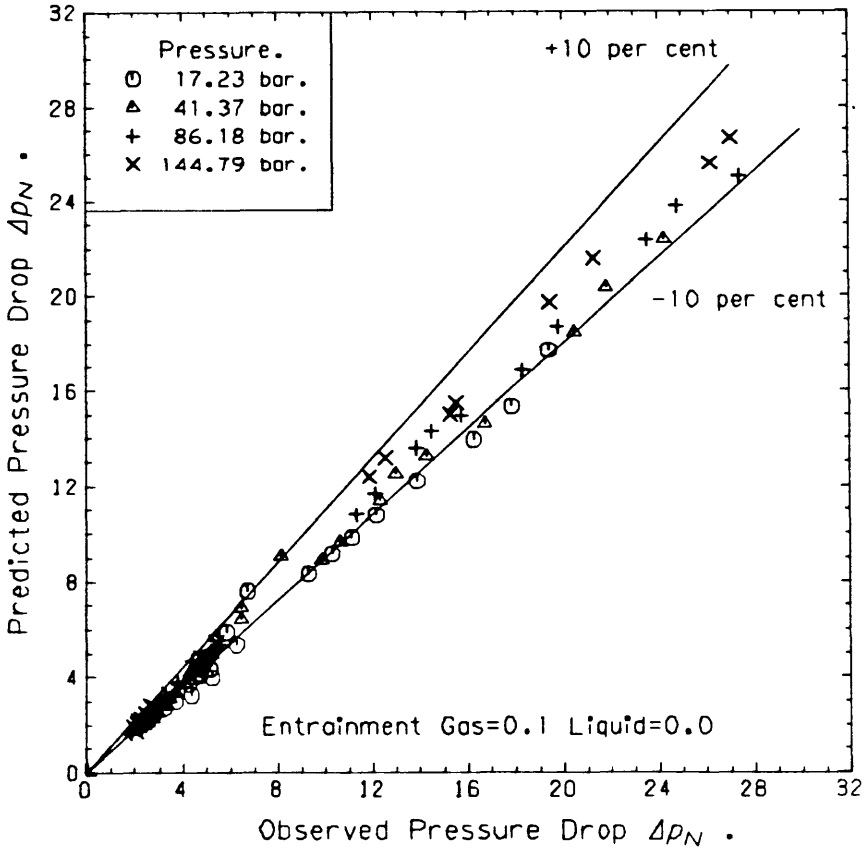

3.7 Comparison between predicted and observed pressure drops with different operating pressures.

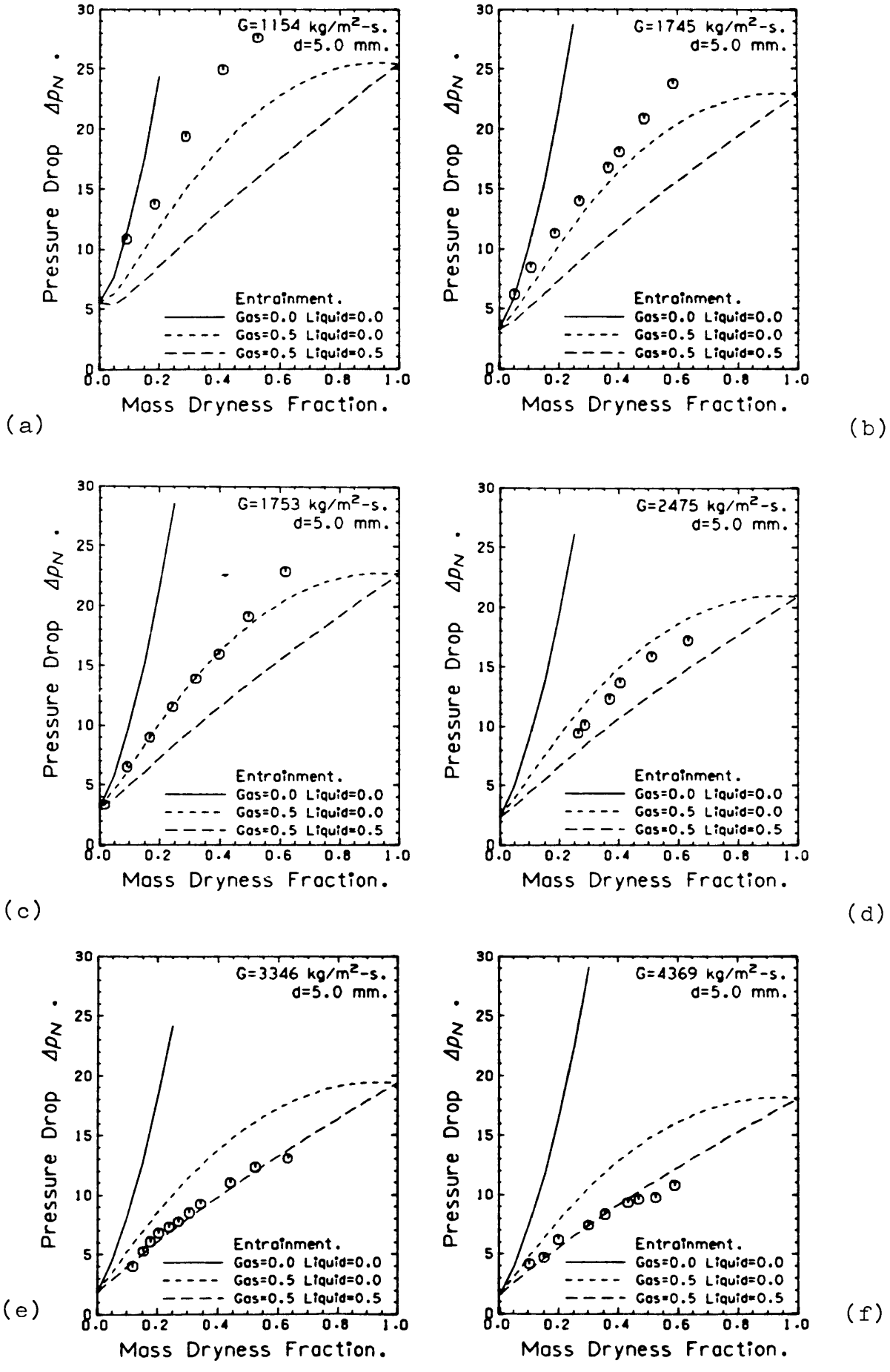

3.8 Normalised pressure drop for pipe flows at 69.69 bar; test length 0.919 m.

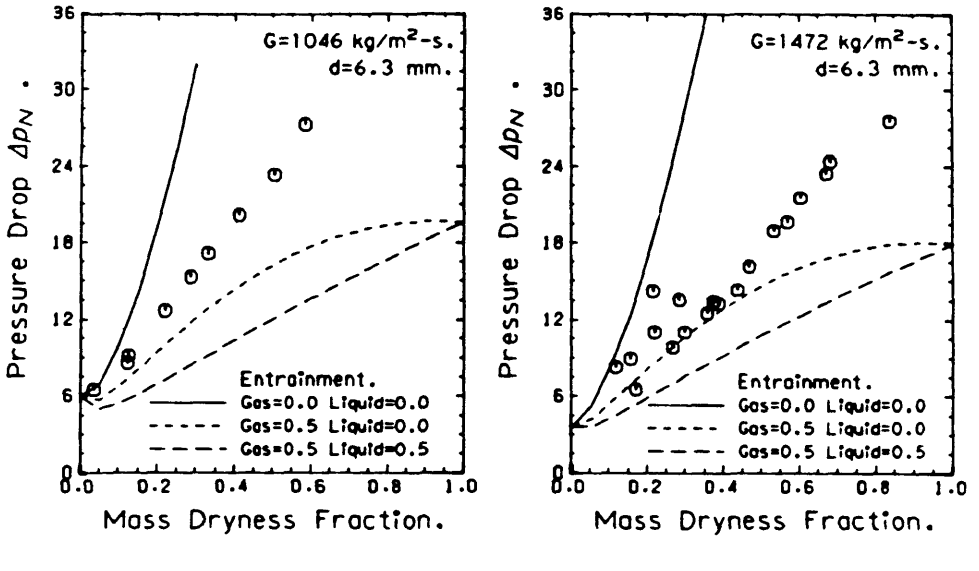

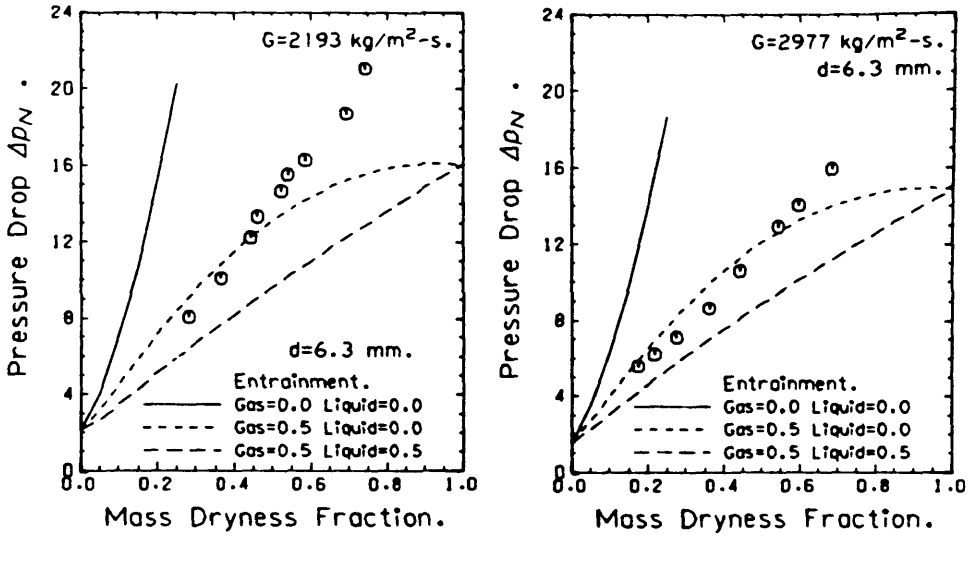

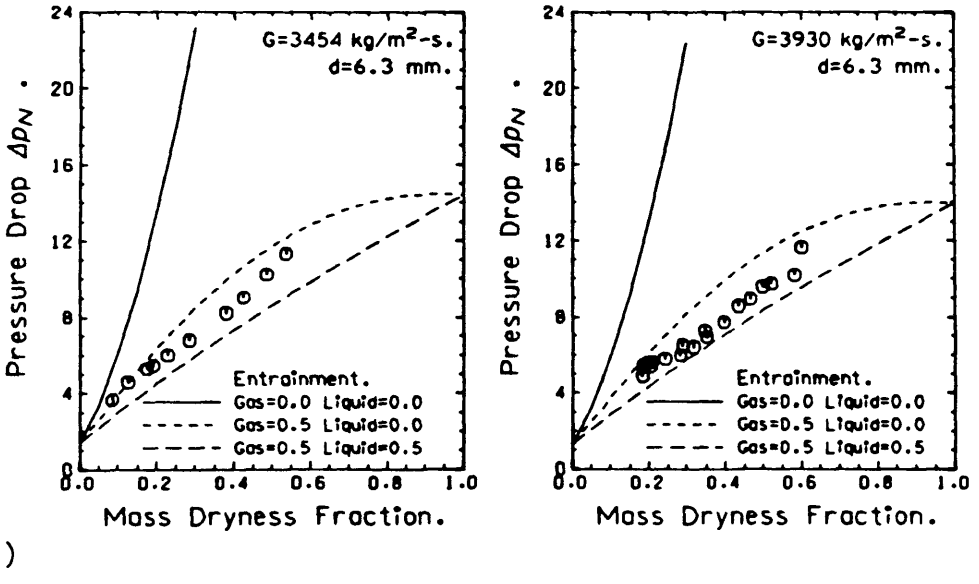

3.9 Normalised pressure drop for pipe flows at 71.13 bar; test length 0.918 m.

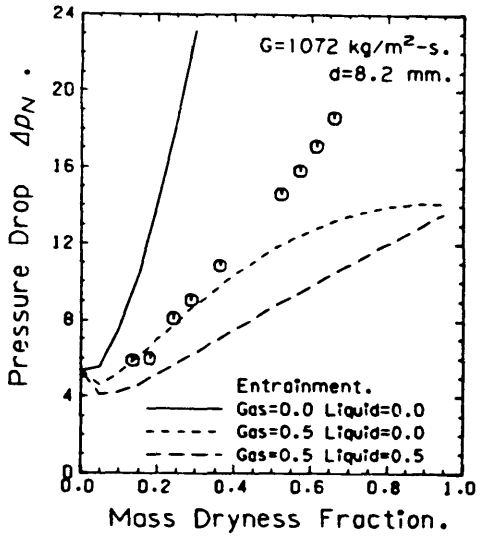

(a)

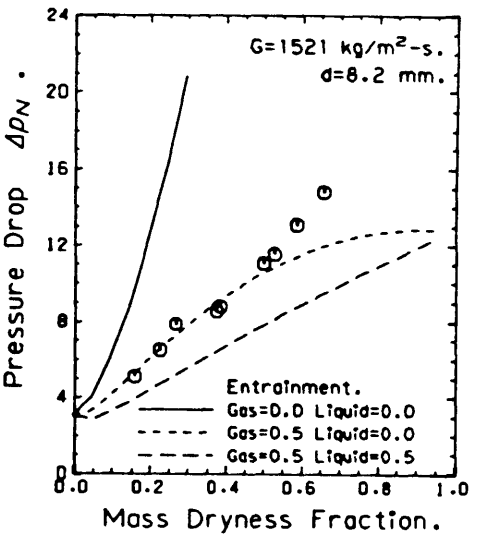

(b)

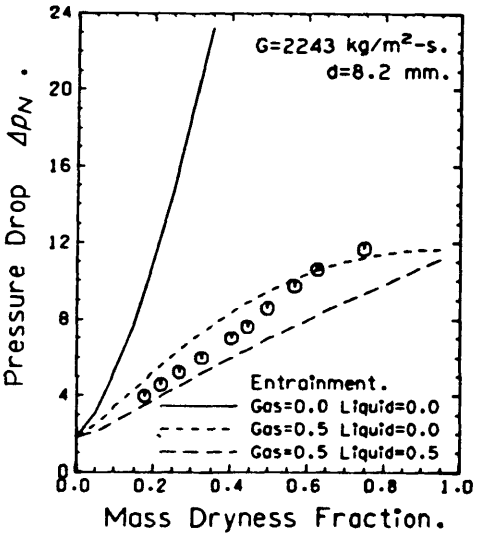

(c)

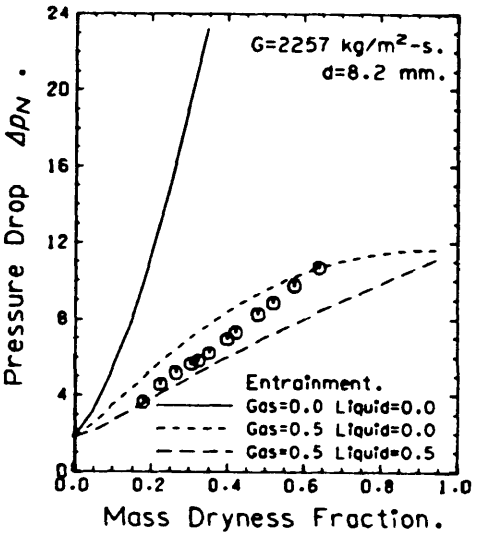

(d)

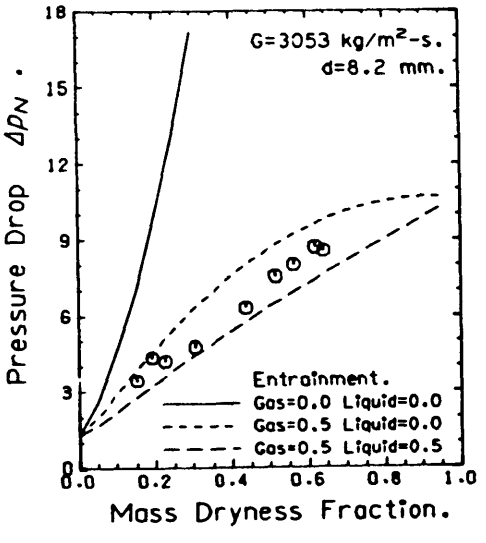

(e)

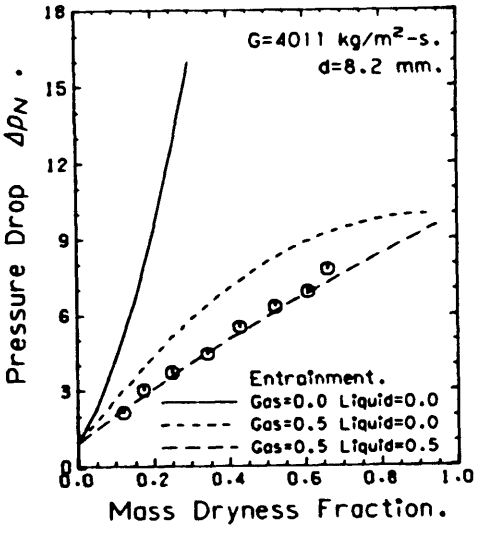

(f)

3.10 Normalised pressure drop for pipe flows at 69.60 bar; test length 0.920 m.

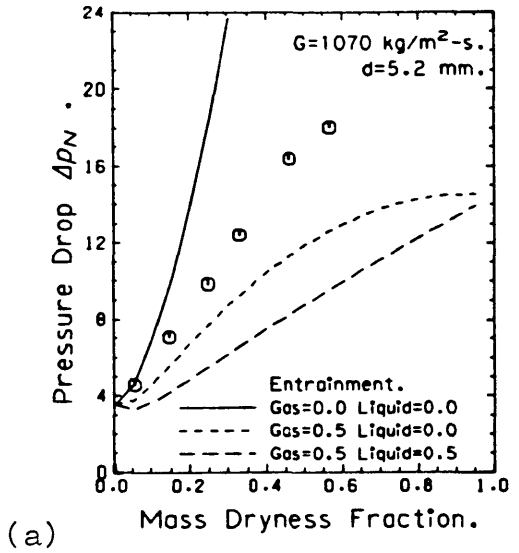

(a)

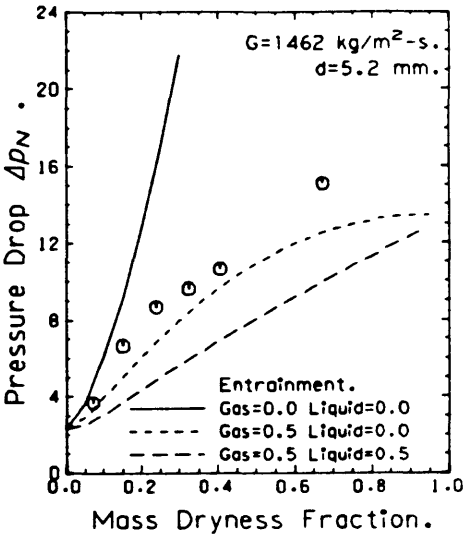

(b)

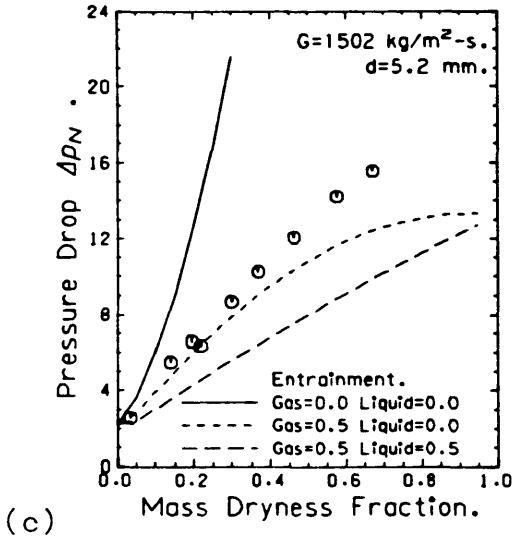

(c)

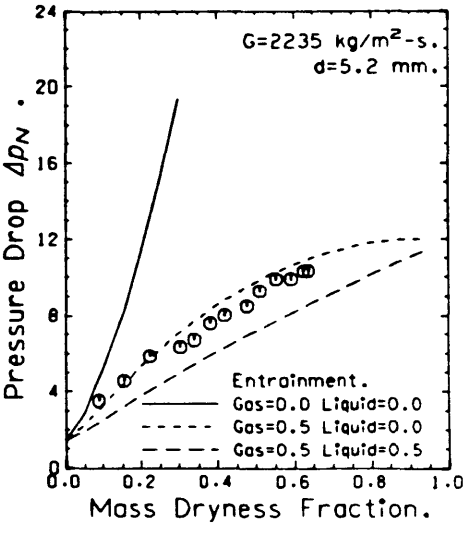

(d)

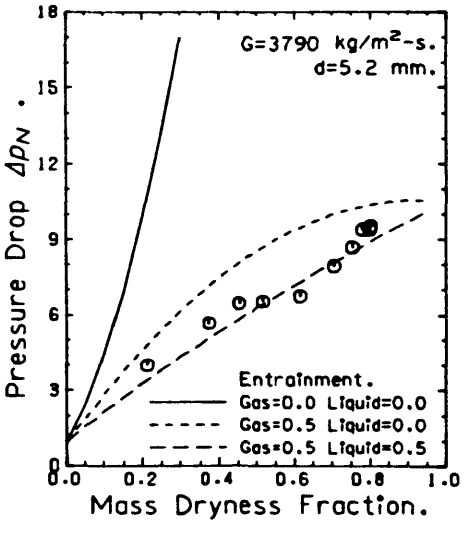

(e)

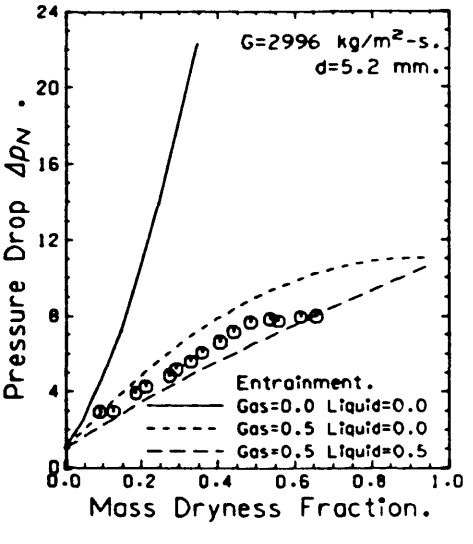

(f)

3.11 Normalised pressure drop for pipe flows at 68.81 bar; test length 0.531 m.

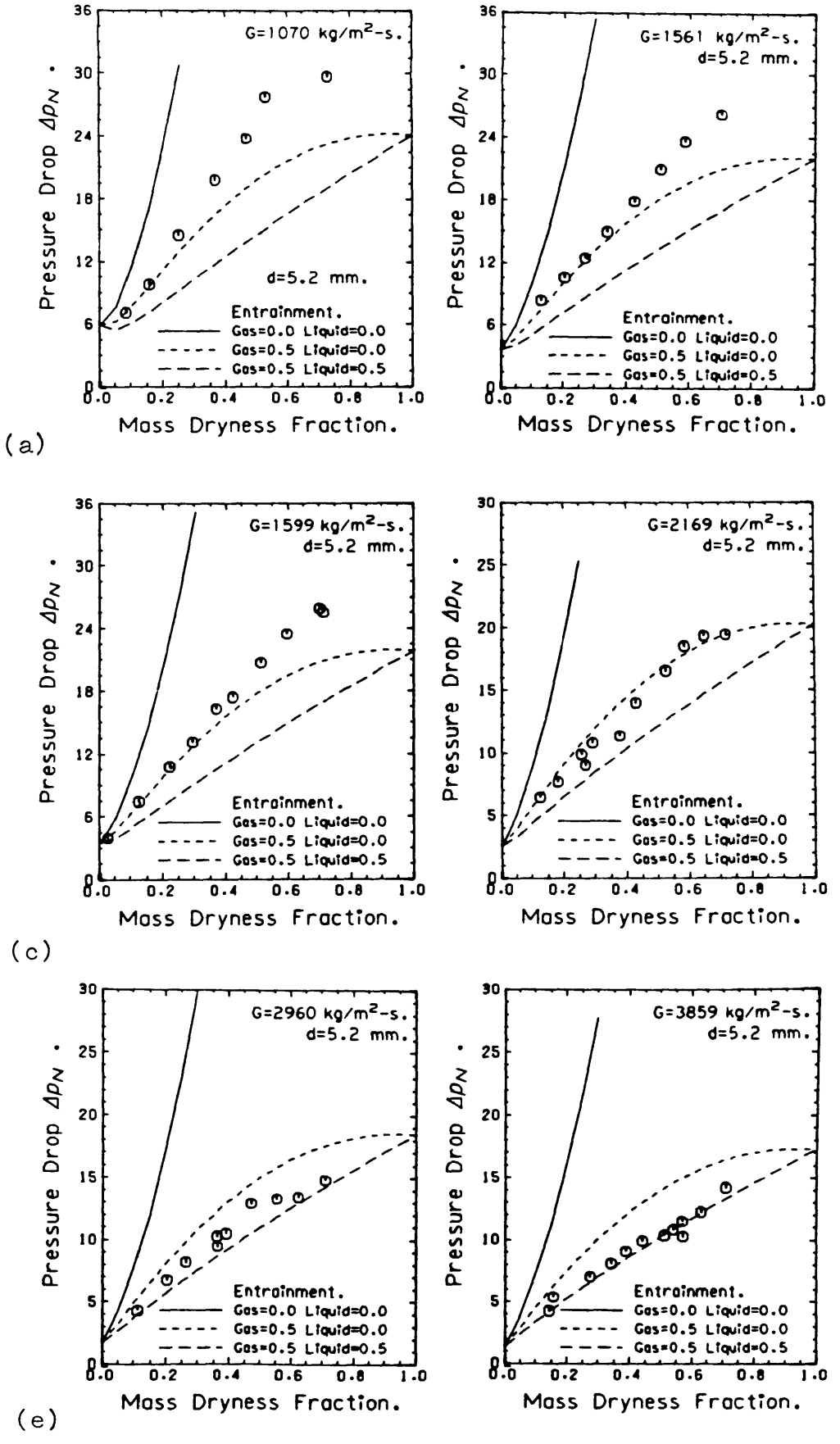

3.12 Normalised pressure drop for pipe flows at 70.07 bar; test length 0.911 m.

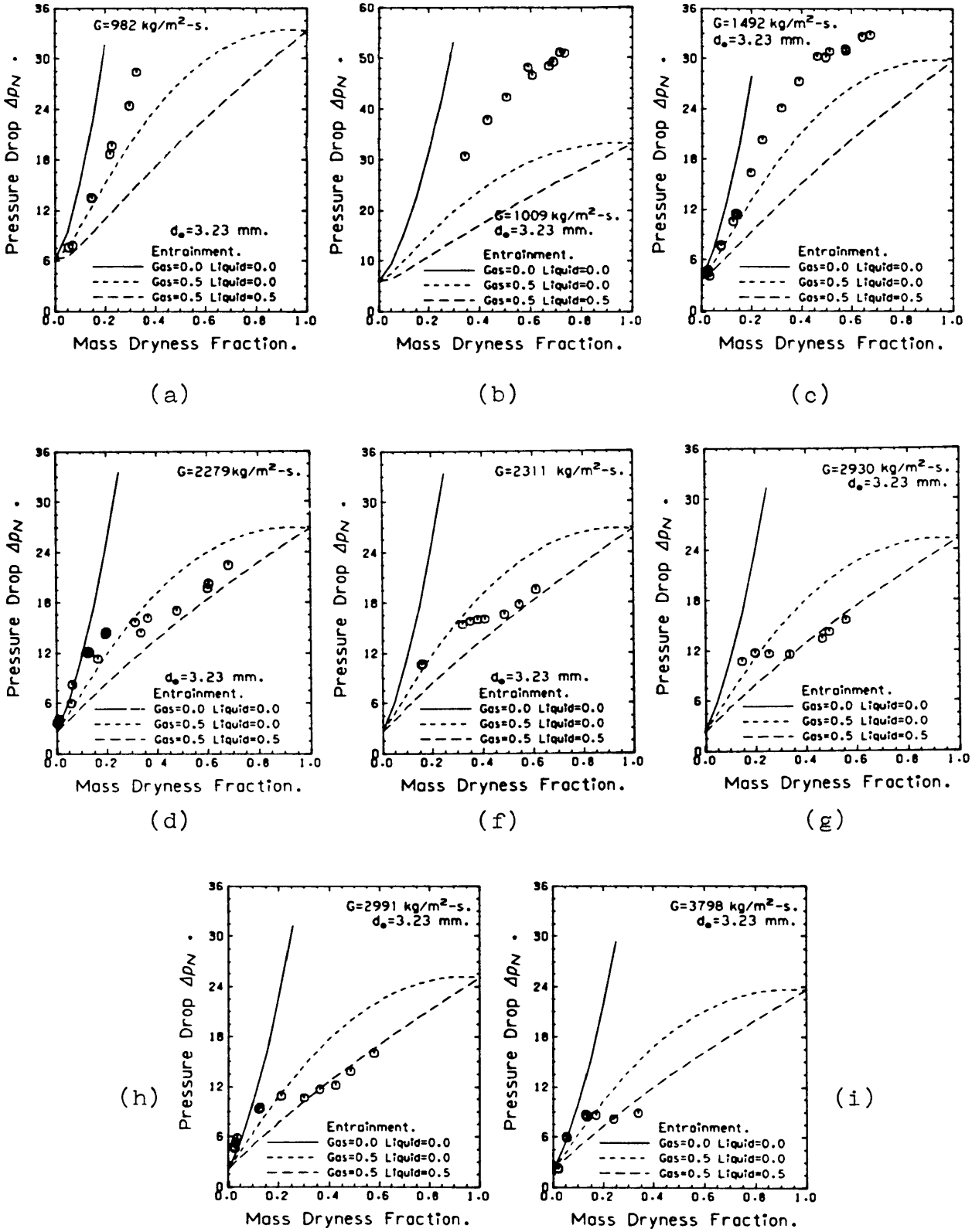

3.13 Normalised pressure drop for flow in an annular passage at 69.90 bar; 50.2 mm inner diameter, 82.5 mm outer diameter. test length 0.674 m.

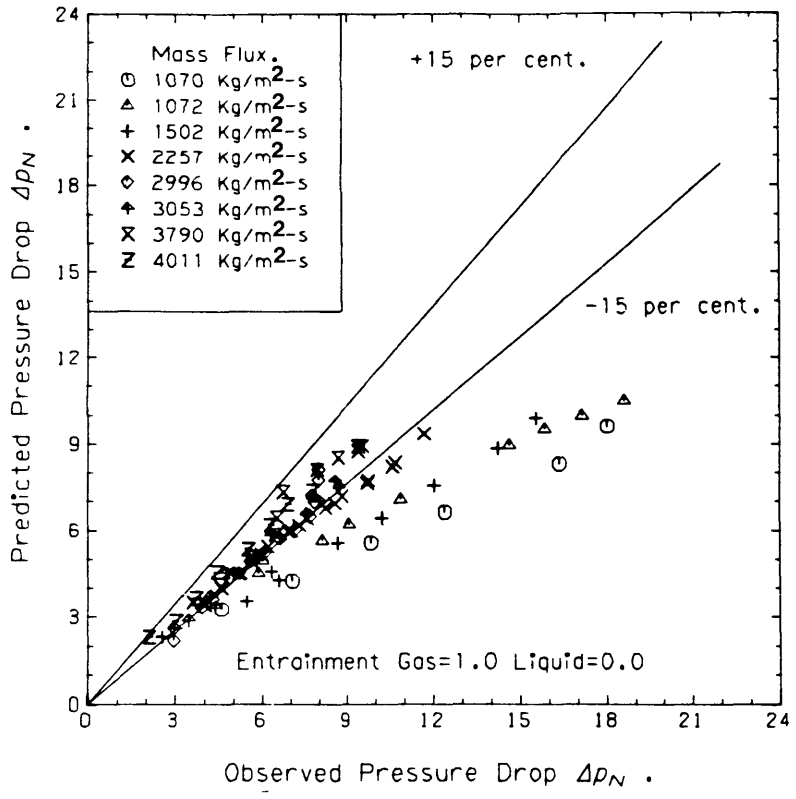

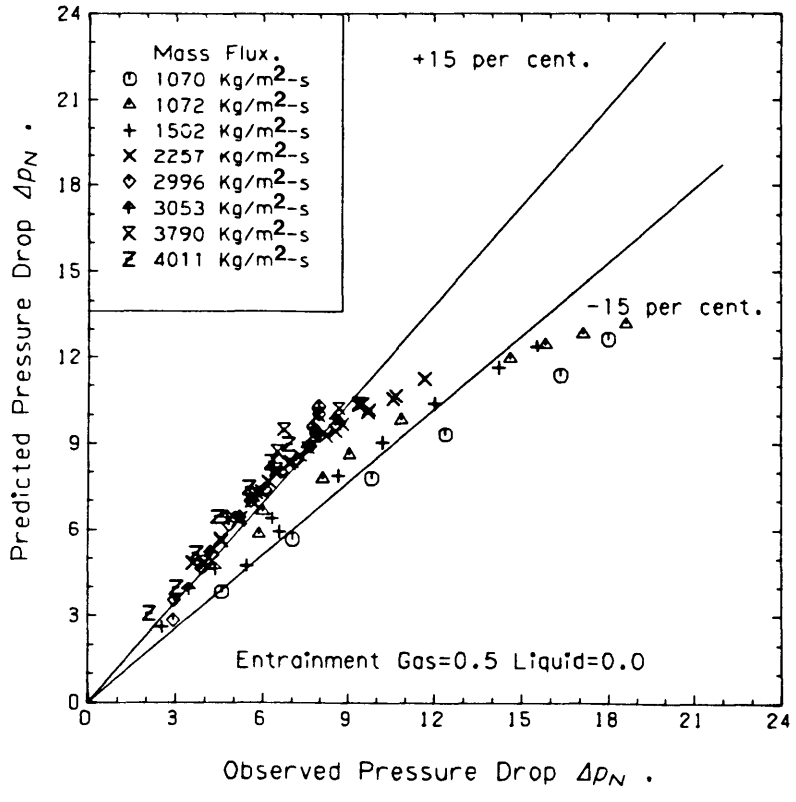

3.14 Comparison between predicted and observed pressure drops at different mass fluxes.

A - 3.2 Tables for Chapter 3.

The predominant phase next to the Wall	LIQUID	VAPOUR
e_1	$\frac{\dot{m}_{\ell 2}}{\dot{m}_\ell} = \frac{(1 - x_2)\,\dot{m}_2}{(1 - x)\,\dot{m}_T}$	$\frac{\dot{m}_{g2}}{\dot{m}_g} = \frac{x_2\,\dot{m}_2}{x\,\dot{m}_T}$
e_2	$\frac{\dot{m}_{g1}}{\dot{m}_g} = \frac{x_1\,\dot{m}_1}{x\,\dot{m}_T}$	$\frac{\dot{m}_{\ell 1}}{\dot{m}_\ell} = \frac{(1 - x_1)\,\dot{m}_1}{(1 - x)\,\dot{m}_T}$
$A_{g1} / A_{\ell 1}$	$(\frac{\rho_\ell}{\rho_g})\,(\frac{e_2}{1 - e_1})\,(\frac{x}{1 - x})$	$(\frac{\rho_\ell}{\rho_g})\,(\frac{1 - e_1}{e_2})\,(\frac{x}{1 - x})$
$A_{g2} / A_{\ell 2}$	$(\frac{\rho_\ell}{\rho_g})\,(\frac{1 - e_2}{e_1})\,(\frac{x}{1 - x})$	$(\frac{\rho_\ell}{\rho_g})\,(\frac{e_1}{1 - e_2})\,(\frac{x}{1 - x})$
α_1	$\frac{e_2\,x}{e_2\,x + (1 - x)(1 - e_1)(\frac{\rho_g}{\rho_\ell})}$	$\frac{(1 - e_1)\,x}{x(1 - e_1) + e_2(1 - x)(\frac{\rho_g}{\rho_\ell})}$
α_2	$\frac{(1 - e_2)\,x}{x(1 - e_2) + e_1(1 - x)(\frac{\rho_g}{\rho_\ell})}$	$\frac{e_1\,x}{e_1\,x + (1 - x)(1 - e_2)(\frac{\rho_g}{\rho_\ell})}$
$\frac{\dot{m}_2}{\dot{m}_1}$	$\frac{(1 - e_2)\,x + e_1(1 - x)}{(1 - e_1)(1 - x) + e_2\,x}$	$\frac{(1 - e_2)(1 - x) + e_1\,x}{(1 - e_1)\,x + e_2(1 - x)}$

3.1 The entrainment flow parameters for liquid or vapour phase occupying region 1.

Experiment	Operat. Pressure (bar).	Diameter (mm)	Length of test section (m).	Inclination to Horizontal.	Mass flow rates (kg/m^2-s)	Figure No.	Description
Anderson Mantzouranis (An60)	1.014	10.85	1.83	90^o	30 to 1363	3.4	Void fraction in adiabatic air-water flows.
Haywood et.al. (Ha61)	17.23 to 144.79	38.00	7.32 2.44	0^o 90^o	750 to 1950	3.5 3.6	Pressure drop in diabatic and adiabatic steam - water flows.
CISE-R-27. Elem. 52,68,88 (Be60)	69.5 to 71.1	5.00 6.30 8.20	0.92	90^o	1046 to 4369	3.8 3.9 3.10	Pressure drop in adiabatic steam - water flows.
CISE-R-27 Elements 54,51 (Be60)	69.0 to 70.0	5.20	0.53 0.91	90^o	1070 to 3859	3.11 3.12	Pressure drop in adiabatic steam - water flows.
CISE-R-31 Element 85 (Ad61)	69.9	Inner 5.02 Outer 8.25 Hydr. 3.23	0.674	90^o	982 to 3798	3.13	Pressure drop in adiabatic steam-water flow in an annulus.

3.2 Summary of the experimental comparisons carried out.

A - 4.1 Figures for Chapter 4.

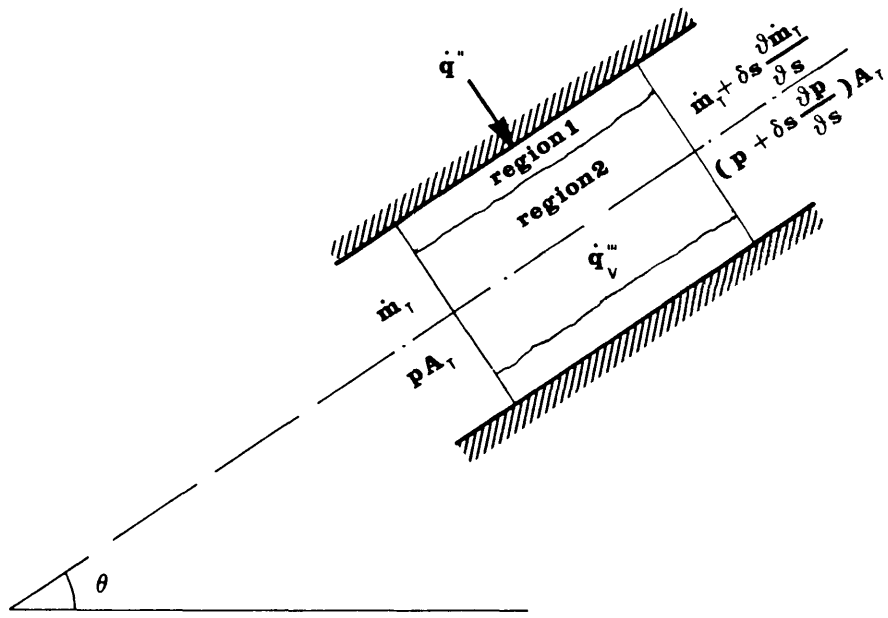

4.1 The control volume of the separated flow conservation equations.

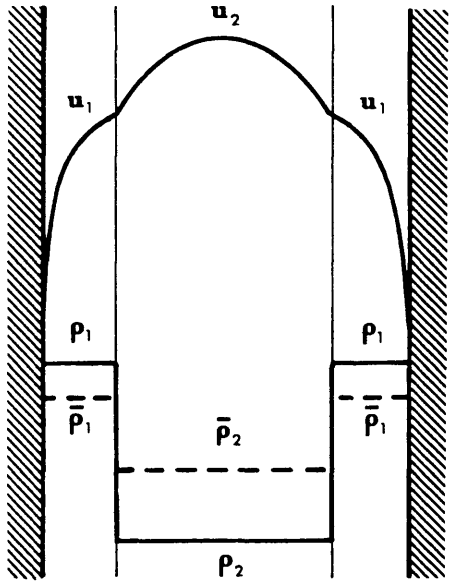

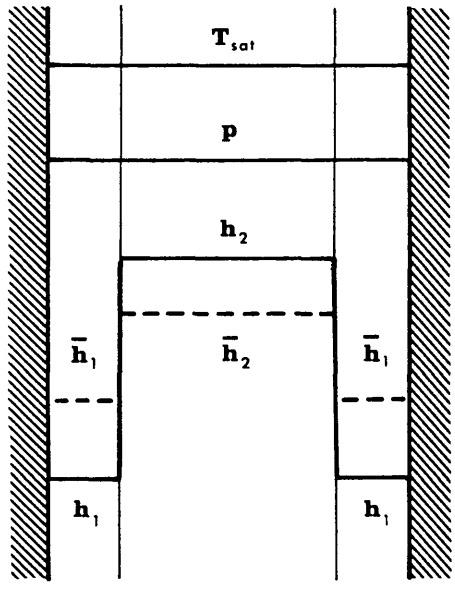

4.2 The assumed transverse distribution of the properties for phases 1 and 2 (L1V2).

(b)

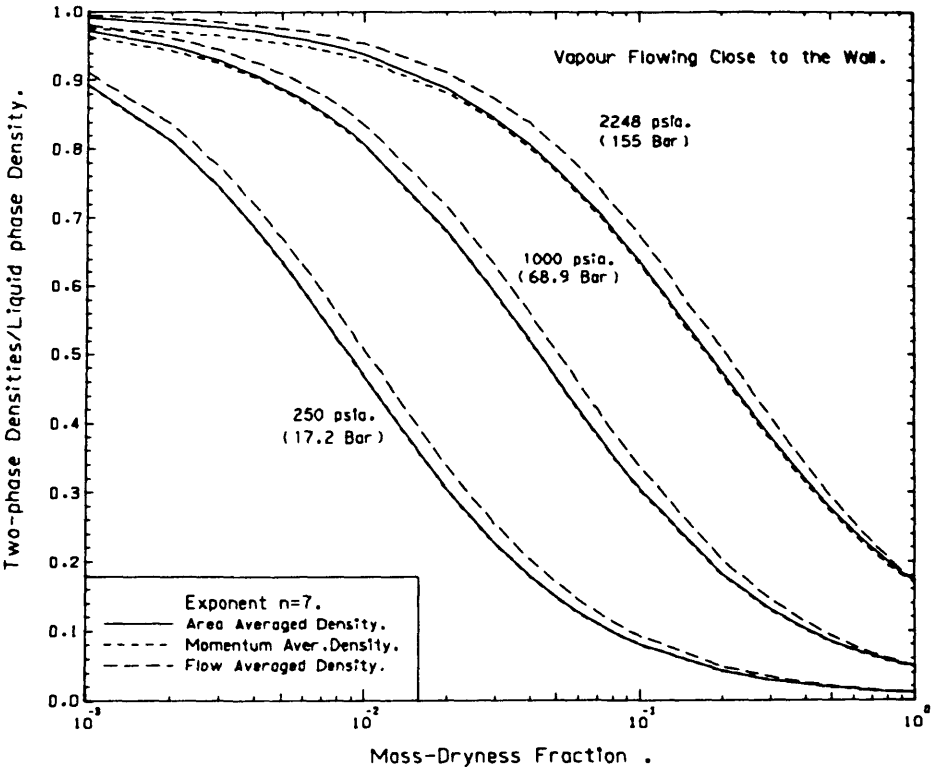

(a)

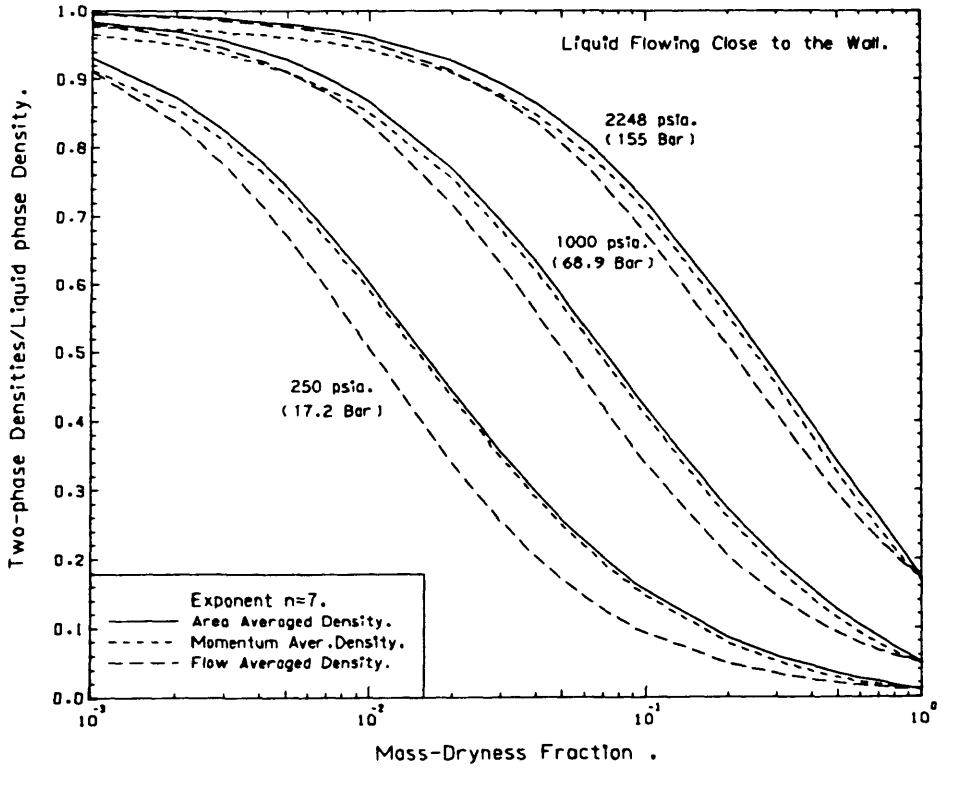

4.3 The two-phase averaged densities for n = 7 when (a) L1V2 and (b) V1L2.

(b)

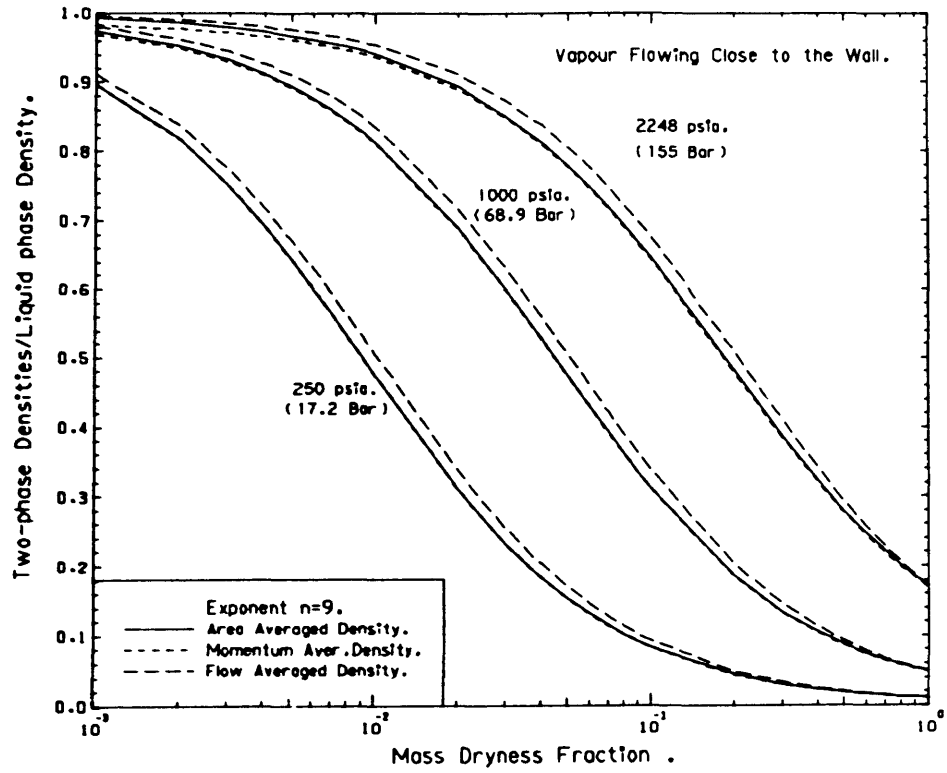

(a)

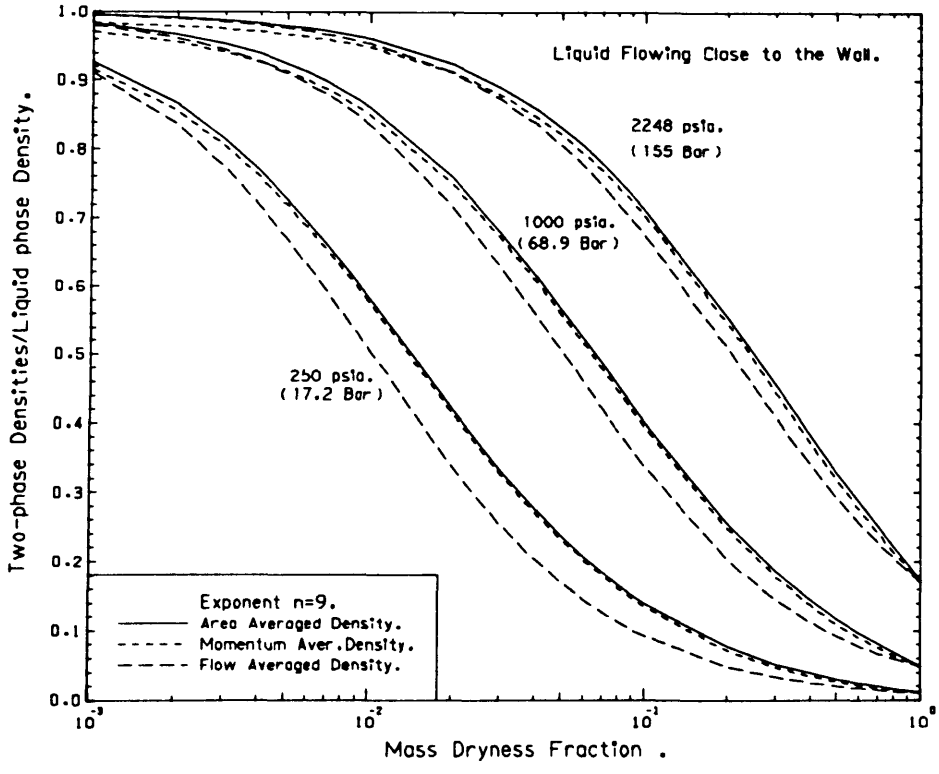

4.4 The two-phase averaged densities for n = 9 when (a) L1V2 and (b) V1L2.

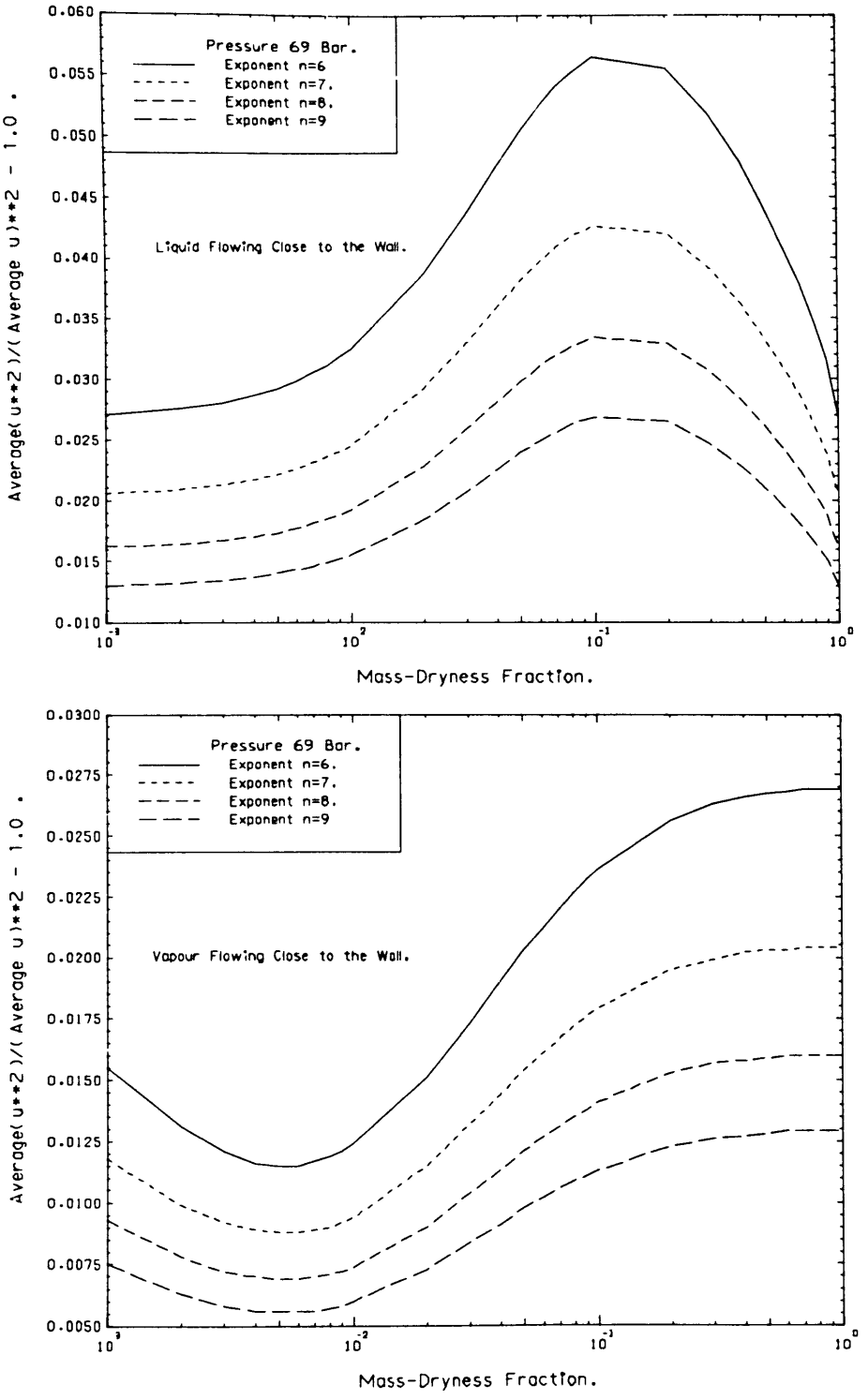

4.5 The ratio $\overline{(u^2)}/(\overline{u})^2$ at 69 bar for L1V2 and V1L2.

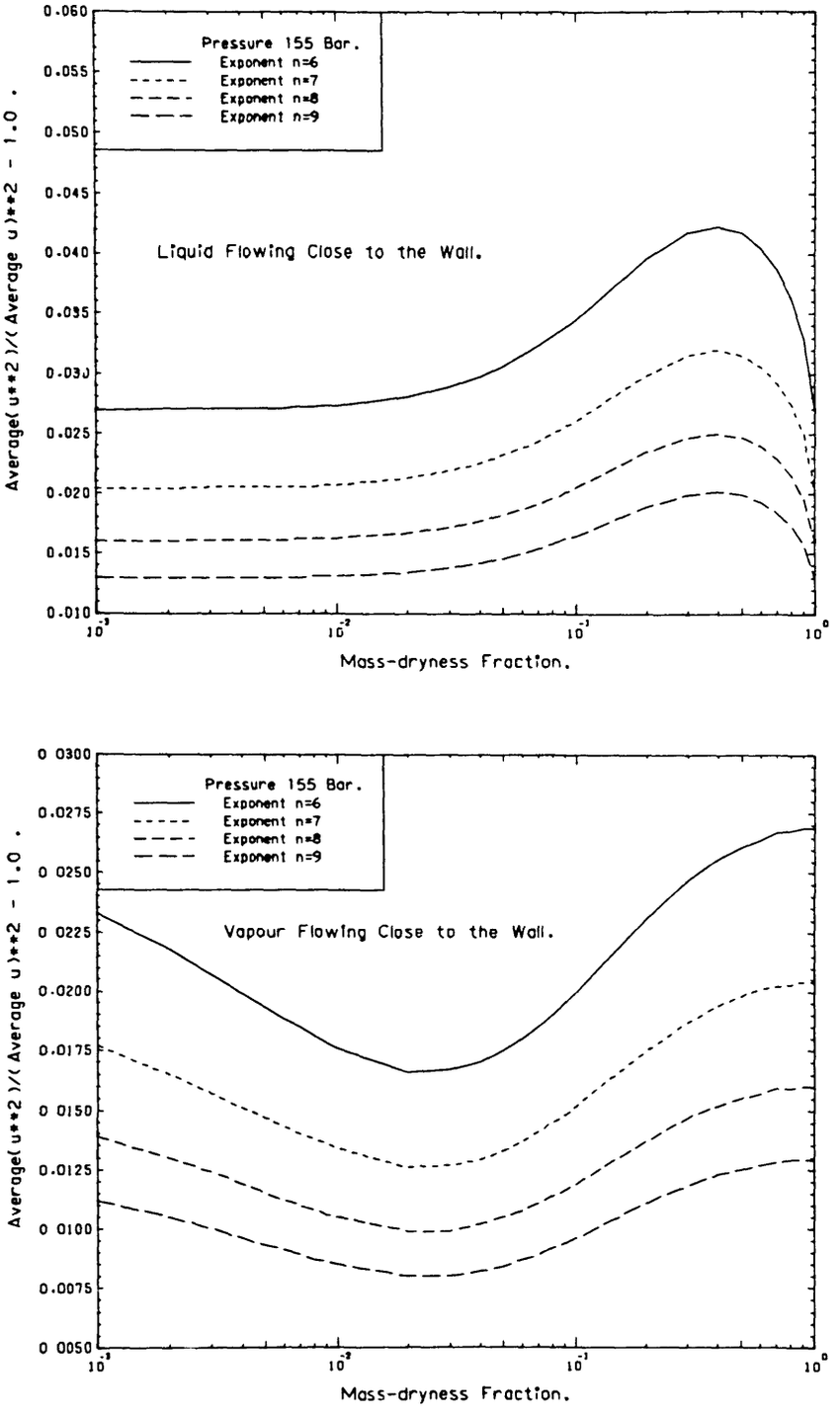

4.6 The ratio $\overline{(u^2)}/(\overline{u})^2$ at 155 bar for L1V2 and V1L2.

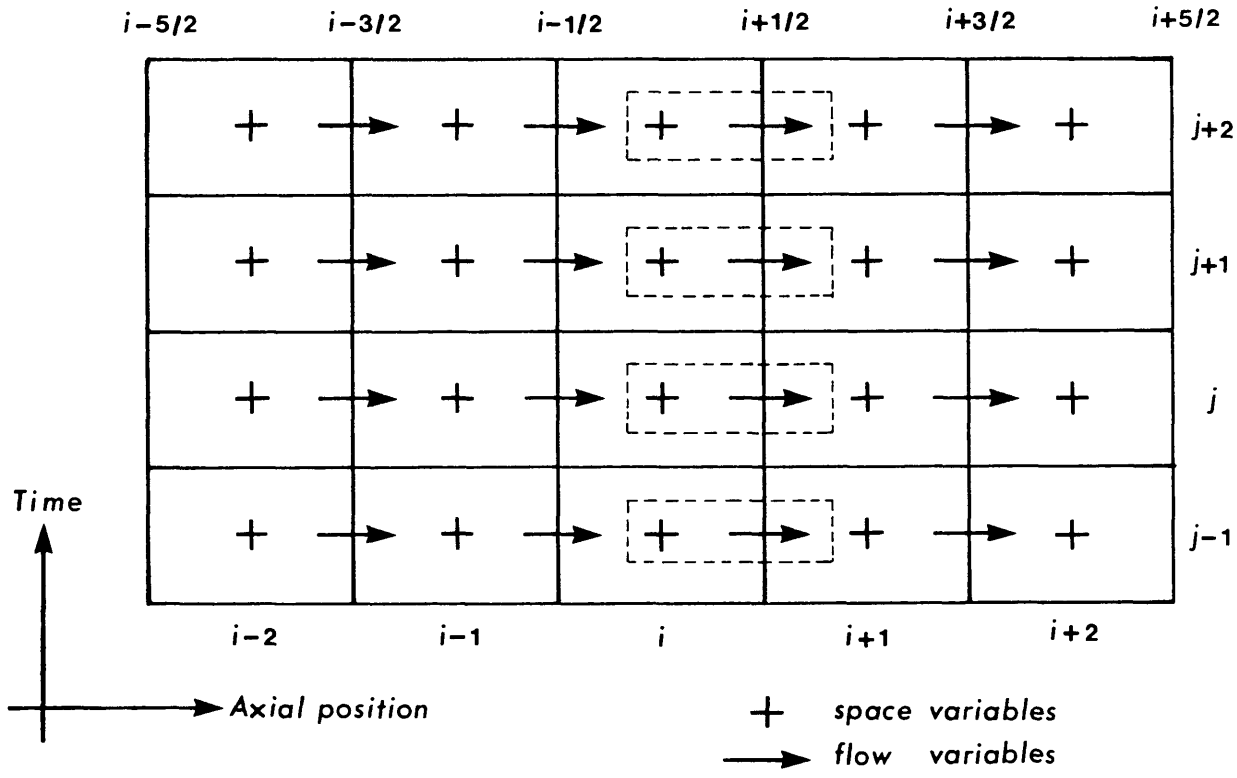

4.7 Staggered grid system.

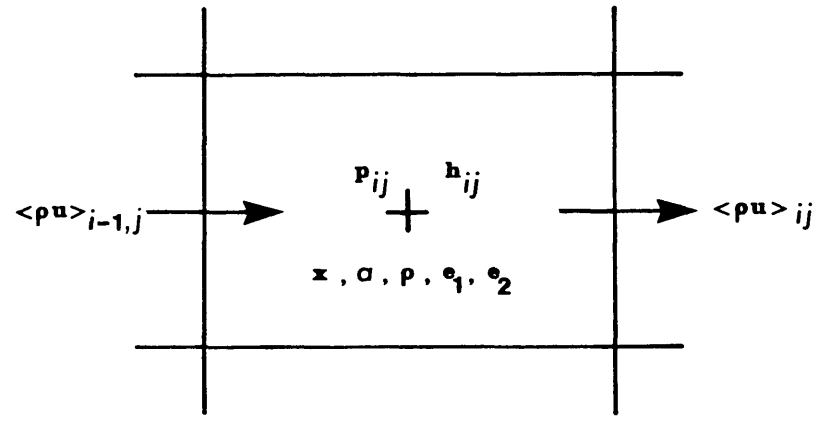

4.8 Arrangement of variables in a typical cell.

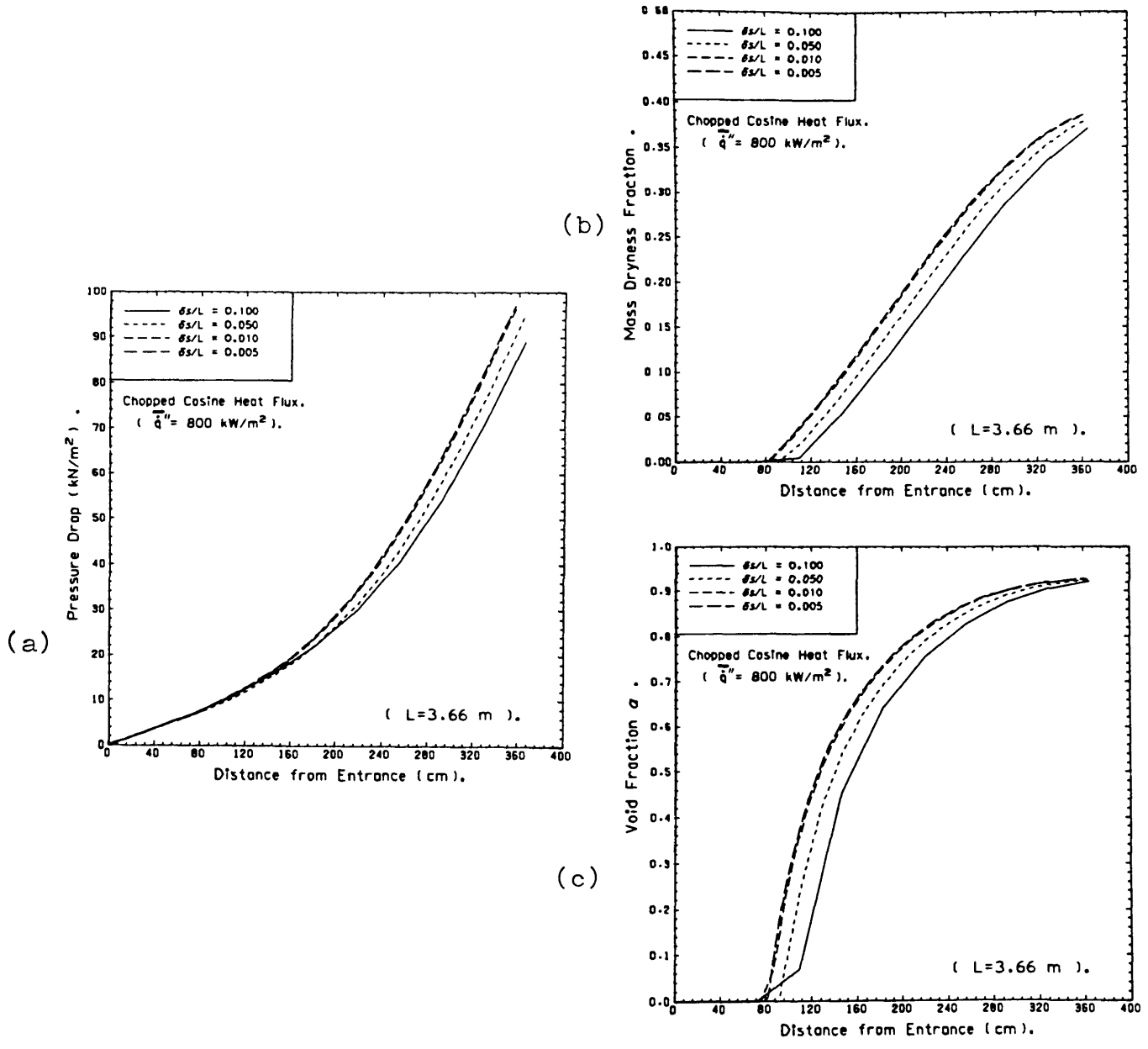

4.9 The effect of grid size on (a) pressure drop, (b) mass-dryness fraction and (c) void fraction, in a cosine heat flux distribution.

(a)

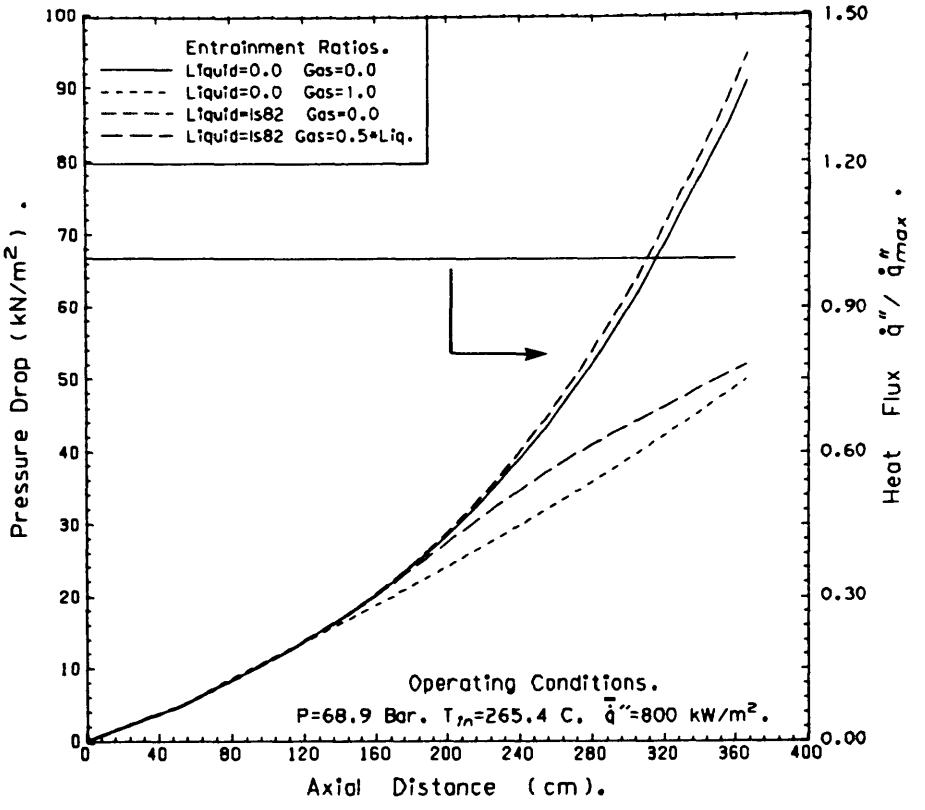

(Is82 = Ishii+Mishima Entrainment Model).

(b)

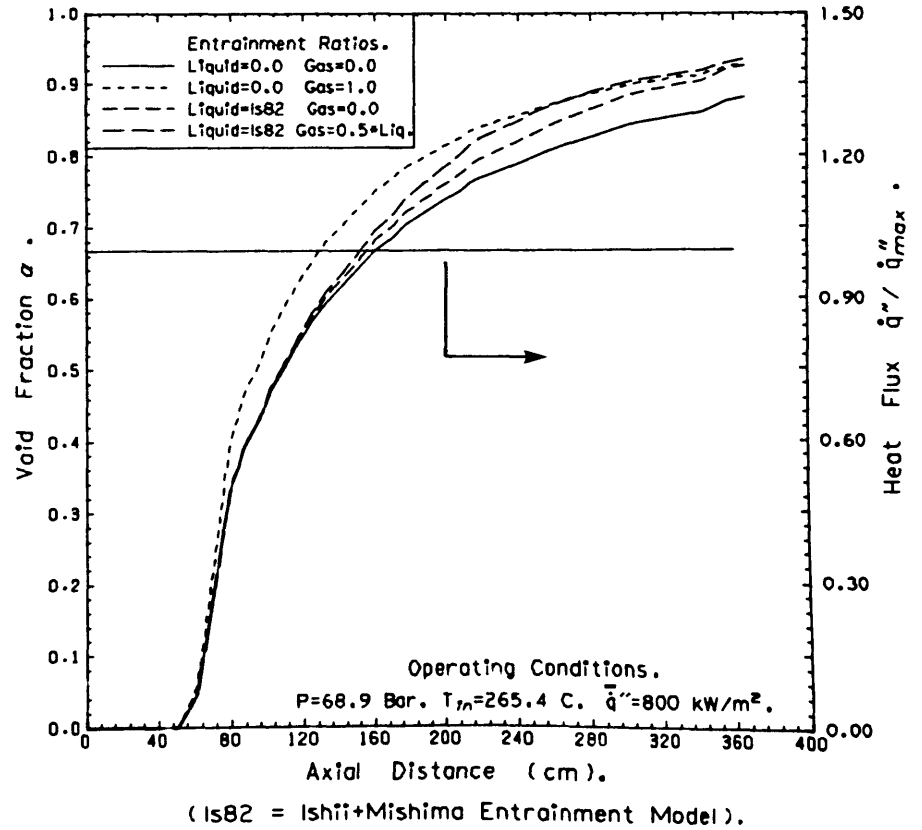

(Is82 = Ishii+Mishima Entrainment Model).

4.10 The pressure drop and void fraction in a uniformly heated pipe for different entrainment models.

(a)

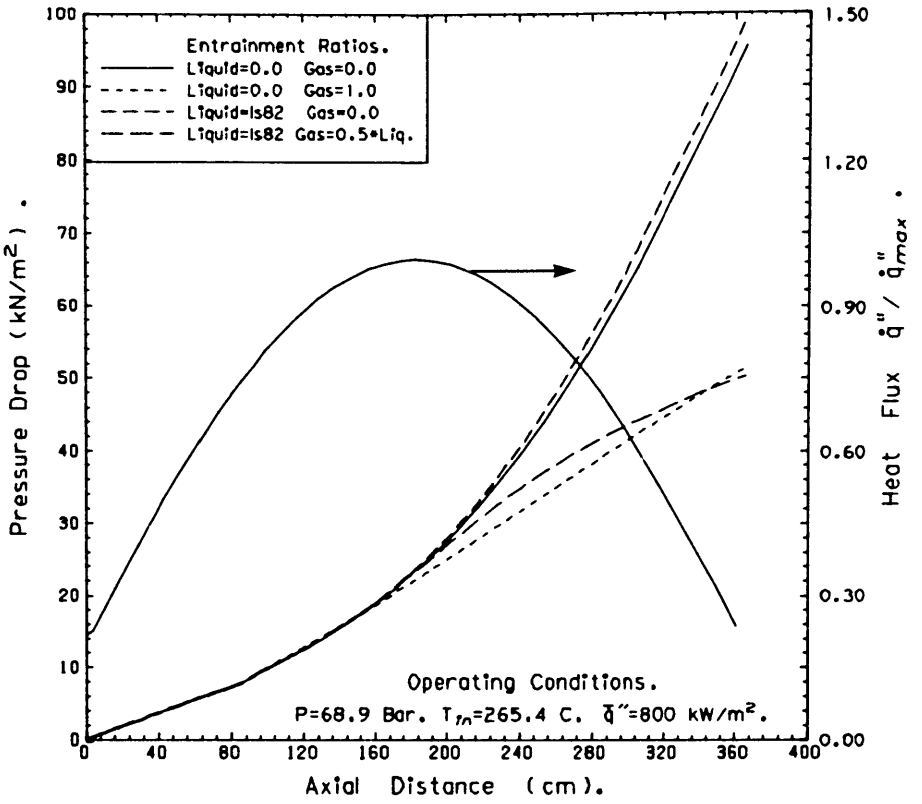

(Is82 = Ishii+Mishima Entrainment Model).

(b)

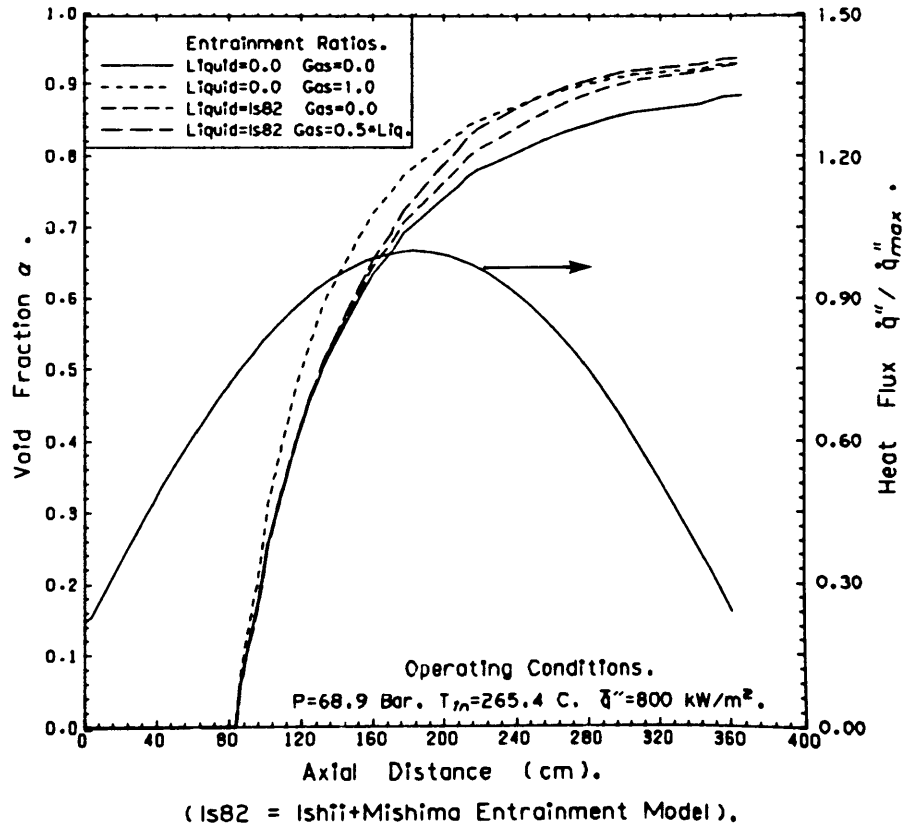

(Is82 = Ishii+Mishima Entrainment Model).

4.11 The effect of entrainment in pressure drop and void fraction for a chopped cosine heat flux.

(a)

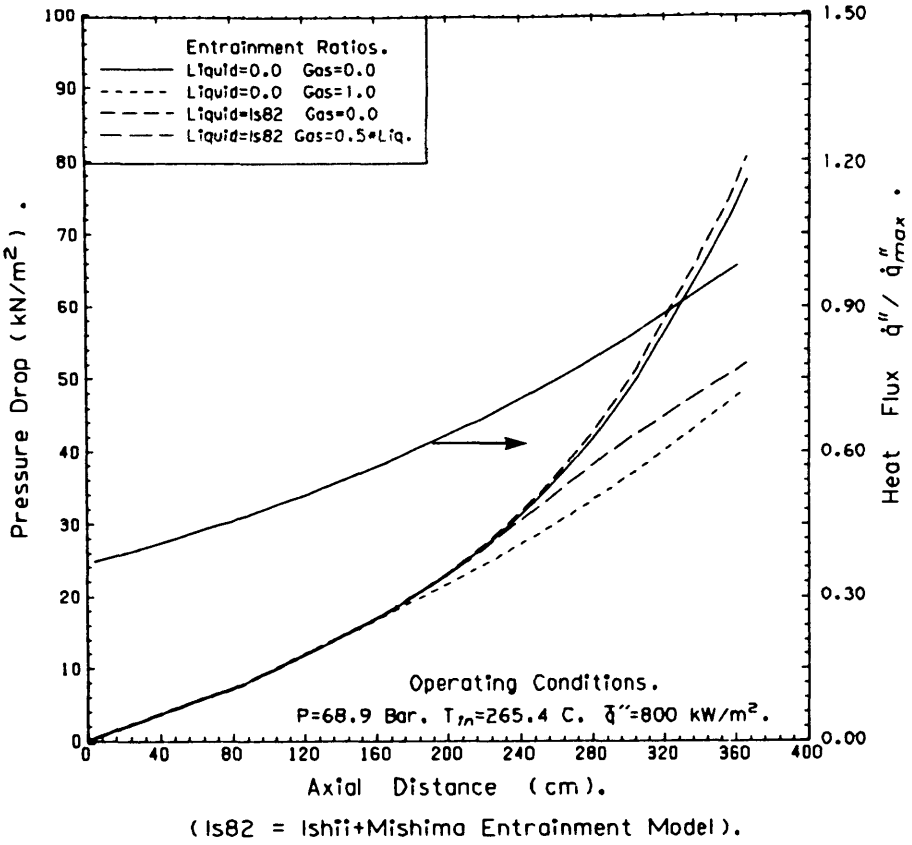

(Is82 = Ishii+Mishima Entrainment Model).

(b)

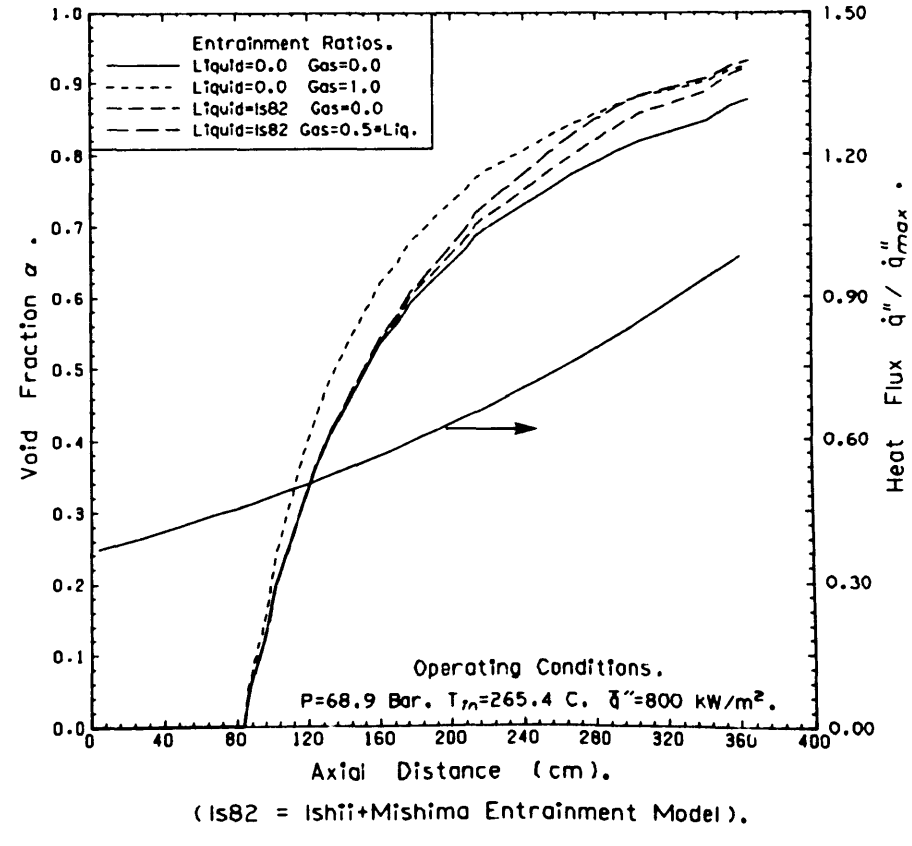

(Is82 = Ishii+Mishima Entrainment Model).

4.12 The effect of entrainment in pressure drop and void fraction for exponential heat flux distribution.

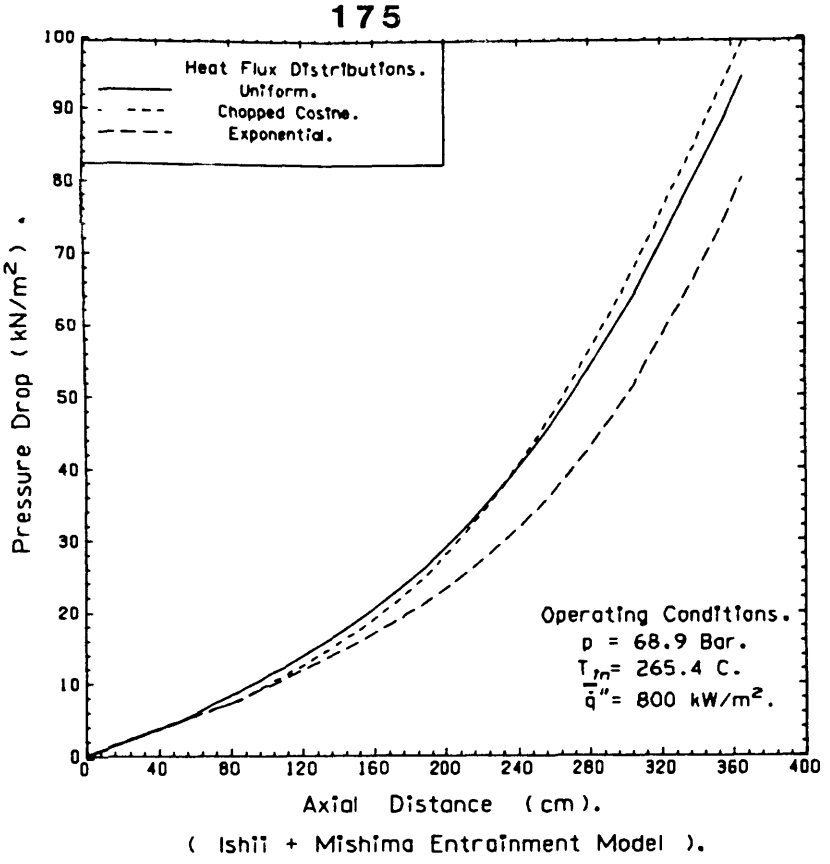

4.13 Comparison of pressure drops predicted for different heat flux distributions.

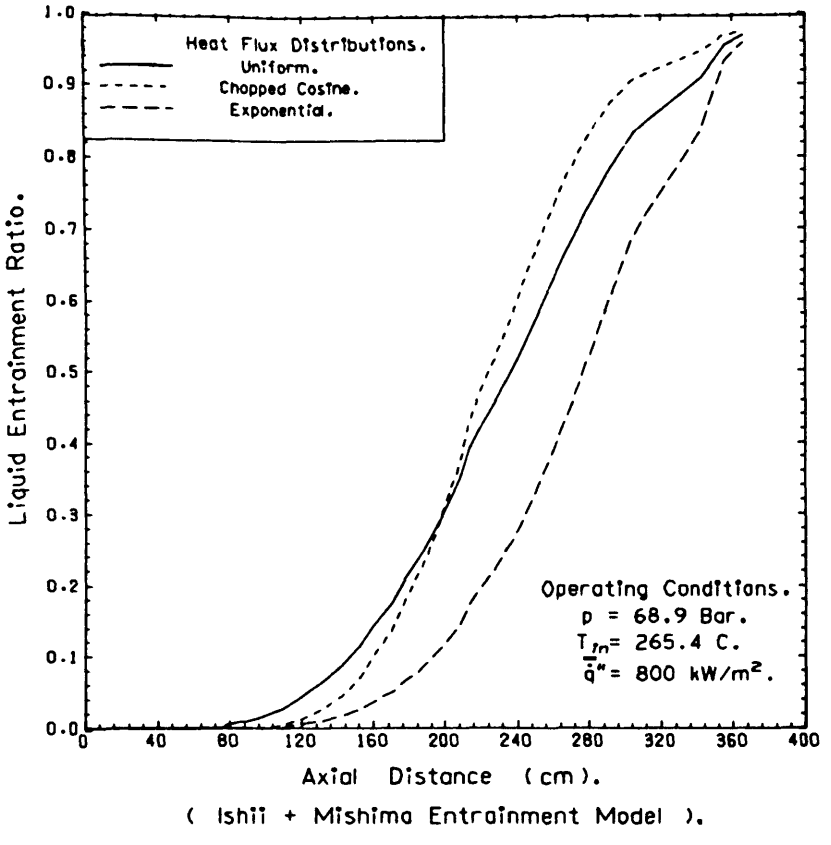

4.14 Comparison of liquid entrainment ratios predicted for different heat flux distributions.

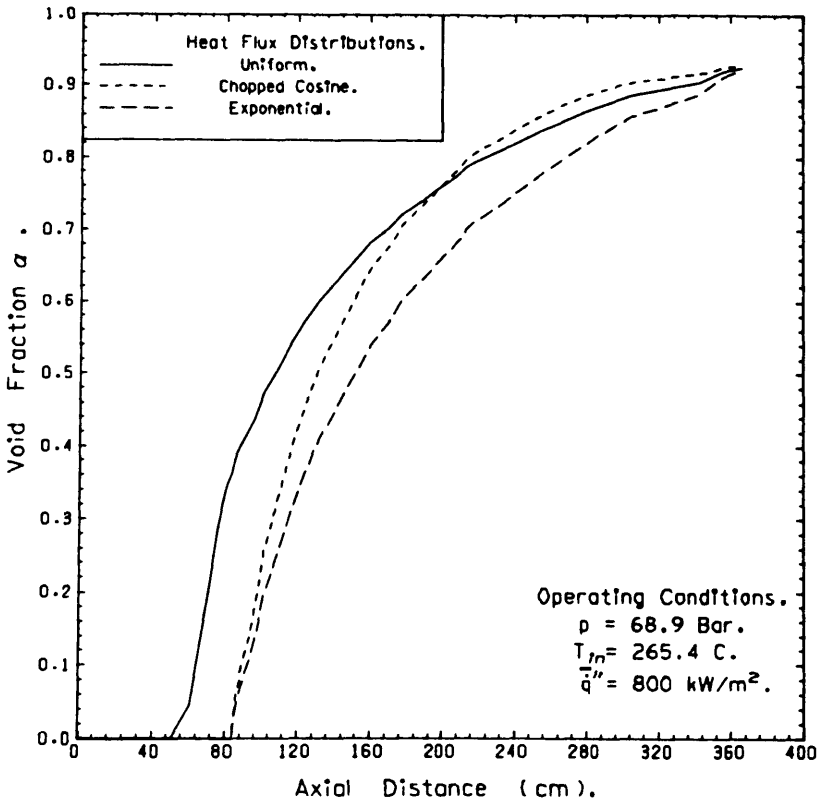

4.15 Comparison of void fractions predicted for different heat flux distributions.

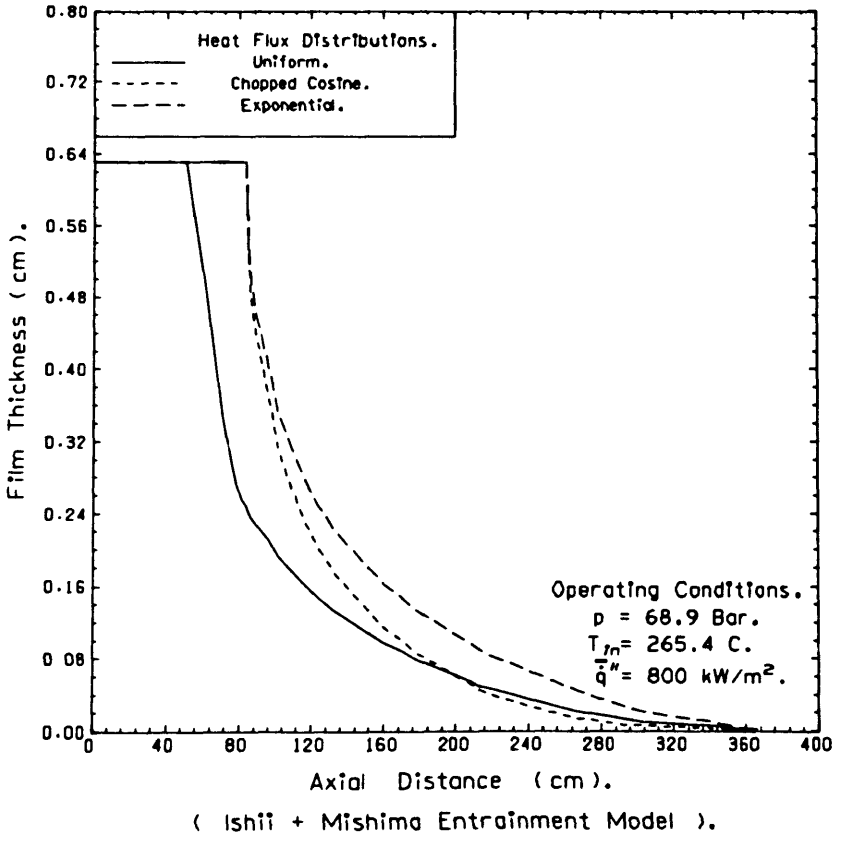

4.16 Comparison of film thicknesses predicted for different heat flux distributions.

A - 4.2 Tables for Chapter 4.

Averaged Densities	Without Entrainment (L1V2)	With Entrainment
$\rho_A = f_1 \bar{\rho}_1 + f_2 \bar{\rho}_2$	$f_1 = 1 - \alpha$ $f_2 = \alpha$	$f_1 = (\alpha_2 - \alpha) / (\alpha_2 - \alpha_1)$ $f_2 = (\alpha - \alpha_1) / (\alpha_2 - \alpha_1)$
$\frac{1}{\rho_F} = \frac{f_1}{\bar{\rho}_1} + \frac{f_2}{\bar{\rho}_2}$	$f_1 = 1 - x$ $f_2 = x$	$f_1 = (x_2 - x) / (x_2 - x_1)$ $f_2 = (x - x_1) / (x_2 - x_1)$
$\frac{1}{\rho_M} = \frac{f_1}{\bar{\rho}_1} + \frac{f_2}{\bar{\rho}_2}$	$f_1 = U_1^2 (1 - x)^2 / (1 - \alpha)$ $f_2 = U_2^2 x^2 / \alpha$	$f_1 = U_1^2 \left[\frac{x_2 - x}{x_2 - x_1}\right]^2 \left[\frac{\alpha_2 - \alpha_1}{\alpha_2 - \alpha}\right]$ $f_2 = U_2^2 \left[\frac{x - x_1}{x_2 - x_1}\right]^2 \left[\frac{\alpha_2 - \alpha_1}{\alpha - \alpha_1}\right]$
$\frac{1}{\rho_E^2} = \frac{f_1}{\bar{\rho}_1^2} + \frac{f_2}{\bar{\rho}_2^2}$	$f_1 = U_1^3 (1 - x)^3 / (1 - \alpha)^2$ $f_2 = U_2^3 x^3 / \alpha^2$	$f_1 = U_1^3 \left[\frac{x_2 - x}{x_2 - x_1}\right]^3 \left[\frac{\alpha_2 - \alpha_1}{\alpha_2 - \alpha}\right]^2$ $f_2 = U_2^3 \left[\frac{x - x_1}{x_2 - x_1}\right]^3 \left[\frac{\alpha_2 - \alpha_1}{\alpha - \alpha_1}\right]^2$

4.1 Definitions of the average densities across the flow flow area.

λ	κ	$\psi_{\kappa\lambda}$	$\Phi_{\kappa\lambda}$
1	1	0	-1
	2	$D_p\ (\rho_A)$	0
	3	$D_h\ (\rho_A)$	0
2	1	1	$-2G / \rho_M$
	2	0	$1 - G^2 D_p(\rho_M^{-1})$
	3	0	$- G^2 D_h(\rho_M^{-1})$
3	1	G / ρ_M	$- h - \frac{3}{2}(\frac{G}{\rho_E})^2$
	2	$hD_p(\rho_H) + \frac{G^2}{2} D_p(\rho_M^{-1}) - 1$	$(G/\rho_E)^3 D_p(\rho_E^{-1})$
	3	$hD_h(\rho_H) + \frac{G^2}{2} D_h(\rho_M^{-1}) + \rho_H$	$- G + (G/\rho_E)^3 D_h(\rho_E^{-1})$

4.2 Definition of the variables used in the conservation equations.

λ	Y_λ	S_λ
1	$< \rho u >$	$- D_{e1} (\rho_A) \frac{\partial e_1}{\partial t} - D_{e2} (\rho_A) \frac{\partial e_2}{\partial t}$
2	p	$- \frac{Z}{A_T} \tau_w - g \rho_A \sin\theta - G^2 D_{e1} (\rho_M^{-1}) \frac{\partial e_1}{\partial s} - G^2 D_{e2} (\rho_M^{-1}) \frac{\partial e_2}{\partial s}$
3	h	$\dot{q}'' \frac{Z}{A_T} + \dot{q}'''_V - g G \sin\theta -$ $- \frac{\partial e_1}{\partial t} (h D_{e1} (\rho_H) + \frac{G^2}{2} D_{e1} (\rho_M^{-1})) - \frac{\partial e_2}{\partial t} (h D_{e2} (\rho_H) + \frac{G^2}{2} D_{e2} (\rho_M^{-1})) +$ $+ \frac{\partial e_1}{\partial s} (\frac{G^3}{\rho_E^3} D_{e1} (\rho_E)) + \frac{\partial e_2}{\partial s} (\frac{G^3}{\rho_E^3} D_{e2} (\rho_E))$

4.3 Definition of the variables used in the conservation equations.

A - 5.1 Figures for Chapter 5.

(a)

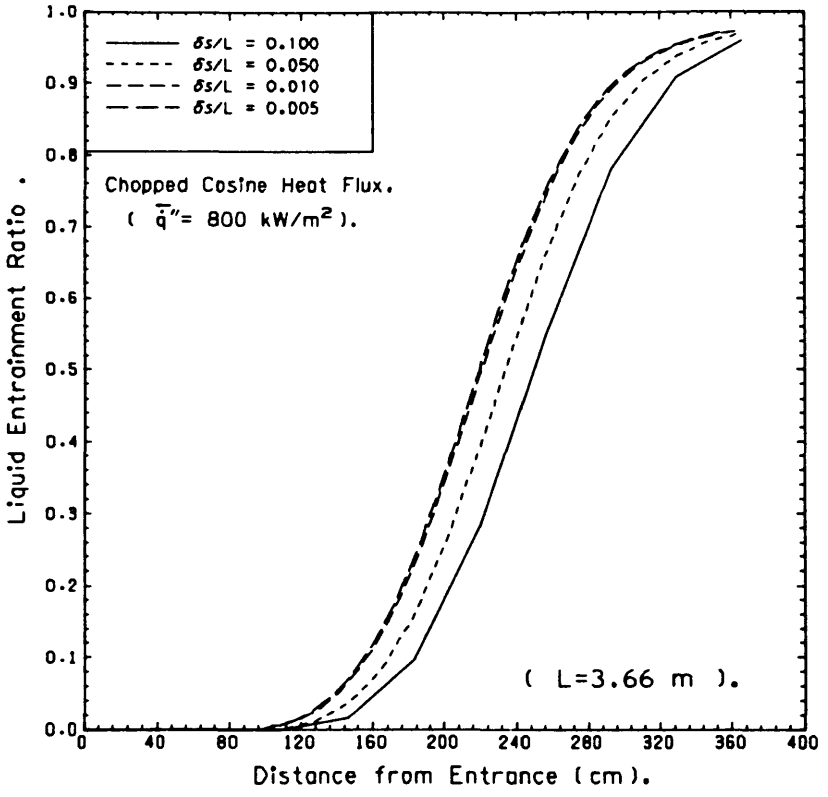

(b)

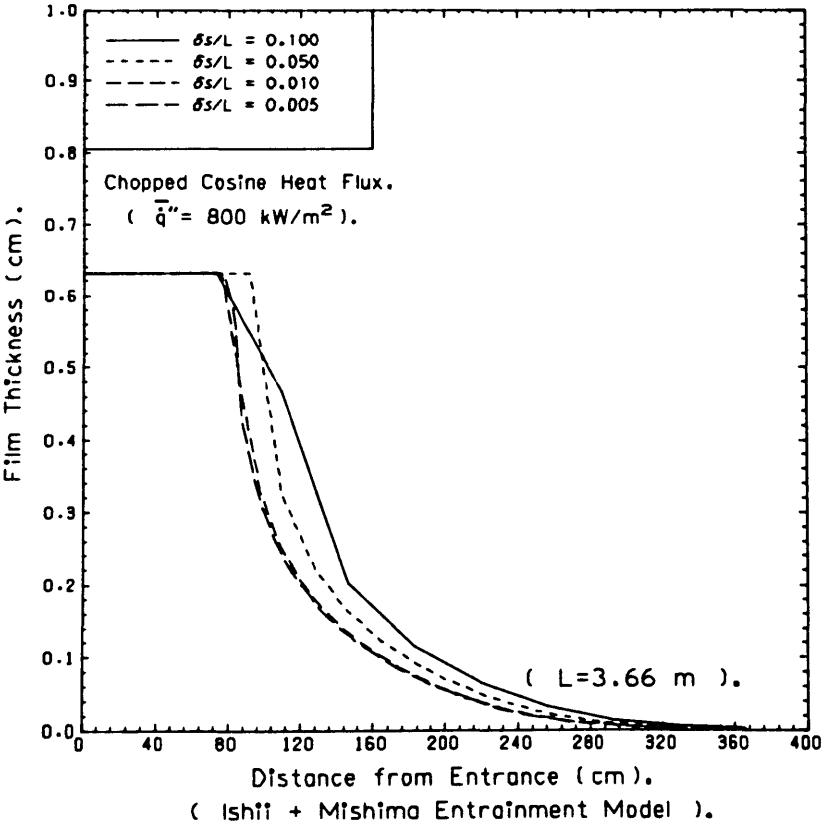

5.1 The effect of grid size on (a) liquid entrainment ratio, (b) film thickness for the Ishii and Mishima entrainment model.

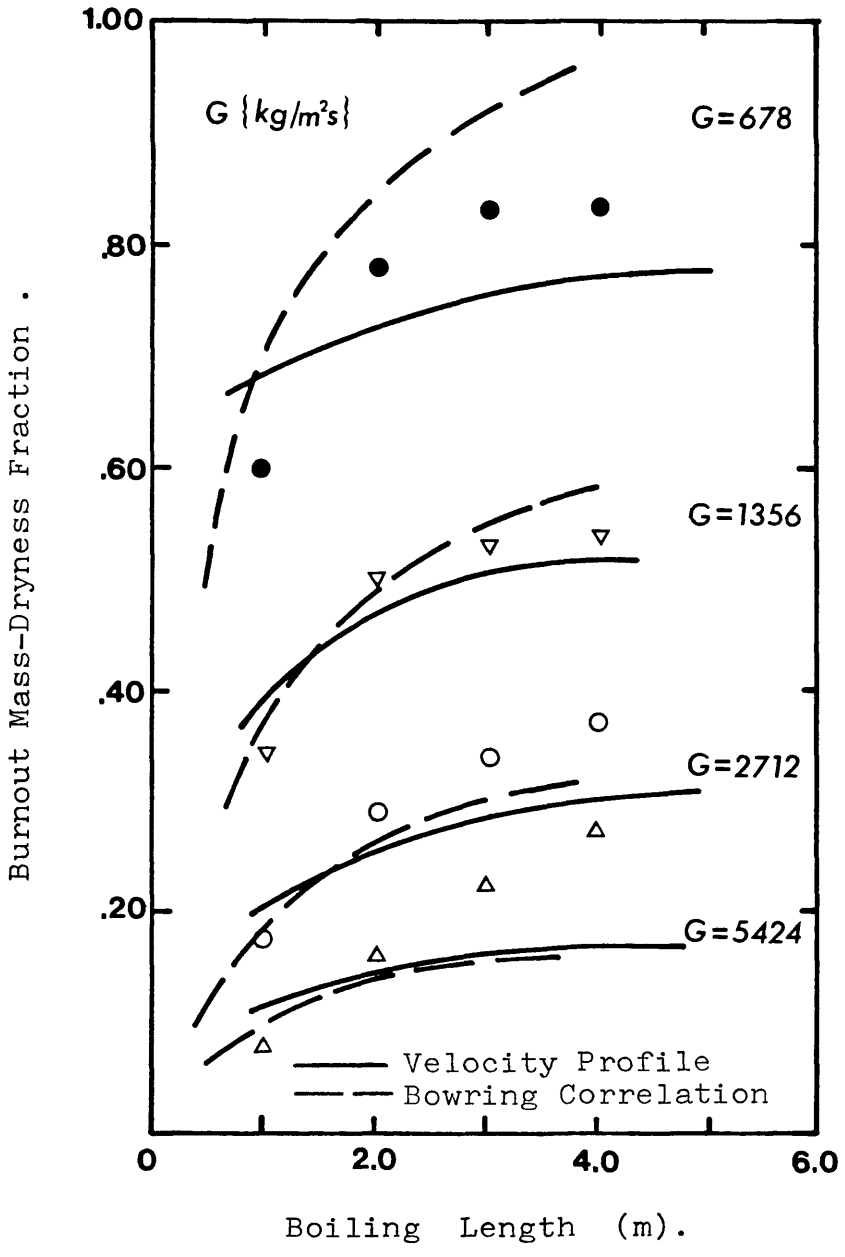

5.2 Burnout mass-dryness fraction at different boiling lengths for a uniformly heated pipe (12.6 mm in diameter).

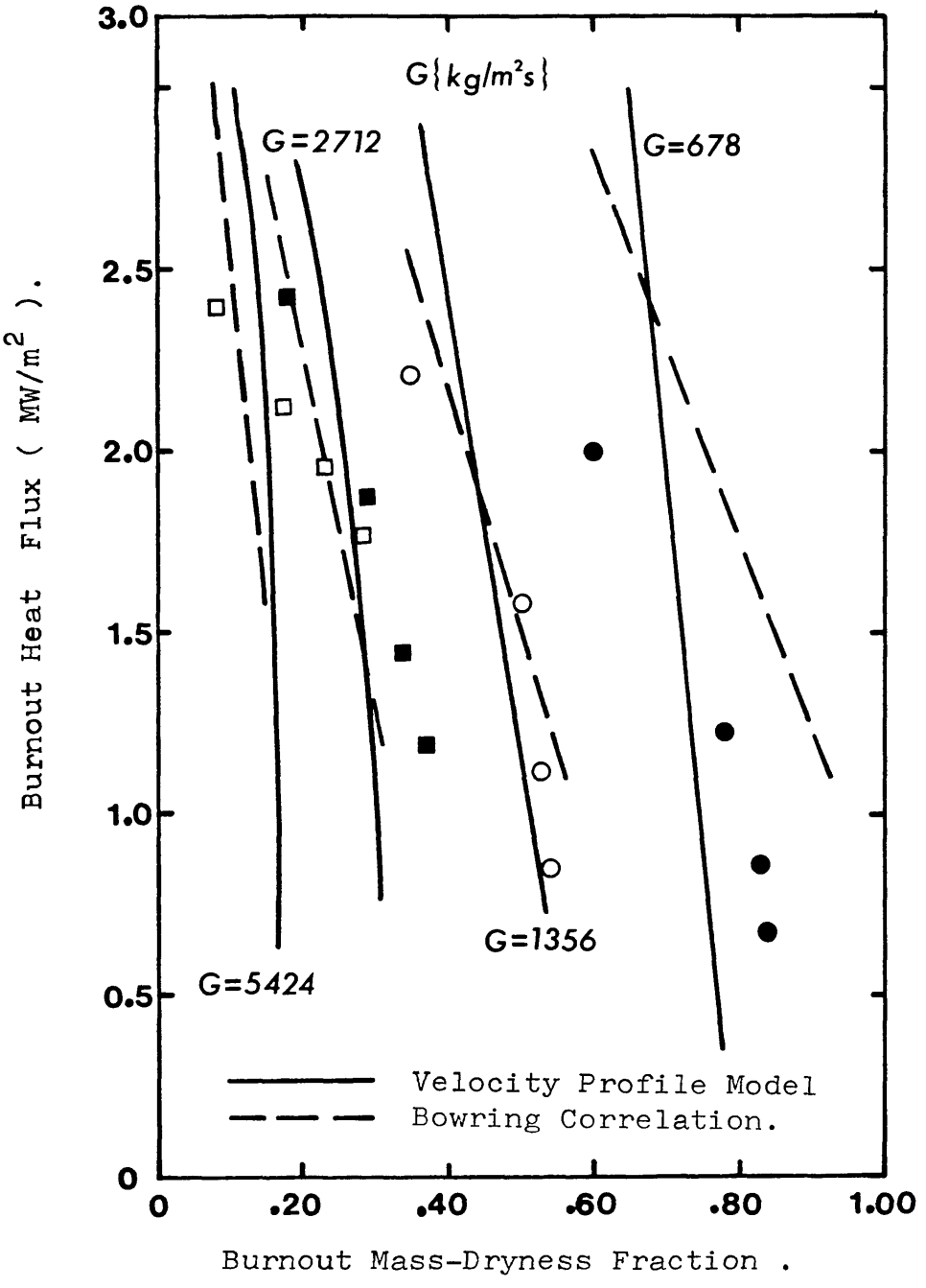

5.3 Burnout heat flux for different dryness fractions in a uniformly heated pipe (12.6 mm in diameter).

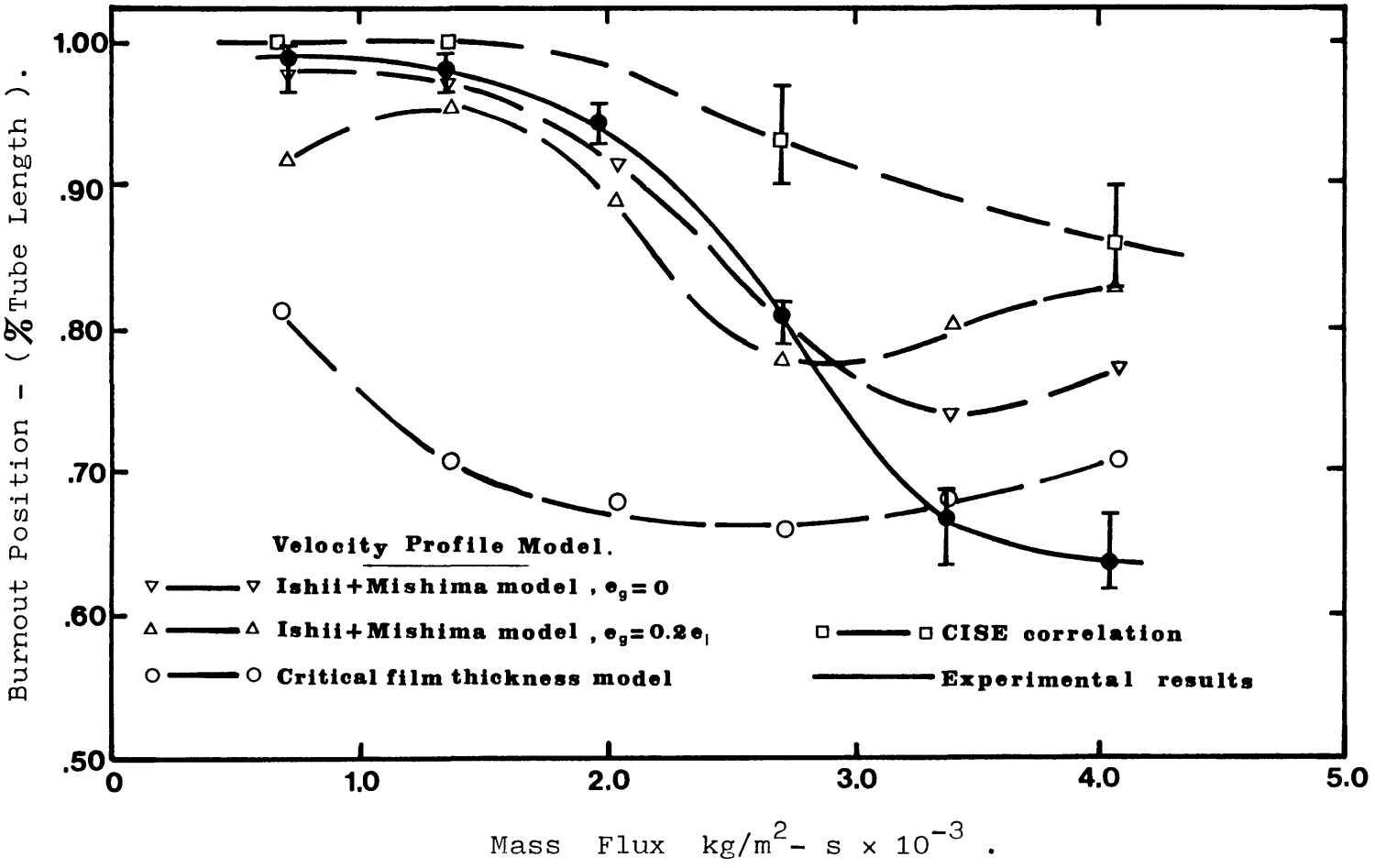

5.4 Burnout position as a function of mass flux for steam-water flow in a tube with a cosine heat flux distribution.

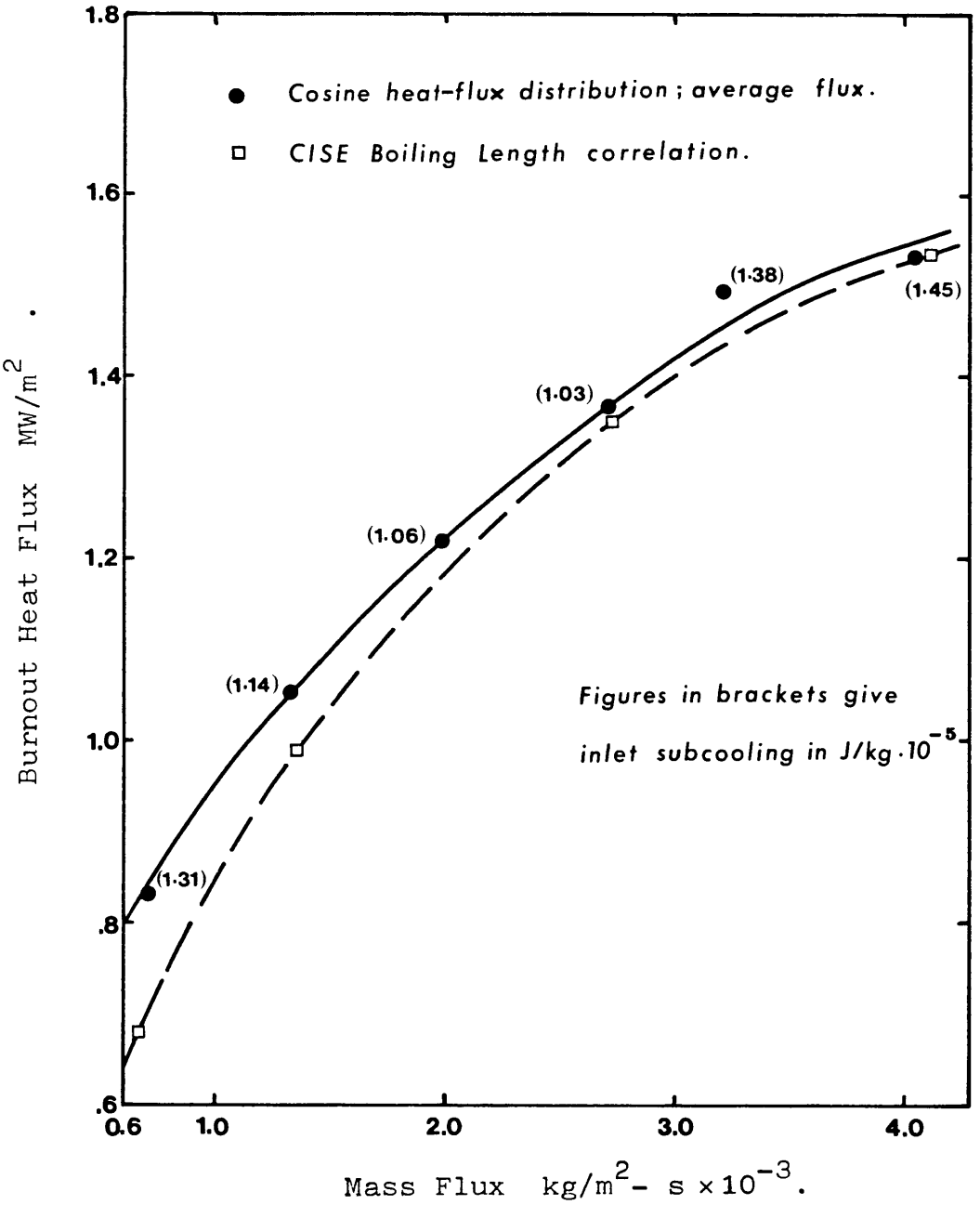

5.5 Burnout heat flux as a function of mass flux for a tube with a cosine heat flux distribution.

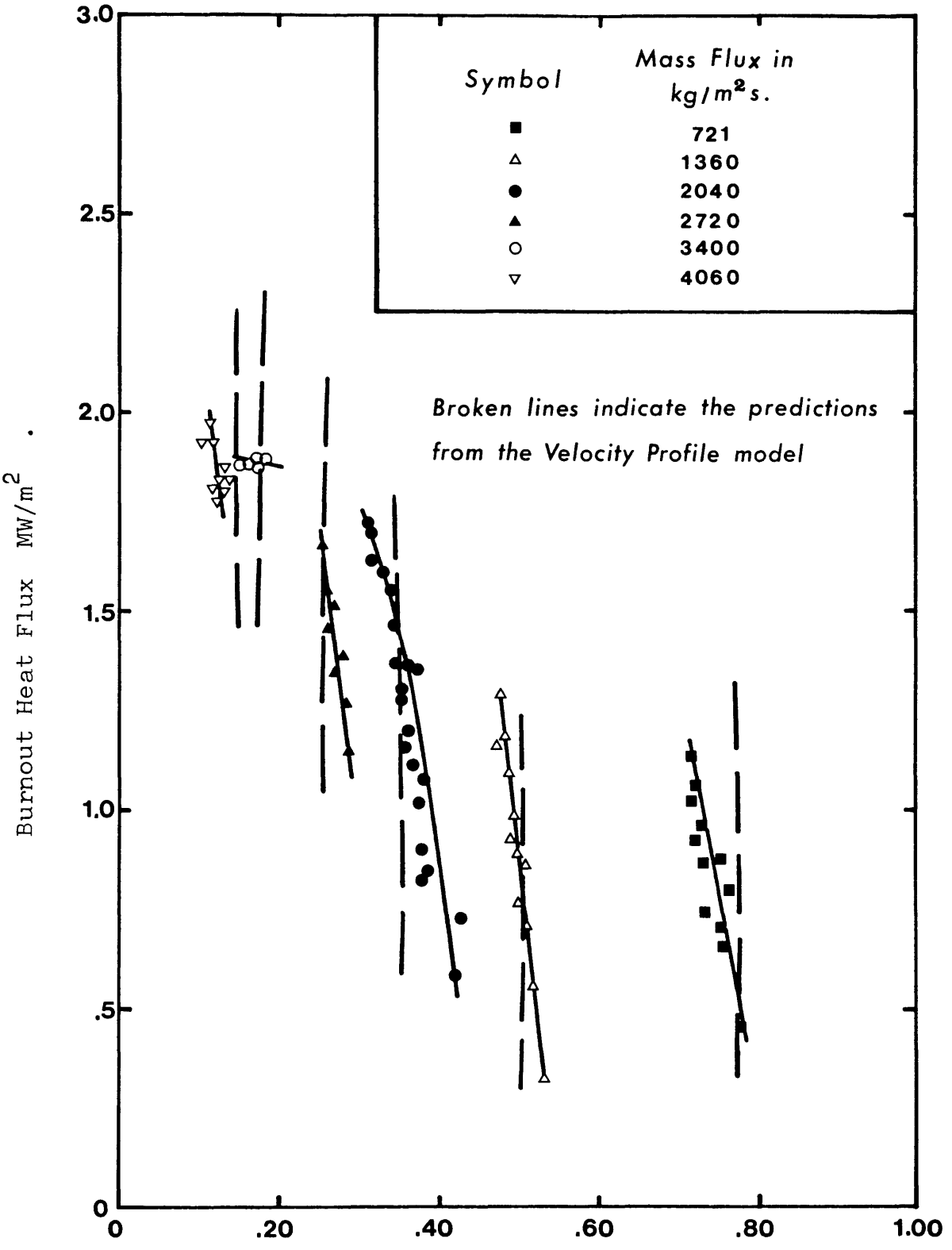

5.6 Comparison of burnout conditions on a local conditions basis for a cosine heat flux distribution.

A - 5.2 Tables for Chapter 5.

Pressure : 68.9 bar. Diameter : 12.6 mm .			Mass flux : 1360 kg/m^2-s . Cold Patch Length : 609.6 mm .			
Case No.	Bottom of Cold patch (mm).	Inlet Subcooling (kJ/kg).	Heat Flux (kW/m^2).	Length to Burnout (m).		
				Experiment	Predicted	Difference(%)
1	423.8	132.6	1121.3	4.2672	4.227	0.9
2	659.4	158.2	1158.2	4.2672	4.318	1.2
3	1273.3	155.8	1152.5	4.2672	4.445	4.2
4	1565.0	255.9	1205.2	4.2672	4.532	6.2
5	1986.1	221.0	1196.4	4.2672	4.572	7.1
6	2570.6	139.6	1178.0	4.2672	4.181	2.0
Predicted length for zero liquid film mass flow rate, without vapour entrainment.						

5.1 Predictions of Burnout length for uniformly heated pipe with a cold patch.

A - 6. Figures for Chapter 6 .

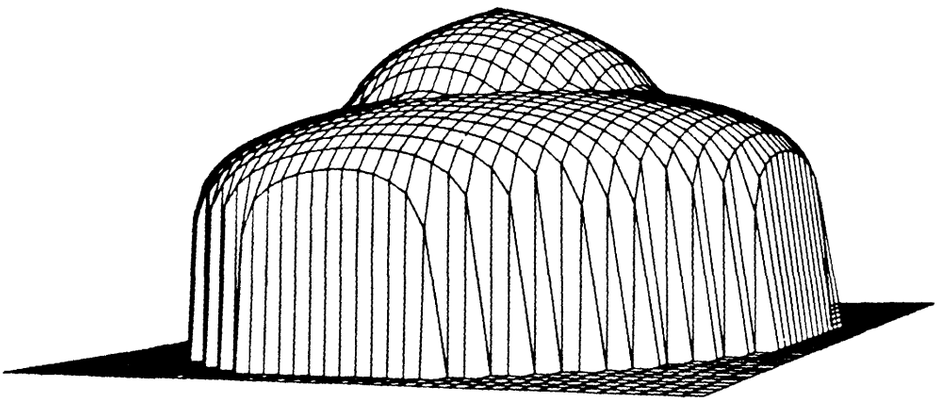

MASS-DRYNESS FRACTION=0.005

PRESSURE=250 PSIA (17.23 BAR)

LIQUID FLOWS CLOSE TO THE WALL

MASS FLOW RATE=100 LB/SEC (45.36 KG/SEC)

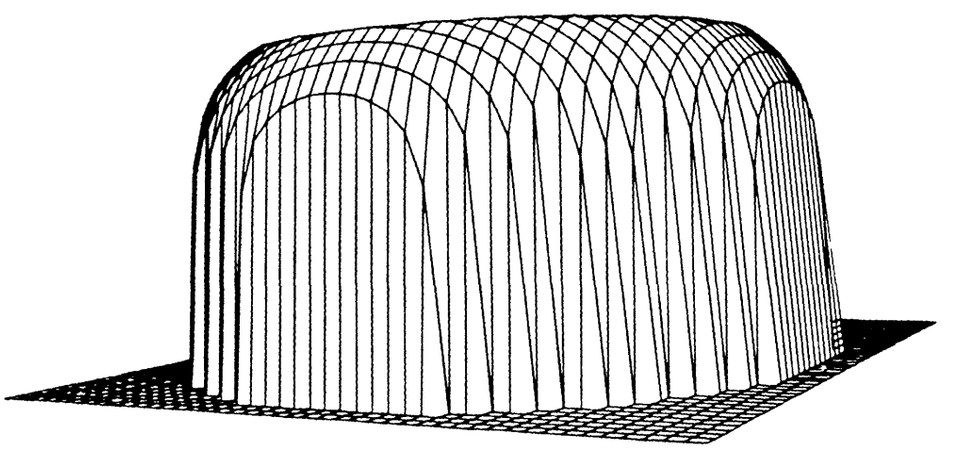

MASS-DRYNESS FRACTION=0.005

PRESSURE=250 PSIA (17.23 BAR)

VAPOUR FLOWS CLOSE TO THE WALL

MASS FLOW RATE=100 LB/SEC (45.36 KG/SEC)

6.1 A three dimensional representation of the velocity profiles.

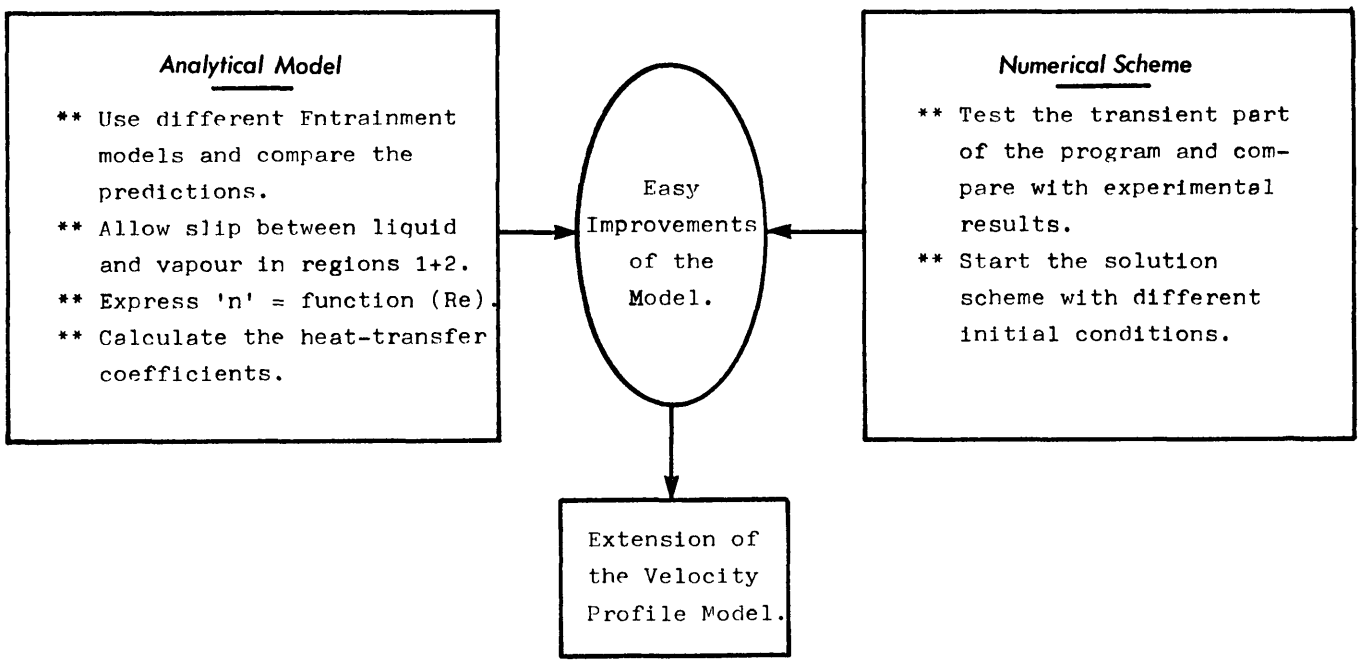

6.2 Diagrammatic representation of the easy improvements of the model.

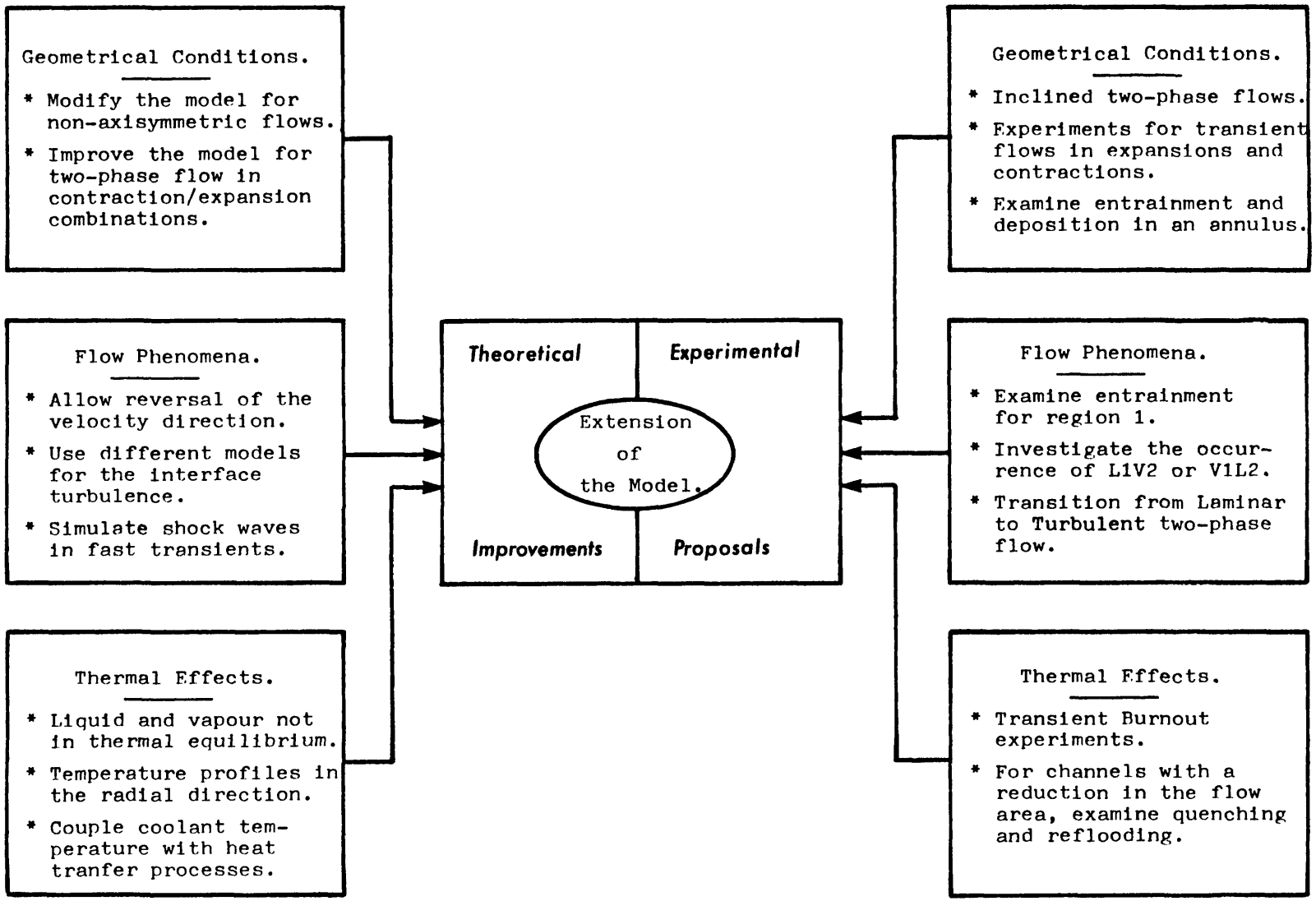

6.3 Further extensions of the velocity profile model.

Appendix B.

The VELPRO Computer Program.

Contents :

APPENDIX B

THE "VELPRO" COMPUTER PROGRAM

B-1 Introduction to the Program.

The "VELPRO" program is designed to calculate the void fraction and pressure drop with the velocity profile model for different mass-dryness fractions and/or mass flow rates in vertical, horizontal or inclined pipe flows, with or without heat transfer.

Because of the great variety of independent variable combinations, the results are usually presented in many different ways. Therefore an interactive computer program is thought to be the easiest solution, with the minimum number of input parameters, which could be flexible enough to allow human intervention even during the calculating stages. With an entrainment option the program can be also made capable of producing results anywhere in the range between the homogeneous and the completely separated types of flow. The corresponding entrainment ratios can be taken to vary with the mass-dryness fraction and either liquid or vapour may be taken as predominant in the wall region. For faster calculations the output from the program can be saved in a magnetic tape or sent directly to the plotter.

A schematic representation of the program construction is shown in figure FB-1 which contains the names of the subroutines used. The main purpose of each subroutine is discussed in the following sections, together with current commands available in the main program to shape the required comparisons. In the final section general remarks from the use of the program are presented, together with some numerical and computational aspects of the calculations.

B-2 General Description of the Program

The program VELPRO, as represented by figure FB.1, consists of a number of subroutines which are used either to form the input part of the main program or to handle the output calculations. Attached to the main program is also a software base of numerical routines and finally the program, with the aid of some software routines, can access the main computer memory base, either for data retrieval and storage or for using the plotting routines.

B-2.1 Description of the Input Part

The input part of program consists of the routines shown in the left hand side of figure FB-1 and contains a number of questions relevant to the options built into the program, and the necessary input parameters. The options that can be used in the description of the two-phase flow problem are those listed in table TB.1. Also at the input, the pipe diameter, angle of inclination to horizontal, the operating pressure and densities are initialised. A complete description of the input is shown in figure FB.2. During the calculations the program has the flexibility to redefine the whole input or part of the physical properties without leaving the execution status.

Immediately after the input to the program, shown in figure FB.2, the routine "VISCOS" is used to calculate the steam-water viscosities. Inside this routine the saturation temperature is first calculated for the operating pressure according to the equation proposed in the Skeleton tables of reference (Ar70). Then for the viscosities the formula proposed in reference (Ba69) is used for the temperature region between 0 to 300 degrees Celsius. Outside this region or for mixtures other than steam-water the program requests the viscosities known from steam tables.

For uniformly heated pipe flows where the inlet conditions are below the saturation point, the routine "PREHEAT" is used to calculate the

length from inlet up to the point of bulk saturation, the pressure drop up to this point, and the mass-dryness fraction at the exit of the specified test section. The same routine can be also used in a different way, to examine whether or not the fluid is subcooled at the inlet to the test section when the mass-dryness fraction at the exit is known. In effect, the routine "PREHEAT" is an application of the momentum and Energy conservation equations for single phase flow.

The entrainment ratios of liquid and vapour at a particular mass-dryness fraction can be also specified at the input. Then for a given table of entrainment ratios at various dryness fractions, the subroutine "ENTRIN" calculates the local entrainment ratios by cubic spline interpolation. This table can be stored in the main computer memory and be retrieved or redefined during any stage of the calculations.

During the calculations we are able to take either the liquid or vapour phases in the region next to the wall. Therefore the properties in region 1 and 2 must correspond to the phases chosen in the input, and any changes are handled by subroutine "FPROP" which is used immediately after the entrainment ratios are found to initialise the transport properties in the flow regions.

B-2.2 Description of the Main Program

The main part of the program is the part where an interactive control of the satellite routines takes place to present or compare void fractions and pressure drops for known mass-dryness fraction or mass-flux. This is achieved by a number of control commands which are shown in figure FB.3, arranged in alphabetical order, together with a short explanation of the action taken. This main part of the program remains always at the execution status until the command "E" is entered.

Thus by suitably choosing the control commands it is easy to examine different aspects of the calculations in many different ways.

It is beyond the purpose of the present thesis to explain in detail what action is taken by these commands. But for a better understanding of their use they can be classed in two main groups as shown by table TB.2. Samples of the outputs produced by the commands CE, CT, EPG, W and PDC are shown respectively in figures FB.4 to FB.8.

However, it is more useful to describe some of the main routines that constitute the heart of the calculations in the main program.

"QUALY" and "VOIDY" are two of the most important routines which are always used for calculating the mass-dryness fraction when the void fraction is known (QUALY), or the void fraction when the mass-dryness fraction is known (VOIDY). Both those routines are developed for the velocity profile model with entrainment and use quadrature routines (Na77) with the method of bisection to find the unique solution for equation (3.2.21) in the interval 0.0 to 1.0. The value accepted as the correct solution is found within error bounds near to the computer accuracy which for the present system is of the order of 1.0 E-15. For similar calculations with different two-phase flow models the program contains the routines "THOM" and "SMITH" for the correlations proposed by J R S Thom (Th64) and S L Smith (Sm70) to predict the void fraction.

"SLIPY" and "VELRAT" are routines that evaluate ratios of the average velocities for the two phases. "SLIPY" is for the ratio of the average velocities of the mixtures in region 1 and 2 and "VELRAT" is for the ratio of $\bar{u}_{1T}$ to the average all liquid velocity with the same mass flow rates. These routines can be used only after the surface of separation and hypothetical radius are calculated from the local void fraction and mass-dryness fraction. Both "SLIPY" and "VELRAT" are useful routines for the pressure drop calculations.

During the pressure drop calculations the program can employ one of the following routines "PDROP", "EDROP" or "GDROP" according to the comparisons requested; "PDROP" gives the calculated pressure drops for different mass-dryness fractions in the region 0.001 to 1.0; "EDROP" is a similar routine but is more suitable for comparisons in an experimental range of mass-dryness fractions. Finally "GDROP" calculates the pressure drop for different mass fluxes when the mass-dryness fraction at the exit is known.

All these routines can be used in the SI or British system of units, and pressure drops can also be normalised to $G^2/2\rho_\ell$. For diabatic pipe flows the same routines are used to calculate the integrals mentioned in section 3-2.3 by a Gaussian (Ce78) integration routine. For the intermediate mass-dryness fractions, during the integral evaluation, the routine "VOIDY" is employed without a significant increase in the computational time.

B-3 Concluding Remarks

Perhaps the most-often-encountered misgiving about existing computer programs, is that they are mostly built with a sophisticated logic which is frequently applicable only to a certain problem for which the program is developed. Therefore such programs require to be extensively rebuilt for application to even a slightly different problem. To avoid this the VELPRO program has been divided into a small number of fundamental satellite routines which can be combined by a series of handling commands to form the solution during different applications.

The main disadvantage of the interactive programs is that they must be reasonable in size and relatively economical. The VELPRO program can satisfy both these requirements and typical execution times for flows

without heat transfer are 0.025 CPS for each different value of dryness fraction, which in the case of diabatic flows becomes 1.793 CPS. The increase is due to the integral evaluation discussed in the last paragraph of section B-2.2. When entrainment was allowed typical times are 0.030 CPS and 1.899 CPS respectively. A substantial improvement of these times is achieved when the "printer-suppress" option is chosen.

About accuracy, as is obvious from the equations related with the velocity profile model described in chapters 2 and 3, it becomes very laborious to check some parts of the program. Nevertheless some parts have been checked manually and for the parts where that was difficult different solution procedures have been applied to examine their influence on the results produced.

Finally in the general flow of the program, infinite or indefinite errors arising from bad input arguments have been dealt with in such a way that they do not interrupt the execution status but they prompt warnings with the necessary action that should be taken next. This is a very useful feature especially for commands which handle files in the main computer base. The important benefit is that the program can be used quite safely by a person who does not know its detailed structure.

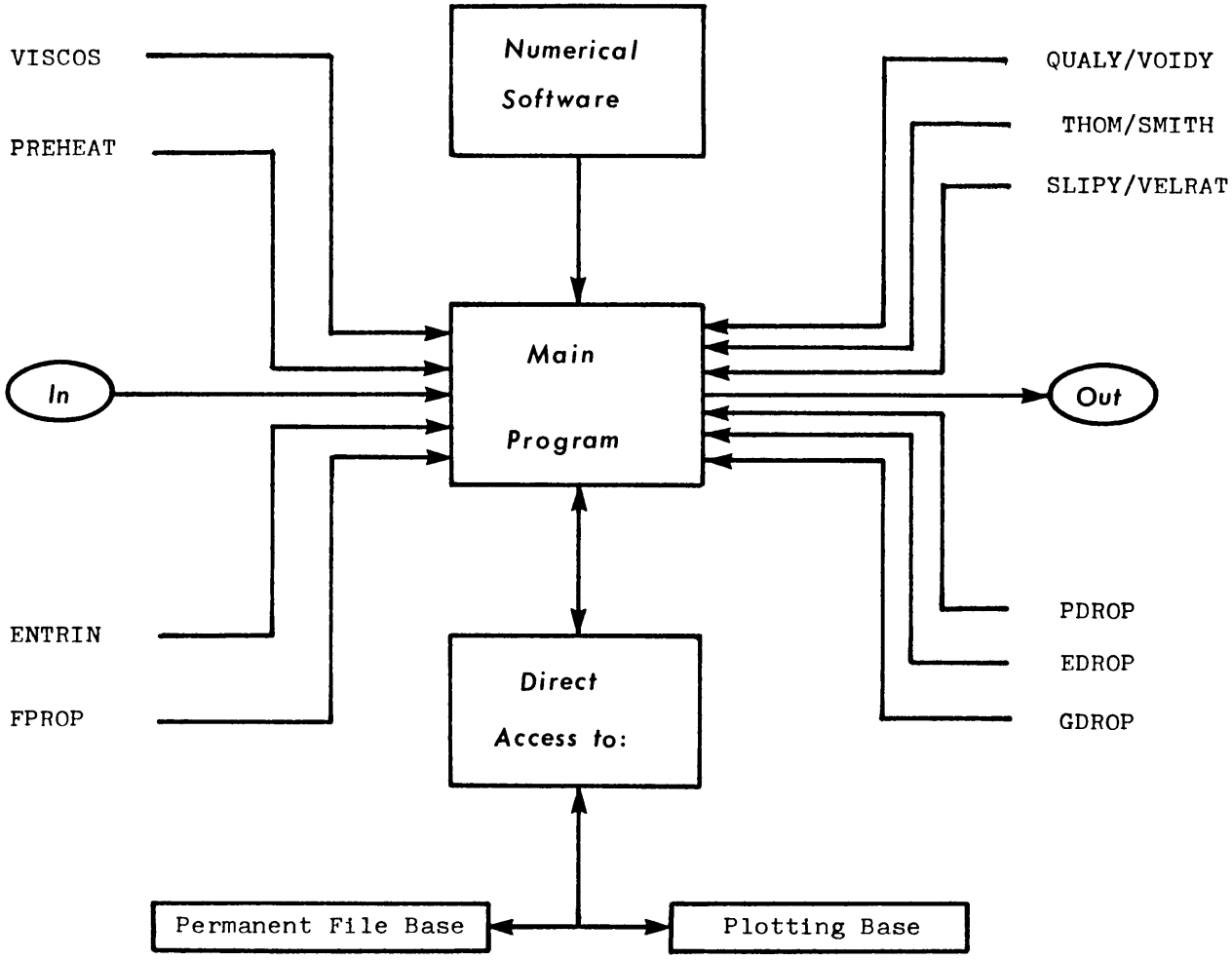

FB.1 Schematic representation of the computer program VELPRO.

```
1 IS THE INLET FLOW LAMINAR OR TURBULENT.?
? turbulent

 ENTER THE VALUE OF THE POWER FOR THE VELOCITY PROFILE.?
  FOR THE TIME BEING THE PROFILES HAVE THE SAME POWER.
? 7.0
 ENTER THE DIAMETER OF THE PIPE IN INCHES.?
 AND THE ANGLE OF INCLINATION TO THE HORIZONTAL.?
? 1.0      90.0
 IS THE CHANNEL HEATED, UNHEATED, OR WITH A PREHEATED INPUT.?
? heated
 WHICH OF THE TWO PHASES IS NEXT TO THE WALL.?
? liquid
 ENTER THE OPERATING PRESSURE (IN PSIA).?
? 1000.0
 ENTER THE DENSITY OF THE VAPOUR AND LIQUID PHASES (IN LB/FT**3).?
?     2.241       46.321
 ARE THE VISCOSITIES MEASURED FOR 544.58 DEG.FAHRENHEIT.?
? no


 ENTER COMMAND OR HELP:?
?
```

FB.2 The input part of the program.

```
help

 ** RATIONALISED VELOCITY PROFILE PROGRAM FOR THE TWO-PHASE FLOW.**

 CURRENT COMMANDS AVAILABLE.:

 BU  BRITISH UNITS ARE USED FOR THE RESULTS PRINTED.
 CE  COMPARES THE VOID FRACTIONS WITH EXPERIMENTAL DATA.
 CT  COMPARES THE 2-PHASE PARAMETERS WITH OTHER THEORIES.
 E   EXIT WITH STORAGE OF THE PROCESSED DATA.
 EP  COMPARES MEASURED PRESSURE DROPS.
 EPC COMPARES MEASURED PRESSURE COEFFICIENTS.
 EPG EXAMINES PRESSURE DROPS FOR KNOWN MASS-FLUXES.
 ECG EXAMINES PRESS.COEFFICIENTS WHEN MASS-FLUX IS KNOWN.
 ETR INITIATES THE ENTRAINMENT OF THE TWO-PHASES.
 H   HELP;DISPLAYS THIS PAGE.
 PC  CHANGE OF THE INPUT PRESSURE.
 PD  GIVES THE PREDICTED PRESSURE DROP OVER THE
     COMPLETE MASS-DRYNESS FRACTION RANGE.
 PDC COEFFICIENTS OF PRESSURE DROP FOR THE COMPLETE
     MASS-DRYNESS FRACTION RANGE.
 PRT SCREEN PRINTER ENABLE.
 PRS SCREEN PRINTER SUPPRESSED (OUTPUT SAVED AS FILE).
 R   REDEFINES THE WHOLE INPUT OF THE FLOW MODEL.
 S   RESULTS SAVED IN THE ALLOCATED PERMANENT FILE BASE.
     (DEFAULT NAMES GIVEN AT THE END OF THE PROGRAM).
 SI  SI UNITS ARE USED FOR THE PRINTED RESULTS.
 W   THE WHOLE  RANGE OF MASS-DRYNESS FRACTION IS EXAMINED
     BY USING THE VELOCITY PROFILE MODEL.


 ENTER COMMAND OR HELP:?
?
```

FB.3 List of the available commands.

```
 ce


 IS THE INPUT DATA STORED UNDER A PERMANENT FILE.?
? no
 IS THE VOID FRACTION MEASURED (REPLY Y/N).?
? no
 ENTER THE MEASURED QUALITY.?
? 0.06547
```

```
 ------------------------------------------------------------------------
 I                                                                      I
 I              OPERATING CONDITIONS                                    I
 I         FOR  LIQUID  FLOWING NEXT TO THE  HEATED  WALL.              I
 I                                                                      I
 I    OPERATING PRESSURE 1000.00 PSIA.   PIPE DIAMETER   1.000    INCHES  I
 I                       68.948 (BAR)                    2.540    ( CM )  I
 I    DENSITIES   OF VAPOUR   2.241      AND LIQUID     46.321    LB/FT**3  I
 I                   VAPOUR  35.897      AND LIQUID    741.9911   KG/M**3  I
 I    OUALITY   .065470                  VOID FRACTION    .506110        I
 I                                                                      I
 I    GAS/LIQUID SLIP VELOCITY RATIO  1.4131                          I
 I    RATIO OF ENTRAINMENT : VAPOUR =       0     LIQUID =       0      I
 I                                                                      I
 ------------------------------------------------------------------------
 ------------------------------------------------------------------------
 I                                                                      I
 I   SEPERATION OF TWO PHASES AT RADIUS =        .35571  IN. OR   .90350 CM.  I
 I   RADIUS OF THE HYPOTHETICAL CYLINDER IS  =   .38744  IN. OR   .98411 CM.  I
 I                                                                      I
 I      IN HEATED PIPE THE AVERAGE                                      I
 I   TWO PHASE FRICTION PRESSURE DROP MULTIPLIER IS =   2.28207         I
 I                                                                      I
 ------------------------------------------------------------------------
 DO YOU WANT TO CHANGE THE MEASURED QUANTITIES.?
? no
```

FB.4 Sample output from the command "CE".

ct

QUALITY	RATIO OF ENTRAINMENT VAPOUR	LIQUID	VOID FRACT. PROFILE METHOD.	VOID FRACT. SJ THOM. REF40/80	VOID FRACT. S.SMITH REF54/80
.001000	0	0	.016427	.012065	.019986
.002000	0	0	.032171	.023865	.038707
.003000	0	0	.047317	.035410	.056299
.004000	0	0	.061917	.046708	.072877
.005000	0	0	.076010	.057765	.088543
.006000	0	0	.089629	.068591	.103381
.007000	0	0	.102803	.079191	.117467
.008000	0	0	.115558	.089574	.130866
.009000	0	0	.127917	.099746	.143637
.010000	0	0	.139901	.109712	.155831
.020000	0	0	.242716	.199346	.254005
.030000	0	0	.322583	.273952	.324330
.040000	0	0	.386834	.337017	.378541
.050000	0	0	.439865	.391026	.422361
.060000	0	0	.484514	.437799	.458977
.070000	0	0	.522712	.478700	.490331
.080000	0	0	.555823	.514768	.517688
.090000	0	0	.584845	.546813	.541911
.100000	0	0	.610523	.575472	.563618
.200000	0	0	.765998	.753086	.705604
.300000	0	0	.841454	.839450	.786432
.400000	0	0	.887204	.890511	.841905
.500000	0	0	.918481	.924242	.883421
.600000	0	0	.941591	.948187	.916105
.700000	0	0	.959667	.966063	.942714
.800000	0	0	.974501	.979920	.964905
.900000	0	0	.987319	.990975	.983754
1.000000	0	0	1.000000	1.000000	1.000000

ENTER COMMAND OR HELP:?
?

FB.5 Sample output from the command "CT".

```
  epg


 ENTER THE LENGTH OF THE TEST SECTION (FT).?
? 20.0
 ENTER THE QUALITY AT THE EXIT.?
? 0.5
 ENTER THE PERMANENT FILE NAME.?
 (THE END OF FILE MUST BE MARKED WITH : 99.99).
? test
```

OPERATING CONDITIONS
FOR LIQUID FLOWING NEXT TO THE HEATED WALL.

OPERATING PRESSURE	1000.00 PSIA.	PIPE DIAMETER	1.000	INCHES
	68.948 (BAR)		2.540	(CM)
DENSITIES OF VAPOUR	2.241	AND LIQUID	46.321	LB/FT**3
VAPOUR	35.897	AND LIQUID	741.9911	KG/M**3
VISCOSITIES OF VAPOUR	.1276E-04	AND LIQUID	.63537E-04	LB/FT*SEC
VAPOUR	.1899E-04	AND LIQUID	.94554E-04	KG/M*SEC

QUALITY	MASS-FLUX (LB/FT2-SEC)	VOID FRACTION	ENTR.RATIO VAPOUR	ENTR.RATIO LIQUID	PRESSURE (PSIA) MEASURE	PRESSURE (PSIA) PREDICT.	DIFFEREN. PER CENT
.5000	50.00000	.91848	0	0	4.5600	2.5638	43.776
.5000	70.67500	.91848	0	0	4.8900	3.1047	36.509
.5000	100.00600	.91848	0	0	5.5900	4.1151	26.385
.5000	150.00000	.91848	0	0	11.5000	6.4487	43.924
.5000	200.00000	.91848	0	0	19.5000	9.5055	51.254
.5000	300.00000	.91848	0	0	34.5600	17.6455	48.942
.5000	400.00000	.91848	0	0	43.6700	28.3327	35.121
.5000	500.00000	.91848	0	0	80.6000	41.4387	48.587

```
 ENTER COMMAND OR HELP:?
?
```

FB.6 Sample output from the command "EPG".

```
 w


 IS THE QUALITY KNOWN.?
? yes
```

OPERATING CONDITIONS
FOR LIQUID FLOWING NEXT TO THE HEATED WALL.

OPERATING PRESSURE 1000.00 PSIA. PIPE DIAMETER 1.000 INCHES
68.948 (BAR) 2.540 (CM)
DENSITIES OF VAPOUR 2.241 AND LIQUID 46.321 LB/FT**3
VAPOUR 35.897 AND LIQUID 741.9911 KG/M**3

QUALITY	RATIO OF ENTRAINMENT VAPOUR	LIQUID	SURFACE OF SEPARATION RADIUS(IN)	HYPOTH. RADIUS (IN).	LIQUID FRICTN. MULTIPL.	GAS/LIQUID SLIP VEL. RATIO.	VOID FRACTION
.0010	0	0	.06408	.1600	1.0170	1.23884	.01643
.0020	0	0	.08968	.1799	1.0339	1.24616	.03217
.0030	0	0	.10876	.1948	1.0508	1.25225	.04732
.0040	0	0	.12442	.2070	1.0678	1.25767	.06192
.0050	0	0	.13785	.2175	1.0848	1.26263	.07601
.0060	0	0	.14969	.2267	1.1019	1.26727	.08963
.0070	0	0	.16031	.2350	1.1190	1.27164	.10280
.0080	0	0	.16997	.2426	1.1362	1.27580	.11556
.0090	0	0	.17883	.2495	1.1535	1.27978	.12792
.0100	0	0	.18702	.2559	1.1709	1.28360	.13990
.0200	0	0	.24633	.3021	1.3496	1.31613	.24272
.0300	0	0	.28398	.3315	1.5378	1.34245	.32258
.0400	0	0	.31098	.3526	1.7355	1.36514	.38683
.0500	0	0	.33161	.3686	1.9428	1.38534	.43986
.0600	0	0	.34804	.3815	2.1595	1.40369	.48451
.0700	0	0	.36149	.3920	2.3856	1.42059	.52271
.0800	0	0	.37277	.4008	2.6209	1.43634	.55582
.0900	0	0	.38238	.4082	2.8652	1.45113	.58485
.1000	0	0	.39068	.4147	3.1184	1.46512	.61052
.2000	0	0	.43761	.4513	6.1151	1.57858	.76600
.3000	0	0	.45865	.4677	9.8948	1.66911	.84145
.4000	0	0	.47096	.4773	14.3925	1.75192	.88720
.5000	0	0	.47919	.4838	19.5616	1.83453	.91848
.6000	0	0	.48518	.4884	25.3655	1.92331	.94159
.7000	0	0	.48981	.4921	31.7736	2.02701	.95967
.8000	0	0	.49358	.4950	38.7587	2.16336	.97450
.9000	0	0	.49682	.4975	46.2942	2.38929	.98732

FB.7 Sample output from the command "W".

```
 pdc


 ENTER THE LENGTH OF THE TEST SECTION (FT).?
 AND THE MASS FLUX AT INPUT (LB/SEC*FT**2).?
? 18.0      350.0
```

OPERATING CONDITIONS
FOR LIQUID FLOWING NEXT TO THE HEATED WALL.

OPERATING PRESSURE	1000.00 PSIA.	PIPE DIAMETER	1.000	INCHES
	68.948 (BAR)		2.540	(CM)
DENSITIES OF VAPOUR	2.241	AND LIQUID	46.321	LB/FT**3
VAPOUR	35.897	AND LIQUID	741.9911	KG/M**3
VISCOSITIES OF VAPOUR	.1276E-04	AND LIQUID	.63537E-04	LB/FT*SEC
VAPOUR	.1899E-04	AND LIQUID	.94554E-04	KG/M*SEC

QUALITY	EXPANSION COEFFIC.	ENTR. RATIO VAPOUR	ENTR. RATIO LIQUID	PRESSURE DROP COEFFICIENTS ACCELER.	FRICTION.	GRAVIT.	TOTAL
0	0	0	0	0	1.31279	10.1437	11.4565
.01271	.25000	0	0	.19656	1.59955	9.2616	11.0577
.02542	.50000	0	0	.38483	1.90406	8.5798	10.8687
.03813	.75000	0	0	.56840	2.22882	8.0265	10.8237
.05084	1.00000	0	0	.74904	2.57389	7.5636	10.8865
.06355	1.25000	0	0	.92780	2.93898	7.1679	11.0347
.07626	1.50000	0	0	1.10545	3.32373	6.8240	11.2532
.08897	1.75000	0	0	1.28254	3.72776	6.5212	11.5315
.10168	2.00000	0	0	1.45949	4.15071	6.2516	11.8618
.11439	2.25000	0	0	1.63663	4.59224	6.0095	12.2383
.12710	2.50000	0	0	1.81426	5.05202	5.7903	12.6566
.13981	2.75000	0	0	1.99260	5.52975	5.5906	13.1130
.15252	3.00000	0	0	2.17185	6.02515	5.4077	13.6047
.16523	3.25000	0	0	2.35219	6.53796	5.2392	14.1293
.17794	3.50000	0	0	2.53377	7.06791	5.0833	14.6850
.19065	3.75000	0	0	2.71672	7.61479	4.9385	15.2700
.20336	4.00000	0	0	2.90116	8.17837	4.8036	15.8831
.21607	4.25000	0	0	3.08721	8.75843	4.6774	16.5231
.22878	4 50000	0	0	3.27496	9.35479	4.5591	17.1888
.24149	4.75000	0	0	3.46451	9.96726	4.4478	17.8795
.25420	5.00000	0	0	3.65593	10.59564	4.3428	18.5944

EXPANSION COEFFICIENT=QUAL*(DENL/DENG-1).
PRES.DROP COEF=PRE.DROP/DENL*VEL(IN)**2.

FB.8 Sample output from the command "PDC".

Laminar	Turbulent	**Flow**
Homogeneous	Separated / Entrained	**Mixtures**
Liquid	Vapour	**Next to the wall**
Unheated	Heated / Preheated	**Pipe wall**
Horizontal	Inclined	**Geometry**

TB.1 Table of the input options.

Setting-up Commands	Calculating Commands
BU / SI	CE
PRT / PRS	CT
ETR	EP / EPC
R / PC	EPG / ECG
S	PD / PDC
E	W

TB.2 Classification of the commands for the main program.

Appendix C.

The Two-Phase Average Densities.

Contents :

APPENDIX C

THE TWO-PHASE AVERAGE DENSITIES

C-1 Calculation of the Average Densities

From the definitions of the average densities used in the flow conservation equations of chapter 4 it is possible to express these densities in terms of the local void fraction, mass-dryness fraction, the entrainment ratios for each phase and the actual densities. The transformations which follow in this appendix are significantly simplified when the definitions of the void fractions and dryness fractions made in chapter 3 are used to find the ratios of total mass flow rate, and similarly for the flow areas A_1 and A_2.

As follows from equation (3.2.6) the total mass flow rate in region 1 is given by

$$\dot{m}_1 = \dot{m}_g - \dot{m}_{g2} + \dot{m}_{\ell 1} \qquad (C.1.1)$$

This equation can be simplified from equations (3.2.2) and (3.2.6) to become

$$\dot{m}_1 = x\,\dot{m}_T - x_2\,(\dot{m}_T - \dot{m}_1) + (1 - x_1)\,\dot{m}_1 \qquad (C.1.2)$$

Further rearrangement gives :

$$(\dot{m}_1 / \dot{m}_T) = (x - x_2) / (x_1 - x_2) \qquad (C.1.3)$$

Also from the definitions of the total mass flow rate as the sum of the flow rates in region 1 and 2

$$\dot{m}_T \equiv \dot{m}_1 + \dot{m}_2 \qquad (C.1.4)$$

From equations (C.1.3) and (C.1.4) it is easily obtained that :

$$(\dot{m}_2 / \dot{m}_T) = (x_1 - x) / (x_1 - x_2) \qquad (C.1.5)$$

In a similar way, the total liquid and vapour area in region 1 is given from

$$A_1 = A_{g1} + A_{\ell 1} = \alpha\, A_T - A_{g2} + A_{\ell 1} \qquad (C.1.6)$$

This equation is further simplified from equation (3.2.8) to become

$$A_1 = \alpha\, A_T - \alpha_2 A_2 + (1 - \alpha_1)\, A_1 \qquad (C.1.7)$$

or,

$$A_1 = \alpha\, A_T - \alpha_2 \,(\, A_T - A_1\,) + (\,1 - \alpha_1)\, A_1$$

Therefore from a similar analysis as equations (C.1.3) and (C.1.5) we obtain :

$$(\, A_1 \,/\, A_T\,) = (\,\alpha - \alpha_2\,) \,/\, (\,\alpha_1 - \alpha_2\,) \qquad (C.1.8)$$

and

$$(\, A_2 \,/\, A_T\,) = (\,\alpha_1 - \alpha\,) \,/\, (\,\alpha_1 - \alpha_2\,) \qquad (C.1.9)$$

For known entrainment ratios e_1 and e_2 it is also possible to use these ratios in equations (C.1.3) to (C.1.9) instead of the void fraction and mass-dryness fraction for each region. This is easily achieved from equations (3.2.2), (3.2.10) and (3.2.11) which give for liquid predominating region 1 :

$$x_1 = (\, e_2 x\,)\, [\, e_2 x + (\,1 - e_1\,)\,(\,1 - x\,)\,]^{-1} \qquad (C.1.10)$$

and

$$x_2 = (\,1 - e_2\,)\, x\, [\,(\,1 - e_2\,)\, x + e_1\,(\,1 - x\,)\,]^{-1} \qquad (C.1.11)$$

The corresponding expressions for α_1 and α_2 are already given by equations (3.2.16) and (3.2.17).

C-1.1 The area-averaged density

From the definition of the area-averaged density given by equation (4.2.5) it is obvious that

$$\rho_A = \frac{1}{A_T}\, [\, \rho_\ell A_{\ell 1} + \rho_g\, A_{g1} + \rho_\ell A_{\ell 2} + \rho_g\, A_{g2}\,] \qquad (C.1.12)$$

This equation is simplified by substitution from equations (3.2.3) and (3.2.4) to become

$$\rho_A = \frac{1}{A_T} \left[\left(\dot{m}_1 / \bar{u}_1 \right) + \left(\dot{m}_2 / \bar{u}_2 \right) \right]$$

or

$$\rho_A = \bar{\rho}_1 \left(A_1 / A_T \right) + \bar{\rho}_2 \left(A_2 / A_T \right) \qquad \text{(C.1.13)}$$

when equations (3.2.6) and (3.2.7) are used. From equations (C.1.13), (C.1.8) and (C.1.9) it is easily derived that :

$$\rho_A = \bar{\rho}_1 f_1 + \bar{\rho}_2 f_2 \qquad \text{(C.1.14)}$$

where :

$$f_1 \equiv \left(\alpha - \alpha_2 \right) / \left(\alpha_1 - \alpha_2 \right)$$
$$f_2 \equiv \left(\alpha_1 - \alpha \right) / \left(\alpha_1 - \alpha_2 \right) \qquad \text{(C.1.15)}$$

C-1.2 The flow-averaged density

The flow-averaged density defined by equation (4.2.6) can be expressed as :

$$\frac{1}{\rho_F} = \frac{1}{\dot{m}_T} \left[\bar{u}_1 A_1 + \bar{u}_2 A_2 \right] \qquad \text{(C.1.16)}$$

or as :

$$\frac{1}{\rho_F} = \frac{1}{\bar{\rho}_1} \cdot \frac{\dot{m}_1}{\dot{m}_T} + \frac{1}{\bar{\rho}_2} \cdot \frac{\dot{m}_2}{\dot{m}_T} \qquad \text{(C.1.17)}$$

when equations (3.2.6) and (3.2.7) are used. Further rearrangement in equation (C.1.17) gives :

$$\left(1 / \rho_F \right) = \left(f_1 / \bar{\rho}_1 \right) + \left(f_2 / \bar{\rho}_2 \right) \qquad \text{(C.1.18)}$$

where f_1 and f_2 are defined from equations (C.1.17), (C.1.3) and (C.1.5) as :

$$f_1 \equiv \left(x - x_2 \right) / \left(x_1 - x_2 \right)$$
$$f_2 \equiv \left(x_1 - x \right) / \left(x_1 - x_2 \right) \qquad \text{(C.1.19)}$$

C-1.3 The momentum-averaged density

As for the area and flow averaged densities the momentum-averaged density defined by equation (4.2.7) can be expressed as :

$$\frac{1}{\rho_M} = \frac{A_T}{\dot{m}_T^2} \left[\rho_\ell \overline{u_1^2} A_{\ell 1} + \rho_g \overline{u_1^2} A_{g1} + \rho_\ell \overline{u_2^2} A_{\ell 2} + \rho_g \overline{u_2^2} A_{g2} \right] \qquad (C.1.20)$$

where $\overline{u_1^2} = \frac{1}{A_1} \int_{A_1} u_1^2 \, dA$ and $\overline{u_2^2} = \frac{1}{A_2} \int_{A_2} u_2^2 \, dA$. (C.1.21)

Equation (C.1.20) can be rearranged to give

$$\frac{1}{\rho_M} = \frac{A_T}{\dot{m}_T^2} \left[(\rho_\ell \bar{u}_1^2 A_{\ell 1} + \rho_g \bar{u}_1^2 A_{g1}) U_1^2 + (\rho_\ell \bar{u}_2^2 A_{\ell 2} + \rho_g \bar{u}_2^2 A_{g2}) U_2^2 \right] \qquad (C.1.22)$$

which is further simplified by substitution from equations (3.2.3), (3.2.4), (3.2.6) and (3.2.7) to give :

$$\frac{1}{\rho_M} = \frac{A_T}{\dot{m}_T^2} \left[\frac{\dot{m}_1^2}{\bar{\rho}_1 A_1} U_1^2 + \frac{\dot{m}_2^2}{\bar{\rho}_2 A_2} U_2^2 \right] \qquad (C.1.23)$$

Then from equations (C.1.3), (C.1.5), (C.1.8) and (C.1.9)

$$(1/\rho_M) = (f_1/\bar{\rho}_1) + (f_2/\bar{\rho}_2) \qquad (C.1.24)$$

where f_1 and f_2 are defined as :

$$f_1 \equiv \left(\frac{x - x_2}{x_1 - x_2} \right)^2 \left(\frac{\alpha_1 - \alpha_2}{\alpha - \alpha_2} \right) U_1^2 \qquad (C.1.25)$$

$$f_2 \equiv \left(\frac{x_1 - x}{x_1 - x_2} \right)^2 \left(\frac{\alpha_1 - \alpha_2}{\alpha_1 - \alpha} \right) U_2^2 \qquad (C.1.26)$$

The average velocity ratios U_1^2 and U_1^2 in equations (C.1.22) to (C.1.26)

are defined as :

$$U_1^2 \equiv \left[\frac{1}{A_1}\int_{A_1} u_1^2\, dA\right] / \left[\frac{1}{A_1}\int_{A_1} u_1\, dA\right]^2$$
$$U_2^2 \equiv \left[\frac{1}{A_2}\int_{A_2} u_2^2\, dA\right] / \left[\frac{1}{A_2}\int_{A_2} u_2\, dA\right]^2 \qquad (C.1.27)$$

which can be easily calculated analytically when the velocity profiles u_1 and u_2 are expressed in terms of r_o , r_h , r_s for laminar or turbulent flows as in section 2.

C-1.4 The energy-averaged density

The method of analysis is similar to the momentum-averaged density except that here the definition is slightly different. Thus

$$\frac{1}{\rho_E^2} = \frac{A_T^2}{\dot{m}_T^3}\left[\rho_\ell \overline{u_1^3} A_{\ell 1} + \rho_g \overline{u_1^3} A_{g1} + \rho_\ell \overline{u_2^3} A_{\ell 2} + \rho_g \overline{u_2^3} A_{g2}\right] \qquad (C.1.28)$$

where $\overline{u_1^3} = \frac{1}{A_1}\int_{A_1} u_1^3\, dA$ and $\overline{u_2^3} = \frac{1}{A_2}\int_{A_2} u_2^3\, dA$ (C.1.29)

In a similar way as for equation (C.1.20), equation (C.1.28) can be rearranged to give :

$$(1/\rho_E^2) = (f_1/\bar{\rho}_1^2) + (f_2/\bar{\rho}_2^2) \qquad (C.1.30)$$

where f_1 and f_2 are defined from the ratios derived by equations (C.1.3), (C.1.5), (C.1.8) and (C.1.9) as

$$f_1 \equiv \left[\frac{x - x_2}{x_1 - x_2}\right]^3 \left[\frac{\alpha_1 - \alpha_2}{\alpha - \alpha_2}\right]^2 U_1^3$$
$$f_2 \equiv \left[\frac{x_1 - x}{x - x}\right]^3 \left[\frac{\alpha_1 - \alpha_2}{\alpha - \alpha}\right]^2 U_2^3 \qquad (C.1.31)$$

As from equation (C.I.29) the average velocity ratios U_1^3 , U_2^3 are defined as :

$$U_1^3 \equiv \left[\frac{1}{A_1}\int_{A_1} u_1^3\, dA\right] / \left[\frac{1}{A_1}\int_{A_1} u_1\, dA\right]^3$$

$$U_2^3 \equiv \left[\frac{1}{A_2}\int_{A_2} u_2^3\, dA\right] / \left[\frac{1}{A_2}\int_{A_2} u_2\, dA\right]^3 \qquad \text{(C.1.32)}$$

The ratios shown in these equations can be calculated analytically when u_1 and u_2 are expressed in the usual way as for chapter 2 for laminar and turbulent velocity profiles.

Appendix D.

Publications.

Contents :

C99/83

An analytical profile model of annular two-phase flow

A N SKOULOUDIS, MSc, DIC and S J PEERLESS, PhD, ACGI, MINucE
Imperial College of Science and Technology, London

SYNOPSIS An analytical model of annular two-phase flow in a tube, in which different power laws are used for the two phases, gives better representation than existing models. Using this model a relationship between the void fraction and mass dryness fraction is derived. Comparisons with experiment show an agreement within ten percent for a wide range of measurements in unheated and heated pipes assuming a continuous transition from bubbly to separated flow. The model is also used to calculate two-phase pressure drops. Agreement with experiment is within fifteen percent.

NOTATION

A	flow area
g	gravitational acceleration
h	specific enthalpy
ℓ	Prandtl mixing length
L	length of pipe over which evaporation occurs
$\dot{m}$	mass flow rate
$\dot{M}$	momentum flow rate
n	power-law exponent
$\dot{q}'$	heat flux per unit length
r	distance from the axis
r_o	pipe radius
R^2	ρ_g/ρ_ℓ for liquid at the wall region; ρ_ℓ/ρ_g for vapour at the wall region
s	distance along the axis
u	local velocity
x	mass dryness fraction
y	$r_o - r$
Z	wetted perimeter
α	area dryness fraction or void fraction
θ	angle of inclination
μ	viscosity
ρ	density
τ	shear stress
Δp	pressure drop

Subscripts

g	vapour phase
h	hypothetical quantity
in	input quantity
ℓ	liquid phase
$g\ell$	property change during evaporation
max	maximum quantity
N	normalised quantity
out	output quantity
s	separation
w	conditions at the wall
T	total

1 = ℓ, 2 = g when liquid flows next to the wall
1 = g, 2 = ℓ when vapour flows next to the wall

INTRODUCTION

In the investigation of flow of a liquid and its vapour along a pipe or duct, knowledge of the division of the flow between the two phases is usually important. The associated parameters are:

(a) the void fraction, α, defined as the ratio of the vapour flow area to the total flow area;

(b) the mass dryness fraction, x, defined as the ratio of vapour flow rate to the total flow rate.

Values of dryness fraction x are normally readily obtainable; from the initial value, local downstream values can be calculated if the heat-transfer conditions are known, and the usual assumption of thermodynamic equilibrium is made.

Void fraction α is less easily determined, but its value is required for the calculation of the frictional, acceleration and gravitational components of the axial pressure gradient. It is also necessary for the calculation of local average density, which is of particular importance in light water nuclear reactors because of the effect on core reactivity.

In the absence of comprehensive analysis of two-phase flow, it is desirable to relate the local values of dryness fraction and void fraction to each other; this can be done only by making simplifying assumptions about the character of the flow.

The paper deals primarily with steady axisymmetric two-phase annular flow in a pipe, in which the two phases can be regarded as flowing separately, divided by a clearly-defined hypothetical surface of separation. Either phase may be taken to occupy the annular space between this surface and the pipe wall.

PREVIOUS WORK

The most widely-known relationship between α and x is that obtained by Martinelli and Nelson (ref. 1). Their approach is an entirely empirical one based on the use of a multiplying

factor which is, in effect, the two-phase pressure gradient normalised by the corresponding pressure gradient for single-phase flow. For low values of mass dryness fraction and high pressure, their predicted void fractions differ from experimental values by more than ten percent, as reported by Smith (ref. 2).

Several authors, wishing to improve on this completely empirical treatment, have proposed a variety of models of two-phase flow. For example, Bankoff (ref. 3) proposed a homogeneous model, in which the flow velocity and the void fraction both vary axially according to a power law. He derived the relationship

$$\alpha = \frac{\beta x}{x + (1 - x)(\rho_g/\rho_l)} \qquad (1)$$

where β is a pressure-dependent variable less than unity. For mass-dryness fractions approaching unity, the void fraction α is considerably underestimated in this model, approaching β instead of unity. A simpler correlation suggested by Thom (ref. 4) removes the discrepancy as $x \to 1$ in Bankoff's model, but retains the assumption of constant slip (γ) between the two phases at constant pressure. Thom's relationship may be written as

$$\alpha = \frac{\gamma x}{\gamma x + (1 - x)} \qquad (2)$$

The slip factor γ is taken as a function of pressure only, although experimental evidence suggests that it should also vary with x.

A similar approach was proposed by Smith (ref. 2). His model assumes an annular liquid flow surrounding a core flow of vapour with entrained water droplets. The annular liquid flow and the mixed core flow are assumed to have equal velocity heads. For the best fit over a wide range of experimental results, Smith suggested that the entrained liquid component of the core flow should be 40% by mass.

All the above models are one-dimensional in the sense that at any station in the pipe, each of the flow properties, including the velocity, has a single value for each of the two phases. The two phases are therefore, to some extent, independent of each other except that together they fill the whole flow area, and the assumed thermodynamic equilibrium governs the local dryness fraction; the general conservation laws apply to the whole flow, of course.

It may be noted at this point that none of the above models predicts any variation of void fraction with mass flow rate.

THE PRESENT MODEL

The most obvious feature of the model proposed here is that in each part of the flow passage the velocity is taken to vary with radius according to a $1/n^{th}$ power law, similar to that sometimes used in the analysis of single-phase pipe flow. The shape of the combined velocity profile depends on whether the heavier phase is flowing in region 1, the annular region next to the wall, or in the circular central region, 2. The two cases are illustrated in Figs. 1(a) and 1(b).

The two parts of the velocity profile are given by

$$\begin{aligned} (u_1/u_{max,1}) &= (1 - r/r_o)^{1/n} \qquad r_s \leq r \leq r_o \\ \text{and} \quad (u_2/u_{max,2}) &= (1 - r/r_h)^{1/n} \qquad 0 \leq r \leq r_s \end{aligned} \qquad (3)$$

When liquid flows next to the wall, subscripts 1 and 2 refer to liquid (l) and vapour (g) respectively; the converse is true when vapour flows next to the wall. The surface of radius r_s is the surface of separation between the two phases; r_h is a hypothetical dimension used in specifying the velocity profile in region 2.

The two parts of the velocity profile are matched by ensuring continuity of velocity and shear stress at the surface of separation, r_s. In terms of Prandtl's mixing-length hypothesis, the turbulent shear-stress expressions for the two flow regions are

$$\begin{aligned} \tau_1 &= \rho_1 \ell_1^2 |du_1/dy| . (du_1/dy) \\ \tau_2 &= \rho_2 \ell_2^2 |du_2/dy| . (du_2/dy) \end{aligned} \qquad (4)$$

where ℓ is the mixing length, which in general varies with radius. At present we assume that the values of ℓ for the two phases at the surface of separation are equal, i.e. that $\ell_1 = \ell_2$. Then from equations 3 and 4 it follows that for continuity of shear stress (ignoring the contribution of molecular viscosity)

$$r_h/r_s = 1 + R(r_o/r_s - 1) \qquad (5)$$

where $R \equiv (\rho_2/\rho_1)^{\frac{1}{2}}$. Defined as the ratio of vapour flow area to the total, the void fraction α is quickly seen to be given by

$$\begin{aligned} (r_s/r_o)^2 &= 1 - \alpha \quad \text{when vapour flows next to the wall} \\ (r_s/r_o)^2 &= \alpha \quad \text{when liquid flows next to the wall} \end{aligned} \qquad (6)$$

The mass flow rates for the two phases are obtained in the normal way:

$$\dot{m}_g \equiv \int_{A_g} \rho_g u_g dA \quad \text{and} \quad \dot{m}_l = \int_{A_l} \rho_l u_l dA \qquad (7)$$

and the ratio of the two mass flow rates can be expressed in terms of the geometric and kinematic parameters by substituting from equations 3 and 5 into equation 7:

$$\frac{\dot{m}_2}{\dot{m}_1} = R^3 \frac{r_h[r_h/(r_h - r_s)]^{(n+1)/n} - r_h - (1+1/n)r_s}{(1 + 1/n)r_s + r_o} \qquad (8)$$

in which the subscripts 1 and 2 have the same meaning as for equation 3.

Since by definition,

$$x = \dot{m}_g/(\dot{m}_g + \dot{m}_l) \qquad (9)$$

this equation, together with equations 6 and 8, constitute an implicit relationship between α and x. There is a single solution everywhere in the range of real physical conditions, i.e. for $0 \leq \alpha \leq 1$ and $0 \leq x \leq 1$.

We thus have a simple two-dimensional model of annular two-phase flow which satisfies the elementary requirement of zero slip at the pipe wall and possesses a small degree of flexibility, since the profile exponent 1/n can be varied empirically to satisfy local flow conditions, if required.

Pressure gradient

An important feature of the new model is that it provides a rational basis for the direct calculation of axial pressure gradient. Application of the force-momentum equation to steady pipe flow in the usual way yields the result:

$$-\frac{dp}{ds} - \frac{Z}{A_T}\tau_w - \frac{1}{A_T}\int_{A_T} \rho g \sin\theta \, dA = \frac{1}{A_T}\frac{d\dot{M}}{ds} \quad (10)$$

where A_T is the total flow area, Z the wetted perimeter, θ the angle of inclination of the channel flow from the horizontal, s the distance along the axis and $\dot{M}$ the momentum flow rate.

Equation 10 can easily be interpreted as showing the axial pressure gradient to consist of three components, which for the present model are evaluated from the following expressions:

(1) The frictional component, $Z\tau_w/A_T$, is calculated from the conditions at the wall, in the same way that it would be if the fluid near the wall filled the whole tube with the complete u_l profile as shown in Fig. 1. For the corresponding steady, fully-developed, uniform-density flow the wall shear stress is given by (ref. 10):

$$\tau_w = \left[c\,\frac{\bar{u}_l}{u_{max,l}}\right]^{-2n/(n+1)} \cdot \left[\frac{\rho_l \bar{u}_l r_o}{\mu_l}\right]^{-2/(n+1)} \cdot \rho_l \bar{u}_l^2 \quad (11)$$

in which the standard value for c when n = 7 is 8.74, and $\bar{u}_l$ is the average velocity over the whole flow area, i.e.

$$\bar{u}_l = \frac{1}{A_T}\int_{A_T} u_l \, dA \quad (12)$$

The use of results for single-phase, uniform-density flow in this way implies that in the two-phase flow conditions are varying only slowly along the pipe.

(2) The gravitational component is expressed in the standard way for annular two-phase flow, thus

$$\frac{1}{A_T}\int_{A_T} \rho g \sin\theta \, dA = [\alpha\rho_g + (1-\alpha)\rho_l] g \sin\theta. \quad (13)$$

(3) The acceleration component of the axial pressure gradient is obtained directly from the velocity profiles for the two parts of the flow:

$$\frac{1}{A_T}\frac{d\dot{M}}{ds} = \frac{1}{A_T}\cdot\frac{d}{ds}\left(\rho_g \int_{A_g} u_g^2 \, dA + \rho_l \int_{A_l} u_l^2 dA\right) \quad (14)$$

where $\dot{M}$ is the momentum flow rate.

The total change of pressure in a given length of pipe, L, can, of course, be obtained by evaluating and adding the integrals of the above three expressions for length L. For the particular case of uniformly heated flow, the mass dryness fraction varies linearly along the pipe, if we again ignore variation of fluid properties, i.e.

$$dx/ds = \dot{q}'/\dot{m}_T h_{gl} \quad (15)$$

where $\dot{q}'$ is the heat flux per unit length and h_{gl} the specific enthalpy of vaporisation. If, in addition, L is measured from the station at which $\alpha = 0$ and the liquid is just saturated, the result is:

$$\Delta p = \Delta p_{fr} + \Delta p_{gr} + \Delta p_{ac} \quad (16)$$

where

$$\Delta p_{fr} = \frac{Z}{A_T}\frac{L}{x_{out}}\int_0^{x_{out}} \tau_w \, dx \quad (17)$$

$$\Delta p_{gr} = \rho_l g \sin\theta \left[L + \frac{\rho_g - \rho_l}{\rho_l}\frac{L}{x_{out}}\int_0^{x_{out}} \alpha \, dx\right] \quad (18)$$

$$\Delta p_{ac} = \frac{1}{A_T}(\dot{M}_{out} - \dot{M}_{in}) \quad (19)$$

Inspection of equations 17, 18 and 11 shows that the following integrals must be calculated.

$$\int_0^{x_{out}} u_l^{2n/(n+1)} dx \quad \text{and} \quad \int_0^{x_{out}} \alpha \, dx \; .$$

These integrals are calculated numerically using the velocity profile model. For this purpose, an interactive computer package (VELPRO) has been developed and used for the calculation presented in this paper.

COMPARISON WITH EXPERIMENT

The void fraction predicted by the velocity profile model is compared below with results from five different experimental sources and two other theoretical correlations - those of S.L. Smith and J.R.S. Thom. In the predictions by the velocity profile method, liquid is taken to flow next to the wall except where otherwise stated.

Haywood *et al.* (ref. 5) presented a series of well-known experimental results, covering the range of:

Pressure: 17.2 to 145 bar

Heat Flux: 20.0 to 140 kW/m^2

Mass Flux: 750 to 1950 kg/m^{2}s

Measurements of the void fraction, taken by the gamma ray absorption method at different scanning positions across the flow area, confirmed that liquid was actually flowing close to the wall. Void fractions were measured for boiling water flowing in a vertical or horizontal channel 38 mm in diameter, and for heated lengths of 4.9 and 7.3 metres. Predictions, as shown in Fig. 2, are in good agreement with experiment.

In Figs. 3 and 4 the present model is compared with results for horizontal and vertical unheated pipes, reported by H.C. Larson (ref. 6) and H. Isbin *et al.* (ref. 7). The operational pressures were 68.95 bar and 1.013 bar with observed void fractions up to 0.90 for mass dryness fractions in the region 0.01 to 0.7.

The velocity profile method also gives good agreement (Fig. 5), with the results of R.A. Egen *et al.* (ref. 8) for vertical flows at high pressure in heated channels. Operating condi-

tions were:

Pressure: 137.90 bar

Heat Flux: 946 to 1577 KW/m^2

Mass Flux: 949 to 1220 kg/m^2s

It is interesting to observe that by changing the power law exponent in equation 8, an explanation is obtained for the slight increase of void fraction with mass flux. This dependence is shown in Fig. 5 for mass fluxes 949 and 1220 kg/m^2s, at 1261 KW/m^2 heating flux, with values of 7 and 8 for n.

Rouhani and Becker (ref. 9) presented void fractions for boiling heavy water in a vertical tube of 6 mm inner diameter and a heated section of 2.5 m in length. The range of their measurements was.

Pressure: 7.0 to 50.3 bar

Heat Flux: 380 to 1200 KW/m^2

Mass Flux: 650 to 2050 kg/m^2s

Samples of their data, for 11 and 49 bars are presented in Fig. 6. No indication is given in their paper as to which phase flows next to the wall. VELPRO predictions for both cases are given, together with the curve obtained by Smith's correlation. The experimental results exhibit some unexpected behaviour in that the lines of experimental points do not seem likely to pass through the points (0, 0) and (1, 1), as thermodynamic equilibrium requires. The deviation at the left hand of Fig. 6 at 49 bar is, of course, exaggerated by the semi-logarithmic plotting, but even so is apparently greater than can be explained by a transition from fluid-next-to-the-wall to vapour-next-to-the-wall.

All these comparisons between theory and experiment are presented in a different way in Fig. 7, which shows that the velocity profile model in its present form agrees with most experimental results to within ±10%, with a tendency to give slightly high predictions at high values of the void fraction, particularly for low pressures. This suggests that the vapour phase should be assumed to have some liquid entrained in it, so that its density is somewhat greater than that of pure vapour only. For a given fraction of entrained liquid, the effect of this will naturally be greater at low pressure when the density difference between the phases is large. However, one could expect the amount of entrained liquid to be greater at high values of the void fraction, where the ratio of the vapour flow rate to that of the liquid is high.

Comparisons between the experimentally determined pressure drops reported by R.W. Haywood et al. (ref. 5) and those predicted by the VELPRO programme are shown in Figs. 9 and 10 for heated vertical and horizontal pipes respectively. All pressure drops are normalised by dividing by $\rho\bar{u}^2$ at inlet conditions, where x = 0, α = 0, i.e.:

$$\Delta p_N \equiv \Delta p/(\rho_l \bar{u}^2_{in}) \qquad (20)$$

Fig. 9 is complicated by the existence of a gravitational component in the pressure drop for a vertical pipe; nevertheless, it is possible to see that the agreement is generally good. Even better agreement is shown, in Fig. 10, for the case of horizontal flow.

The various intercepts on the vertical axes of these two figures indicate the normalised pressure drops for uniform-density liquid flow along the test section. Fig. 11 shows the agreement between observed and calculated pressure drops.

CONCLUSION

In its present simple form, the velocity profile method relates void fraction and mass-dryness fraction at least as well as other existing methods over the whole range of possible flow conditions. It contains a small degree of flexibility conferred by variation of the profile exponent, n, and is thereby able to predict the slight dependence of void fraction on mass flow rate noticeable from some experimental investigations. It gives a better description of physical reality than "one-dimensional" models, and allows direct calculation of axial pressure gradient. It thus represents a significant advance on most existing models.

Even so, the velocity profile model cannot claim to be more than a highly simplified description of a complex physical reality, and further development may be desirable. One obvious possibility is the addition of entrained liquid to the vapour steam. In the present state of knowledge about the behaviour of the liquid-vapour interface, even this change would have to be largely empirical in character.

This and other developments are under active consideration, but it is already clear that further progress will, to a considerable extent, depend on the existence of more detailed observation of actual two-phase flows.

REFERENCES

1. MARTINELLI R.C. and NELSON D.B. Prediction of pressure drop during forced-circulation boiling of water. Trans. Am. Soc. Mech. Engrs., 1948, 70, 695-702.

2. SMITH S.L. Void fractions in two-phase flow: a correlation based upon an equal velocity head model. Proc. Inst. Mech. Engrs., 1969-1970, 184, 647-657.

3. BANKOFF S.G. Variable density single-fluid model for two-phase flow with particular reference to steam water flow. J. Heat Transfer, Trans. Am. Soc. Mech. Engrs., 1960, 82, 265-272.

4. THOM J.R.S. Prediction of pressure drop during forced circulation boiling of water. Int. J. Heat Transfer, 1964, 7, 709-724.

5. HAYWOOD R.W., KNIGHTS G.A., MIDDLETON G.E. and THOM J.R.S. Experimental study of the flow conditions and pressure drop of steam-water mixtures at high pressures in heated and unheated tubes. Proc. Inst. Mech. Engrs., 1961, 175, 663-747.

6. LARSON H.C. Void fractions of two-phase steam-water mixture. MS Thesis, University of Minnesota, 1957.

7. ISBIN H.C., SHER N.C. and EDDY K.C. Void fractions in two-phase steam water flow. AIChE

Journal, 1957, 136-42.

8. EGEN R.A., DINGEE D.A. and CHASTAIN J.W. Vapour formation and behaviour in boiling heat transfer. Battelle Memorial Report No. 1163, 1957.

9. ROUHANI S.Z. and BECKER K.M. Measurements of void fraction for flow of boiling heavy water in vertical round ducts. Rep. AE-106, A.B. Atomenerg., Sweden, 1963.

10. SCHLICHTING H. Boundary layer theory. Pergamon Press: London, 1955, Chapter XXI.

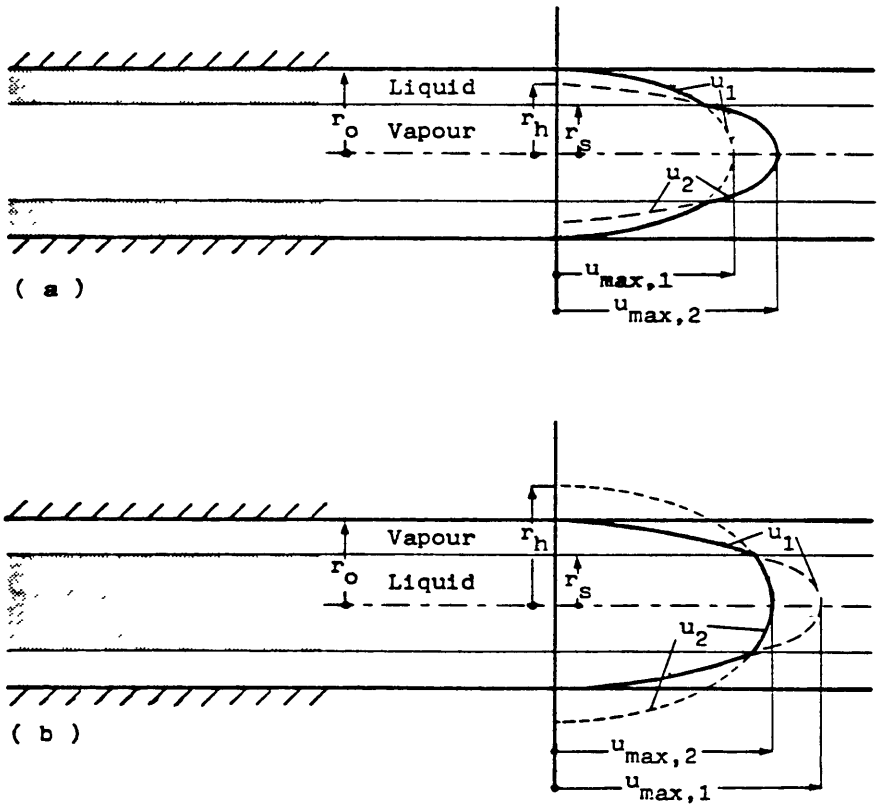

Fig 1 The assumed velocity profiles for annular two-phase flow

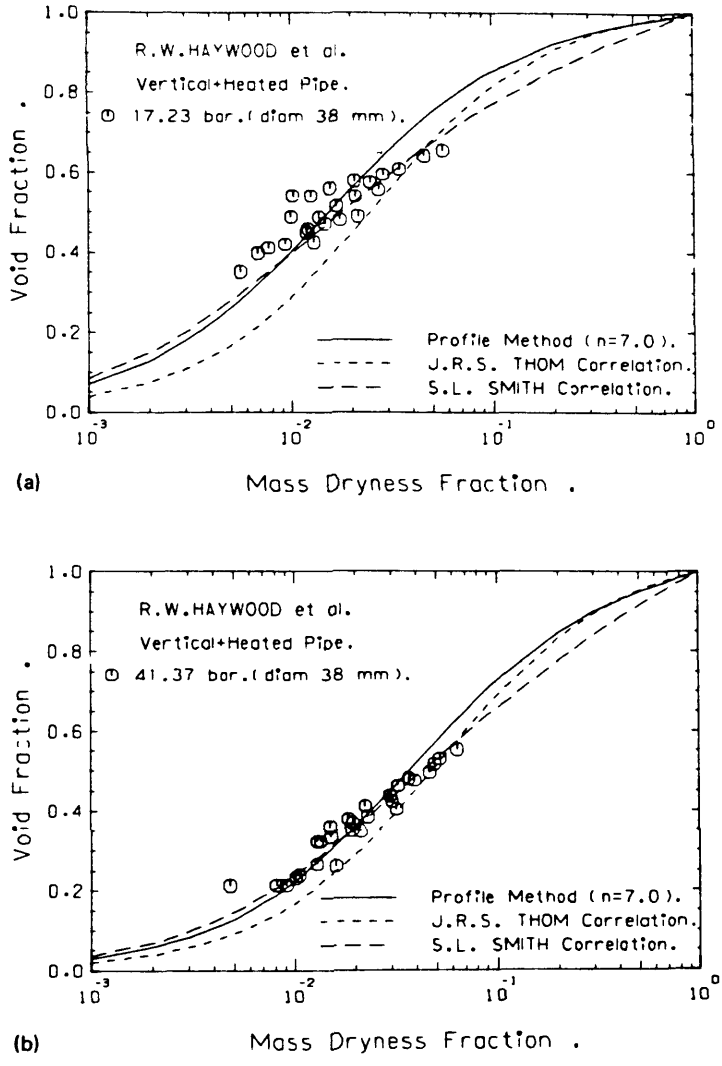

Fig 2 The void fraction, mass-dryness fraction relation for boiling water in vertical heated pipe

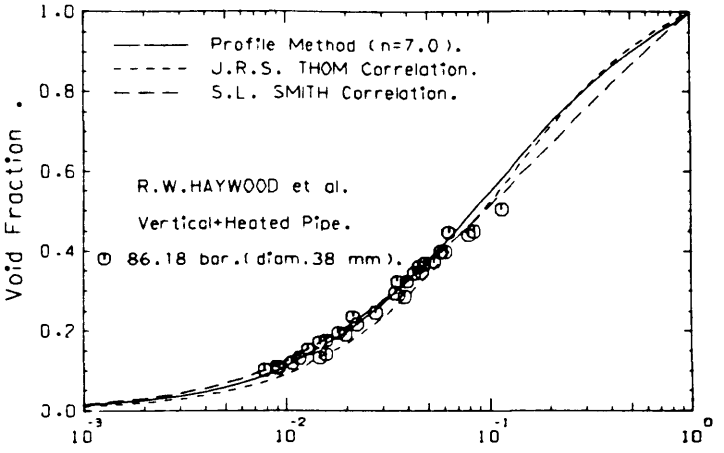

(c)

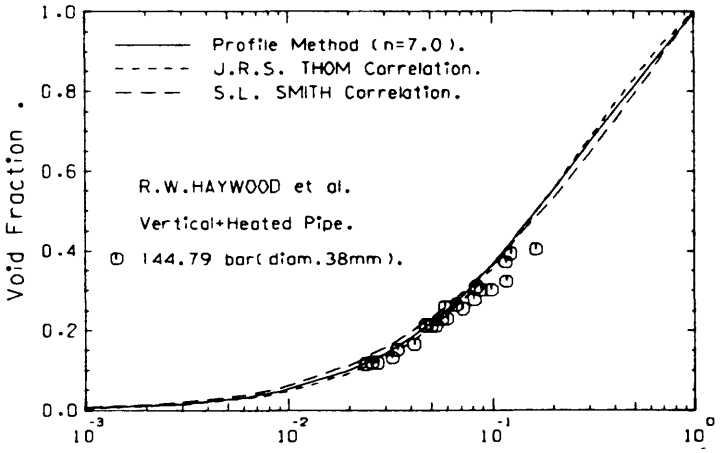

(d)

Fig 2 The void fraction, mass-dryness fraction relation for boiling water in vertical heated pipe

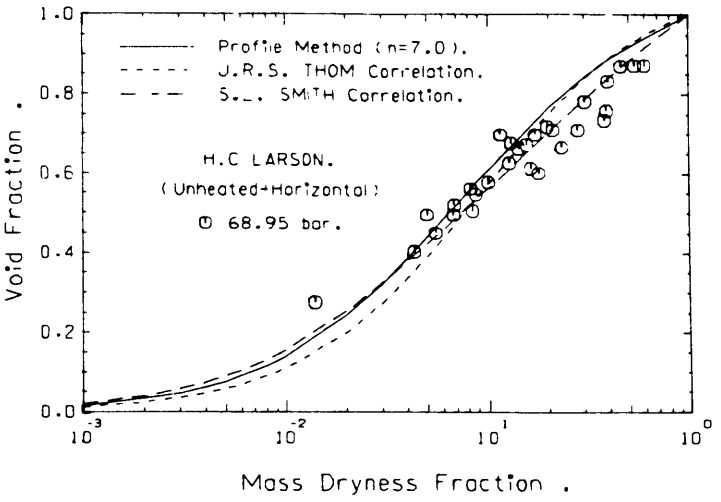

Fig 3 The void fraction, mass-dryness fraction relation in horizontal unheated pipe

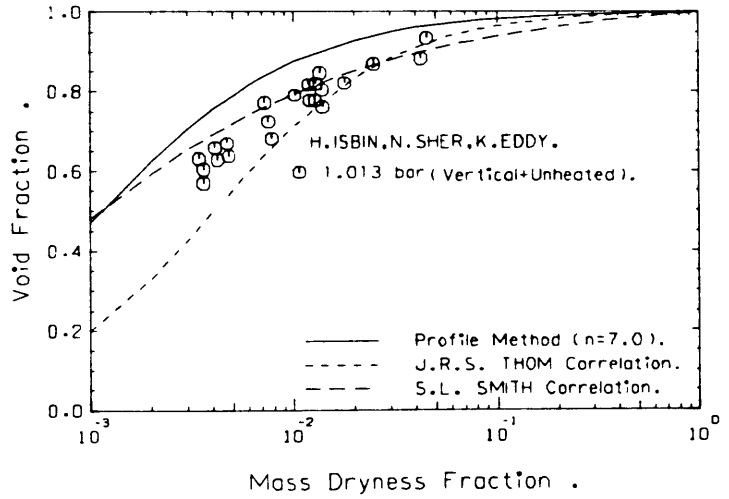

Fig 4 The void fraction, mass-dryness fraction relation in vertical unheated pipe

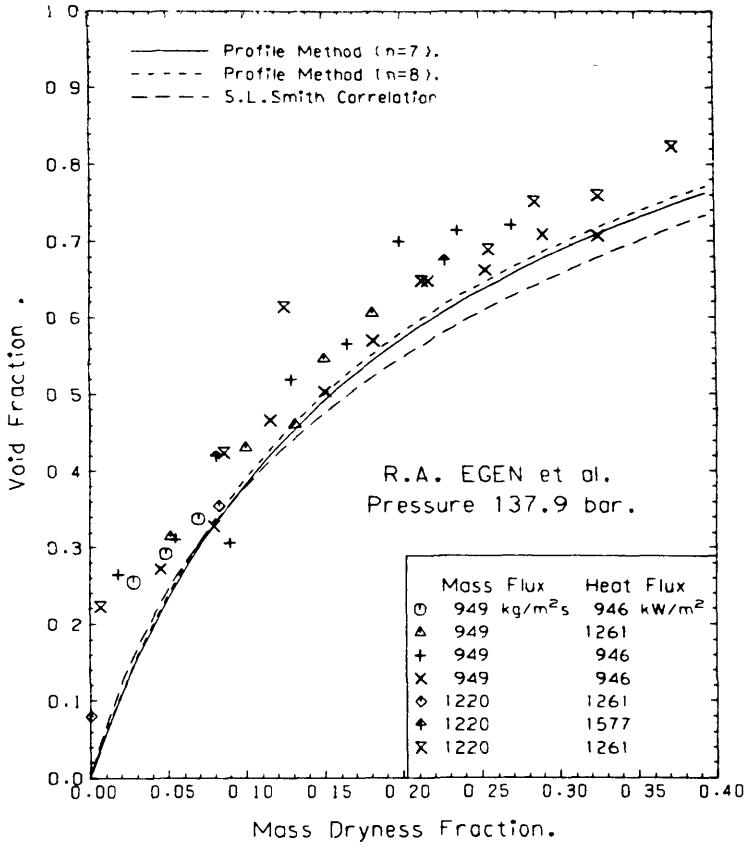

Fig 5 The void fraction, mass-dryness fraction relation in vertical heated pipe

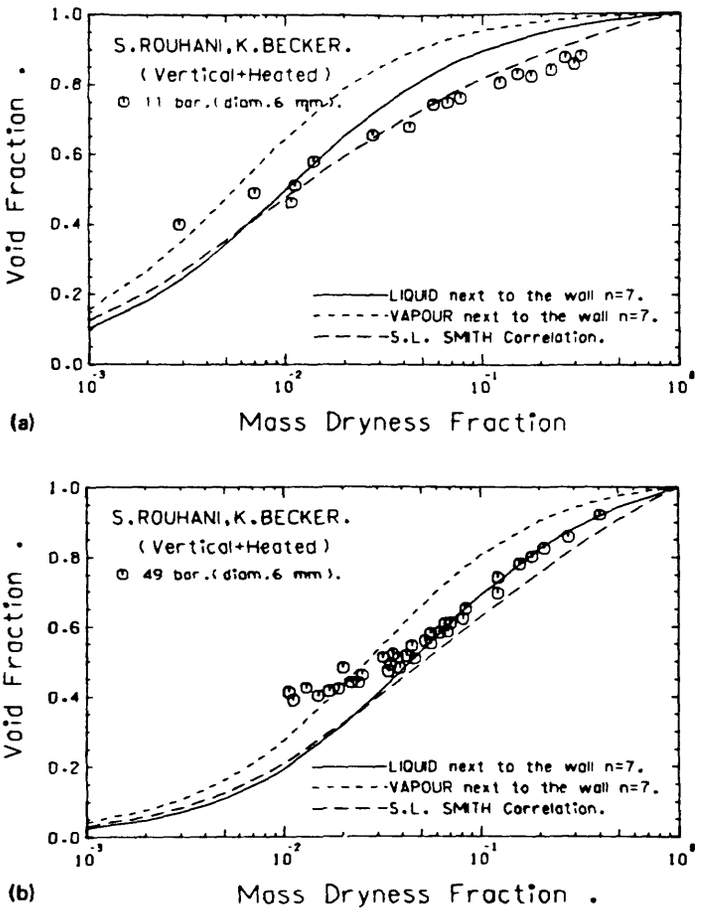

Fig 6 The void fraction, mass-dryness fraction relation for boiling heavy water in vertical pipe

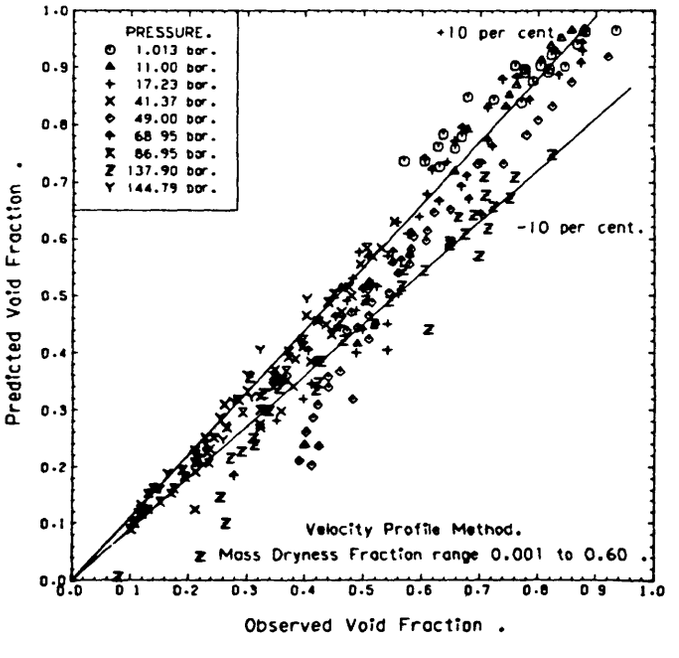

Fig 7 Comparison between predicted and observed void fractions

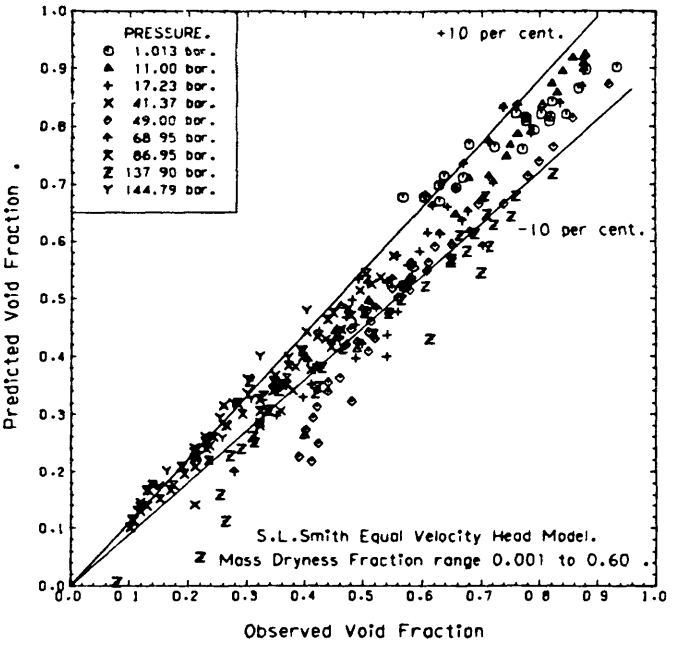

Fig 8 Predicted and observed void fractions by S L Smith

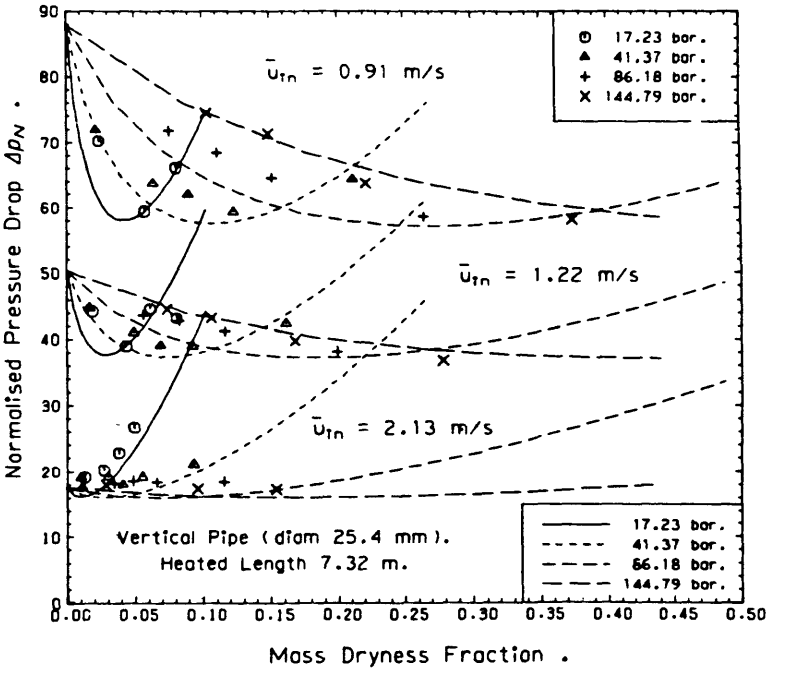

Fig 9 Normalised pressure drop for vertical flow

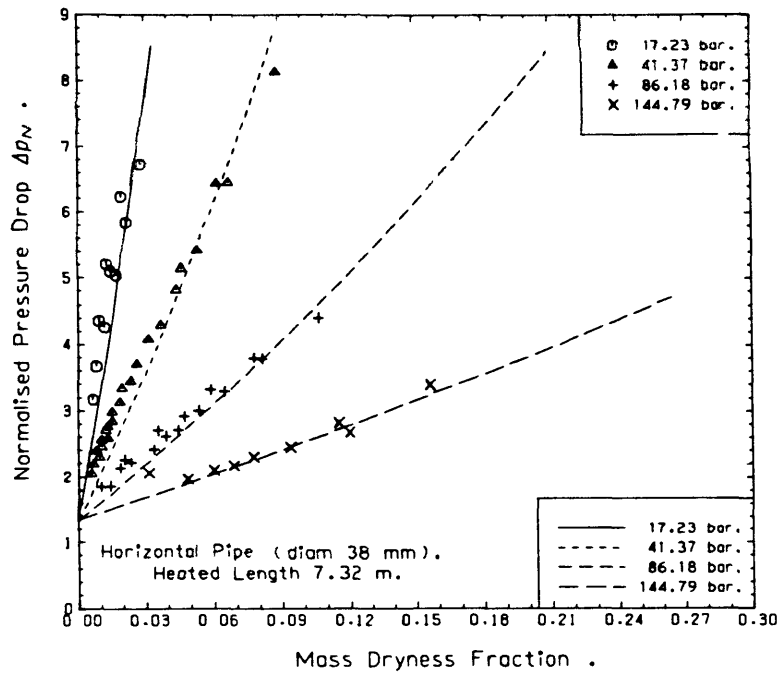

Fig 10 Normalised pressure drop for horizontal flow

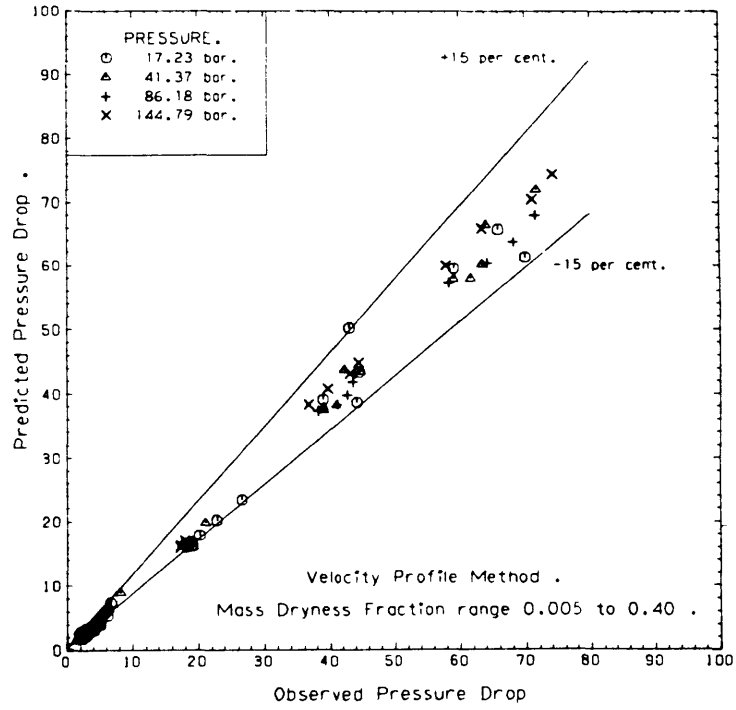

Fig 11 Comparison between predicted and observed pressure drop

A VELOCITY PROFILE MODEL FOR TWO-PHASE FLOW WITH LIQUID AND VAPOUR ENTRAINMENT

A.N. Skouloudis and S.J. Peerless

Department of Mechanical Engineering, Imperial College of Science and Technology, London SW7 2BX

1. SUMMARY

An analytical model of annular two-phase flow in a tube, in which a composite velocity profile based on a power law is used, gives better representation than existing models for both heated and unheated flows. The model allows both liquid and vapour entrainment and assumes equilibrium between the two phases. Predicted pressure drops for steam-water mixtures agree with experimental values to within 15% in a wide range of operating conditions.

2. INTRODUCTION

Mixed flows of liquid and vapour along pipes and similar passages occur widely in engineering, and the ability to analyse them is of considerable importance. This is particularly so for liquid-cooled nuclear reactors, in which phase transitions not only directly affect the heat-transfer rate from the fuel, but also indirectly affect the thermal power.

Two-phase flow analysis is complicated by the existence of a wide variety of possible flow patterns [1], and the absence of clear criteria governing transitions between them. Consequently, the calculation of axial pressure gradients, with which this paper is primarily concerned, has been based almost entirely on empirical correlations. A recent collection of such correlations and their suggested ranges of application is presented by Hewitt [2].

Relatively simple analysis is possible when the flow can be represented as a homogeneous mixture of liquid and vapour; the main difficulty in this case arises from ignorance about the effective viscosity of such a mixture.

Another relatively simple flow pattern is that in which

the liquid and vapour can be considered to flow entirely separately, one phase occupying a central cylindrical core, the other occupying the surrounding annulus. However, one-dimensional analysis of this type of flow still requires some rather crude assumptions, e.g. that the velocity heads for the two phases are equal.

A recent analysis presented by the present authors [3] constitutes a two-dimensional approach to separated two-phase flow. Using a compound power-law profile, good agreement was obtained between theoretical and experimental correlations between void fraction α and mass dryness fraction x. Void fraction is the fraction of the total flow area occupied by the vapour; mass dryness is the ratio of the vapour mass flow rate to the total.

In the present work we extend the range of application of this velocity-profile model by allowing the two phases to be partly entrained in each other, while retaining a clearly defined surface of separation between the two regions of the flow. By varying the amounts of entrainment it is possible to cover the whole range from the homogeneous fluid to the fully-separated type of flow.

Using this extended model we analyse the dependence of streamwise pressure gradient on flow rate and mixture quality, and give some tentative comparisons with experimental results for diabatic and adiabatic flows in vertical and horizontal pipes.

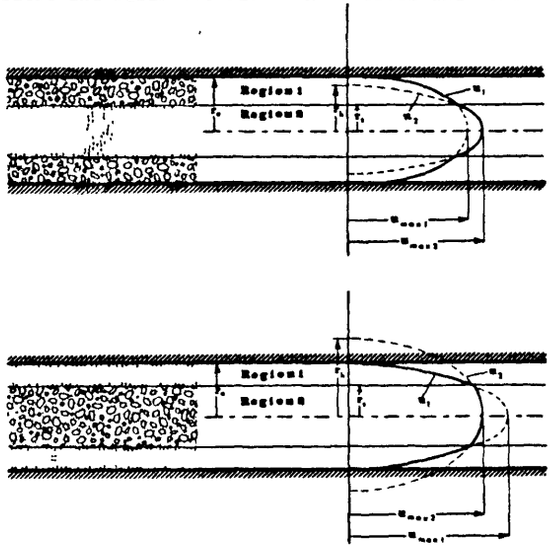

Fig. 1 The assumed velocity profiles for two-phase flow.

3. DESCRIPTION OF THE MODEL

The form of the assumed velocity profile is indicated by Fig. 1. Within each of the two regions of the flow passage the fluid velocity is taken to vary with radius according to a $1/n^{th}$ power law, as sometimes used in single-phase pipe flow analysis. Each region is assumed to be occupied mainly by one phase, but with some of the other phase uniformly mixed in with it, sufficiently intimately to allow the velocity to be assigned a single value at each point.

The shape of the velocity profile will depend on whether the heavier mixture is flowing in the annular region next to the wall (1), or the central circular region (2); the two cases are shown in Fig. 1 (a) and (b). The two parts of the velocity profile are defined by

$$u_1/u_{max,1} = (1 - r/r_o)^{1/n} \qquad r_s \le r \le r_o \qquad (1a)$$

$$u_2/u_{max,2} = (1 - r/r_h)^{1/n} \qquad 0 \le r \le r_s \qquad (1b)$$

where radius r_s defines the surface of separation, and r_h is a hypothetical dimension used in specifying the profile in region (2).

We make the usual assumption of local thermodynamic equilibrium between the vapour and liquid phases at any cross-section of the pipe, so that the familiar concept of dryness fraction, x, can be used to relate the total mass flow rates of vapour and liquid, $\dot{m}_g$ and $\dot{m}_\ell$:

$$x = \frac{\dot{m}_g}{\dot{m}_g + \dot{m}_\ell} \qquad (2)$$

Similarly, a dryness fraction can be defined for each region of the flow:

$$x_1 = \frac{\dot{m}_{g1}}{\dot{m}_{g1} + \dot{m}_{\ell 1}} \quad , \quad x_2 = \frac{\dot{m}_{g2}}{\dot{m}_{g2} + \dot{m}_{\ell 2}} \qquad (3)$$

The mean density of each of the mixtures can then be easily expressed in terms of the relevant dryness fraction:

$$\frac{1}{\bar{\rho}_1} = \frac{x_1}{\rho_g} + \frac{1 - x_1}{\rho_\ell} \quad , \quad \frac{1}{\bar{\rho}_2} = \frac{x_2}{\rho_g} + \frac{1 - x_2}{\rho_\ell} \qquad (4)$$

and the mass flow rates in the two regions are

$$\dot{m}_1 = \dot{m}_{g1} + \dot{m}_{\ell 1} = \bar{\rho}_1 \int_{A_1} u_1 \, dA \qquad (5a)$$

$$\dot{m}_2 = \dot{m}_{g2} + \dot{m}_{\ell 2} = \bar{\rho}_2 \int_{A_2} u_2 \, dA \qquad (5b)$$

The physical laws describing mass-transfer at the surface of separation are not sufficiently developed to provide a basis for analysis. We can, nevertheless, incorporate the idea of entrainment into our model by introducing an 'entrainment ratio'. Since entrainment can presumably occur in both directions there will in general be two entrainment ratios in each of the two flow cases. For the case in which liquid predominates in the region (1) (next to the wall), we write

$$e_1 = \frac{\dot{m}_{\ell 2}}{\dot{m}_\ell} = \frac{(1-x_2)\dot{m}_2}{(1-x)\dot{m}} \qquad (6a)$$

$$e_2 = \frac{\dot{m}_{g1}}{\dot{m}_g} = \frac{x_1\dot{m}_1}{x\dot{m}} \qquad (6a)$$

Entrainment ratio is thus the proportion of the total flow rate of a phase which flows in the region in which that phase is not the predominant one.

The two parts of the velocity profile are matched by ensuring continuity of shear stress at the interface, r_s. As in the earlier, simpler, model of reference [3], we do this by assuming that Prandtl's mixing-length hypothesis is valid in the neighbourhood of the interface, with equal mixing-lengths for the two mixtures. Consequently,

$$r_h/r_s = 1 + R(r_o/r_s - 1) \qquad (7)$$

where $R \equiv (\bar{\rho}_2/\bar{\rho}_1)^{\frac{1}{2}}$

The shape of the velocity profile, so established, can be related to the mass flow rates of the two phases and the entrainment ratios; the result is

$$\frac{(1-e_2)\dot{m}_g + e_1\dot{m}_\ell}{(1-e_1)\dot{m}_\ell + e_2\dot{m}_g} = R^3\left[\frac{r_h\left(\frac{r_h}{r_h-r_s}\right)^{(1+1/n)} - r_h - \left(\frac{n+1}{n}\right)r_s}{\left(\frac{n+1}{n}\right)r_s + r_o}\right] \qquad (8a)$$

An alternative form of the left-hand side of this equation is

$$\frac{(1-e_2)x + e_1(1-x)}{(1-e_1)(1-x) + e_2 x} \qquad (8b)$$

which clearly shows that the geometric parameters of the velocity profile, r_h and r_s, depend on the entrainment ratios and the overall dryness fraction, x.

Since r_s implicitly defines the void fraction, α, we now have a relationship between α and x; it has a single solution for all values of α and x between 0 and 1.

Pressure Drop Calculation

For pressure drop calculations the force-momentum relation applied to steady pipe flow yields the result

$$-\frac{dp}{dz} - \frac{P}{A}\tau_W - [\alpha\rho_g + (1-\alpha)\rho_\ell]g\sin\theta = \frac{1}{A}\frac{d\dot{M}}{dz} \qquad (9)$$

where A is the total flow area, P the wetted perimeter, θ the angle of inclination and M the momentum flow rate.

Following the same method as for our earlier model, the wall shear stress τ_W is assigned the same value as that in a hypothetical homogeneous fluid flow in which the whole pipe is filled with the mixture occupying region (1), and the velocity distribution is the u_1 profile extended to the pipe axis; the calculation uses standard $1/n^{th}$ power law analysis, and gives

$$\tau_W = \left(C \cdot \frac{\bar{u}_1}{u_{max,1}}\right)^{\frac{-2n}{n+1}}\left(\frac{\bar{\rho}_1\bar{u}_1 r_o}{\bar{\mu}_1}\right)^{\frac{-2}{n+1}} \cdot \left\{\bar{\rho}_1\bar{u}_1^2\right\} \qquad (10)$$

where $\bar{u}_1$ is the average velocity for this hypothetical flow, and C is a numerical factor, with the value 8.74 when n = 7; $\bar{\mu}_1$ is the viscosity of the mixture, obtained from the expression

$$\frac{1}{\bar{\mu}_1} = \frac{x_1}{\mu_g} + \frac{1-x_1}{\mu_\ell} \qquad (11)$$

The last term in equation (9) is obtained by integration over the two parts of the combined velocity profile:

$$\frac{d\dot{M}}{dz} = \frac{d}{dz}\left(\bar{\rho}_1\int_{A_1} u_1^2 dA + \bar{\rho}_2\int_{A_2} u_2^2 dA\right) \qquad (12)$$

If it is assumed that the phase densities are varying only slowly along the pipe then equation (9) can be integrated to give the total pressure drop; for diabatic flows this requires a numerical solution for the wall shear stress and the void fraction.

All calculations based on this model can be performed by an interactive computing package 'VELPRO 2', which can handle both laminar and turbulent flows, varying entrainment ratio, heated and unheated tubes, etc.

Application of the model in its present form requires the entrainment ratios for the two phases to be specified as part of the input data; this information is required in addition to a statement about which phase is predominant in each of the two regions of the flow. In the absence of such detailed information, comparison with experimental results must be rather tentative.

4. COMPARISONS WITH EXPERIMENT

In the comparisons which follow, calculations made with the velocity profile model have been based on the assumptions that

(a) the liquid phase is predominant next to the pipe wall (region 1), with the vapour phase mainly occupying the central core, and

(b) no liquid entrainment into the central core occurs.

Results are presented for different amounts of vapour entrainment into region (1). No attempt has been made to optimise the agreement by varying the entrainment ratio; the values used have been chosen rather arbitrarily to demonstrate the effect of introducing entrainment into the model. In all the comparisons presented here, pressure drop has been normalised against $\rho_\ell \bar{u}_\ell^2$, for all liquid flow at the same mass flow rate.

The well-known experimental results of Haywood et al. [4] were obtained in heated and unheated, horizontal and vertical tubes of 25.4 mm and 38.1 mm diameter and various lengths from 1.5 m to 7.3 m. Their heat and mass-fluxes were in the ranges:

Heat flux: 20.0 to 140 kW/m^2
Mass flux: 750 to 1950 kg/m^{2}s

Comparisons with their results for heated horizontal tubes are shown in Fig. 2. As previously found in reference [3], good agreement is obtained over most of the range of these experiments without introducing entrainment.

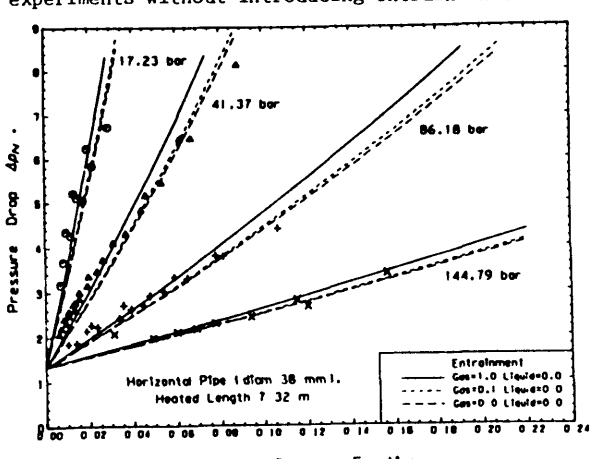

Fig. 2 Calculated and measured pressure drops: horizontal pipes.

However, inspection of Fig. 2 suggests that agreement would be improved by increasing the gas entrainment ratio for low values of outlet mass-dryness fraction.

Fig. 3 shows comparisons with the Haywood results for flows in unheated vertical tubes. For these conditions also the flow can apparently be adequately modelled by assuming complete separation of the two phases, without any entrainment.

It is interesting to note the decreasing effect of entrainment on the predicted pressure drop as pressure increases and the density difference between the two phases decreases.

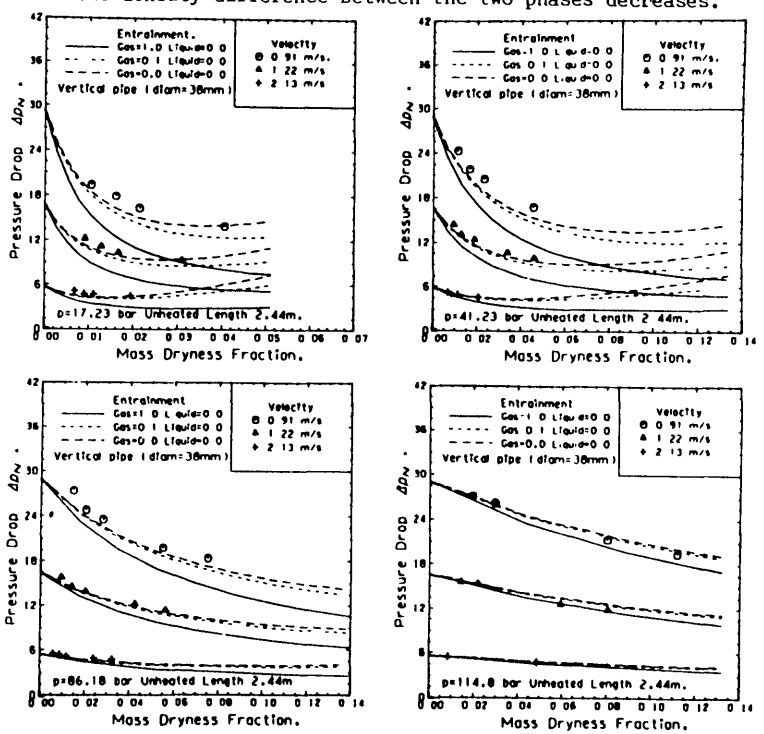

Fig. 3 Calculated and measured pressure drops: vertical pipes.

Markedly different conclusions follow from comparison with the experimental results from CISE, reference [5]. Their experiments were carried out in unheated tubes of 5.0 mm to 10.1 mm diameter, within the following ranges:

Pressure: 41.0 to 82.4 bar
Mass dryness fraction: 0.01 to 0.8
Test section length: 0.53 to 0.92 m

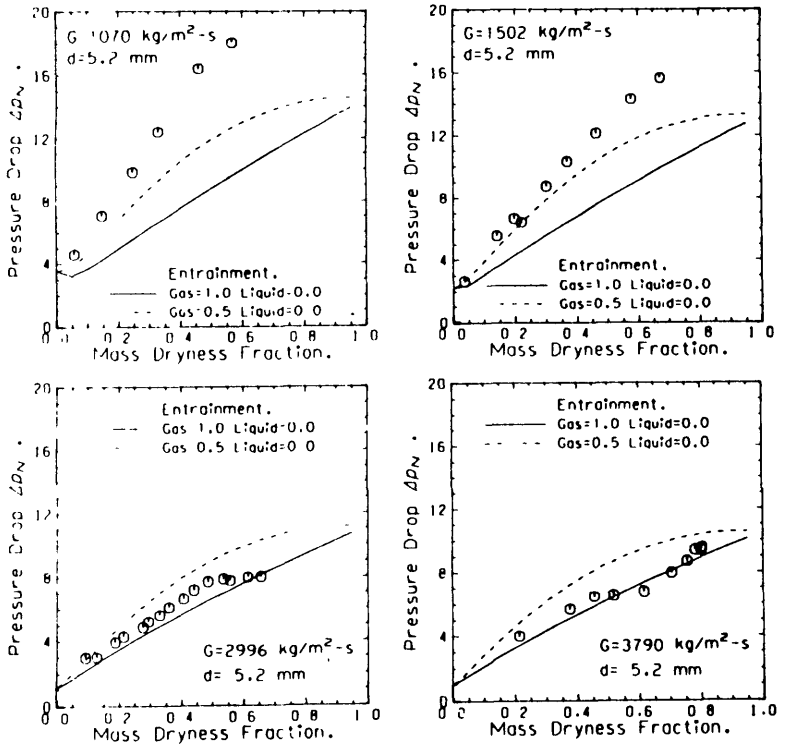

Fig. 4. Calculated and measured pressure drops: vertical unheated pipes; length 53 cm; pressure 68.8 bar.

Sets of results for various mass fluxes are shown in Figs. 4 and 5 for tube diameters of 5.2 mm and 8.2 mm respectively. On each graph curves are drawn for gas entrainment ratios of 0.5 and 1.0; the latter value represents the case in which all the vapour is entrained, so that the whole tube is filled with a homogeneous vapour/liquid mixture. In order to achieve close agreement with the experimental results, the entrainment ratio has clearly to be increased as the mass flux increases.

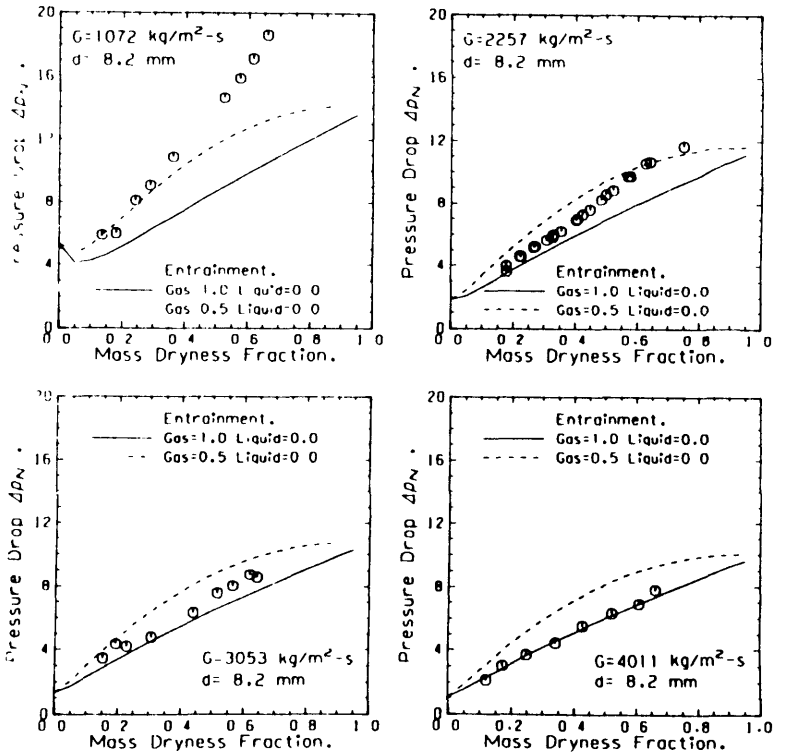

Fig. 5. Calculated and measured pressure drops: vertical unheated pipes; length 92 cm; pressure 69.6 bar.

The same point is made in a different way in Fig. 6, in which predicted pressure drops are plotted against the observed values for a larger number of mass fluxes. The upper graph is drawn for the homogeneous-mixture model (gas entrainment ratio = 1) and shows good agreement for high mass fluxes, but increasingly poor agreement for decreasing mass flux. The lower graph shows the effect of reducing the gas entrainment ratio to 0.5.

It is interesting to note that Muscettola [6], in analysing the CISE results using a variety of models of two-phase flow, obtained the best agreement with the homogeneous-mixture model.

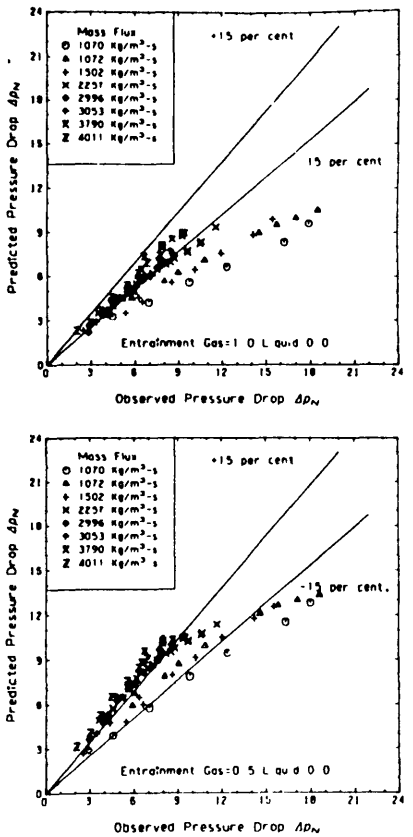

Fig. 6. Comparison of measured pressure drops with calculated values using two entrainment ratios.

5. CONCLUDING DISCUSSION

It will be appreciated that even with the added feature of inter-phase entrainment, the velocity profile model remains a highly-idealised representation of two-phase flow, particularly in its sharp division into two flow regions. The measured transverse distributions of relative density obtained by Haywood et al. [4] clearly indicate a gradual transition across most of the tube radius.

In the calculated results displayed in this paper only entrainment from the vapour phase into the liquid region has been allowed, for simplicity. Entrainment can of course generally be expected to occur in both directions. In the present form of the model the values of the entrainment ratio(s) appropriate to local flow conditions have to be available as input data. The encouraging indication from the comparisons shown above is that when this information is given the model will give reasonably accurate predictions of the axial pressure gradient.

It is clearly desirable to extend the model further so that entrainment ratio(s) are calculated internally. Such a development is being actively pursued, but may require more extensive experimental results than at present exist, for its satisfactory conclusion.

6. REFERENCES

1. COLLIER, J.G. - Convective Boiling and Condensation, McGraw-Hill Company (UK) Ltd., 1981.

2. HEWITT, G.F. - Handbook of Multiphase Systems, Gad Hetsroni, Hemisphere Publishing Corporation, 1982, pp. 2.44-2.75.

3. SKOULOUDIS, A.N., PEERLESS, S.J. - An Analytical Profile Model of Annular Two-Phase Flow, Proceedings Heat and Fluid Flow in Nuclear and Process Plant Systems, Institution of Mechanical Engineers, London, 17-18 May 1983.

4. HAYWOOD, R.W., KNIGHTS, G.A., MIDDLETON, G.E., THOM, J.R.S., Experimental Study of Flow Conditions and Pressure Drop of Steam-Water Mixtures at High Pressures in Heated and Unheated Tubes, Proc. Inst. Mech. Engrs., Vol. 175, pp. 663-747, 1961.

5. BERKOWITZ, L., BERTOLETTI, S., LESAGE, J., PETERLONGO, G., SOLDAINI, G., WECKERMANN, F.J., ZAVATTARELLI, R. - Results on Wet Steam Cooling Experiments, CISE Report R-27, October 1960.

6. MUSCETTOLA, M. - Two-Phase Pressure Drop - Comparison of the Momentum Exchange Model and Martinelli and Nelson's Correlation with Experimental Measurements, UKAEA Report AEEW-R.284, 1963.

Appendix E.

References.

REFERENCES

Ad61 : N Adorni, G Gaspari, G Germani, G Peterlongo, "Experimental Data in Annuli and Cluster".

CISE, Report R-31, 1961.

An60a : G H Anderson, G B Mantzouranis, "Two-Phase Flow Phenomena - I".

Chem. Eng. Sci., 12, 1960, pp 109 - 126.

An60b : G H Anderson, G B Mantzouranis, "Two-Phase Flow Phenomena - II Liquid Entrainment".

Chem. Eng. Sci., 12, 1960, pp 233 - 242.

Ar70 : E Arnold, "UK Steam Tables",

E Arnold (Publishers) Ltd., 1970.

Ba60 : S G Bankoff, "A Variable density single fluid Model for Two-phase Flow with Particular Reference to Steam-Water Flow".

J Heat Transfer, Trans. ASME, 82C, 1960, pp 265 - 272.

Ba69 : K J Bar, "Properties of Water and Steam in SI - Units", 1969.

Be60 : L Berkowitz, S Bertoletti, J Lesage, G Peterlongo, G Saldaini, F J Weckermann, F J Zavattarelli, "Results on Wet Steam Colling Experiments".

CISE, Report R-27, October 1960.

Be64 : S Bertoletti, G P Gaspori, G Lombard, G Peterlongo, M Silvestri, F A Tacconi, "Heat Transfer Crisis With Steam Water Mixtures".

Energia Nucleare, 12(3), 1964, pp 121 - 172.

Be65 : A W Bennett, G F Hewitt, H A Kearsley, R K F Keeys, P M C Lacey.
UKAEA Report, AERE - R4874, 1965.

Be66 : A W Bennett, G F Hewitt, H A Kearsley, R K F Keeys, D J Pulling, "Studies in Burnout in Boiling Heat Transfer to Water in Round Tubes with Non-uniform Heating".

UKAEA Report, AERE - R5076, 1966.

Be67 : A W Bennett, G F Hewitt, H A Dersey, R K F Keeys, D J Pulling, "Studies of Burnout in Boiling Heat Transfer".

Trans. Inst. Chem. Eng., 45, 1967, T319 - 333.

Be77 : A E Bergles, "Burnout in Boiling Heat Transfer. Part 11 : Subcooled and Low-Quality Forced Convection Systems".

Nucl. Saf., 18(2), 1977, pp 154 - 167.

Bo72 : R W Bowring, "A Simple but Accurate Round Tube, Uniform Heat Flux, Dryout Correlation over the Pressure Range 0.7- 17 MN/m^2".

UKAEA Report, AEEW - R789, 1977.

Br77 : W M Bryce, "A new Flow Dependent Slip Correlation which gives Hyperbolic Steam-Water Mixture Flow Equations".

A E E Winfrith, AEEW - R1099, 1977.

Ce78 : Cern Computer Centre Program Library,
"Gaussian Intregration".
Routine D103, 1978 version.

Ch58 : D Chisholm and A D K Laird,
"Two-Phase Flow in Rough Tubes".

Trans. Amer. Soc. Mech. Enginrs, 80, 1958, pp 276 - 286.

Ch73 : D Chisholm, "Pressure Gradient due to Friction during the Flow of Evaporating Two-Phase Mixtures in Smooth Tubes and Channels".

Int. J Heat and Mass Transfer, 16, 1973, pp 347 - 358.

Ci65 : CISE R-99 (1964) See Reference (Be64).

Co72 : J G Collier, "Convective Boiling and Condensation".

McGraw-Hill Book Company, Maidenhead, 1972.

Co81 : J G Collier, "Introduction to Two-phase Flow Problems in the Power Industry", Chapter 19.

Two-Phase Flow and Heat Transfer in the Power and Process Industries, Hemisphere Publishing Corporation, 1981.

Eg57 : R A Egen, D A Dingee, J W Chastain, "Vapour Formation and Behaviour in Boiling Heat Transfer.

Battelle Memorial Report, No. 1163, 1957.

Fa76 : S Fabic, "Review of Existing Codes for Loss-of-Coolant Accident Analysis".

Adv. Nucl. Sci. Technol., 20, 1976, pp 365 - 404.

Gi81 : M Giot, "Friction Factors in Single Channels".

Chapter 11, Thermohydraulics of Two-Phase Systems for Industrial Design and Nuclear Engineering.

Hemisphere Publishing Corporation, 1981.

Ha61 : R W Haywood, G A Knights, G E Middleton, J R S Thom "Experimental Study of the Flow Conditions and Pressure Drop of Steam-Water Mixtures at High Pressures in Heated and Unheated Tubes".

Proc. Instn. Mech. Eng., 175, 1961, pp 669 - 748.

Ha64 : D E Hartley, W Murgatroyd, "Criteria for the Break-up of Thin liquid Layers Flowing Isothermally over a Solid Surface".

Int. J Heat Mass Transfer, 7, 1964, pp 1003 - 1015.

He63 : G F Hewitt, H A Kearey, P M C Lacey, D J Pulling, "Burnout and Nucleation in Climbing Film Flow".

UKAEA Report No. AERE - R4373, 1963.

He65/66 : G F Hewitt, H A Kearsey, P M C Lacey, D J Pulling, "Burnout and Film Flow in the Evaporation of Water in Tubes".

Proc. IME, 180 (part 3c), 1965/66, pp 206 - 215.

He70 : G F Hewitt, N S Hall-Taylor, "Annular Two-Phase Flow".

Pergamon Press, Oxford (1970).

He78 : G F Hewitt, "Critical Heat Flux in Flow Boiling".

Proc. 6th Int. Heat Transfer Conf., 6, 1978, pp 143 - 171.

He81 : G F Hewitt, "Burnout", Chapter 9.

"Two-Phase Flow and Heat Transfer in the Power and Process Industries".

Hemisphere Publishing Corporation, 1981.

He82 : G F Hewitt, "Burnout", Chapter 6.4.

Handbook of Multiphase Systems (G Hetsioni),
Hemisphere Publishing Corporation, 1982.

Hu62 : G A Hughmark, "Hold-up in Gas-Liquid Flow".

Chemical Engineering Progress, 58, 1962, pp 62 -65.

Hu73 : P Hutchinson, P B Whalley, "A possible
Characterization of Entraninment in Annular Flow".

Chem. Eng. Sci., 28, 1973, p 974.

Is57 : H C Isbin, N C Sher, K C Eddy, "Void Fractions in
Two-Phase Steam-Water Flow".

AIchE Journal, 1957, pp 136 - 142.

Is61 : H Isbin, R Vanderwater, H Fauske, S Singh, "A Model
for Correlation Two-Phase, Steam-Water, Burnout Heat
Fluxes".

J Heat Treansfer, Trans. ASME, 83, 1961, pp 149 - 157.

Is75 : M Ishii, M A Grolmes, "Inception Criteria for Droplet Entrainment in Two-Phase Concurrent Fil, Flow".

AIchE J, 21, 1975, p 308.

Is82 : M Ishii, "Wave Phenomena and Two-Phase Flow Instabilities", Chapter 2.4.

Handbook of Multiphase Systems (G Hecsroni) Hemisphere Publishing Corporation, 1982.

Is82b : M Ishii and K Mishima, "Liquid Transfer and Entrainment Correlation for Droplet-Annular Flow".

Proc. 7th Int. Heat Transfer Conf., 5, 1982, pp 307 - 312.

Ke70 : R K F Keeys, J C Ralph, D N Roberts, "The effect of Heat Flux on Liquid Entrainment in Steam-Water Flow in a Vertical Tube".

UKAEA Report, AERE - R6294, 1970.

Ke72 : R K F Keeys, J C Ralph, D N Roberts, "Post burnout Heat Transfer in High Pressure Steam-Water Mixtures in a Tube with Cosine Heat Flux Distribution".

UKAEA Report, AERE - R6411, 1972.

La57 : H C Larson, "Void Fractions of Two-Phase Steam-Water Mixture".

Ms Thesis, University of Minnesota, 1957.

La75 : R T Lahey, "Boiling Transition. Lecture notes for Two-Phase Flow and Heat Transfer in Water-cooled Nuclear Reactors, Dartmouth College 1975.

Le60 : S Levy, "Steam Slip-Theoretical Prediction From Momentum Model".

Journal of Heat Transfer, Trans. ASME, 82, 1960, pp 113 - 124.

Le66 : S Levy, "Prediction of Two-Phase Annular Flow with Liquid Entrainment".
Int. J Heat and Mass Transfer, 9, 1966, pp 171 - 188.

Lo49 : R W Lockhart, R C Marinelli, "Proposed Correlation of Data, for Isothermal Two-Phase, Two Component flow in Pipes".

Chemical Engineering Progress, 45, 1949, pp 39 - 48.

Ma48 : R C Marinelli, D B Nelson, "Prediction of Pressure Drop during Forced Circulation Boiling of Water".

Trans. ASME, 79, 1948, pp 695 - 702.

Ma75 : V Marinelli, "Critical Heat Flux: A Review of Recent Publications", paper 3.0

European Two-Phase Flow Group Meet., Haifa 1975.

Mu63 : M Muscettola, "Two-Phase Pressure Drop-Comparison of the Momentum Exchange Model and Marinelli and Nelson's Correlation with Experimental Measurements".

Atomic Energy Research Establishment Winfrith, AEEW - R284, 1963.

Na77 : "The NAG Fortan Library, Mark 8".

Routine CO5ACF, Numerical Algorithms Group Ltd., 1977.

Ne54 : D M Newitt, N Dombrowski, F H Knelman, "Lipuid Entrainment: 1, The Mechanisms of Drop Formulation from Gas or Vapour Bubbles".

Trans. Inst. Che,. Eng., 32, 1954, pp 244.

Ro63 : S Z Rouhani, K M Becker, "Measurements of Void Fraction for Flow of Boiling Heavy Water in Vertical Round Ducts".

Rep. AE - 106, A B Atomenerg, Sweden 1963.

Ro67: D H Rooney, "Natural Circulation Velocity Prediction with Paricular Reference to Water Tube Boilers".

PhD Thesis (1967) Univ. of Strathclyde Glasgow.

Sc55 : H Schlichting, "Boundary Layer Theory".

Pergamon Press, London, 1955, Chapter XXI.

Sm70 : S L Smith, "Void Fractions in Two-Phase Flow: A Correlation Based upon an Equal Velocity Head Model".

Proc. Instn. Mech. Eng., 184, 1970, pp 647 - 664.

Sm78 : G D Smith, "Numerical Solution of Portial Differential Equations: Finite Difference Methods".

Oxford University Press, 1978.

Th64 : J R S Thom, "Prediction of Pressure Drop during Forced Circulation Boiling of Water".

Int. J Heat and Mass Transfer, 7, 1964, pp 709 - 724.

Wa69 : G B Wallis, "One Dimensional Two-Phase Flow".

McGraw-Hill, New York (1969).

We57 : J C Westmoreland, "Prediction of the Pressure Loss and Density Factors for Two-Phase Annular Flow with or without Heat Generation".

Am. Soc. Mech. Eng. Paper 57-A-50, 1957.

Wh74 : P B Whalley, P Hutchinson, G F Hewitt, "The Calculation of Critical Heat Flux in Forced Convection Boiling".

Proc. 5th Int. Heat Transfer Conf., 4, 1974, pp 290 - 294.

Zu66 : N Zuber, F W Staub, "Stability of Dry Patches Forming in Liquid Films Flowing over Heated Surfaces".

Int. J Heat Mass Transfer, 9, 1966, p 897.